Characterization of the spin and attitude of the ESA Huygens probe during its descent onto Titan using the engineering dataset.

Study carried out by Alain Sarlette
under supervision of
Dr. J.-P. Lebreton
Dr. O. Witasse, Ir. M. Pérez Ayúcar
Pr. J.-P. Swings

during a training period at ESA/ESTEC Noordwijk, The Netherlands
from February to April 2005

Liège University
Faculty of Applied Sciences

European Space Agency Liège University

Characterization of the spin and attitude of the ESA Huygens probe during its descent onto Titan using the engineering dataset.

Graduation thesis written by Alain Sarlette in order to obtain the diploma of civil engineer in physics, orientation space technologies.

Acknowledgements

I want to thank

My supervisors at ESA/ESTEC, Dr. Jean-Pierre Lebreton, Dr. Olivier Witasse and Ir. Miguel Pérez Ayúcar, as well as the whole RSSD team who accepted and helped me during the 3 months I spent in Noordwijk. Special thanks to Ir. Miguel Pérez Ayúcar who supported me a lot by sharing his research work on similar topics;

My promoter, Prof. Jean-Pierre Swings, who allowed me to make this wonderful experience of a training period at the European Space Agency's research centre;

All the people who supported me, morally or financially, in order to allow me to carry out this enriching work.

Characterization of the spin and attitude of the ESA Huygens probe during its descent onto Titan using the engineering dataset.

•

Abstract

The Huygens probe is the ESA's main contribution to the Cassini-Huygens mission, carried out jointly by the ESA, the NASA and the ASI. It was designed to descent into the atmosphere of Titan, Saturn's largest moon, on January 14, 2005, providing surface images of the farthest object a man-made probe has ever landed on. Its main purpose was to study Titan's atmosphere during the descent phase.

Of course, priority has been given to the scientific instruments for data recovery but a small engineering dataset was also sent back to Earth. The goal of the present work was, using these engineering data, to characterize the instantaneous orientation of the Huygens probe during its descent, in order to allow correct analysis of the scientific data.

The methods used concern evaluation of reduced accelerometer data, analysis of the telecommunication link's power level using the accurately known antenna gain pattern and a comparison between the Huygens mission and the more fully instrumented SM2 test probe which was dropped in the Earth's atmosphere in 1995. Some basic dynamic modelization has also been done to investigate likely behaviours and try to identify consistent approximations.

In addition to this report, the results of my work include Excel ® files containing probe orientation (support) data as well as a MATLAB ® routine which allows to compute a probe's azimuth from the (manually pre-processed) telemetry link gain and the positioning dataset. A user-friendly program for the visualization of the evolution of all involved variables - including a 3D probe orientation display - was also planned, but could not be finished since a complete characterization of the probe's attitude (tilt-related motions) was not achieved yet before writing the present report.

As a whole bunch of people spread over the world were working on the subject of the probe's orientation using different information, the conclusions of all teams had to be compared. This was continually done by e-mail while working on the subject; a final meeting on April 22 & 23, 2005 was meant to clarify the situation before publishing first official results.

•

Alain Sarlette, student in physical engineering (orientation space technologies), University of Liège, 2004-2005.

Caractérisation du spin et de l'attitude de la sonde Huygens de l'ESA pendant sa descente vers Titan à partir des données utilisées pour le contrôle des opérations.

•

Abstract(FR)

La sonde Huygens constitue la contribution principale de l'ESA à la mission Cassini-Huygens, effectuée conjointement avec la NASA et l'ASI. Elle a été conçue pour descendre dans l'atmosphère de Titan, le plus grand satellite de Saturne, le 14 janvier 2005. Les images de la surface de cet objet, le plus éloigné sur lequel l'homme ait jamais posé une sonde, ont fait le tour du monde. Mais le principal objectif de la mission était l'étude de l'atmosphère de Titan pendant la descente.

Il est logique que les mesures scientifiques aient été privilégiées en ce qui concerne le rapatriement des données, mais un petit ensemble de donnes opérationnelles a également été envoyé vers la Terre. Le but du présent travail était la reconstitution de l'orientation instantanée de la sonde Huygens pendant la descente en se basant sur ces informations dont disposent les ingénieurs, afin de permettre aux scientifiques d'interpréter correctement leurs résultats.

Les méthodes utilisées comportent l'évaluation de données d'accéléromètres, la comparaison de la puissance du lien de télécommunication au diagramme de gain de l'antenne ainsi que l'analyse d'une possible analogie entre le mouvement de la sonde Huygens lors de sa mission et celui de la maquette SM2, spécifiquement instrumentée pour observer le comportement de la sonde lors d'une descente dans l'atmosphère terrestre effectuée en 1995. Une brève étude dynamique simplifiée a également été effectuée afin de tenter d'identifier des régimes probables et des approximations cohérentes.

En plus de ce rapport, les résultats de mon travail comprennent des fichiers Excel ® contenant des données sur l'orientation de la sonde ainsi qu'une routine MATLAB ® permettant de calculer l'azimuth d'une sonde à partir d'un jeu de données opérationnelles disponibles (en particulier, gain de la télécommunication prétraité manuellement et données de localisation). Un programme a également été prévu pour la visualisation conviviale de l'évolution des variables concernées - incluant un affichage 3D de l'orientation de la sonde; celui-ci n'a malheureusement pas pu être terminé à cause d'une caractérisation encore insuffisante de l'attitude de la sonde au moment de la publication du présent rapport.

Vu le nombre de personnes, distribuées dans le monde, travaillant sur le sujet du comportement de la sonde en utilisant des sources d'informations différentes, les conclusions de toutes ces équipes devaient être comparées. Cela s'est fait continuellement par courriel au cours des avancées des analyses; une réunion à l'ESTEC les 22 et 23 avril 2005 devait clarifier la situation avant la publication des premiers résultats officiels.

•

Alain Sarlette, étudiant ingénieur civil physicien (orientation techniques spatiales), Université de Liège, 2004-2005.

Contents

Acronyms and abbreviations

ACP : Aerosol Collector and Pyrolyser

AGC : Automatic Gain Control

AGP : Antenna Gain Pattern

ASI : Italian Space Agency

BCSS : Back Cover SubSystem

BIU : Bus Interface Unit

CASU : Central Acceleration Sensor Unit

CDMS : Command and Data Management System

CDMU : Command and Data Management Unit

CFRP : Carbon Fibre Reinforced Plastic

DCSS : Descent Control SubSystem

DDB : Descent Data Broadcast

DGB : Disk Gap Band

DISR : Descent Imager / Spectral Radiometer

DM : Descent Module

DTWG : Descent Trajectory Working Group

DWE : Doppler Wind Experiment

EM : Engineering Model

EPSS : Electrical Power SubSystem

ESA : European Space Agency

ESTEC : European Space research and TEchnology Centre

FM : Flight Model

FRSS : FRont Shield Subsystem

GCMS : Gas Chromatograph and Mass Spectrometer

HASI : Huygens Atmospheric Structure Instrument

HGA : High Gain Antenna

HSWT : Huygens Science Working Team

IF : Intermediary Frequency

JPL : Jet Propulsion Laboratory (NASA)

MLI : Multi-Layer Insulation

MTU : Mission Timer Unit

NASA : National Aeronautics and Space Administration

PAA : Probe Aspect Angle

PCDU : Power Conditioning and Distribution Unit

PDD : Parachute Deployment Device

PDRS : Probe Data Relay System

PI : Principal Investigator

POSW : Probe Onboard SoftWare

PSA : Probe Support Avionics

PSE : Probe Support Equipment

PTT : Probe Transmitting Terminal

RASU : Radial Acceleration Sensor Unit

RAU : Radar Altimeter Unit

RF : Radio Frequency

RFE : Receiver Front End

RHU : Radioisotope Heater Unit

RSSD : Research and Scientific Support Department (ESTEC)

RUSO : Receiver Ultra-Stable Oscillator

SED : Spin Eject Device

SEPS : SEParation Subsystem

SM2 : Special Model 2

SOI : Saturn Orbit Insertion

SSP : Surface Science Package

STPM : Structural, Thermal and Pyrotechnic Model

THSS : THermal SubSystem

TUSO : Transmitter Ultra-Stable Oscillator

VLBI : Very Large Baseline Interferometry

Part I
Introduction

1 Presentation of the Huygens mission

1.1 Generalities about the Cassini-Huygens mission

The Cassini-Huygens mission is a joint mission from NASA, ESA and ASI. Its goal is to study the planet Saturn as well as some of its satellites. It consists of two parts.

- An orbiter, called Cassini[1] and provided by NASA, which constitutes the main spacecraft. Its goal is to study Saturn, its rings, its magnetosphere and a large number of its moons from orbit around Saturn. It carries all necessary equipment for an interplanetary mission, including a power supply, propulsion devices for trajectory corrections and a High Gain Antenna for telecommunication with ground stations on Earth.
- A probe, called Huygens[2] and provided by ESA, which was carried by Cassini until release in December 2004.

Since a direct injection towards Saturn is impossible using our current propulsion systems, several gravity assists were planned to finally reach the energy of a transfer orbit crossing Saturn's one.

The 5650 kg heavy spacecraft was launched from Cape Canaveral Air Station in Florida on October 15, 1997 by a Titan(what chance)4B/Centaur rocket. Liberated from Earth attraction, it operated a 4-fold gravity assist composed of a first Venus flyby in April 1998, a second Venus flyby in June 1999, an Earth flyby in August 1999 and a Jupiter flyby in December 2000 to finally reach Saturn on the first of July 2004.

[1] In memory of *Giovanni Domenico Cassini*, Franco-Italian astronomer: born in Perinaldo (Italy) in 1625, he became a French citizen in 1673 and was director of the famous Observatoire de Paris. He spent a lot of his time observing Saturn, its rings and its satellites. Among others, he discovered the saturnian moons Iapetus, Rhea, Tethys and Dione, as well as the now called "Cassini division", the largest gap in Saturn's rings; he was also the first to come up with the hypothesis that the rings should actually consist of a myriad of separate objects, too small to be distinguished individually. He died in Paris in 1712 after having initiated a whole dynasty of renowned astronomers working at the Observatoire de Paris.

[2] In memory of *Christiaan Huygens*, Dutch astronomer: born in 1629 near Den Haag, he took benefit of an excellent education through his father, who was a councillor of the Prince of The Netherlands. After studying Law and Mathematics, he specialized in Mechanics (conceiving among others the pendulum clock) and Optics. He built his own telescopes which he occasionally pointed to Saturn; after determining that its strange, changing shape could only be due to the presence of a ring around the planet, he also discovered a big moon close to it, later called Titan. He died in 1695. Although he wasn't considered as a major scientific personality during his life, his research work is nowadays recognized as of fundamental importance.

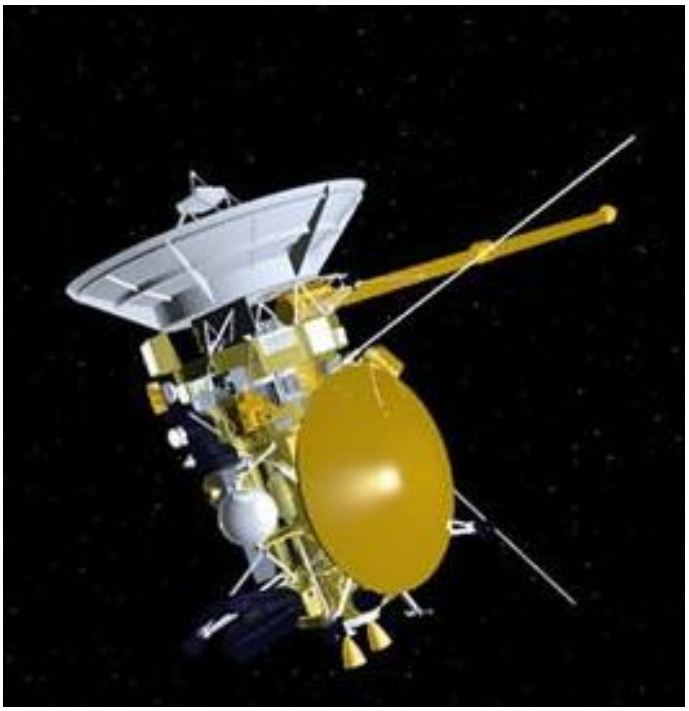

FIG.1: *The Cassini-Huygens spacecraft as it travelled from the Earth to Saturn.*

The seven-year cruise phase before starting the actual Huygens mission was not only critical from a psychological point of view. During all this time, the spacecraft had to survive without any maintenance. System checks were carried out every 6 months, during which some parts of the orbiter and probe were "awakened" to verify proper operation and prevent them from "cramps" due to a too long inactivity[3]. Nevertheless, some systems had to work properly after seven years without any check-out nor activity. Other classical problems encountered for interplanetary missions include the very different thermal conditions to which the spacecraft was subjected between Venus and Saturn and the impossibility to use solar power at the large distances to be explored.

Arriving at Saturn, a Saturn Orbit Insertion propulsive manoeuvre was executed; this put the spacecraft into a highly elliptical orbit around the planet, from which several observations have already been carried out. Among them, one distant observation and two closer flybys of Titan have provided important information about this moon from orbit even before dropping the Huygens probe. The latter was successfully ejected from the orbiter 21 days before the third encounter. From this point on, the two vehicles operated separately, Huygens flying on a Titan-collision trajectory while Cassini deflected its trajectory to avoid Titan and have a proper view of the Huygens landing site (indeed, the Cassini orbiter served as a telecommunication relay to broadcast the Huygens data to Earth); this deflection also set up the subsequent satellite encounters for the further 4 years / 77 orbits carried out by the Cassini mission.

[3]These "cramps" can result from space environment effects such as cold welding, local spacecraft charging effects, degradation of material properties due to high energy electromagnetic or particular irradiation or improper thermal conditions.

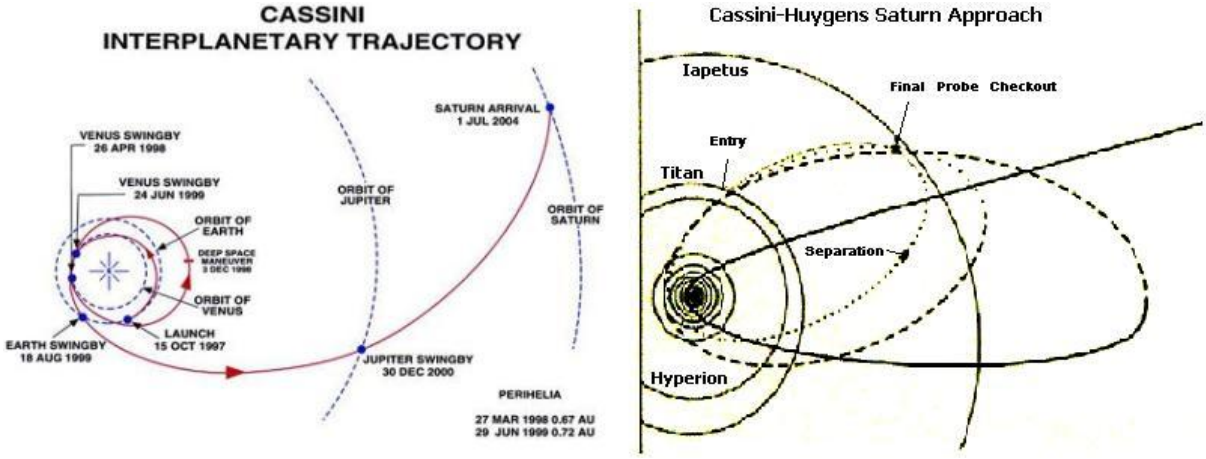

FIG.2: *The trajectory of the Cassini-Huygens spacecraft on its way to Saturn and during the first orbits after SOI.*

Before examining the Huygens mission in more detail, let's have a quick look at the targeted celestial object to understand the scientists' special interest in Titan observations.

1.2 The saturnian satellite Titan

Titan is the biggest of a large and still increasing number (at least 30) of saturnian moons and the second biggest moon in the solar system (just after the jovian satellite Ganymede); with its 2575 km radius, it is only about 2.5 times smaller than the Earth itself. But the most interesting fact is that it is the only known moon to possess a significant atmosphere, and it's a thick one: the surface pressure reaches 1.5 bar. As for the Earth, it is mainly composed of nitrogen (> 95 % of N_2); other major constituents are hydrogen (0.2 % of H_2) and methane (a few percent of CH_4), whose presence is not satisfactorily explained yet. It was speculated that argon might also be present in some quantity.

These constituents are very similar to what was present on Earth before the appearance of life; lightning could also be present and might stimulate chemical processes, so that scientists hope to gain important insight in the chemical processes involved in the creation of the basic molecules of living organisms. However, the large distance to the sun involves much reduced solar irradiation and low temperatures of 94 K at the surface and 70 K at the tropopause; the latter is located at an altitude of about 45 km, for a total atmosphere thickness of about 200 km. As a consequence, water could only be present in the form of ice on the surface.

The main objectives of the Huygens mission were to study the atmosphere, whose composition and activity will be much more accurately known after full evaluation of the Huygens data, and the surface, which in majority remains hidden behind the thick atmosphere when viewed from an orbiter.

From a challenging point of view, Titan is the farthest celestial object on which a manmade vehicle has ever landed.

1.3 The Huygens probe

1.3.1 The entry and descent scenario

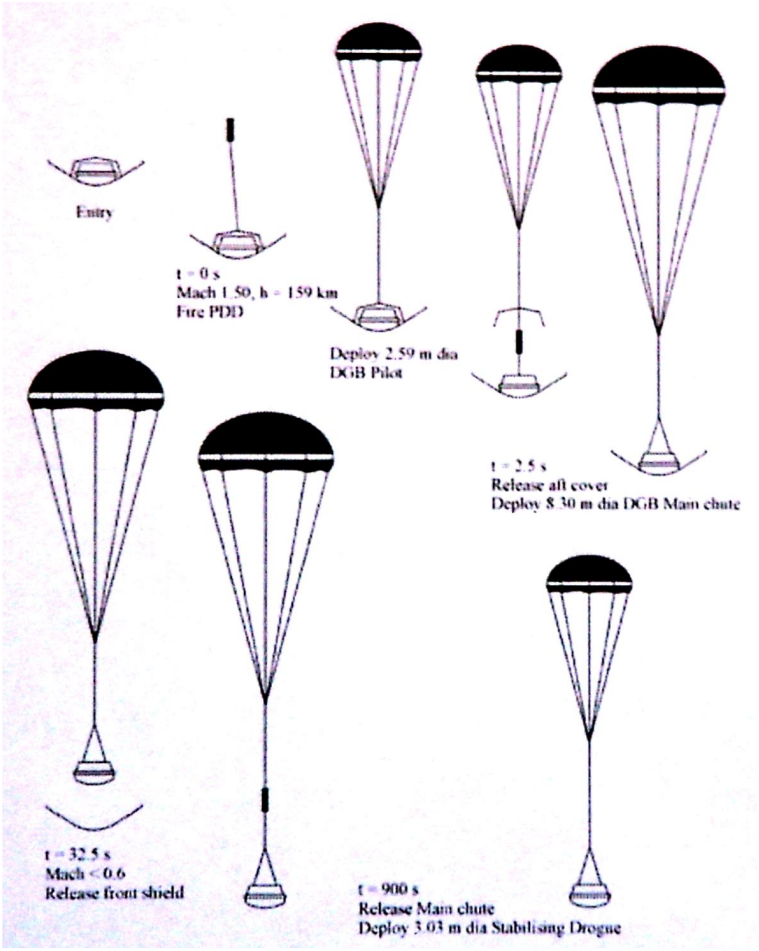

FIG.3: *The entry and descent sequence of the Huygens probe.*

As already mentioned, the Huygens probe has been ejected from Cassini about three weeks before its landing which occurred on January 14, 2005. To enhance the stability of the trajectory, a spin of 7 *rpm* was given to the probe by the Spin Eject Device, in counterclockwise direction as seen from behind.

During this operation and during the subsequent three weeks long coasting phase, the Huygens probe was still "sleeping" to save energy. Only the Mission Timer Unit was initiated, activated before separation and powered during the coasting phase, its role being to awaken the probe at the right time; it consisted of three hot-redundant clocks to prevent the probe from having a critical "hangover" leading to an entire mission loss. Indeed, no telecommand link to Cassini[4] was established during this phase, the probe had to operate completely autonomously.

[4]Nor to Earth of course, which would have required huge amounts of power and a high gain antenna and would anyway have been of little use for probe command since Saturn is at more than one light-hour from Earth.

The probe was switched on 4 hours before entry. This event activated the onboard computers which controlled all onboard operations and allowed sufficient warm-up of the probe equipment, in particular of the clock that generated the data-stream modulation frequency.

At an altitude of 1270 km, the entry phase officially started. As the JPL had the responsibility to bring the probe to this point at the right time and with the right velocity vector, from here on ESA took over the entire responsibility of the Huygens mission. The probe's aeroshell decelerated it in about 4.5 minutes from the entry speed of 6 km/s to 400 m/s at an altitude of about 170 km.

When the CASU accelerometer system detected that the deceleration dropped under 10 m/s^2, the Descent Control SubSystem was initiated and the descent phase began. This time is known as S_0. Exactly 6.375 seconds later, at T_0, a mortar firing liberated the pilot parachute; this one deployed within 1-2 s and, after back cover cut-off, ejected it pulling out the main parachute, under which the probe made the first phase of its descent. T_0 corresponded to 9 h 10 mn 21.770 s UTC local (Titan) time on January 14.

After having passed through the transsonic phase, 30 s after main chute inflation, the front shield was released, liberating the instruments which successfully ejected their covers and deployed their booms to start carrying out their measuring tasks. The radio link to the Cassini orbiter, which had turned its High Gain Antenna to listen to Huygens and record the data on its solid state recorder for later transmission to Earth, was started roughly 50 s after T_0.

As an entire descent under main chute would have been too slow to reach the surface of Titan before Cassini had passed behind the horizon, the main parachute was ejected after 15 mn and a smaller stabilizer parachute was inflated for use during the second phase of the descent. This lasted about 2 h 12 mn, before Huygens touched the moon's ground. As the probe survived the landing on a solid ground and the batteries worked longer than minimal assumptions stated, surface analysis and imaging could be pursued until Cassini disappeared behind Titan's horizon and the telecommunication link was definitively broken at 12 h 50 mn 24 s, after 3 hours and 40 minutes of successful mission.

1.3.2 The scientific goals and instruments

The scientific objectives of the Huygens mission were defined as follows:

- Determine the abundance of atmospheric constituents, including isotope ratios for abundant elements, in order to constrain possible scenarios for the formation and evolution of Titan and its atmosphere;

- Observe vertical and horizontal distributions of trace gases and search among those for more complex organic molecules; investigate possible energy sources for atmospheric chemistry and model the photo-chemistry of the stratosphere; study the formation and composition of aerosols;

- Measure winds and global temperatures; investigate cloud physics, general circulation and seasonal effects in Titan's atmosphere; search for lightning discharges;

- Determine the physical state, topography and composition of the surface; infer the internal structure of the satellite;

- Investigate the upper atmosphere, its ionization and its role as a source of neutral and ionized material for the magnetosphere of Saturn.

Analysis of the data will keep scientists busy for several years, but it is clear that the scientific return of the Huygens mission will be very high.

To achieve these scientific objectives, the payload was composed of 6 instruments.

GCMS , the Gas Chromatograph and Mass Spectrometer, was designed to measure the chemical composition of Titan's atmosphere and determine the isotope ratios of the major gaseous constituents. It has also analyzed gas samples from ACP and investigated the composition of several candidate surface materials. It was composed of a quadrupole mass-spectrometer and three gas chromatograph columns.

ACP , the Aerosol Collector and Pyrolyser, was designed to collect aerosols which GCMS analyzed for their chemical composition. A deployable sampling device was operated twice during the descent to collect samples at two different altitudes; a pump drew the atmosphere through a filter which captured the aerosols. For each sample, the filter was passed to a furnace which conducted a stepwise pyrolysis, the products being flushed into GCMS for analysis.

DISR , the Descent Imager / Spectral Radiometer, provided the most popular data of the mission, namely the pictures. This optical remote-sensing instrument consisted of a set of upward and downward looking photometers, visible and IR spectrometers, a solar aureole sensor, a side-looking imager and two down-looking imagers (medium and high resolution). To take pictures in different directions, the probe was meant to spin in a controlled manner; DISR tried to check the precise spin rate with the sun sensor in order to coordinate the pictures it took with the probe's orientation. To be able to carry out spectral measurements in the bottom layers of Titan's thick atmosphere and of the surface, it had to turn on a lamp a few hundred meters above the surface.

DWE , the Doppler Wind Experiment, was not an instrument on its own, in the sense that the useful information was actually obtained by observing the probe's signal from the Cassini orbiter (and accessorily from Earth where radio-telescopes were able to detect the very faint signal of the Huygens probe). Its objective was to determine the direction and strength of Titan's zonal winds to a precision better than 1 m/s. It used one of the 2 redundant chains of the probe-to-orbiter radio link, to which two Ultra-Stable Oscillators were added, one at the probe Transmitter (TUSO) and one at the orbiter Receiver (RUSO), to perform Doppler processing of the received carrier signal on board of the orbiter. Unfortunately, channel A of the telecommunication link, on which DWE was mounted, was not received by Cassini, leading to the loss of this experiment. However and fortunately, a set of 17 radio-telescopes on Earth successfully detected the carrier of the channel A signal, allowing the measurement of winds along the line of sight.

HASI , the Huygens Atmospheric Structure Instrument, was multi-sensored to measure the atmosphere's physical and electrical properties. It consisted of a 3-axis piezo-accelerometer

and a 1-axis servo-accelerometer, specifically optimized to measure entry deceleration for the purpose of inferring the atmospheric structure; a coarse and a fine temperature sensors; a multi-range pressure sensor; a microphone to listen for thunder; and an electric field sensor array, composed of a relaxation probe to measure the atmosphere's ionic conductivity and a quadrupolar array of electrodes, in active mode measuring the permittivity of both the atmosphere and the surface material, and in passive mode detecting atmospheric electromagnetic waves, such as those produced by lightning. The HASI sensors were mounted on meter long booms which were deployed as soon as possible to reduce the influence of the probe itself on the atmospheric measurements.

SSP , the Surface Science Package, finally got the unique opportunity to characterize Titan's surface by direct contact, as the Huygens probe successfully survived the landing. It included a force transducer for measuring the impact deceleration and sensors to measure the index of refraction, temperature, thermal conductivity, heat capacity, speed of sound and dielectric constant of any material at the impact site; a microphone was also turned on a few hundred meters above the surface to sound the atmosphere's bottom layer and evaluate the depth of a potential liquid at the landing site (which was not done since the probe landed on a solid surface). A tilt sensor was also included to indicate the probe's attitude after impact.

Figure 4 shows the location of these different instruments on the Huygens probe.

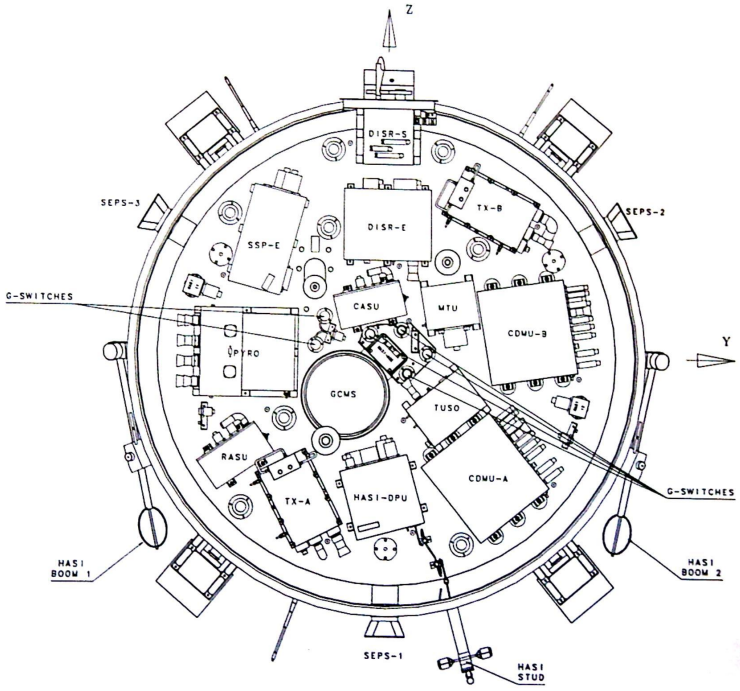

FIG.4: *Map of the Huygens probe experiment platform as seen from above.*

1.3.3 The Huygens probe technical design

As a summary, the mission requirements for the design of the Huygens probe are

1. to carry the probe experiments while attached to the Cassini spacecraft during 7 years;
2. to ensure a clean separation from the orbiter;
3. to withstand entry into Titan's atmosphere, protecting the instruments from excessive heat flux and contamination;
4. to authorize a start of payload operation at high altitude;
5. to ensure a descent through the atmosphere to the surface within a precise period of time (2-2.5 hours) while presenting motions (spin, pendulum and coning) compatible with RF link and experiments requirements;
6. to rely on a passive mechanical/thermal design to save resources for scientific equipment.

The Huygens probe system consisted of two principal elements: the probe itself, which detached from the orbiter to enter in the atmosphere of Titan and the Probe Support Equipment, an element that remained attached to the orbiter after separation and supported its operations. Relatively large uncertainties about the encountered environment on Titan required a robust and versatile design. For example, the bottom part of the probe and the SSP instrument were optimized to permit an interesting use on both a solid and a liquid ground. The probe's mass of 320 kg at launch progressively decreased, to 311 kg after entry[5], 289 kg after main chute deployment, 208 kg after front shield release and finally 202 kg under stabilizer chute.

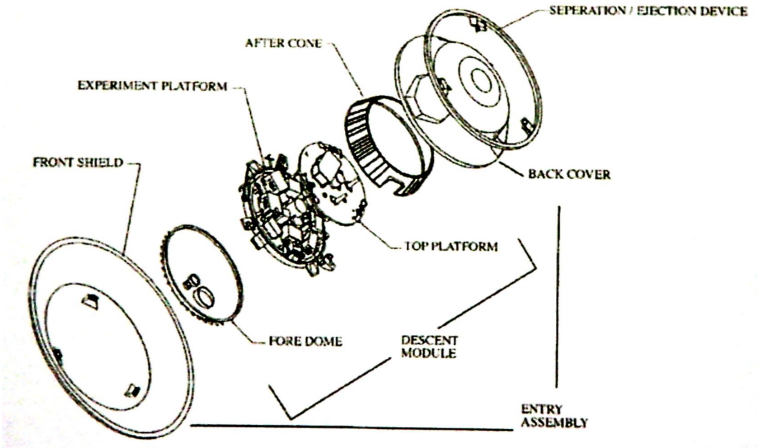

FIG.5: *The Huygens probe's general architecture (exploded view).*

[5]Ablation of MLI and AQ60 tiles, see below.

The probe support equipment

The PSE consisted of

- a Spin Eject Device. The probe was installed on the orbiter by its supporting ring and maintained in place by spring loaded pyrotechnic devices; when these latter were fired, the springs pushing on the probe made it turn in the guide rails of the ring to eject it along a helical track, with a relative velocity of 0.3 m/s and a spin of 7 rpm;
- a harness including the "umbilical connector" between probe and orbiter (and PSE equipment). During the cruise, this electrical connection provided power, command, temperature monitoring and RF and data links;
- two redundant radio Receiver Front Ends and the DWE Receiver Ultra Stable Oscillator (the HGA of Cassini acting as receiving antenna, only the receivers had to be provided in the PSE).
- two redundant Probe Support Avionics electronic boxes. Composed of both analog and digital parts, their role was to handle the received radio signal, performing frequency tracking and conversion down to intermediary frequency, decoding the IF signal, transforming the received transfer frame into telemetry packets, as well as to generate its internal housekeeping data and to distribute the telecommands from the orbiter Bus Interface Unit.

The probe aeroshell

It was composed of only two parts, the front shield and the back cover, that enclosed and protected the Descent Module during cruise and entry phases. The aeroshell and the descent module were attached to each other by pyro-associated mechanisms at three points (3 large struts passing through the whole probe for shock reduction on the DM platform structures); as already explained, the back cover was jettisoned at descent initiation, liberating the main chute, while the front shield was released a bit later once the sub-Mach regime was established and liberated the instruments. The aeroshell was wrapped into a MLI thermal protection for the cruise phase: since the encountered thermal environments between Venus and Saturn were very different, passive thermal regulation was difficult and the best way to obtain temperature regulation was shielding/insulation with respect to exterior influences associated with an inner radio-isotope heat source.

The 79 kg, 2.7 m diameter, 60-degree half-angle coni-spherical front cover was designed as an entry shield, implying thermal and aerodynamic requirements. The CFRP honeycomb supporting structure was covered with 'AQ60' tiles (ablative material consisting of phenolic resin reinforced by silica fibres) on the front side to provide protection against the entry thermal flux of up to 1.4 MW/m^2; Prosial (a suspension of hollow silica spheres in silicon elastomer) was directly sprayed on the aluminium structure of the rear surfaces, experiencing much lower heat fluxes. This design rejected heat by all thermal capacity, radiation, ablation and limited conduction during the short transient entry phase. A radiative window was implemented on the spherical part of the front face to increase heat transfer to space during probe thermal control hot cases; this one was composed of 8 white painted aluminium sheets directly bonded on the AQ60.

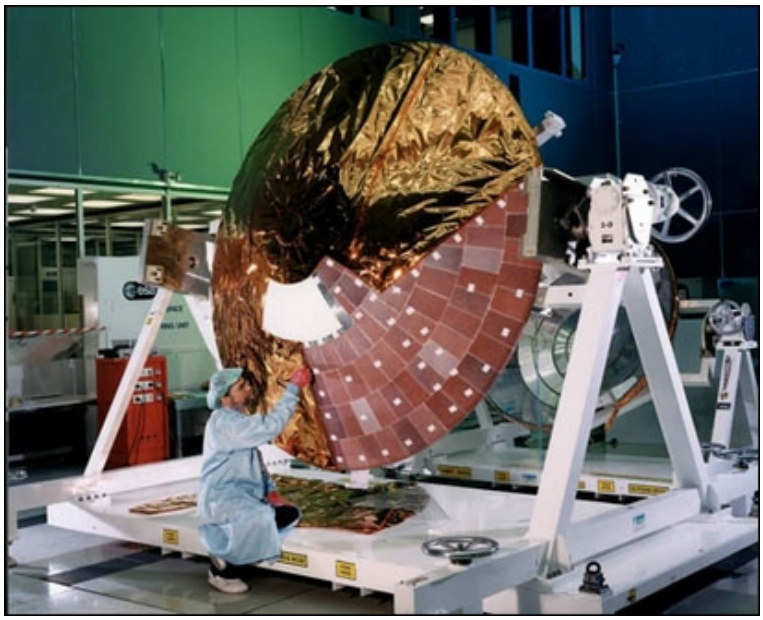

FIG.6: *The Huygens probe's front shield.*

The back cover was also covered by a Prosial spray for entry protection and a MLI for the cruise and coast phases. A whole pierced through its surface ensured depressurisation during launch and repressurization during entry. Its stiffened aluminium structure was connected to the front shield by a labyrinth sealing joint providing a non-structural thermal and particulate barrier.

The Descent Control SubSystem

The DCSS was meant to control the descent speed and provide the stability of the Huygens probe during descent. It mainly consisted of the parachutes and their deployment and jettison devices.

All three parachutes (pilot chute, main chute and stabilizing drogue) were of Disk Gap Band type, made of Kevlar lines and nylon fabric. While the pilot chute had a single gap, double gap technology was used for the main and stabilizer chutes; by increasing the porosity from 13.1 % to 22.4 %, this significantly reduced their angle of attack and enhanced their stability. The 2.59 m diameter pilot chute pulled out the 8.30 m diameter main chute, designed to rapidly slow down the probe under Mach 1 in order to allow an early front shield release; the stabilizing parachute, deployed after jettison of the main chute 15 minutes later to accelerate the probe's descent velocity, had a diameter of 3.03 m and was housed in the same canister on the DM's top platform.

The probe hung under the parachutes using a three-point attachment to ensure horizontal stability, the three wires connecting to a single one about 4 m above the probe's top platform. A swivel was incorporated in the middle of this vertical axis in order to decouple the spin of the probe from the parachute's motions; this was done to allow the probe spin constantly in the same direction, providing a view of the whole panorama to the instruments, which were fixed on the probe's structure.

The structure of the Descent Module

The DM was a 1.3 m diameter, 0.65 m high cylinder, comprising two platforms, a fore-dome and an after-cone. It provided mounting support for the payload and the equipment subsystems and was fully sealed (among others to allow floating on a hypothetic liquid impact surface) except for a venting hole of about 6 cm^2 on the top. The architecture of the module had to take into account that the mass distribution should approach axial symmetry to ensure dynamic stability through a centred barycentre.

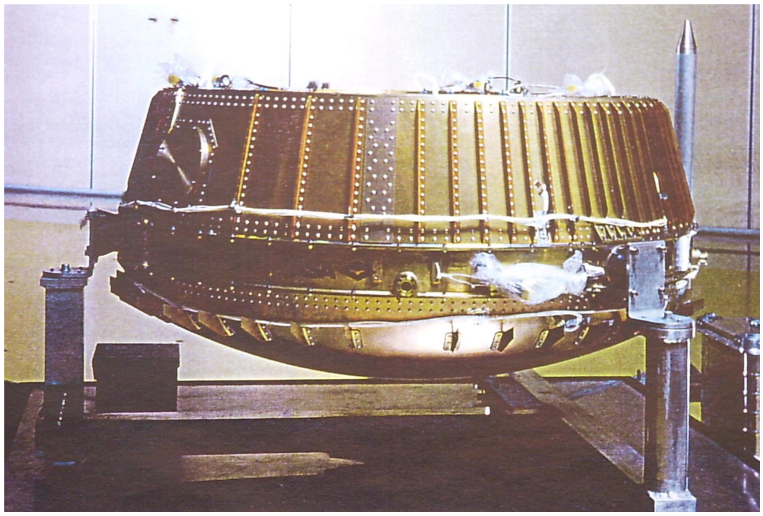

FIG.7: *Picture of the Huygens descent module.*

The two platforms were made of aluminium honeycomb sandwich structures. The 73 mm thick experiment platform supported the majority of the experiments and subsystem units, together with their associated harnesses, while the 25 mm thick top platform carried the DCSS and the two RF transmitting antennas.

The after cone and fore dome were aluminium shells linked by a central ring; 36 spin vanes have been mounted on the periphery of the fore dome to maintain a spin movement during the whole descent through aerodynamic interaction with the atmosphere. The critical moment for their efficiency was supposed to be at the end of the main chute phase, when dynamic pressure was the lowest and a small friction torque in the parachute swivel might have stopped the spin movement. This led the dimensioning constraints, resulting in an inclination of 2.2 deg, which was increased to 3 deg after reduced efficiency was observed during the SM2 test flight.

Three radial titanium struts served as SEPS interface and provided thermal decoupling between the probe and the orbiter, while three vertical struts linked the two platforms and transferred the parachute deployment loads through the whole DM.

The Thermal SubSystem

The role of the probe's THSS was to maintain all experiments and subsystem units within their allowed temperature ranges during all mission phases; while the PSE was thermally

controlled by the Cassini orbiter, the Huygens probe itself was (partially) thermally insulated from the orbiter.

During cruise, small inner temperature variations had to be ensured despite variations of the solar flux from 3800 W/m^2 (near Venus, but only shortly since the probe was normally shadowed behind Cassini's High Gain Antenna) to 17 W/m^2 (approaching Titan). That's why all external areas were packed in an MLI blanket, except for the small thermal window in the front shield to allow controlled heat rejection (about 8 W during cruise), in order to decouple Huygens' thermal behaviour from the changing environment to a maximal extent. Thirty-five Radioisotope Heater Units, providing about 1 W each all the time, mounted on the experiment and top platforms, generated the necessary internal heat to avoid the probe freezing (remember that all systems were asleep during cruise). The RHU/heat window combination was meant to reduce the sensitivity of thermal performances to the MLI efficiency.

During entry, the MLI was burnt and torn away, uncovering the 'AQ60' tiles of the front shield and the other, Prosial-covered aeroshell surfaces that protected the probe in this hot phase.

During descent, convective cooling by Titan's cold atmosphere was prevented by using gas-tight seals and lightweight foam covers on the internal walls of the DM's shell.

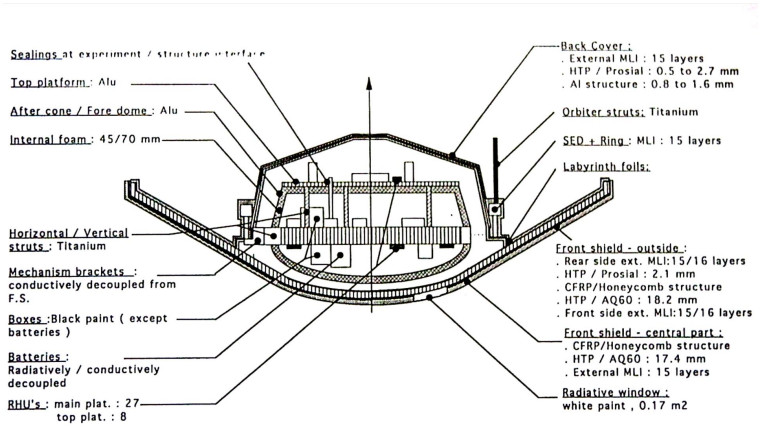

FIG.8: *The thermal control systems on the Huygens probe.*

The power source

The Electrical Power SubSystem comprised five $LiSO_2$ batteries providing the mission's electrical power. Each battery consisted of two modules of 13 cells in series. This nominal battery capacity of 2059 Wh included a 520 Wh margin for energy loss due to the 7-year storage during cruise phase, a 355 Wh margin for battery failures (ensuring enough power if 1 cell in each string and one of the 10 strings failed) and a 195 Wh margin assuming a single experiment and a single probe unit failure. These margins were partially used for the pre-heating required by the mission recovery solution (see below).

The interested reader can have a look at specific reports to get the exact energy budget of the Huygens mission; let's just pick out that

- during entry, 125 W were consumed (mainly by the CDMS and by payload preparations);

- during descent, 180 W were fed to the payload, 83 W to the RF link subsystem and 30-40 W to the CDMS at 28 V (maximal available power: 400 W);

- during cruise, the power was provided by the orbiter through a 28 V power bus in the umbilical link, the probe batteries being isolated (this power was just needed during the bi-annual checkouts).

Finally, 325 Wh of the initial 2059 Wh (or actually 972 Wh after loss margin deduction) were foreseen for the payload, 214 Wh for communication needs (PDRS) and 246 Wh for command and data management (CDMS).

The power was managed and distributed by a specifically dedicated Power Conditioning and Distribution Unit. Losses within that unit consumed an energy of about 128 Wh.

As third and last subsystem of the EPSS, the pyro unit which triggered the separation mechanisms consisted of two redundant sets of 13 pyro lines, directly connected to the centre tap of two batteries. Their power consumption of 5 Wh was truly negligible. For safety reasons, the pyro firings were commanded through three independent levels of control relays in series: an energy intercept relay activated by the PCDU after coast phase, arming relays activated by the arming timer hardware after entry deceleration detection at S_0 and selection relays activated by the CDMS. In addition, active switches and current limiters controlled the firing current.

The radio link

The Probe Data Relay Subsystem was split in two parts: the PSE subsystems on the Cassini orbiter and the Probe Transmitting Terminal on Huygens. The latter was composed of two hot-redundant S-band transmitters and their circularly polarized transmitting antennas. Channel B used left-hand circular polarization, a simple temperature controlled oscillator providing the carrier frequency around 2097.995 MHz; channel A, right-hand polarized, used the Ultra-Stable Oscillator of the DWE experiment to very precisely fix the carrier frequency of 2040 MHz.

The signal itself was of residual carrier type, phase modulated by a 131.072 kHz subcarrier signal carrying the PCM encoded data stream. Each telecommunication channel was designed to support a constant data rate of 8192 b/s during the entire mission[6].

The transmitted power was regulated by a 10 W power amplifier using automatic level control to provide a minimal but sufficient output power. To understand the received power variations, we should consider the following link properties.

- The transmitting antenna gain depended on azimuth and inclination (with respect to vertical) of the link direction. Exact antenna characterization was carried out prior to launch to have an exact gain pattern for each antenna. *Figure 9* represents the evolution of minimal and maximal antenna gain patterns as a function of inclination,

[6]This transmission rate might seem quite reduced; however, remember that Cassini's closest approach to Titan was 60000 km above the surface and that the available power for telecommunication was much reduced: given the minimal total energy of 972 Wh foreseen for feeding the entire probe, during the whole descent and surface phases, the already large portion of 214 Wh allocated to the PDRS could not be increased. In fact, you could say that they had to achieve a performance similar to a far Earth-to-satellite link with the reduced power of two satellites; the resulting lower signal-to-noise ratio implied a much reduced useful bit rate.

showing that a significant gain drop occurred after $60 - 70$ *deg* of inclination; a gain of 1.6 *dB* and 1.8 *dB* for channels A and B respectively was guaranteed for Probe Aspect Angles under 60 *deg*.

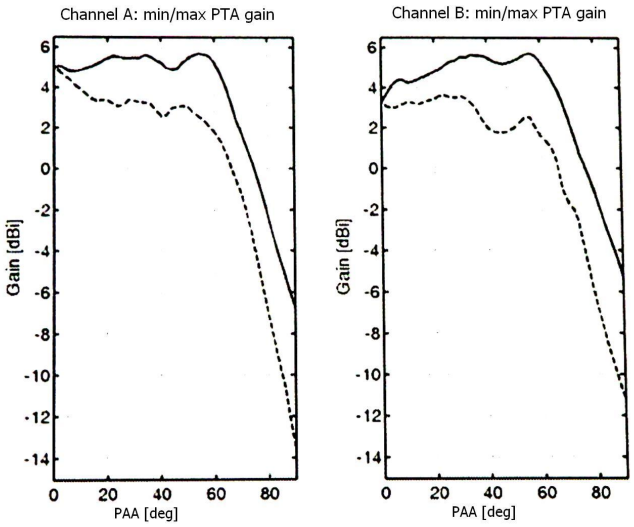

FIG.9: *Gain of the probe transmitting antennas as a function of the angle to vertical (minimum and maximum curves depending on different azimuths).*

We will come back later on the azimuthal variation of the antennas' gains.

- The receiving HGA gain varied from 34 *dBi* on axis to 26.6 *dBi* at 1.7 *deg* off axis (worst case for channels A and B). This very low pointing error was due to the fact that Cassini oriented its HGA towards the expected Huygens landing site to listen to Huygens in an efficient way.

- The variation in distance from probe to orbiter resulted in a slowly varying loss in power density (1.6 *dB* variation for a telecommunication distance between 72000 and 60000 *km*).

- Atmospheric losses were very low: the theoretical upper limit was 0.05 *dB* during the whole descent.

- Near the surface, a multi-path-link interference pattern (due to reflection on Titan's ground) could arise. In practice, this should explain the observed gain variations when the probe had landed.

Unfortunately, channel A of the radio link did not properly operate during the Huygens mission, leading to significant data loss especially for the DWE instrument; channel B worked perfectly, losing no data packet during descent and only a few during the surface extended phase.

Onboard engineering sensors and command units

The Command and Data Management Subsystem was divided between CDMUnits on the probe itself and PSE elements on the orbiter, the PDRS providing the RF link between those two during descent (the umbilical link taking over this job during cruise). It had two primary functions:

- autonomous control of probe operations after separation from the orbiter and
- management of data transfer from the equipment subsystems and experiments to the probe transmitters for relay to the orbiter and finally to Earth.

To carry out these tasks, the CDMS used the specific Probe Onboard SoftWare, for which it also provided the necessary processing, storage and interface capabilities. To make this vital element of the probe single point failure-tolerant despite the fact that no telecommand access could be accomplished for operation or POSW changes after separation, a very safe multi-hot-redundancy scheme had been selected.

Two identical CDMUs executed their own POSW simultaneously, each one being able to run the entire mission independently. The two different telecommunication channels were each dedicated to one of the CDMUs. To avoid data loss in case of a temporary break in the telemetry link, the chain B telemetry was delayed by about 6 s. However, since only one of the two channels actually worked during the Huygens mission, this potential advantage has had absolutely no effect.

A set of probe parameters, called the Descent Data Broadcast, was distributed by the CDMUs to all payload instruments, so that they used the same reference parameters for sequence initiation and operation. It contained as information: probe time, spin rate, internal temperature, altitude, special-event flags and a 'Processor Valid' status flag reflecting the result of each CDMU's health check.

The Mission Timer Unit used to activate the probe at the end of the coast phase was also a mission critical device; it would surely have been stupid to lose a healthy mission just because it wasn't switched on. For this reason, three independent hot-redundant timer circuits, powered by independent batteries and followed by two hot-redundant command circuits were used; their correct (independent) loading with the exact predicted coast phase duration was verified prior to separation. The timers consumed about 300 mW during the 21 days of the coast phase and returned to standby mode after probe switch-on. Additional redundancy was achieved by incorporating two g-switches to turn on the probe in the event of atmospheric entry without the time signal from any of the timer boards; these purely mechanical devices would close when the deceleration reached 5.5-6.5 **g**.

To facilitate understanding of the accelerometer (see below) and g-switches operations, it might be useful to have a look at the following schematic representation of the probe's deceleration during the entry phase.

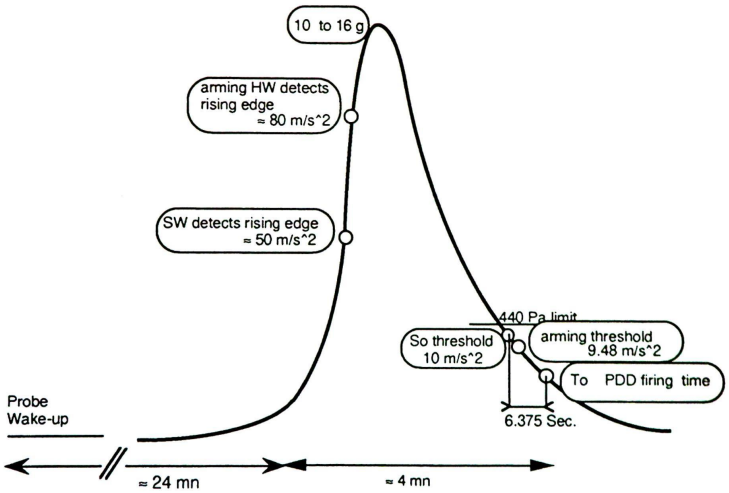

FIG.10: *Schematic overview of the expected deceleration of the Huygens probe during entry and related events.*

A triply redundant Central Acceleration Sensor Unit measured axial deceleration at the centre of the experiment platform during entry and descent. Its purpose was to detect the S_0 event defined as a 10 m/s^2 deceleration reached while coming down from the entry deceleration peak. The CASU operated within 0-10 **g** and used a scale factor of 0.512 $V/\mathbf{g}$. Two hot-redundant input power lines made it single point failure-tolerant. The three accelerometers were followed by a conditioning block with a low-pass filter of 2 Hz cut-off frequency to avoid aliasing. In this context, I forgot to mention that the basic data sampling rate for all telemetry operations was 8 Hz.

S_0 detection, triggering parachute deployment at T_0 and launching the processes controlling all subsequent operations, was made by majority voting of the 3 CASU units and backed up by two pairs of mechanical g-switches closing at 1.2 and 5.5 **g** in case the prime CASU system was inoperative.

A Radial Acceleration Sensor Unit composed of two radially oriented accelerometers was mounted at the periphery of the experiment platform. Its design was based on the CASU unit, including the same conditioning block with a 2 Hz cut-off frequency low-pass filter, but its range was adapted between 0 and 120 $m\mathbf{g}$ with a scale factor of 41.67 $V/\mathbf{g}$. The measured centrifugal acceleration output signal was processed by the CDMUs to compute the probe's spin rate, which was distributed to the experiments within the DDB.

The Radar Altimeter Unit used two proximity sensors, each consisting of separate electronics, transmitting and receiving antenna. Starting their altitude measurements 25 km above Titan's surface, each of the four antennas was a planar slot radiator array with a symmetrical full beam width of 7.9 deg. The chirp-like signal obtained by frequency-modulation of the carrier waves at 15.4 GHz and 15.8 GHz with a rising and falling ramp allowed accurate delay determination for altitude estimations and was also passed to the HASI instrument for further onboard processing to characterize Titan's surface roughness and topography.

The verification models and checkouts

For interplanetary missions such as Huygens, the absolute reliability factor takes even more importance than it already has for other space missions. Not only, the absolute impossibility of in-flight repairs, the seldom launch opportunities and the reduced launch windows impose tight schedules and a careful design, but the mission is also much longer and passes through different environments; moreover, usually no results are obtained during the first phase of the mission, so that an in-flight failure after a few years would lead to total loss of the mission.

The careful design and verification activities required four development models to be built.

A Structural, Thermal and Pyro Model was made to qualify the probe design for all structural, thermal and mechanical parts (including all mechanisms activated by pyrotechnic devices).

An Engineering Model was used to verify the electrical performance of the probe, including the payload instruments and the interfaces with the orbiter. This model has been upgraded with flight standard spare equipment for use as a test bed at the Huygens Probe Operations Centre in Darmstadt, Germany; as a matter of fact, the one-time occurrence nature of the Huygens mission called for special ground facilities for test and validation of any operation to be made on the onboard software and for simulation and diagnostic of different effects encountered during the mission. It was extensively used during characterization of the Huygens receiver anomaly (see hereunder).

A balloon drop test model, known as Special Model 2 (an SM1 model had been foreseen early in the program but was eventually not built), was dropped in the Earth's atmosphere for a validation of the complete descent sequence in the most realistic way achievable on Earth, with many flight standard items; we will come back to this test in more detail.

Finally, the Flight Model which has been launched only contains specifically built flight units, none of them having been used for instrumenting any of the test models. Flight spare units of all electrical subsystems and of all payload instruments had also been built to minimize delays in case of any unit failure.

Since after its launch, the probe system remained in a dormant state for seven years as the spacecraft was following its cruise trajectory, bi-annual health checks of the Huygens probe were scheduled during this phase. These in-flight checkouts lasted 3-4 hours and were designed to follow as closely as possible the pre-programmed descent scenario. Their purpose was to perform periodic instrument maintenance and regular payload sensor calibration. Additionally, the PSE alone was activated to perform in-flight end-to-end testing of the receiving elements of the Huygens telecommunication system, using the NASA Deep Space Network Antenna to mimic the probe radio transmissions. The power for the checkouts was pumped from Cassini through the umbilical link between probe and orbiter.

Some words about the Huygens receiver anomaly

We cannot close the subject of Huygens' engineering issues without at least evoking a major problem which was discovered during an in-flight end-to-end test of the Huygens telecommunication system, and the solution found, known as the "Huygens Mission Recovery Plan".

The Huygens receiver anomaly was discovered as a result of the first end-to-end relay test carried out in February 2000. The systems functioned as expected when receiving the RF

signal through the umbilical link, but unexpected behaviour was observed on both Huygens PSE receivers while receiving mission mimicking data from a ground station. In fact, a design fault in the data-transition-tracking-loop of the symbol synchronizer resulted in poor phase tracking and ultimately cycle slipping: the bit synchronizer had a bandwidth which was too narrow to accommodate the Doppler shift of the data stream frequency, due to the probe-orbiter relative motion. At a certain combination of the parameters frequency offset, signal to noise ratio and data transition density, cycle slips would have occurred, causing data corruption, onboard synchronization detection failures and ultimately decoding failures. In summary, this design fault, uncovered, would have resulted in nearly complete loss of the data during the Huygens mission.

To recover the full Huygens scientific return, engineers could play with the three parameters involved, which cause cycle slips in a deterministic way. The first two parameters depend on the relay link geometry, so a first consequence was to strongly adapt the mission profile, adopting a totally different scenario for the spacecraft's first Saturn orbits, Huygens' release and Cassini's orbit around Titan after release to listen to the probe during its descent (the orbiter passing further away than previously planned, so that relative velocity and thus frequency shift was reduced). The transmitting frequency could be slightly adapted by adjusting the temperature of the temperature controlled crystal oscillator: pre-heating the oscillator during 4 hours allowed this shift; the data stream was finally left unchanged. These changes in mission profile had also to be discussed with the Cassini team at the NASA, but it was really worth the investment since finally an acceptable mission recovery scenario was found, which obviously succeeded.

2 Contribution of the present work

2.1 The goal of the study

The aim of the present study is to analyze a part of the so-called "engineering" dataset, the science data being processed and analyzed by the respective Principal Investigator teams.

The purpose of my work was to provide the orientation of the Huygens probe during the descent phase under main and stabilizer parachute, as well as its final position on the surface. As a matter of fact, knowledge of this information is very important for the interpretation of some of the scientific data, especially those from DISR and HASI-PWA.

The design of the Huygens mission didn't include any attitude control: ensuring the stability of a passive descent was preferred to a complex avionics system coupled to propulsion devices. This allowed saving resources for science operations, but it also includes that no complete set of gyroscopes was built in to permit rapid and accurate probe motion reconstruction. As a consequence, the accurate reconstruction of the Huygens probe's motion during the mission is not a straightforward task.

Referring to the mission requirements for the engineering design of the Huygens probe, this work fits in the post-mission verification of the fifth point: ensuring a safe descent with spin, pendulum and coning motions compatible with RF link and experiments requirements. Let's have a closer look at those requirements.

Obviously, the scientists might be interested in the orientation of the probe while their measurements were performed in order to know exactly where they are looking, and in a certain stability to allow correct function of the experiments. But a control of Huygens' motions was also necessary for several other reasons.

From an operational point of view, many tasks of the DCSS could only be successfully carried out because a proper probe orientation had been foreseen. These included correct detection of special event times by the DCSS sensors, parachute firings and inflations and ejection of the front shield and some instruments' protecting covers (the windows for the DISR camera for example were covered during entry phase to avoid a contamination by disintegration residuals from the ablative front shield) without making them hit the probe.

The antennas should not be oriented too exotically with respect to a normal, vertical state to allow a reasonable telecommunication link to Cassini. Knowing that the orbiter was already not so high above the horizon ($20 - 70$ *deg* during descent), even without any eclipsing, significant power losses could result from an exaggerated tilt since the antenna gain strongly decreases when the angle between communication direction and vertical would go beyond $60 - 70$ *deg*.

A last element needing probe orientation control was the DISR imager. Here, sufficient stability was needed to allow taking sharp images, but a purely static probe would have taken all the images in the same direction, so that a minimal spin had to be guaranteed in order to look around, providing whole panoramic views of the surrounding. As a result, the spin rate had to be maintained between 1 and 15 *rpm*; that was the role of the spin vanes mounted on the fore-dome of the descent module.

We evidently are not the only team working in this field and the present work is continuously being discussed with other Huygens attitude reconstruction working teams. The

principal concerned actors met at ESTEC for this reason shortly before the conclusion of my work, on April 22 & 23, 2005. This work will be part of the desired probe orientation information given to the scientists, allowing them to better interpret the scientific data.

2.2 Available information for attitude reconstruction

Different types of information may be used to gain insight into the probe's orientation and motions during the descent phase.

2.2.1 Data from scientific instruments

Very accurate and directly usable data have been acquired by specific sensors on three instruments.

- Two perpendicular inclinometers on SSP were meant to measure the probe's tilt on the surface; they were already switched on during descent where they provided the same information.

- A sun sensor was used on DISR to evaluate the spin rate of the probe for proper imaging synchronization: a "sun lock" signal was sent every time the sun crossed a detection slit close to the imager. This information could be gathered as soon as the DISR cover had been ejected and until the atmosphere became too dense to detect the sun's direction in a sufficiently certain way. The 8 Hz sampling rate of the sun sensor lock signal implies a good accuracy on the spin period and directly provides an absolute azimuth at discrete steps (in fact, telling when a particular azimuth was crossed) so that the accumulating error on azimuth which would result from a continuous spin integration can be avoided. The down-looking visual spectrometer might also provide some information about the sun's position.

- The HASI instrument comprised an acceleration sensor package, which was much more high performance than the basic engineering accelerometers. It consisted of one highly sensitive vertical axis servo-accelerometer and three orthogonal piezo-resistive accelerometers for three-axis measurements.

  The servo-accelerometer was mounted exactly at the probe's centre of mass; it sensed the displacement of a seismic mass and drove it back to a null position, the required current being a direct measurement of the acceleration. The range of the two output channels of its amplifier could be switched between high and low resolution; their respective resolution was 1 or 10 $\mu\mathbf{g}$, while the absolute sensor accuracy in high resolution, high gain attained $\pm$ 35 $\mu\mathbf{g}$.

  The piezo-accelerometers consisted of a suspended seismic mass supported by a cantilever whose displacement was determined by two strain-dependent resistances; using them in a Wheatstone bridge, a resolution of 0.1 $\mathbf{g}$ and an accuracy of $\pm$ 0.4 $\mathbf{g}$ were obtained.

These sensors have not been provided by the ESA project but by the scientific instruments' teams; these teams will analyze the data from their respective instruments while we examine the engineering sensors to provide complementary results, allowing useful verifications.

2.2.2 The SM2 test flight

More than 2 years before the launch of the Cassini-Huygens mission, on May 14, 1995, a model of the Huygens probe called "Special Model 2" was test-dropped in the Earth's atmosphere to verify the behaviour of the probe under realistic, dynamic conditions. This test took place at the ESRANGE balloon launch site of Kiruna (Sweden) and was a collaboration between the ESA and its industrial partners Aerospatiale, Fokker Space and Martin-Baker.

The primary objective of this test flight was to demonstrate the proper function of the DCSS sequence under dynamic conditions as close as possible to those encountered at Titan. The successive steps to be verified included

- ejection of the back cover pulling out the main chute;
- deployment, inflation and structural strength and stability of the main chute;
- front shield release without making it touch the probe after separation;
- main chute release followed by stabilizer chute deployment and inflation;
- structural strength and stability of the stabilizer chute;
- decoupling of the probe's spin motions with respect to the parachute during the whole descent through correct swivel operation.

At the end of this sequence, a recovery chute was added to the SM2 to avoid probe damage caused by a simple crash on Earth; indeed, the probe was to be examined for scratches, impacts and other damages resulting from in-flight operations.

Secondary objectives of this test were

- to gain further insight into the (aero-)dynamic behaviour of the probe-parachute system, in particular the spin vanes, during subsonic flight. Correlations with predictions, wind tunnel tests and additional helicopter drops of small-scale models have been analyzed and will be briefly discussed when presenting the test flight's results and conclusions;
- to provide behaviour patterns and parameters with a test model fully instrumented to determine the probe's dynamic behaviour. This would facilitate the complex study of the probe's orientation from an incomplete dataset for the Huygens mission at Titan.

A flight standard philosophy was used to build the SM2 specimen: the full inner and outer structure, all separation subsystems and the DCSS including parachutes, mechanisms (swivel and pyro devices) and command subsystems were exactly matching (current) flight standard elements. At the command level, full onboard descent control was achieved, ground contact being reduced to ascent phase control and telemetry recovery.

On the top platform, the antennas mounted beside the parachutes were slightly adapted for the needs of the test. Test-specific batteries, sensors and electrical systems also replaced the instruments on the experiment platform; additional mass was added at different places to reach flight standard mass ($\approx 300\ kg$) and mass balance despite these changes.

The whole probe was suspended under a gondola for a balloon raise to an altitude of 37.4 km. There, it was dropped without any initial velocity and spin movement, to fall

down to Earth in about 15 minutes (less than 10 minutes useful flight before recovery chute deployment) following its own predefined flight sequence as for the actual Huygens mission.

FIG.11: *The SM2 test probe attached under the raising gondola before its balloon launch.*

Unlike that case, data was not only sent to heaven on a RF S-band uplink (here recovered by the gondola which directly sent them back to Earth on an L-band downlink), but also directly sent to the ground station via an S-band downlink and recorded on board, all systems backing up the same information. The achieved 38400 bit/s data stream, powered with 2 W only, was more than two times higher than on Huygens (due to the enormously reduced distance of course).

The measurements made by SM2 included

- altitude and horizontal position through dual GPS tracking;
- acceleration and velocities through the dual GPS system and a 3-axes accelerometer set;
- roll, yaw and pitch rates through the accelerometers and a 3-axes gyroscope system;
- temperature and pressure;
- visual images (video camera) to monitor the separation events;
- internal health and housekeeping data as a switch monitor, an analogue voltage monitor and the DCSS event timing.

All kinematic data, as well as the video extracts (see 7.3), can help to gain information about the probe's dynamic behaviour. The properties of the corresponding instruments are summarized in the following table.

	Range	Resolution	Sampling rate
X accelerometer	$\pm$ 7.5 **g**	0.41 m/s^2	200 Hz
Y,Z accelerometers	$\pm$ 5 **g**	0.31 m/s^2	200 Hz
High range roll gyro	$\pm$ 240 deg/s	1.9 deg/s	40 Hz
High range pitch/yaw gyros	$\pm$ 600 deg/s	4.7 deg/s	40 Hz
Low range pitch/yaw gyros	$\pm$ 60 deg/s	0.47 deg/s	40 Hz
GPS Velocity	-	1 m/s	1 Hz

Notice the very high frequency at which the measurements were carried out; this also provides additional information on probe motions compared with the Huygens mission, though the 200 Hz signal of the accelerometers is already characterizing vibration modes.

A direct comparison between the SM2 test flight and the actual Huygens mission requires the characterization and, if possible, subtraction of environment-difference-related effects. In fact, the conditions in Earth and Titan atmospheres are somewhat different (mainly temperature and gravity) and the relatively low launch, and resulting lower velocity, of SM2 gives additional differences; this led to some discussions before launch, based on adimensional parameters, on the most representative test scenario achievable with reasonable resources.

At PDD initiation, the Titan mission navigated at $Mach$ 1.46-1.47 and a dynamic pressure of 315-317 Pa. To obtain supersonic velocities with a probe drop in the Earth's atmosphere, a minimal altitude of 60 km is necessary. This was impossible using a simple balloon ascent; an additional rocket firing could have been considered, as had been done for Viking tests to reach $Mach$ 1.2 at parachute deployment, but was finally rejected for operational needs. The same argument refuted the possibility of additional, jettisonable ballast used to reach a higher descent limit speed or a drag coefficient variation, although these techniques would anyway have led to higher dynamic pressure so that both parameters could not match the Titan case; indeed, as dynamic pressure and Mach number are both related to the speed[7] and to parameters which are fixed by the planet's atmosphere, they cannot be independently fixed. Finally, $Mach$ 0.9 and a matching dynamic pressure (340 Pa) was accepted as a trade-off.

At Front shield release, the Huygens probe above Titan was expected to experience $Mach$ 0.4 and a dynamic pressure of 34 Pa. The main problem was to reach such low dynamic pressure in the Earth's larger gravitational field[8]. To reduce the ballistic coefficient $\frac{m}{C_D A}$, either other parachutes had to be used or a very light probe after a mass ejection had to be implemented. The first solution was rejected because of the flight standard philosophy of the test and the second because the implementation would have been too difficult; as a conclusion, a higher dynamic pressure with Titan-case $Mach$ was accepted.

Considering other similarity indicators, using Titan atmospheric properties

- surface pressure = 1.5 bar
- temperature decreasing from 94 K at the surface to 70 K at 40 km, then increasing again to 200 K at 200 km
- mean molar mass of $\simeq$ 28 g roughly equal to the Earth's atmosphere's one

[7] $Q_dyn = \frac{1}{2}\rho v^2$ and $Mach = v/v_{sound}$.

[8] Titan's gravity acceleration at the surface is 1.354 m/s^2, seven times lower than the Earth's 9.81 m/s^2 attraction.

and the fact that $\mathbf{g}_{Titan} \approx \frac{1}{7}\mathbf{g}_{Earth}$, we can compute a scale factor of about 20 km for Titan's atmospheric characteristics (to be compared with 8-9 km for the Earth). As pressure is higher and temperature lower on Titan's surface, the density is higher (by a factor of 5 assuming perfect gas behaviour), which explains the large aerodynamic deceleration (the scale factor being larger, this density difference initially even increases with altitude) of the probe. The velocity of sound in Titan's atmosphere, computed using $v_s = \sqrt{\frac{\gamma RT}{\bar{M}_{molar}}}$ where $\gamma = 1.4$, R and $\bar{M}_{molar}$ are identical for both celestial bodies, varies from 200 m/s near the surface to 260 m/s at the hotter high altitude of 160 km where the main chute deployment was initiated; for the SM2 test, totally carried out at lower altitudes, less variation from the 330 m/s at Earth surface to 300 m/s at the cold tropopause was experienced.

As a third parameter, the Reynolds number $Re = \frac{vL\rho}{\mu}$, considered using the probe's diameter as the characteristic length, indicates a highly turbulent regime of $Re \sim 10^6$ for the SM2 test. Since L does not vary (flight standard probe model), the speeds are approximately equal (slightly lower $Mach$ number on Earth for slightly higher sound velocity) and the atmosphere's constitutions too, significant differences on Re for the actual mission could only arise from density and viscosity dependence on atmospheric pressure and temperature. Since for gases, μ has nearly no dependence on pressure and varies as the square root of the temperature, we obtain using the perfect gas state equation

$$Re_{Titan} \approx \frac{(P/T^{3/2})_{Earth}}{(P/T^{3/2})_{Titan}} Re_{Earth} \approx \frac{1.5}{\left(\frac{100K}{270K}\right)^{3/2}} Re_{Earth} > Re_{Earth}$$

so that we were still in highly turbulent regime, quite similar to the SM2 test. However, the Reynolds number is important for parachute characterization, as it changes the cloth's porosity and thus the aerodynamic coefficient of the chutes. This effect had no influence on the SM2 test results, whose goals could easily be achieved with flight standard chutes. In fact, the proper characterization of the probe's parachutes had already been done, using different Reynolds numbers to carry out an extrapolation to Titan case; precise parachute knowledge was required for accurate modelization of the descent schedule.

The following table summarizes the comparison between the SM2 and Huygens flight conditions.

		SM2 (Earth)	**Huygens (Titan)**
	Mean gravity	9.81 m/s^2	1.354 m/s^2
Atmospheric properties	**Temperature**	$\sim$ 270 K	70-200 K
	Surface pressure	1 bar	1.5 bar
	Typical $\mathbf{v_{sound}}$	330 m/s	200 m/s
	Typical scale factor	8-9 km	20 km
Flight properties	**Typical Re**	$\sim 10^6$	$\sim 10^7$
PDD init. \ Fr.shield rel.	**$\mathbf{Q_{dyn}}$**	340 \ 90 Pa	316 \ 34 Pa
PDD init. \ Fr.shield rel.	**Mach**	0.9 \ 0.4	1.465 \ 0.4

Results and/or data analysis of the SM2 test flight will be presented in regard with the specific motion studies throughout this work. Let's just unveil that the descent sequence and separation operations successfully worked (some minor improvements, like better fixing some

structural elements that had been torn off, had to be made), the spin vanes obviously worked less efficiently (but without any valuable reason to be found) so that their angle of attack was increased from 2.2 *deg* to 3 *deg* for the Huygens mission and an unsatisfactory stability was observed under the single gap stabilizer chute, which could partially be imparted to windy conditions after additional helicopter drop tests but nonetheless led to the use of a much stabler double gap not only for the main chute but also for the stabilizer of the Huygens mission.

As complete data analysis, including an attitude reconstruction based on the full gyroscope set, has been carried out by industry to provide test reports, we will focus on

- likely probe motions which could be inferred for Huygens from comparison with SM2;
- correlations between gyroscope and accelerometer measurements to see how accelerometer measurements on Huygens could be related to attitude issues as would be seen by gyroscopes.

The interested reader should have a look at references [5], [14] and [15] for more details on SM2.

2.2.3 Data from engineering sensors on the probe

The acceleration sensor units in the probe's onboard engineering and command units seem to be the most straightforward information source about its motions.

As the RASU was specifically dedicated to spin deduction, there was a certain hope that the azimuthal behaviour of the probe would be directly known with enough accuracy. Since the probe's other motions and vibrations were obviously superimposed on the centrifugal force signal, averaging was necessary for this purpose. Unfortunately, no negative value quantification was foreseen so that when, for low spin and strong perturbations by other movements, the acceleration on RASU was actually negative, the output telemetry blindly indicated 0. This led to a non-negligible error on the averaged centrifugal force estimation and hence on the spin evaluation obtained. Moreover, several more accurate data sources even provide absolute azimuth, allowing a much better reconstruction of the probe's orientation, so that the onboard spin deduction from RASU found in the DDB really has to be regarded as a coarse approximation, and even the conclusions obtained from post-mission analysis of the direct RASU accelerometer signal can easily be surpassed.

But as RASU was a fully operational one-directional accelerometer, very useful information about the "perturbing motions" can be obtained after subtraction of the accurately known spin-induced centrifugal acceleration signal. The design and range of RASU have been given while describing the engineering design of the Huygens probe (see 1.3.3). We just have to add that the RASU signal received on Earth comprises only one of the two accelerometer data, for which samples are present at a 4 Hz frequency, the Nyquist limit frequency for aliasing avoidance of 2 Hz lying just on the analog low-pass filter's cut-off frequency. The quantification steps of 0.005 **g** provided a reasonable accuracy.

The CASU was actually not mounted exactly on the probe's centre of mass, which was occupied by HASI's high-precision servo-accelerometer, but directly next to it. Primarily designed for entry deceleration detection, it naturally kept on measuring the acceleration along the vertical axis during the whole descent. As a result, probe attitude movements as

pendulum or coning motions may be seen on its signal when the deceleration component was not too dominant and can be efficiently subtracted (accurate trajectory information obtained from post-mission data processing should provide a satisfactory estimation of the probe-parachute system's deceleration). The frequency of periodic variations on the deceleration signal could also give hints about some periodic behaviour.

Unfortunately, the CASU signal sent to Earth was undersampled at 1 Hz without any prior treatment after having passed the 2 Hz analog filter, leading to frequency spectrum pollution by aliasing; for this reason, correlations with other data sources will be necessary to identify the correct movement periods.

As can be seen from CASU's description in the previous section, the inherent resolution of the three sensors, which have all been operative and transmitted, is relatively low. But an accurate evaluation of the average acceleration can be obtained when the signal is sufficiently varying - Appendix A contains an example showing how this works. This was the case during the whole descent, thanks to noise and motion influences that do not result in constant vertical axis acceleration. Just on the surface, the steady probe did not allow us to get a more accurate resolution than CASU's 0.04 **g** quantification steps.

As accelerometer units operating in probe-related reference frame were present on both the SM2 and the Huygens flight model, it seems unavoidable for a proper evaluation of the data to calculate what such accelerometers are actually exactly measuring, *i.e.* which motions have which (primary or secondary) effects on different, occasionally uncentred, accelerometers.

To do this, let's first introduce the probe's reference frames in accordance with the following *figure 12* (left part). In the official probe reference frame, $\mathbf{X_P}$ points to heaven along the vertical axis, $\mathbf{Z_P}$ indicates DISR camera direction in the probe's horizontal reference plane and $\mathbf{Y_P}$ completes the trihedron. To simplify the notations, let's introduce another reference frame when considering the accelerometers: vector $\mathbf{e}_x$ vertically points to heaven, vector $\mathbf{e}_y$ radially points from the probe's centre of mass towards the measuring accelerometer and vector $\mathbf{e}_z$ completes the trihedron.

After this, we have to decide how to describe the probe's orientation. As pendulum motions seem to be a basic component of the probe's movement under parachute, the use of the angles θ and ϕ, respectively measuring the angle between $\mathbf{e}_x$ and the vertical direction and the orientation of the plane containing the vertical axis and $\mathbf{e}_x$ with respect to a fixed horizontal direction, seems to be natural; allowing a 360 deg variation for both angles leads to multiple (actually exactly 2 using the intuitive sign convention) possibilities to define a particular position of the probe, but the continuity of ϕ and θ is needed to permit easy description of pendulum and coning motions. As a third variable, I've chosen - for the present accelerometer study - to define the azimuth of $\mathbf{e}_y$ as the angle ψ between $\mathbf{e}_y$ and the same horizontal reference direction as before, if the probe was not tilted; indeed, tilting the probe changes the azimuth of probe-related directions with respect to ground coordinates and the present choice for accelerometer analysis allows to skip these corrections.

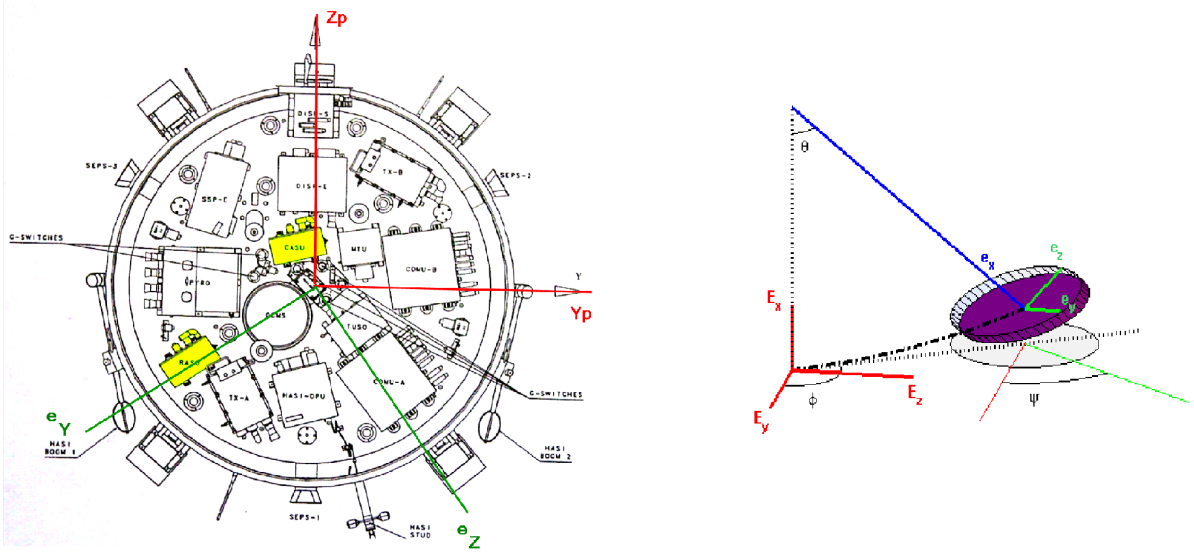

FIG.12: *Left part: definition of the probe axes. Right part: the angles used to characterize the probe's orientation.*

After a few geometrical observations using an intermediary reference frame, the relation between the vectors relative to the ground coordinate system and those attached to the probe may be expressed as

$$\begin{aligned}
\mathbf{e}_x &= \cos(\theta)\mathbf{E}_x - \sin(\theta)\cos(\phi)\mathbf{E}_y - \sin(\theta)\sin(\phi)\mathbf{E}_z \\
\mathbf{e}_y &= \cos(\psi-\phi)[\sin(\theta)\mathbf{E}_x + \cos(\theta)\cos(\phi)\mathbf{E}_y + \cos(\theta)\sin(\phi)\mathbf{E}_z] \\
&+ \sin(\psi-\phi)[-\sin(\phi)\mathbf{E}_y + \cos(\phi)\mathbf{E}_z] \\
\mathbf{e}_z &= -\sin(\psi-\phi)[\sin(\theta)\mathbf{E}_x + \cos(\theta)\cos(\phi)\mathbf{E}_y + \cos(\theta)\sin(\phi)\mathbf{E}_z] \\
&+ \cos(\psi-\phi)[-\sin(\phi)\mathbf{E}_y + \cos(\phi)\mathbf{E}_z]
\end{aligned}$$

or inversely

$$\begin{aligned}
\mathbf{E}_x &= \cos(\theta)\mathbf{e}_x + \sin(\theta)\cos(\psi-\phi)\mathbf{e}_y - \sin(\theta)\sin(\psi-\phi)\mathbf{e}_z \\
\mathbf{E}_y &= -\sin(\theta)\cos(\phi)\mathbf{e}_x + [\cos(\theta)\cos(\phi)\cos(\psi-\phi) - \sin(\phi)\sin(\psi-\phi)]\mathbf{e}_y \\
&+ [-\cos(\theta)\cos(\phi)\sin(\psi-\phi) - \sin(\phi)\cos(\psi-\phi)]\mathbf{e}_z \\
\mathbf{E}_z &= -\sin(\theta)\sin(\phi)\mathbf{e}_x + [\cos(\theta)\sin(\phi)\cos(\psi-\phi) + \cos(\phi)\sin(\psi-\phi)]\mathbf{e}_y \\
&+ [-\cos(\theta)\sin(\phi)\sin(\psi-\phi) + \cos(\phi)\cos(\psi-\phi)]\mathbf{e}_z \ .
\end{aligned}$$

Let's now examine what accelerometers which are attached on the probe's body would measure. This is equivalent (except for the straightforwardly added influence of gravity) to computing the acceleration of the probe's reference frame with respect to absolute space and to express it in probe reference frame. We designate the length of the cable leading to

pendulum movements by l - describing the motion of its attach point by $\ddot{x}$, $\ddot{y}$ and $\ddot{z}$ - and the distance from probe centre of mass to the accelerometer by r. After tedious but trivial derivation and algebraic work, we get the following expressions for onboard accelerometer measurements on the probe.

$$
\begin{aligned}
\mathbf{Acc}\cdot\mathbf{e}_x &= \{\cos(\theta)\ddot{x} - \sin(\theta)\cos(\phi)\ddot{y} - \sin(\theta)\sin(\phi)\ddot{z} \\
&+ l[\dot{\theta}^2 + \sin^2(\theta)\dot{\phi}^2] \\
&+ r[\cos(\psi-\phi)\ddot{\theta} + \cos(\psi-\phi)\sin(\theta)\cos(\theta)\dot{\phi}^2 + \sin(\psi-\phi)\sin(\theta)\ddot{\phi} \\
&\quad -2\sin(\psi-\phi)\dot{\theta}(\dot{\psi}-\dot{\phi}) + 2\cos(\psi-\phi)\sin(\theta)\dot{\phi}(\dot{\psi}-\dot{\phi})]\} \\
\mathbf{Acc}\cdot\mathbf{e}_y &= \{\sin(\theta)\cos(\psi-\phi)\ddot{x} + (\cos(\theta)\cos(\phi)\cos(\psi-\phi) - \sin(\phi)\sin(\psi-\phi))\,\ddot{y} \\
&+ (\cos(\theta)\sin(\phi)\cos(\psi-\phi) + \cos(\phi)\sin(\psi-\phi))\,\ddot{z} \\
&+ l[\cos(\psi-\phi)\ddot{\theta} - \cos(\psi-\phi)\sin(\theta)\cos(\theta)\dot{\phi}^2 + \sin(\psi-\phi)\sin(\theta)\ddot{\phi} \\
&\quad +2\sin(\psi-\phi)\cos(\theta)\dot{\phi}\dot{\theta}] \\
&- r[\Big(\cos(\psi-\phi)\dot{\theta} + \sin(\psi-\phi)\sin(\theta)\dot{\phi}\Big)^2 + \Big((\dot{\psi}-\dot{\phi}) + \cos(\theta)\dot{\phi}\Big)^2]\} \\
\mathbf{Acc}\cdot\mathbf{e}_z &= \{-\sin(\theta)\sin(\psi-\phi)\ddot{x} - (\cos(\theta)\cos(\phi)\sin(\psi-\phi) + \sin(\phi)\cos(\psi-\phi))\,\ddot{y} \\
&\quad + (-\cos(\theta)\sin(\phi)\sin(\psi-\phi) + \cos(\phi)\cos(\psi-\phi))\,\ddot{z} \\
&+ l[-\sin(\psi-\phi)\ddot{\theta} + \sin(\psi-\phi)\sin(\theta)\cos(\theta)\dot{\phi}^2 + \cos(\psi-\phi)\sin(\theta)\ddot{\phi} \\
&\quad +2\cos(\psi-\phi)\cos(\theta)\dot{\theta}\dot{\phi}] \\
&+ r[\sin(\psi-\phi)\cos(\psi-\phi)\dot{\theta}^2 + (\ddot{\psi}-\ddot{\phi}) - \sin(\psi-\phi)\cos(\psi-\phi)\sin^2(\theta)\dot{\phi}^2 \\
&\quad + \cos(\theta)\ddot{\phi} - 2\cos^2(\psi-\phi)\sin(\theta)\dot{\theta}\dot{\phi}]\}
\end{aligned}
$$

This shows that actually, lots of effects are superimposed in the data of the accelerometers' outputs, whatever primary measurement purpose was envisaged. Analysis of these relations will be presented in regard with the concerned issues in the continuation of this work. Just notice that Titan's gravity can be accounted for by including an extra gravity acceleration term in addition to the attachment points' motion in $\ddot{x}$.

2.2.4 Indirect methods

Maybe the most useful information, though also the most economically obtained, comes from the analysis of signals which by no means were intended to be envisaged in the way of attitude reconstruction.

A first telemetry parameters, which was still quite related to probe motions but could just potentially be used as an additional parameter to validate some strange behaviour, is the altimeter lock/unlock signal. This signal indicated if the probe's Radar Altimeter Unit succeeded in deducing useful altitude measurements, thus permitting to know whether we had a stable probe orientation, not too far from vertical, or not. This engineering signal required a very thin place in the data stream, but also did not provide much information on the probe's motions.

The possibilities of the second indirect parameter, concerning the radio link, are much more interesting. As already mentioned, the antennas' gain patterns quite strongly depended

on azimuth (1-4 dB), not only on elevation. It was a very nice surprise that this azimuthal gain variation pattern was clearly recognizable on the AGC signal while the probe was spinning around during its descent. In fact, the 8 Hz sampling rate of the AGC signal makes it the most accurate data we have for attitude reconstruction. Since a direct relation exists between the position of the orbiter in the antenna-related reference frame and the antenna gain, part of the probe's orientation might be directly deduced from the transmitted B-channel signal. As this relation can not be reversed, sufficiently strong assumptions inferred from other considerations should be made on hypothetic motions.

In addition, trajectory information about the Huygens probe and the Cassini orbiter was used to subtract trajectory-related effects from the other data, in order to investigate the other motions more accurately. This was the case for example for probe deceleration on the CASU measurement and Probe Aspect Angle for the analysis of the AGC variations. As these results come from other working groups within the Huygens team, the way of obtaining them will not be discussed anymore after this brief summary.

As for inferring the attitude, observations which were not foreseen during the probe's development were added for a better accuracy on the reconstruction of the probe trajectory. These included

- Position tracking and attitude reconstruction of the orbiter between Huygens release and trajectory deflection: as the post-separation trajectory mainly depended on the separation dynamics experienced during the very short separation process, its knowledge could be improved by continuing to observe the orbiter for some time after the separation process (this is a routine check which had been foreseen since the beginning);
- Magnetometer observation of the Huygens probe by Cassini (to infer the spin rate);
- Probe imaging by the Cassini orbiter a few days after separation: offering the possibility to determine relative separation errors by using optical navigation techniques;
- Ground-based tracking of the Huygens Probe during its descent: the faint radio signal of the probe being received using radio tracking stations on Earth, the recording could be used to determine the Doppler shift of the signal and hence infer the velocity of the probe in the direction of Earth. This information was also meant to complement the one obtained by the DWE in the probe-to-orbiter direction to determine wind speeds in Titan's atmosphere;
- Direct detection of the Huygens radio signal by VLBI: the feasibility of Very Long Baseline Interferometry observations of the Huygens probe radio signal using a telescope network on Earth implies a sub-kilometric probe localisation at a few seconds time resolution during the whole descent. Work is ongoing at the time of writing.

Part II
First evaluation of the CASU & RASU accelerometer and the SM2 accelerometer and gyroscope data

Before going on to the detailed analysis, we want to present the data from the Huygens accelerometers, which would at first sight seem to be the dedicated instruments for the characterization of the probe's movements and orientation, as well as the SM2 gyroscope and accelerometer data, to point out some features related to their analysis.

3 Presentation of the time signals and event localization

First of all, let's have a look at the time signals provided by the vertical accelerometers. By using the plural, we mean that we will consider both the actual Huygens mission and the SM2 drop test. In fact, the three accelerometers of the CASU sensor indicated very close values: they were designed for nothing else than hot-redundant backup; furthermore, the guaranteed precision on their calibration, position and orientation, associated with their reduced resolution, makes the deduction of useful information by fine detail difference analysis on those three signals impossible, so that we will always consider only one CASU signal.

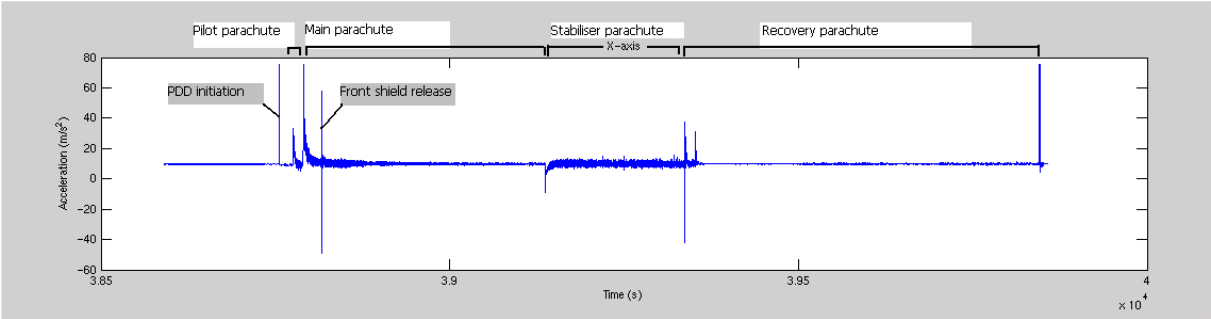

FIG.13: *Vertical axis accelerometer signal for the SM2 test flight.*

Looking first at the SM2 signal, we can clearly identify the different special events, which lead to enormous peaks followed by progressive stabilization of the probe's movements; we successively encounter

- Mortar firing at PDD initiation (shock on the probe)
- Pilot parachute deployment (deceleration
- Back cover jettison and main parachute deployment (shock + deceleration)
- Front shield release (shock on the probe)

- Main parachute jettison and stabilizer parachute deployment (acceleration w.r.t. main chute)

- Stabilizer jettison and recovery parachute deployment in two phases (shock + 2 successive decelerations)

- Impact on the ground (deceleration shock).

Between these events, an idea of the probe's stability can be obtained by examining the amplitude of the accelerometer signal oscillations. We see that from a very smooth free fall, the probe is perturbed by the parachute's deployments more than by firing shocks. The slower the probe's descent velocity, the more the oscillations resulting from this instability were damped: while an acceptable and a strong damping leading to good stability were observed under main and recovery chute respectively, the probe's oscillations were not damped at all under stabilizer chute. It was first feared that an oscillation mode coupling parachute and probe motions could be responsible for this last movement, resulting in dangerous oscillations which didn't meet mission specifications; but after additional wind tunnel tests, helicopter drop tests of similar systems and a detailed wind analysis for the day of the SM2 test flight, it was concluded that the large, undamped oscillations were induced by strong wind gusts and vertical wind gradients present on that day and which could not be encountered on Titan.

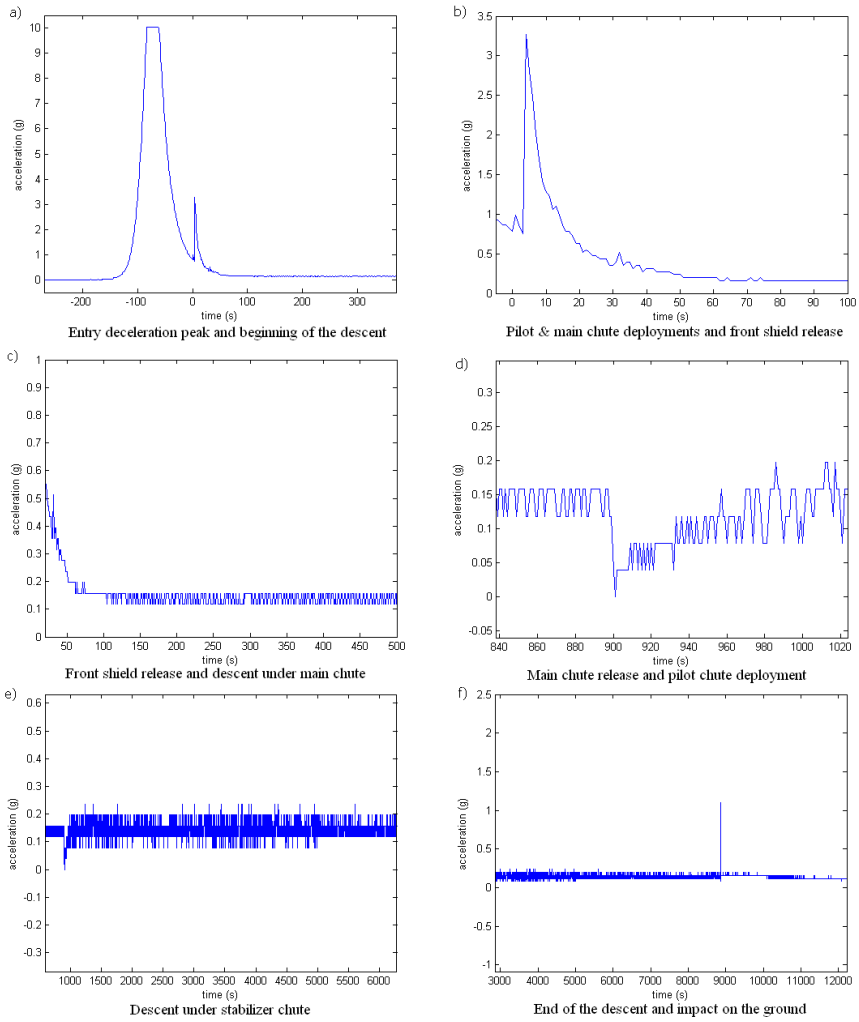

FIG.14: *Some views of the time signal of the CASU A-accelerometer for the Huygens mission flight.*

The longer CASU signal for the actual Huygens mission has to be split into many plots to allow proper visualization. Notice the different scales of the successive figures; time is related to T_0.

On picture *a*), you can recognize the entry deceleration pattern; the peak is not wholly drawn because the accelerometer saturated at 10 **g**. Detection of the S_0 event took place when the deceleration curve crossed the horizontal line at 10 $m/s^2 \approx 1$ **g** (by majority voting of the three accelerometers to be precise). After this, the PDD mortars were fired at $T_0 = S_0$+6.375 s and the parachutes successively deployed. You cannot see the shock of the firing on the accelerometer, which is probably due to its 0.5 Hz time resolution[9]; remember that the peak was very narrow on SM2, which sampled at 200 Hz. The large peak on the right is due to main chute inflation, starting the descent phase under main chute.

Picture *b*) is a zoom on the initial phase of the main chute descent. It shows a first small bump before the main chute inflation peak, corresponding to the deployment of the pilot chute, and a second one about 30 seconds after main chute deployment, due to the front

[9]This shock has apparently been detected by the HASI accelerometer dataset.

shield release. We can notice that the perturbation caused by this last event seems to be smaller (however, remember the reduced sampling rate so that the shock itself is probably skipped) than on the SM2 test flight; this is certainly related to the reduced dynamic pressure of the Huygens mission case with respect to the test flight at this event (see SM2/Huygens mission comparison in 2.2.2).

Looking at this picture and the picture *c*), damping of the oscillations seems to be quite rapid, leading to a very stable probe: after about 60 s, the oscillations of the accelerometer signal remain at the limit of its resolution, switching between 0.12 and 0.16 **g** (remembering Titan's gravity of 0.138 **g**, this could correspond to very tiny oscillations since the average value $\mathbf{g}_{Titan} + Deceleration \approx 0.14\mathbf{g}$ under main chute is very close to the quantification limit). This 0.04 **g** very maximal oscillation is much less than the about 0.5 **g** amplitude oscillation which lasted at least 100 seconds on SM2. Even when stabilized, a 0.1 **g** oscillation remained for the test flight; as predicted, the descent through Titan's atmosphere was much smoother than on Earth, the SM2 test validation thus being really very strict.

Picture *d*) shows the main chute jettison/stabilizer chute deployment event. The deceleration shortly drops down to a zero minimum, indicating a (very) short period of free fall, the probe accelerating to the new limit velocity corresponding to the smaller parachute.

As for the test flight, the probe was much less stable during the stabilizer phase, though the parachute was upgraded to double gap to ensure acceptable limits for oscillations. As can be seen on the last pictures (*e*) and *f*)), the extreme accelerometer values are 0.08 to 0.24 **g** during the first half and 0.12 to 0.20 **g** during the second half of the descent; this should not be imparted to a discontinuity in the probe's behaviour: since we go down by one quantification step, it is much more probable that the oscillations were just slowly decreasing, the discontinuity simply arising when we crossed the quantification limit. The fact that this limit is crossed nearly together for both oscillation directions - *i.e.*, passing from 0.08 to 0.12 probably at 0.10 **g** and from 0.24 to 0.20 at 0.22 **g** - might be explained as an accidental appearance due to the particular shape of the signal and its offset at roughly $\mathbf{g}_{Titan} + Deceleration$.

The final peak indicates surface touchdown at $t = 8869.77030\ s$ after T_0 (this very accurate value was provided by another, specifically dedicated SSP sensor of course). The accelerometer did not saturate at all and shows a 1.1 **g** peak - which is quite inaccurate due to its short duration and the low sampling rate[10] - followed by a few damping oscillations. The positive value when the probe is stabilized on the surface corresponds to Titan's gravity (quantified); in fact, to justify the indicated value of 0.12 **g**, the analog value of the accelerometer measurement should lie between 0.1 **g** and 0.14 **g** which agree with Titan's gravity of 0.138 **g** and allow a tilt between 0 and 43 *deg*.

Remark: You maybe noticed that the value of CASU A stays too high during approximately 1000 s before decreasing to its final, acceptable (meaning lower than $\mathbf{g}_{Titan}$) value. In fact, acceleration and tilt sensors on other instruments also showed a decreasing tendency, while no evolution at all was observed by the imaging camera. As a consequence, those variations were attributed to temperature effects. RASU, which might be less sensitive to actual tilt variations because of its horizontal orientation and might experience other temperatures given its different location on the probe, stays frozen in agreement with the pictures, but the strange thing is that the two other CASU sensors did not experience such a measurement change either; it would be possible to explain this by slightly different

[10]The SSP touchdown sensor, sampling at 200 Hz, recorded the whole profile of the touchdown peak with a maximum at 15 **g**.

values if the evolution was less than one quantification step, but the tendency on CASU A clearly starts around 0.18 **g** (to reach the 0.20 **g** quantification step value), which is much too high according to Titan's 0.138 **g** gravity, before decreasing towards at least 0.14 **g**(to reach the 0.12 **g** quantification step value). In-flight checkouts before reaching Saturn showed some unexplained spiking on the CASU A sensor which led to less confidence in its results, but during the descent its behaviour was actually very close to the measurements of the other accelerometer outputs.

As a conclusion of this first analysis, we can already say that the low resolution in both acceleration and time of the CASU sensor strongly limits the possibilities for a more detailed analysis.

Making the same comparison to tell useful information about the other accelerometers is not so easy since they were different on Huygens and SM2: the RASU on Huygens was placed at the boarder of the probe and radially oriented, while the SM2 accelerometers were all three located at the same, uncentred place and the $Y-$ and $Z-$axes were both subject to radial and tangential forces (see *figure 15* below). To have a first idea of what might be seen on those signals, spectral analysis and cross-correlation investigations will have to be carried out. But let's first present the time signals that we are going to look at.

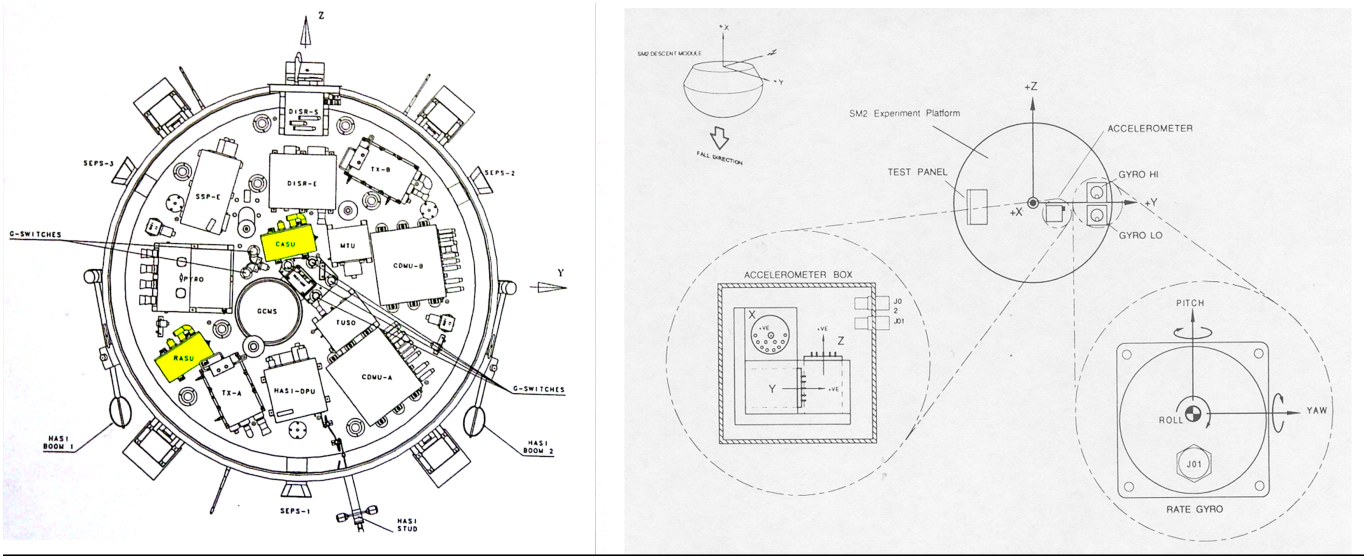

FIG.15: *Location and orientation of the accelerometers on Huygens (left part) and of the accelerometers and gyroscopes on SM2 (right part).*

The remaining accelerometers on SM2 both show the same events as the X-axis accelerometer, and nearly to the same extent (notice the similar acceleration scales); interpretation of the direction of the shocks is more difficult since their effect on horizontal accelerometers depends on structural propagations. It is not surprising to also observe the same oscillation amplitude variations along those axes, since the orientation perturbations will lead to tangential and centrifugal accelerations along all directions.

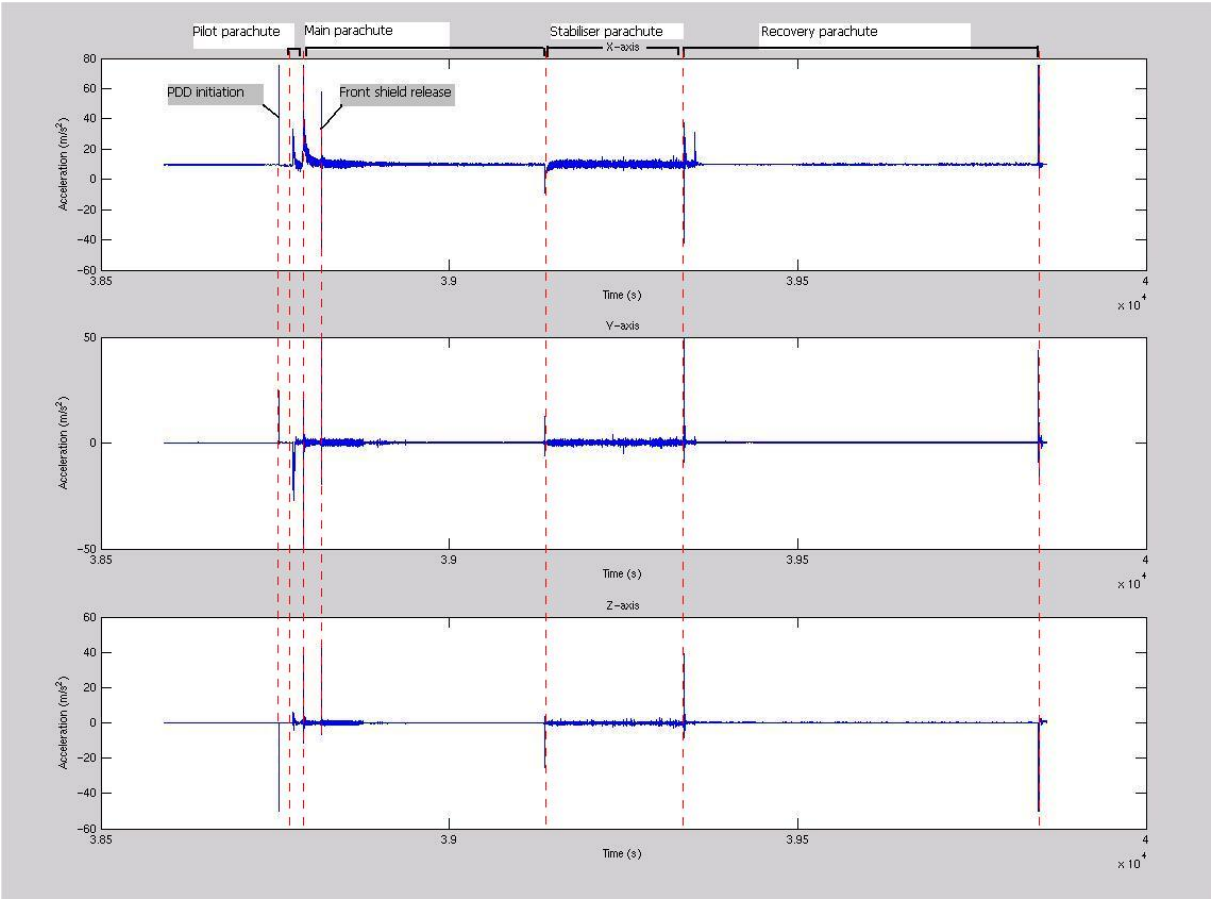

FIG.16: *The time signals of the three SM2 accelerometer sensors.*

Gyroscopes are much more interesting for orientation studies since they directly provide variations of specified angles; unlike the accelerometers, which could provide rotation speeds through centrifugal force measurements, they also indicate the direction of rotation. Reconstructing the attitude from a full gyroscope set should actually be straightforward, but unfortunately, we did not have any on Huygens. Looking at the gyroscope measurements of the SM2 test flight, we actually observe two different things.

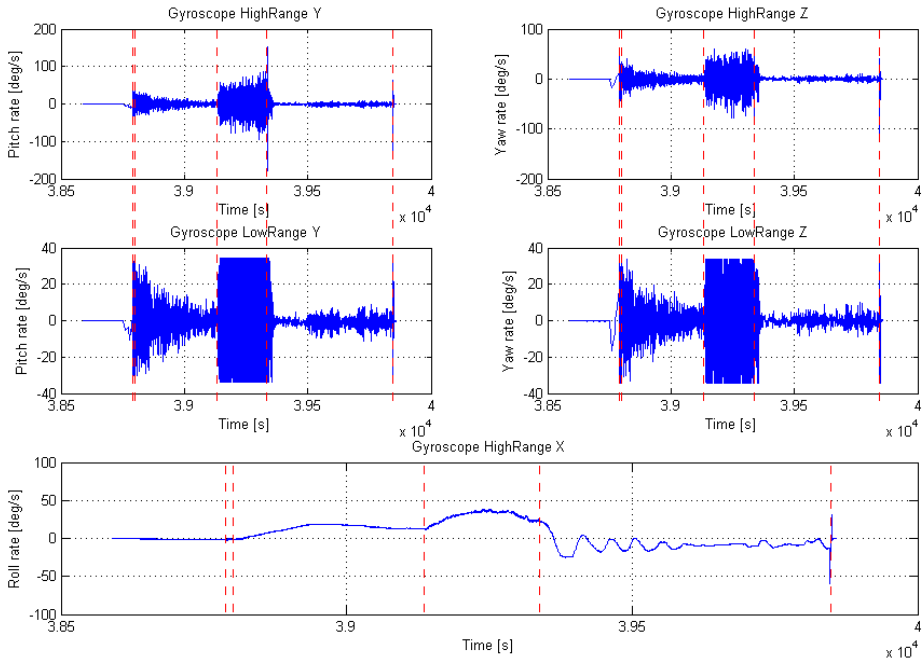

FIG.17: *The time signals of the SM2 gyroscope sensors.*

The X-axis gyroscope, oriented along the particular probe vertical direction, characterizes the spin movement on its own. We can see that through the whole descent under main and stabilizer chute, it was not much perturbed, evolving in a smooth way. In particular, it is not an alternating signal but always stays positive, meaning that the probe spun straightforwardly in the same direction, adjusting its spin rate to the intervening torques; this shows that the swivels and spin vanes properly worked to respectively allow/produce a constant spin of the probe. When the recovery chute was deployed, the spin begins to oscillate, showing that the probe alternately spun in one direction and the other. This agrees with the fact that no swivel was mounted on the recovery chute: the chute's big inertial behaviour held the top end of the suspension cable fixed, while the bottom end was spinning with the probe; the resulting oscillating spin movement is the same as that of any *mobile* suspended at a fixed point, the cable acting as a torsion spring. However, looking more carefully at this time signal, one can see that the oscillations are not around zero, but rather a negative value of $-8.5\ deg/s$. This seems to indicate that the parachute was indeed holding the top end of the suspension cable, but that it was moving itself at a roughly constant spin rate rather than being at rest. This is an interesting information, as it gives an idea of the parachute's spin motion, which is expected to be, but might actually not be, totally decoupled from the probe's one for all other test phases and for the Huygens mission. According to this justification, the spin rate of the recovery parachute would be about $-1.4\ rpm$ (the negative sign indicating a counterclockwise direction as seen from above if the sensor orientation maps were correctly interpreted).

We will talk later about the fact that, based on $figures$15 and 17, the spin direction of the SM2 probe is clockwise, which was not expected.

The Y- and Z-axes gyroscopes rather capture attitude variations; they are thus expected to oscillate as the accelerometer signals while the probe is moving. Comparing the high and low range gyroscopes along each direction, a similar signal is observed - except that the low

range gyroscopes saturated at some points - confirming their proper functioning. Here also, it is obvious that initial perturbations were successfully damped during the stable main chute phase, while the oscillations remained at the same amplitude - or even increased - during the whole less stable stabilizer phase.

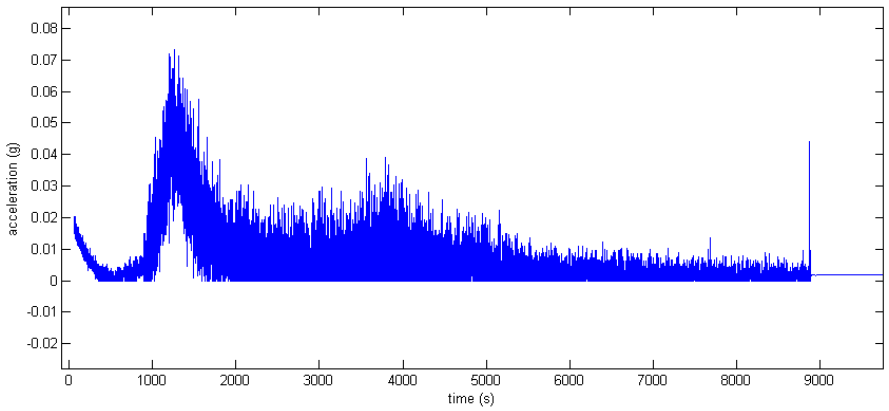

FIG.18: *The RASU time signal.*

Much less information was provided for the actual Huygens mission, since no gyroscopes were on board and the only thing we may add to CASU which was presented earlier is one radial accelerometer from RASU. As its name indicates, it measured radial acceleration on the probe and, as will be showed in the next section, by this provided mainly information about the probe's spin. We can make the same remark about the oscillations around the mean value, showing a rather stable probe under main chute (at the very left of *figure 18*, before 900 s) and a noisier behaviour under stabilizer. It can also be seen that no representation of negative acceleration values had been foreseen: the accelerometer value saturated at 0 as the lowest output, leading to significant data loss. The impact on the ground can be seen at the end, after which a non-zero value indicates that the probe had to be tilted in a way that Titan's gravity induced a positive acceleration on RASU. Further comments on this signal will be made when studying the spin and azimuth issues.

4 Spectral analysis

Let's now turn to a frequency analysis of these signals; local Fourier transforms are used to visualize the spectra's evolution in time.

As already mentioned, the SM2 data were sampled at a much higher rate than the Huygens data, which had to be reduced for telemetry budget reasons: the accessible spectrum for the SM2 accelerometers is up to 100 Hz (20 Hz for the gyroscopes), while RASU can maximally access 2 Hz motions and CASU even 0.5 Hz. As a consequence, very different information is visualized when simply plotting the spectra of all those signals (see *figure 19* below), so that a useful comparison is challenging.

However, frequencies as high as 100 Hz cannot describe probe motions; they are rather characterizing vibration modes of the structure. The present work does not have to pay attention to those, though it might have been interesting for structural engineers to analyze

them; so, we are going to filter them out of the SM2 signals in order to obtain a more realistic spectrum for orientation variations, limited to a maximum of 4 Hz[11].

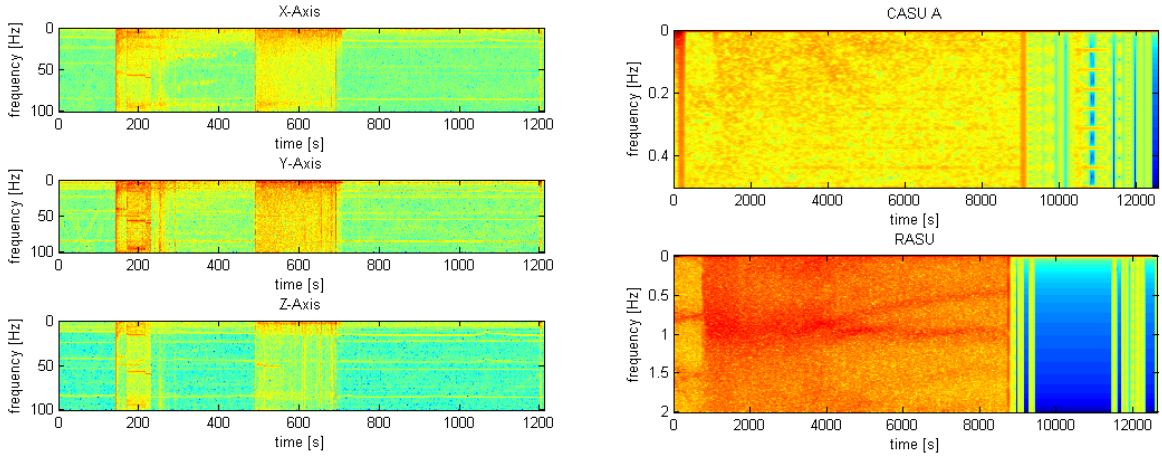

FIG.19: *The raw spectra of the SM2 (left) and Huygens (right) accelerometer signals as a function of time.*

Let's first have a closer look at the Huygens CASU and RASU spectra; we will separate main chute and stabilizer chute phases as the behaviour of the probe was clearly different for those two cases (this had indeed always been expected).

Starting with the main chute, we can identify two clear lines on the RASU spectrum. Given the analog low-pass filter cutting at 2 Hz in its conditioning block, there are many chances that they represent real frequencies (and not aliasing coming from strong vibration lines analog to those observed on the SM2 spectra above); this view is also supported by the fact that the lines, at 0.75 - 0.8 Hz and at 1.5 - 1.6 Hz, are in a fundamental frequency / first harmonic ratio. Their constancy indicates a very smooth flight, agreeing with the observations made on the time signal.

On CASU, a weak and broad line can be seen around f = 0.2 - 0.25 Hz. But since the sampling rate was four times lower than required to avoid aliasing as on RASU, this line may actually be an aliasing effect; remember that aliasing copies the original spectrum f at frequencies

$$f_{observed} = nf_{sampling} + mf$$

where n is integer and $m = \pm 1$. As there was a filter at 2 Hz, the observed line could be originally situated at $f + 1$ Hz, $1 - f$ Hz or even $2 - f$ Hz. The second of these possibilities would imply an actual frequency of 0.75 - 0.8 Hz, perfectly agreeing with RASU.

We can thus conclude that the movement under main chute includes a periodic component at a frequency between 0.75 Hz and 0.8 Hz. The lower background than under stabilizer chute also indicates that the movement was less noisy.

Indeed, the following descent phase under the smaller stabilizer chute starts, as the previous one, with a filled spectrum reflecting the large transitory perturbations caused by the

[11]This value was chosen because the full SM2 attitude reconstructions carried out in 1995, directly using the gyroscope data, showed an important periodic movement around 2.5 Hz under stabilizer parachute.

parachute inflation, but now those perturbations are very slowly damped. No spectral lines can be made out on CASU, while a slowly oscillating line around 1 Hz can be found on RASU's spectrum, out of which a second line starts about 3500 s after T_0, progressively descending towards 0.45 - 0.5 Hz at the end of the descent.

Finally, the very sharp horizontal lines on CASU's spectrum do not represent probe motions; in fact, you can see them prolonging in the strange patterns appearing after the probe has landed. They are signal processing artefacts.

Movements at a 1 Hz frequency seem to be very rapid for such a probe's orientation variations, so we might wish to zoom in on the lower frequencies; we may for example hope to find frequencies characterizing the spin rate, which was expected between 1 $rpm = 0.017$ Hz and 10 $rpm = 0.17$ Hz. But when doing this, no result was obtained at all, which could imply that

- either all dominant motions took place at those high frequencies. This hypothesis has to be rejected at least for the spin movement, since a spin of one turn per second would clearly not have allowed a proper operation of the probe; for example, it would have been impossible to take sharp pictures;

- or the general movement was too noisy to make the low frequency periodic components appear on CASU and RASU. This could eventually mean that there were no low frequency periodic attitude variations;

- or maybe the Fourier transform tool we used is not adapted to explore the low frequencies; indeed, to reach a sufficient spectral resolution at frequencies around 0.05 Hz, the length of the signal samples to be considered for each Fourier transform covers several hundreds of seconds, so that the flight conditions may vary too much over one integration period to recover a regular movement component.

Let's now see what similarities and / or differences are observed on the accelerometer spectra of the SM2 test. Remember that the last, longest part of the spectrum on the right is the final descent under recovery parachute; the descent under stabilizer parachute was shortened due to the lower launch altitude and the higher gravity.

As for the Huygens mission, the spectral lines are much clearer on the horizontal accelerometer(s) than on the vertical one. The same sharp lines are observed on the $Y-$ and $Z-$ axes accelerometers. The fundamental frequency can be identified on the $Y-$ axis accelerometer; it starts around 1.4 - 1.5 Hz and slowly increases towards 1.6 - 1.7 Hz. A first harmonic is very clear on both accelerometers, as well as a reversed harmonic whose presence is unexplained since the signal was sampled at 100 Hz. Another strange feature is that they remain during the whole descent, unperturbed by parachute transitions, and are actually already present before opening the first parachute. This is very intriguing, since in addition to the shocks associated with parachute exchanges which should strongly perturb the probe's vibrations, other parachutes and suspension rope lengths should also imply other characteristic frequencies for its motions.

As a consequence, I cannot satisfactorily explain the presence of those lines by probe motions; they do not seem to be associated to measurement artefacts so their presence simply remains unexplained to me. Anyway, such lines were not observed during the Huygens mission.

More useful spectral lines are the broad ones observed on all three sensors, quite regular between 2 Hz and 2.2 Hz under main chute and much noisier around 2.6 Hz under stabilizer. Those are very similar to the lines observed on RASU during the Huygens mission and could thus probably characterize similar motions. The possible nature of those ones will be discussed in the appropriate section later in this report.

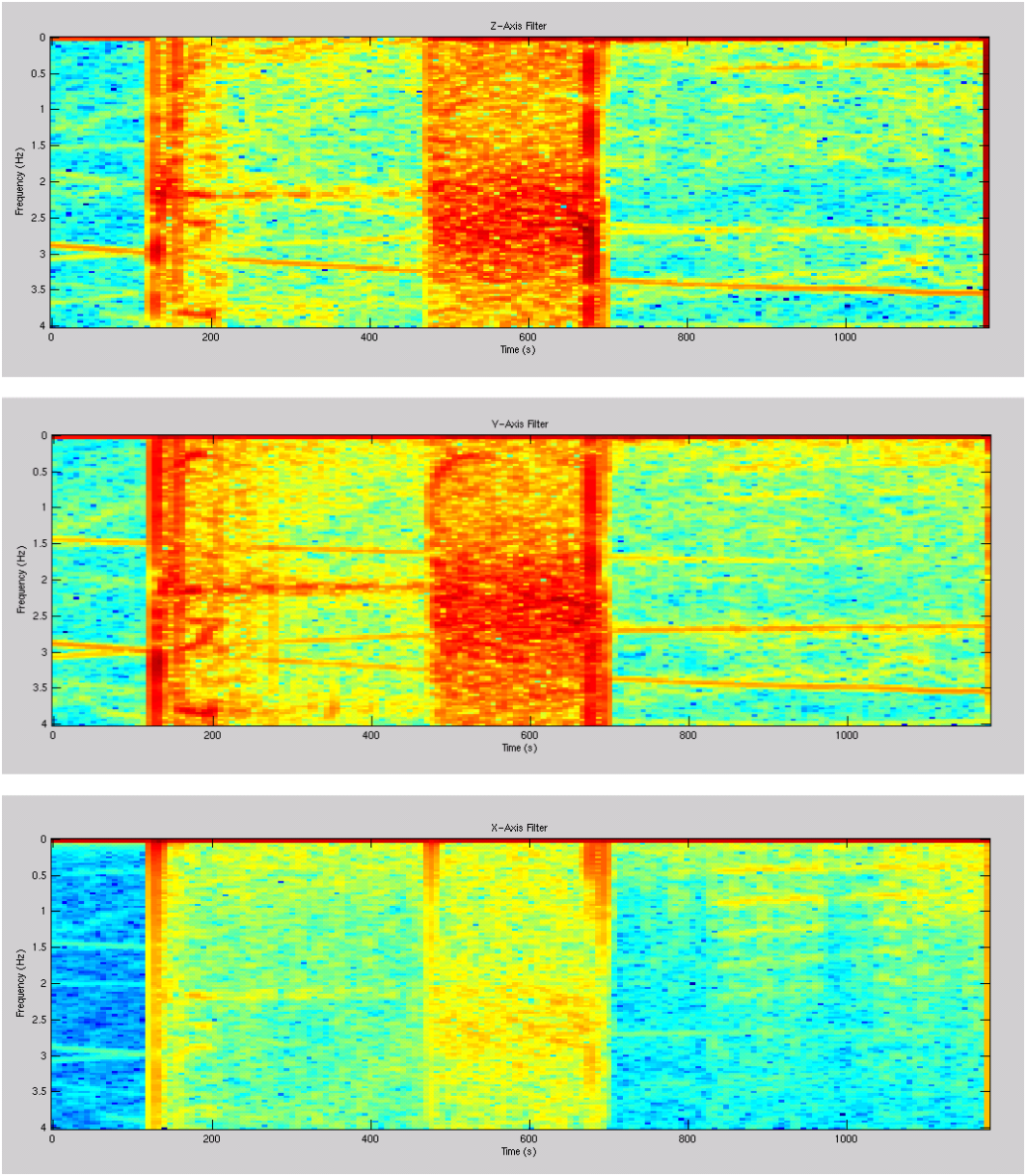

FIG.20: *Low frequency spectrum of the SM2 accelerometers.*

On the gyroscope spectra, which will not be presented in detail as they lead to no direct comparison with the Huygens mission, the same characteristic broad lines are observed. These spectra also feature narrow lines extending through the whole mission, but their frequencies are different from the ones observed on the accelerometers; as the gyroscope data were sampled at a different frequency, this could be explained by the fact that the lines are due to aliasing,

but as the gyroscope sensor set was located somewhere else on the probe, they could also be due to real low-frequency vibrations that would differ from one place to another on the probe.

Finally, no lower frequency lines were observed for the SM2 test flight either, while we know that the spin rate was not unreasonably high; this means that the method using the Fourier transform on accelerometer measurements is not adapted to deduce spin movements. The attitude motions will be discussed later.

5 Looking for correlations

The goal of this issue was at one hand, to see in general whether the movements of the probe seem to involve common oscillations on the Huygens accelerometers and SM2 sensors (just for verification) and at the other hand, to try to find strong cross-correlations involving a gyroscope and an accelerometer on SM2; indeed, it would be of great benefit if we could directly relate the Huygens accelerometer measurements to gyroscope values, which would provide the orientation of the probe in a direct way. A third point which could lead to useful information is that we should observe regularly spaced peaks on a cross-correlation and/or autocorrelation function in case the movement was significantly periodic.

Two methods have been considered for our search for correlations in the Huygens accelerometer and the SM2 accelerometer and gyroscope signals. To produce relevant results, we did not use the signal as a whole for our analysis but cut out the parachute deployment phases in order to consider a same system during the totality of each analyzed period.

The first method just involves the classical computation of the cross-correlation of two signals (or the autocorrelation if we consider two copies of the same signal) as a function of the delay added to the second one.

Before starting a uselessly huge analysis, we have first quickly checked that the sensors which were expected to measure the same thing actually show the same results. As we already noticed a great match on the time signals, it is not surprising that the high and low range gyroscopes along the same axis - Y or Z - turn out to be strongly correlated. The correlation between the three CASU sensors is even nearly perfect, justifying the fact that we only considered the first one until now. In fact, we will also suppress the low range gyroscopes from our analysis as they turn out to be very good copies of the high range ones[12].

The following functions were obtained (strongly zooming in of course) when autocorrelating the Huygens sensors.

[12]The lower cross-correlation probably resulting from the fact that the low range gyroscopes saturated.

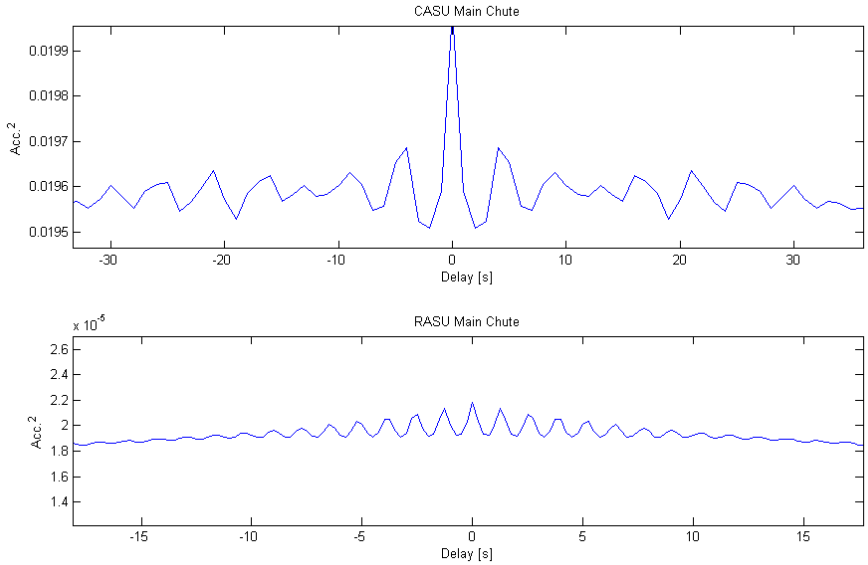

FIG.21: *Zoom on the centre of the autocorrelation functions for the CASU A and RASU signals under main chute.*

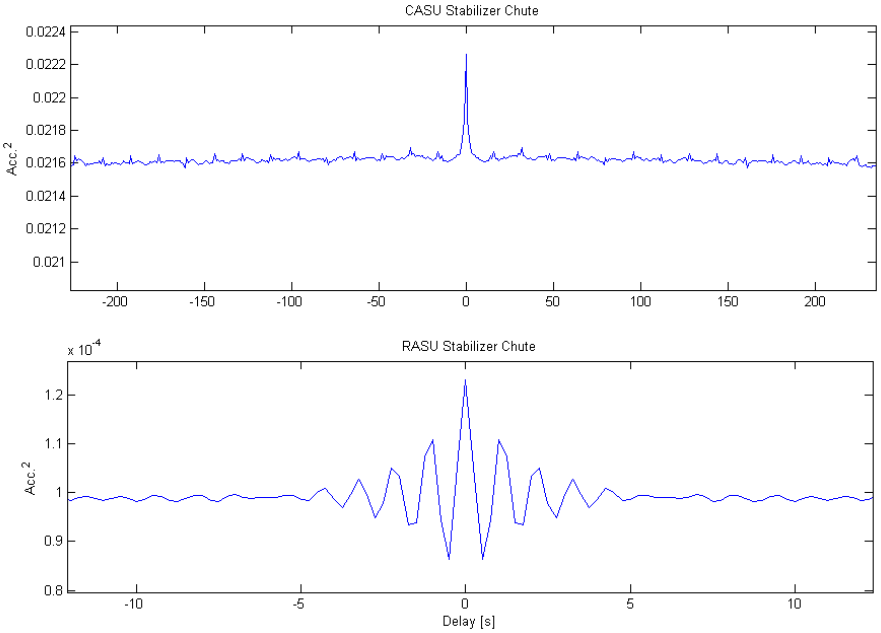

FIG.22: *Zoom on the centre of the autocorrelation functions for the CASU A and RASU signals under stabilizer chute.*

They obviously show a periodic behaviour on each sensor and for each phase. The corresponding periods are

- for CASU under main chute: $4\ s \Leftrightarrow f = 0.25\ Hz$;

- for RASU under main chute: 1.3 $s \Leftrightarrow f = 0.77\ Hz$;

- for CASU under stabilizer chute: 16 $s \Leftrightarrow f = 0.0625\ Hz$;

- for RASU under stabilizer chute: 1.1 $s \Leftrightarrow 0.91\ Hz$.

Remember that CASU is subject to aliasing, so the basic frequencies to be considered are those on RASU.

Notice the very regular shape of its autocorrelation oscillations under main chute, very slowly decreasing. This supports the fact that we had a very smooth, regular movement under main chute, which might maybe even be considered periodic.

However, a periodic movement resulting from proper frequency oscillations at about 1 Hz seems quite amazing under a parachute which is located 27 m (for the main chute) or 12.03 m (for the stabilizer chute) above the probe; the same conclusion applies to a spin rate of about 50 rpm, which would in addition be totally incompatible with mission requirements. However, no lower frequencies than those indicated in the above summary were observed on the autocorrelation functions. So, even if periodic, the movements involved have to be aerodynamically induced; we will thus call them vibrations, in the sense of high[13] frequency movements appearing under (probably) steady flow conditions.

As you have probably already noticed, the very clear frequency observed on RASU under main chute perfectly matches with what we deduced from the spectral analysis, which showed a bright line between 0.75 Hz and 0.8 Hz. The other RASU frequency, under stabilizer, agrees with the steadier spectral line which was observed between 0.85 Hz and 1.15 Hz during the whole descent under this parachute.

The (probably aliased) frequencies observed on CASU under main chute also agree, while the second spectral line of RASU under stabilizer cannot be deduced from our autocorrelation analysis. This can be explained by the fact that it only appears after 3000 s - nearly half of the descent under stabilizer - and moves, so that it should not be very clear when averaging over the whole period.

We can thus conclude that the autocorrelation and the Fourier frequency analyses show matching results.

One exception to the rule of high frequency movements is the frequency observed for CASU under stabilizer. As this one is significantly lower, it may turn out to be related to proper frequency or spin movements (the corresponding spin rate would be 3.75 rpm). The repeating peak signal is not as strong as on RASU, but extends quite far[14]. A correspondence with actual movements could be investigated when those have been characterized in a sufficient way.

To answer to our first two questions, let's now have a look at the cross-correlations. Starting with the Huygens mission, we saw that the RASU and CASU sensors present no correlation at all. But this might also result from the different sampling rate. So we looked at the SM2 sensors, where absolutely no correlation was found between the X-Y and X-Z accelerometers and just a tiny peak indicated common things between $Y-$ and $Z-$ axes under main chute. Since those two accelerometers were replaced by the single RASU on

[13] Compared to the proper frequency pendulum oscillations / regular spin.

[14] At least 6-7 periods in each direction, corresponding to more than 200 s of "autocorrelation", *i.e.* signal regularity, implying causal continuity over this duration.

Huygens, our conclusions are that it seems logical, according to an analogy with SM2, that no correlations were observed between CASU and RASU.

Going on with the gyroscopes, a similar pattern was found:

- no correlation between the $X-$ axis and the other axes. This is normal since the spin measured by the $X-$axis was aerodynamically controlled in order to stay above a certain value while the other axes show oscillating movements.

- no correlation between $Y-$ and $Z-$ axes under stabilizer chute, but well under main chute and this time significantly. It is difficult to guess what type of movement would cause strong correlations between $Y-$ and $Z-$ axes gyroscopes, or rather which ones would not, since they both describe the motions of the probe's horizontal plane. But an important piece of information that should be pointed out is that the behaviour of the probe seems to have been different under main and stabilizer chutes; so, at least for the SM2 test, the larger oscillations observed on the signal are maybe not just due to higher amplitudes of the same movement, but arise from different, probably much noisier motions[15].

Now turning to the cross-correlation between accelerometers and gyroscopes, the first thing to verify may be the relevance of a radial accelerometer to deduce the probe's spin. In fact, we discovered that the $X-$ axis gyroscope showed no significant correlation with any accelerometer. This seems to indicate that there could be some serious problems about RASU's spin deduction purpose. However, remember that

- none of the two horizontal accelerometers was really radial and

- the SM2 accelerometer set was located near the centre of the probe, not at its boarder to increase centrifugal forces as was done for RASU

so that other motions may take much more importance on SM2 accelerometers than on Huygens' RASU. In fact, the oscillations induced by the probe's motion are so big that the small bias due to the spin-induced centrifugal force is drowned, specially when computing the correlation on a whole timeslot; the offset can be seen though by looking very carefully at the SM2 accelerometer signals and even as a constant positive offset, whatever delay is considered, on the cross-correlation function between $GyroX$ and $AccY$.

Investigating cross-correlations between other gyroscope-accelerometer pairs, we noticed that

- the $X-$ accelerometer showed no correlation with any gyroscope. This seems to indicate that it will be difficult to infer indications about the probe's orientation from the CASU measurements for the Huygens probe.

- finally, peaks could thus only appear on Y-Z pairs, and they do in fact. This is not such a good news since it confirms what we previously suspected, namely that RASU's measurements would be strongly perturbed by attitude variations of the probe; on the other hand, it also means that RASU will turn out to be useful (let's see in what extent) for attitude reconstruction.

[15]Or at least, producing much noisier gyroscope output since no correlation was found between the two horizontal gyroscopes.

As will be clear after its description, the following second method should prove much more adapted to investigate how accelerometer variations could be directly related to gyroscope measurements.

This method is known as the "plunging method". It is used to study chaotic phenomena when the presence of a so-called strange attractor is suspected, or more generally to reconstruct the behaviour of a strongly unknown system where, in particular, the number of measured variables is too low with respect to what would be required to fully monitor its evolution.

The initial idea is that if all variables are coupled through differential equations, as would be the case on a complex system, the evolution of a single, measured variable should reflect, in some way, the behaviour of the whole system.

As a result, the proposed method consists in plotting delayed samples of the same variable, let's say

$$x_i(t)\ ,\ x_i(t+\tau)\ ,\ x_i(t+2\tau)\ ,...\ x_i(t+(n-1)\tau)$$

in an n-dimensional space, rather than the full variable set[16]

$$x_1(t)\ ,\ x_2(t)\ ,\ x_3(t)\ ,...\ x_n(t)\ ,$$

where the time t is of course considered as a parameter when reconstructing the trajectory. Despite the fact that we consider only one variable, this is more than a simple autocorrelation computation since we really draw a geometrical structure, which should be very close to a projection of the actual trajectory that takes place in $(x_1...x_n)$ space.

When, as will be the case here, the number of dimensions required to characterize the (expected) recurrent movement is unknown, the shape of the obtained geometrical object should become more and more accurate when increasing the number n of delayed signal components, approaching a somehow projection of the attractor in an n-dimensional x_i space. Computing the fractal dimension of the attractor at each step while n is augmented, an increase is observed as long as n is too low to allow reproducing all features of the trajectory, after which the computed dimension stabilizes at the dimension of the real attractor.

All this might sound quite strange, but it works and was demonstrated on lots of chaotic systems, among which the famous Lorentz equations which initiated the interest in this subject.

Using this method, we thus hoped to overcome the lack of measured kinematic variables for the Huygens mission, at least to investigate a possible movement along a strange attractor. Indeed, the presence of clear frequency lines on the RASU spectrum as well as on the SM2 sensors seemed to indicate nearly-periodic, *i.e.* recurrent, motions.

But do not await a miracle: the convergence of this special method is very sensitive to the choice of the delay, τ. The smaller its value, the higher are the chances to observe a regular movement (if present). But this means that we should use a very high sampling rate to provide lots of very close measurements and it implies a long computation time before getting the results; in general, a trade-off has to be chosen between measurement and computation investments and convergence/accuracy. Anyway, in the present case we don't have much

[16] Whose number of members may be too high to measure them all. Actually, the method was developed for the particularly useful case where the minimal needed number of variables to draw the trajectory is unknown.

choice since the 4 Hz and 1 Hz sampling rates on RASU and CASU respectively are already quite low.

As a consequence, the results are disappointing: a full and disordered wool ball showing no regular feature is invariably obtained (reducing to its projection when considering 2 dimensions) using both the RASU and CASU signals. This might indicate that no recurrent movement is present or simply that the minimal possible value for τ is still too high to highlight an existing attractor. In fact, the wool balls which are obtained seem to be very similar to what we have been shown for cases where the convergence of the plunging method failed. Anyway, it does not provide any useful information on correlations for the Huygens mission.

However, we made additional trials after having applied different low-pass filters to eliminate some noise. We have also applied the same method, with and without low-pass filters, to the SM2 data (gyroscopes and accelerometers), which were sampled at a much higher frequency and thus allowed lower values for τ. Without filtering, the same big noisy wool ball is observed on all SM2 data, while a smoother, curved but still filled object appears after having filtered the data; I think that this smoothing is produced by the filter itself, since it does add some regularity, and does not give any hints about potential attractors for the probe's motion.

We must thus unhappily conclude that this issue turned out to be a dead end for our investigations. It is a pity since the tool seemed to be well adapted to our purpose and could have provided useful information, but the fact that it did not is not that surprising; indeed, we are not studying a perfect, closed system but a probe which is interacting with its changing environment - actually it is moving in the environment - so that many perturbations induced by variations of external effects are just logically inducing too much irregularity to allow a stabilization of the probe's movement on an attractor.

Anyway, let's close this subject and move on to a detailed analysis to, at length, get results in a profitable way. We will start with the easiest issue given the data at our disposal, namely the spin and azimuth of the probe, then going on with the probe's orientation after touchdown where the absence of motion should help us in our data analysis before addressing the much more complicated attitude issue, where the motion is obviously quite noisy (since it is these movements that give raise to the oscillations observed on the CASU and RASU signals and we did not find any attractor) and no dedicated engineering sensor exists.

•

Part III
Characterizing the spin and azimuth

6 The spin rate and azimuth (part 1)

6.1 Pre-mission analysis

The spin of the Huygens probe had to be controlled not only in order to remain under an acceptable limit (that would have been obtained automatically by sufficient friction) but also to stay above a minimal rotation rate of 1 *rpm* in order to allow looking around and regularly taking pictures (or measurements for the other instruments) in different directions.

To allow a free rotation of the probe, unaffected by the parachute's inertial and aerodynamic damping influence, a swivel was incorporated in the suspension cable between probe and parachute. Furthermore, to maintain a sufficient spin despite the continuous and unavoidable friction losses in the atmosphere of Titan, this same atmosphere was used in an aerodynamic trick taking advantage of Huygens' descent velocity towards the attracting planet.

Thirty-six little winglets, known as "spin vanes", were placed on the front dome of the descent module, slightly tilted with respect to vertical (2.2 *deg* initially). These acted as turbine blades, making the probe rotate while experiencing the vertical air flow due to the probe's fall; the probe actually screw itself through Titan's atmosphere in a similar way maple fruit do on Earth.

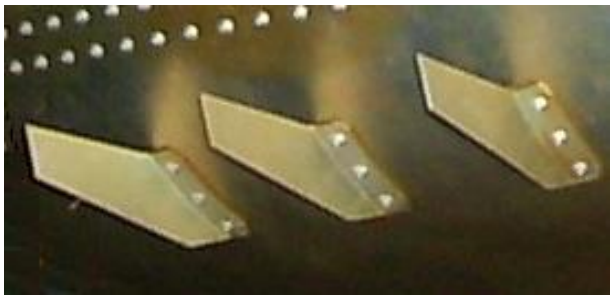

FIG.23: *Zoom on some of the 36 spin vanes.*

After the primary conception, aerodynamic design calculations and wind tunnel tests and qualification were carried out by industry and provided the adopted configuration. Using realistic models for the different aerodynamic and friction terms

M_1 = Spin vanes motor torque

M_2 = Damping torque due to protrusions in external flow

M_3 = Damping torque due to protrusions in separated viscous flow (stiffeners,...)

M_4 = Damping torque due to viscous skin friction on the DM

M_5 = Swivel torque

and the law $I\frac{d\omega}{dt} = \sum_i M_i$, spin profile predictions versus time and altitude were elaborated for the Huygens mission for different atmosphere models, to show that the probe's motions would meet specifications.

A secondary objective of the SM2 test flight was to validate these calculations using parameters for the Earth's atmosphere. The spin rate of the specially instrumented test probe was directly accessible through the vertical axis gyroscope, whose time signal was presented above. The observed spin rate fitted quite well under main chute, where it was lower than nominal case but within predictions; under stabilizer however, it was as much as twice too slow, so that the required minimal spin rate of 1 *rpm* was not achieved.

Searching for the reason of this anomaly, the sensitivity of the spin rate profile to variations of the torques M_1 to M_5 was studied numerically. It turned out that, to obtain the observed spin rate under stabilizer chute by varying one of those parameters, a variation of at least

$\div 2$ on M_1

$\times 5 - 10$ on M_2

$\times 100$ on M_3

$\times 10$ on M_4

$\times 50$ on M_5

was needed; even by considering combined variations of several parameters, the values lie well above the supposed uncertainties about them. Furthermore, it was impossible to find a common match for both stabilizer chute and main chute phases.

The possibility that a tilt of the probe, thus changing the flow's incidence angle, may change its aerodynamic properties in order to produce a lower spin rate was also invoked; this hypothesis seemed in good agreement with observations since the spin rate was much lowered under stabilizer chute, when the attitude was the most unstable. But after testing, it was found that, far from reducing the spin rate, a tilt actually increased the efficiency of the spin vanes.

Having found no valuable reason, the reduced spin rate was finally attributed to a "reduced efficiency of the spin vanes under flight conditions", though they actually were supposed to have been characterized for precisely these conditions. The inclination of the spin vanes was increased to 3 *deg* on the Huygens flight model to ensure a sufficient rotation speed for imaging needs at Titan.

6.2 RASU measurements

The first information source which was used during the mission to evaluate the spin rate was the RASU accelerometer. Indeed, it was meant to measure the centrifugal force due to the probe's rotation around the X-axis, in order to deduce the spin rate by the simple formula

$$a_{centrif.} = r\dot{\psi}^2$$

where $\dot{\psi}$ is the angular spin rate in rad/s.

Knowing that the radial position of the RASU sensor was at 0.353 m of the probe's symmetry axis and that its measurement output is given in multiples of $\mathbf{g} = 9.81\ m/s^2$, the numerical value of the spin rate in rpm would be readily computed by the formula

$$Spin = \frac{60}{2\pi}\sqrt{\frac{9.81 \cdot RASU_{out}}{0.353}}\ .$$

It was clear from the beginning that perturbations would induce oscillations on RASU's measurement; these include centrifugal and tangential accelerations due to other movements, as well as a bias by the gravitational influence of Titan when the probe was not horizontal (see the expression of $\mathbf{Acc} \cdot \mathbf{e}_y$ in section 2.2.3). That is why the RASU signal was averaged over a few samples (over 128 s actually) before applying the above formula to compute an onboard spin rate estimation; this estimation was delivered to all instruments, and also sent back to Earth, as a part of the DDB. The azimuthal orientation of the probe should then be obtained by integration of the spin rate, starting at a particular, known azimuth (which could come from an image taken at a certain moment and whose direction is known or from the orientation of the probe after touchdown if it can be determined by any independent source of information); unhappily, the error on the spin rate would then accumulate as time goes on during integration, leading to a high and increasing uncertainty on the azimuthal orientation which would finally be totally undetermined when the uncertainty reaches 180 deg after several rotations.

The spin estimation of the DDB may be checked with a "reconstructed DDB spin profile" by averaging the RASU signal over a few seconds (we took 49 samples, representing about 12 s, to see what happens when having a better time resolution). The following first estimations of the spin profile appear; of course, the two signals (computed from RASU accelerations and present in the DDB) perfectly agree, except that a longer period was taken by the POSW to compute the DDB average. In addition, as the POSW was working in real time, without any possibility to look at future accelerations to enhance the average's accuracy, the spin rate present in the DDB was delayed with respect to our computations using centred means by 64 s.

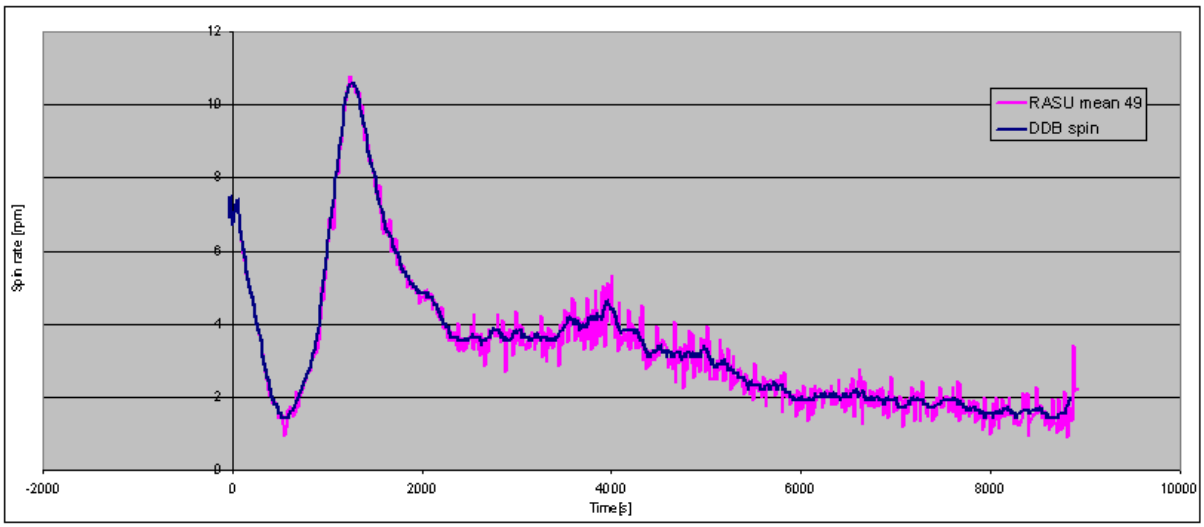

FIG.24: *Spin profile provided in the DDB and computed from RASU average.*

At first sight, nearly everything seems to agree with predictions: starting around 7 *rpm*, which was the initial spin value given to the probe when ejected from Cassini, the movement was slowed down by friction in Titan's atmosphere until a very low spin rate was reached before main chute jettison; the spin rate then increased under higher descent velocity until a maximum was reached before the increasing density of the atmosphere again slowed down the movement during the remaining part of the descent. The only strange behaviour is the very low value of the local minimum around 600 *s*.

But there also is an inherent problem in the POSW's determination of the spin rate. Unhappily, the fact that all negative values of the accelerometer were considered as 0 introduced a strong bias on the average: the computed mean value does actually not correspond to the DC component of the analog accelerometer signal so that all spin values were overevaluated when negative values appeared, that means during nearly the entire descent (see the RASU time signal in chapter 3). This can be seen by superimposing the computed average on the RASU signal: the curve is slightly too high with respect to what we would call the average value from inspection.

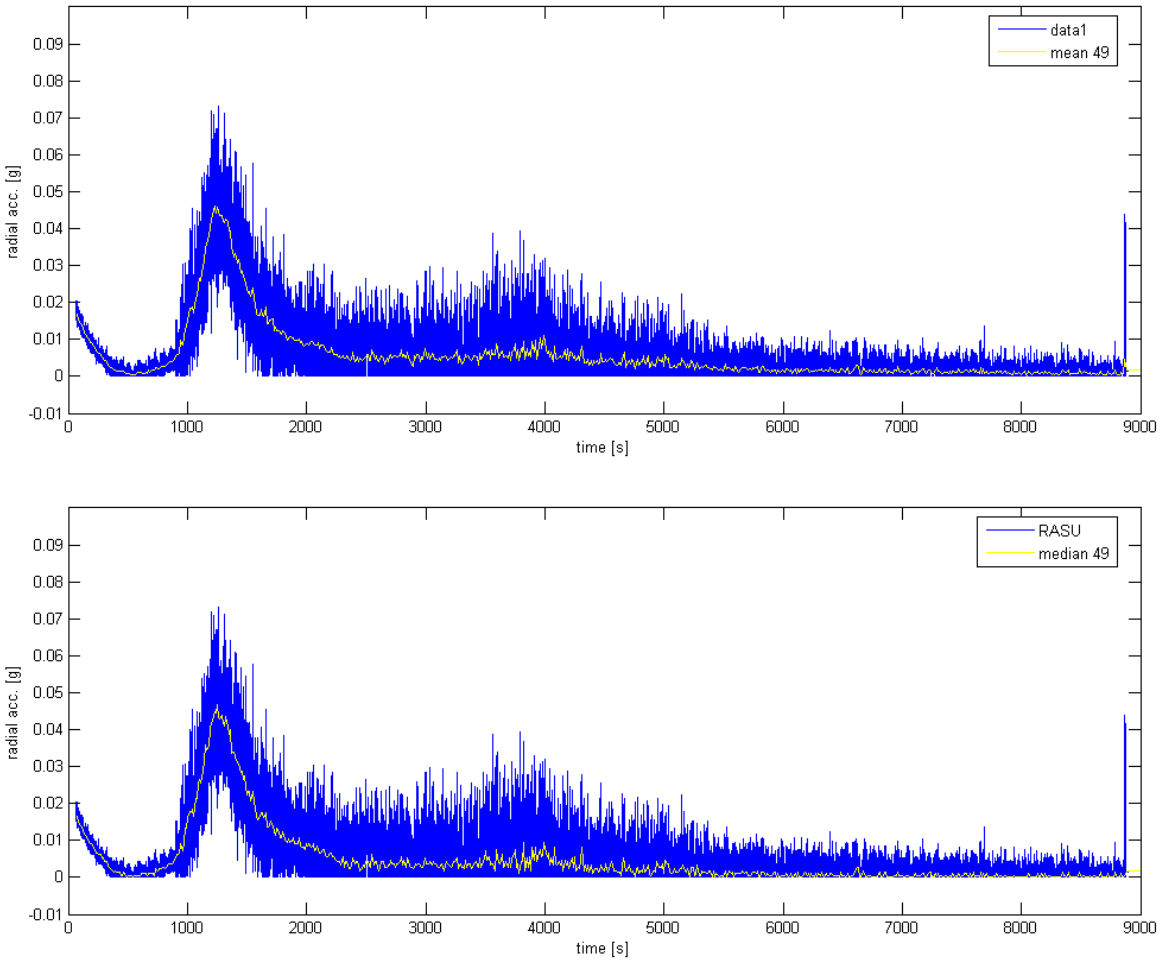

FIG.25: *Superposition of the computed RASU digital output average (upper part) and median (lower part) on the RASU signal.*

This means that, trying to justify the observed low minimum spin rate by measurement errors, we discovered that it was not underevaluated but overevaluated so that it is actually even lower. To quantify this assertion more accurately, we should examine "what we would call the DC component from inspection", that is the median value of the signal. The difference in agreement with the analog acceleration's mean can barely be seen on *figure 25*, but a different spin profile is obtained especially at low spin rates (see *figure 26*).

This spin profile, still using 49 samples for the median to approximate an average over 12 s, should already be much more accurate than before, but still suffers from some bias.

In fact, averaging was supposed to suppress all perturbing accelerations on RASU's measurements by eliminating all terms that depend on the probe's azimuth in the expression of $\mathbf{Acc} \cdot \mathbf{e_y}$. In practice, this is equivalent to deleting all linear terms in $\cos(\psi - \phi)$ and $\sin(\psi - \phi)$. Indeed, it seems plausible to assume that the other motions of the probe took place at frequencies which were different and independent from the controlled and varying spin rate so that the variations of ϕ and θ should not interfere.

But this does not directly provide the spin rate $\dot{\psi}$: the actual result obtained is

$$\mathsf{Av}\left[\mathbf{Acc}\cdot\mathbf{e_y}\right] = r\left(\frac{(\dot{\theta}^2+\sin^2(\theta)\dot{\phi}^2)}{\sqrt{2}}+\left(\dot{\psi}+\dot{\phi}(\cos(\theta)-1)\right)^2\right) .$$

The first term is positive and would thus induce another positive offset on RASU spin deductions when we assume that $\mathsf{Av}[\mathbf{Acc}\cdot\mathbf{e_y}] = r\dot{\psi}^2$. Its effect is dominant for a high pendulum velocity (since the tilt should remain low, producing a low value for $\sin^2(\theta)$).

The presence of the coning velocity in the second term will have a different effect depending on the relative spin and coning directions (both of them were initially supposed to stay the same during the whole descent): if they are the same, the offset will be negative, compensating the error induced by the first term, while opposite spin and coning directions would lead to one more positive offset component.

Analysis of the attitude (part V) is needed to accurately quantify the influence of those terms on RASU and show that we are effectively mainly measuring the spin rate; on the other hand, RASU deviations might be explained by - or even better, give hints about - pendulum and coning motions.

Let's finally have a look at the results of our computations. The following *figure 26* shows the spin profile deduced from RASU accelerations using the median and (wrong) average estimations in comparison with the predicted spin profile for a nominal descent (which finally was the model closest to reality).

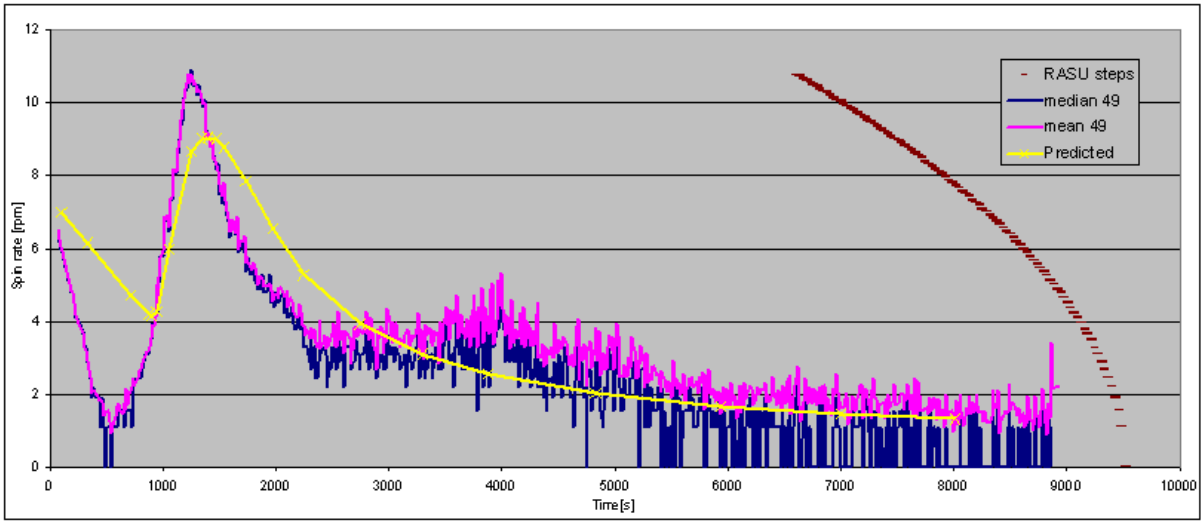

FIG.26: *Spin profiles deduced from RASU accelerations (median and average estimation) compared to the predicted spin profile for a nominal descent; the brown steps indicate the quantification steps of RASU.*

As expected, the spin profile is lower for the median estimation. Both spin estimations turn out to agree quite well with the predicted spin profile, except for the same strange feature: the spin rapidly drops down at the beginning, reaching a much lower value than expected, then increasing rapidly before it reaches the expected spin rate and follows more or

less the predicted curve for the remainder of the descent. In fact, the value of the minimum spin rate is zero, though we should be somewhat careful about this statement since the square root performed to deduce the spin rate from the acceleration distorts the linear quantification scale chosen on acceleration so that we have a very bad resolution for low spin values (see the brown quantification steps at the right of the figure): the repeating zero values at the end are clearly not real, but from visual inspection, an annihilation around 600 s, where much less noise is superimposed on the mean value, really seems to take place.

However, the minimum spin rate seems to be much lower than predicted on both RASU estimations. Remembering the other influences which should be visible on RASU's average, we observe that

- this implies a much reduced influence of the pendulum velocity, at least around this moment, since a positive offset should be observed if its addition had a significant effect.

- it might be (though sounding quite amazing) that a strong coning velocity in the same direction as the spin is actually the cause of the RASU drop, making us deduce a reduced spin rate which was actually not present; even further, it is possible that a similar frequency for the spin and some other motions of the probe led to wrong averaging assumptions (*i.e.*, we are not accurately deleting the $\cos(\psi - \phi)$ and $\sin(\psi - \phi)$ terms since the other variables involved in the integration vary with a similar frequency) which artificially create what seems to be a spin drop. However, the very regular evolution of the difference, starting at the beginning of the signal[17] and increasing until the minimum after which it decreased until the nominal curve was reached, seems to be in contradiction with such interferences.

How strange such behaviour may seem to be, we have to look for an explanation of this apparent spin anomaly. To rule out the possibility of dominating secondary effects on RASU, a good idea would be to check the spin rate with independent information; this is the purpose of the following section.

Let's just make a final remark about the chosen averaging period before leaving the RASU–Spin issue. To provide a correct evaluation of the average as we want it, the 12 s used for its calculation should cover at least one entire period of the spin movement; in the ideal case, an entire number of periods should be used, or at least such a high number of turns that the remaining oscillation bias coming from an incomplete period becomes negligible with respect to the offset.

Looking at the spin profile, we see that it just briefly exceeds the 5 rpm spin rate corresponding to our 12 s period; our median/average evaluation is thus far from best-guessed; the DDB, using 128 s integration time (but updating the spin much more often, thus superimposing the consecutive data windows used), did a much better job in this way. But a longer integration period implied a much reduced resolution, which would among others skip the spin annihilation points. As those seemed to be real when looking at the RASU signal, we chose to keep a reduced averaging period; as a result, rapid oscillations on the

[17] Notice that telemetry acceleration data from RASU start roughly 70 s after T_0, meaning that the front shield had already been jettisoned and the spin vanes were thus active. The DDB spin values have been recovered since 24 s after T_0, meaning with the 64 s delay that we have the average spin from $T_0 - 40$ s on. The constant 7 rpm spin before front shield release can be seen on the first figures of this section.

RASU-acceleration deduced spin signal should be discarded since they probably arise from this incomplete averaging.

6.3 The spin signature on the AGC signal

The AGC signal reflects received power of the telecommunication link during the Huygens mission; we will explain later what this exactly implies and how probe motions and, even better, orientations, can be related to it. Let's just have a quick look at this signal which was not presented yet; the green curve represents the actual AGC signal, while the blue curve, very close to it, is the same signal where the influence of the slow probe-to-orbiter distance variation has been subtracted.

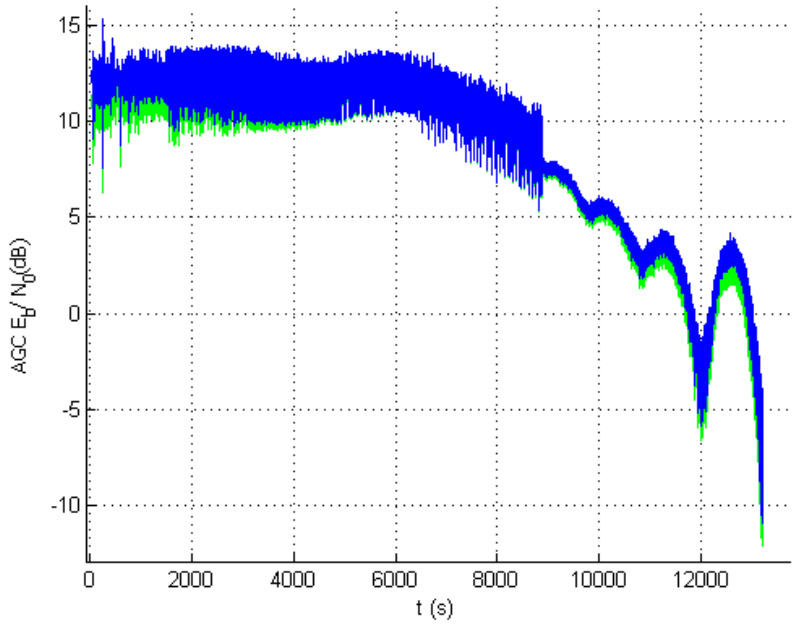

FIG.27: *The time signal of the AGC (channel B) during the whole descent phase and after touchdown.*

The reason why we slightly anticipate the presentation of the AGC is that, at first sight, a clear periodic variation has been observed (see *figure 28*), and it turned out as expected to be correlated with the probe's spin motion as deduced from RASU; the reason of this feature will become clear when the AGC signal is understood.

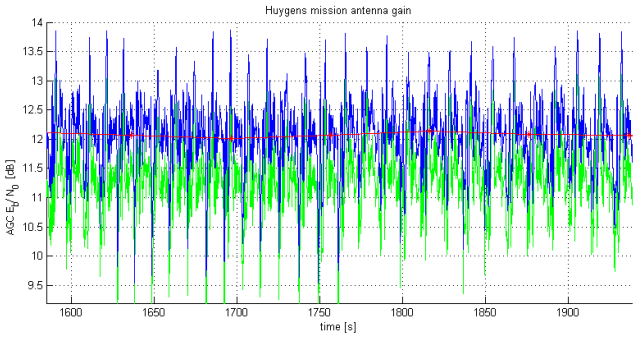

FIG.28: *Zoom on the time signal of the AGC (channel B) to show the periodic variation due to the probe's spin.*

Looking at the local Fourier transform of this signal (where high frequencies were filtered as the expected spin rates should maximally - remember that RASU tends to overevaluate the spin - reach 11 $rpm = 0.1833\ Hz$ and the AGC signal was sampled at 8 Hz), clear lines appear showing patterns very similar to what RASU measurements made us deduce for the probe's spin rate: a barely visible decrease at the beginning followed by a minimum close to 0 Hz; then increasing towards a maximum from which the signal slowly decreases with some oscillations[18]. Trying to compare the place of the spin annihilation (big red spots at the bottom), you should notice that the presented AGC specgram is also delayed in time, but in the opposite direction as the DDB was, due to MatLab's computation of the Fourier transforms: while the actual first sample of the AGC was obtained about 46 s after T_0 and the width of the window used to compute the Fourier transform covers 512 s so that another 256 s delay is introduced before getting the first spectrum, MatLab's scale just starts at $t = 1$ s.

We tried to follow the lower curve as accurately as possible to deduce a spin profile, zooming on less clear parts. The fact that many harmonics are visible allowed a reduction of the positioning error of the fundamental frequency curve by checking the superposition of the manually retraced curve at higher frequencies. We actually used both the fundamental frequency and the clearly visible first harmonic to retrace the curve before checking and correcting it with higher harmonics. There is just one timeslot around 5000 s where the behaviour of the signal was not clear; this will be explained when the AGC is analyzed in more detail.

[18] All these features might not be clearly visible on the following *figure 29*; it is a fact that the spin signal is much less visible during the beginning of the descent, but using different scales actually allows to follow the whole line.

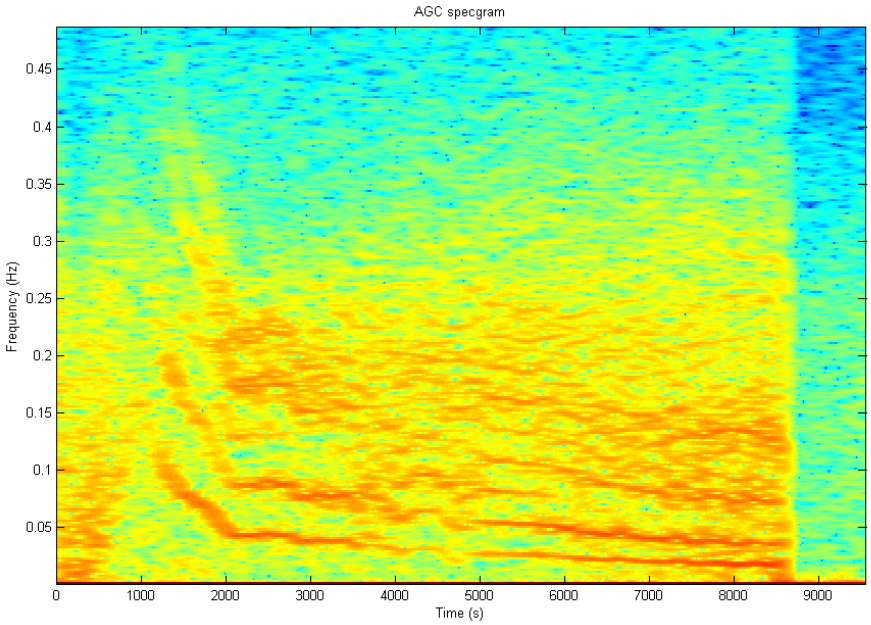

FIG.29: *Low frequencies of the local Fourier transform (specgram) of the AGC signal, clearly showing a frequency line that seems to follow the RASU-deduced spin frequency and related harmonics.*

Here is the result we obtained.

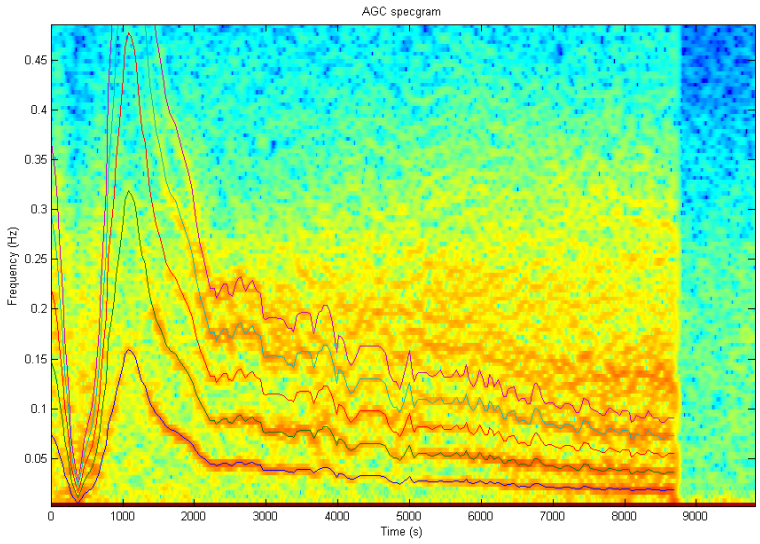

FIG.30: *Superposition of the manually reconstructed main frequency and its first four harmonics on the previous signal.*

The conversion to *rpm* for a comparison with predictions and with the RASU-deduced spin profile is straightforward and yields the following figure.

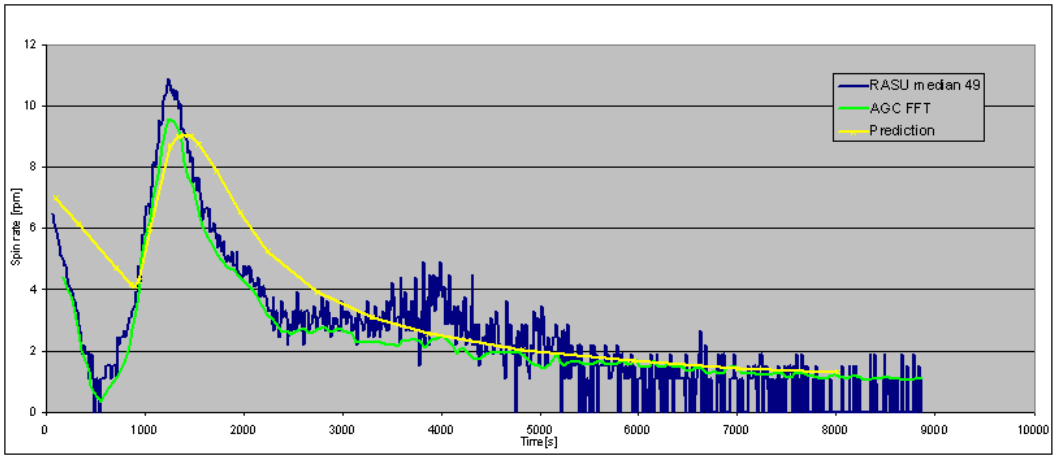

FIG.31: *Comparison of the spin profile deduced from the RASU median and from the AGC spectrum, in regard with the predicted spin profile.*

The observed spin profile agrees very well with what we deduced from RASU and thus confirms that we are observing the same phenomenon, namely the spin of the probe, on both independent signals; despite RASU's reduced resolution, several common secondary peaks are identified in the oscillations after the spin maximum, but at some places a peak appears on only one of the sensors or is reversed on one of the signals (which doesn't make any sense regarding spin movements of course). This indicates that other effects dominate the variations on at least one of the sensors at those places[19].

We also notice that the spin rate deduced from RASU, even using our computed median value, is mostly a bit higher than what is obtained from the AGC Fourier transform evaluation. As the spin rate deduced from the AGC cannot suffer from any constant offset - because indeed, it is not measuring any acceleration or speed but directly a frequency which has to correspond to a physical reality - , this again seems to show the biasing influence of the pendulum and coning motions on RASU, which were already discussed earlier. But the general agreement is unquestionable.

The AGC Fourier curve is even closer to the predicted spin profile, though its deceleration is much faster at the beginning. The descent was a bit longer than expected and that is why the predicted spin curve stops before the real ones. The previously unexplained feature - the annihilation around 700 s - is present on both signals; this was thus not an artefact of the particular RASU measurement method, but a real behaviour of the probe's spin rate during the Huygens mission. As this was definitely not predicted, a specifically dedicated section investigating this problem has to be introduced, and is presented next.

[19]We know that actually both signals are subject to bias and/or oscillating perturbations by, among others, the other probe motions (tilt angle and tilt direction).

7 The spin direction anomaly

7.1 Early observations

The fact that the spin seemed to drop to zero between 516 and 540 s after T_0 has led to some discussion within the Huygens team. In fact, it seemed difficult to accept that the probe would stop spinning at a certain moment and then start again. However, the zero spin moment was clearly seen on RASU and confirmed by the AGC Fourier transform analysis.

Knowing the precise mission timeline, the predicted spin minimum is at the end of the main chute phase, when the descent velocity of the probe is minimal. The release of the main chute and deployment of the smaller stabilizer leading to higher velocity again, the spin vanes experience faster flow and the spin rate increases. Now you might think that this could explain the spin annihilation: the probe's spin rapidly decelerated under high friction of an improperly operating main chute swivel until it blocked; after main chute release, a fresh stabilizer chute swivel and increased descent velocity liberated the spin movement which accelerated towards the predicted spin rate that was followed until the end of the mission.

The problem is that the observed spin annihilation does not occur at the end of, but **during** the main chute phase. This can be clearly seen by comparing the spin rate curve to the descent sequence.

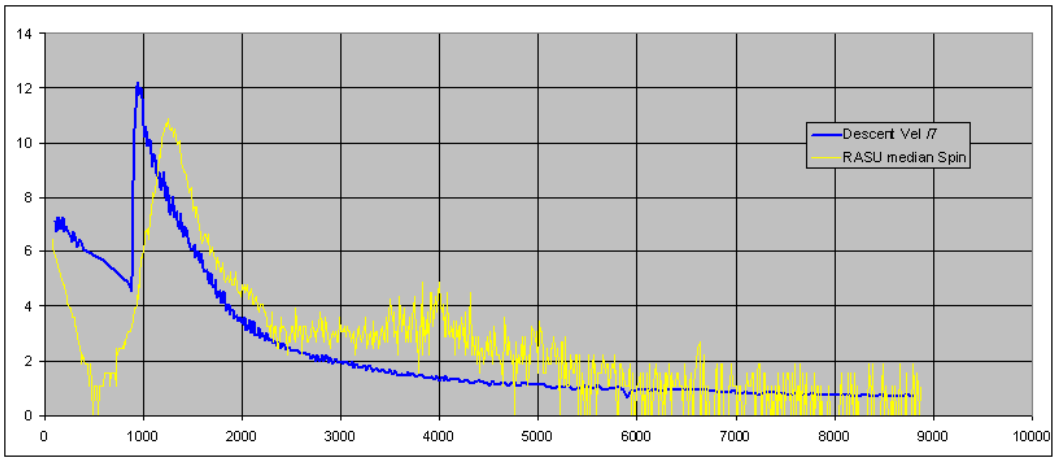

FIG.32: *Huygens mission (processed) data: the descent velocity (from DTWG) and the spin rate (RASU median) as a function of time.*

The minimum and related sudden increase in descent velocity corresponds to main chute release. It is obviously at this point that the local spin minimum should appear, the spin vanes' induced rotating torque depending directly on descent velocity; in fact, we can even see a change in the slope of the spin rate at this point.

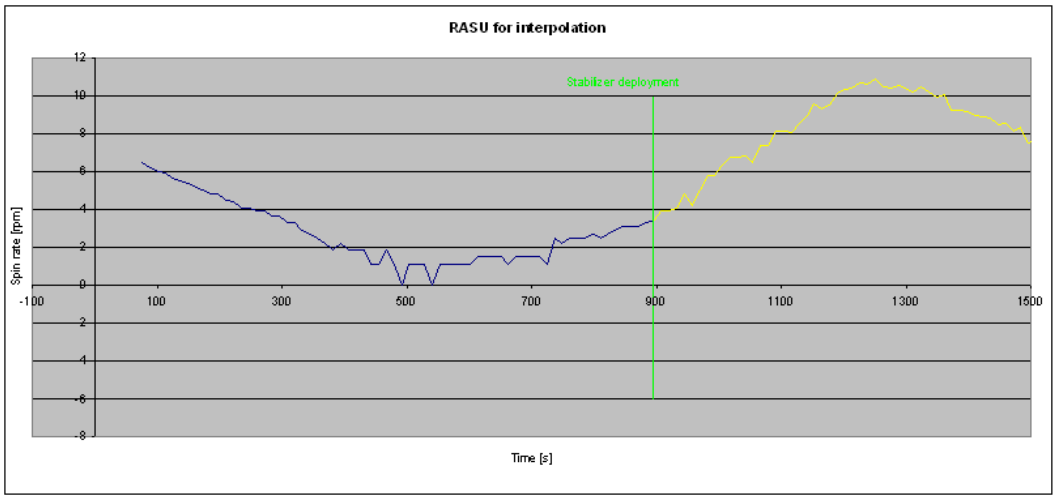

FIG.33: *Zoom on the spin rate (RASU median) during the beginning of the descent. A discontinuity is seen on the slope when passing from main to stabilizer chute.*

The spin annihilation definitely occurred at a strange time, where nothing particular happened in the descent sequence, and in place of staying at rest for a moment until something else would appear in the descent sequence, the probe directly started spinning again.

The most reasonable way to justify this punctual annihilation obviously was to suppose a reversal in the spin direction. This hypothesis was supported by information from the DISR-team: from the first days after data recovery, they were wondering if the probe was not spinning "the wrong way" while the camera took its surface images during the late descent phase; indeed, it was the only way to make a consistent recombination of their panoramic views. An impressive demonstration at a later meeting confirmed that this had to be the case. So, the camera indicated that during the late descent phase, the probe was spinning clockwise (as seen from above), while it was ejected from the Cassini orbiter with a counterclockwise spin, which should have predominated at least during coast and entry phases where no torque at all could be induced, normally, until front shield release. Between those two movements, a spin reversal would have to take place, and actually that is what we observe here.

Thinking this way, the observed spin profile looks much more plausible, as can be seen on the following figure.

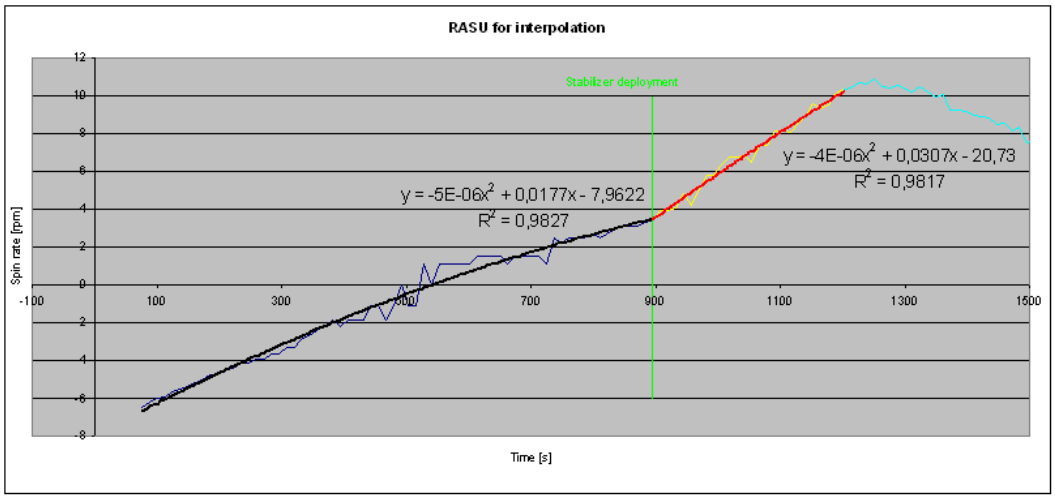

FIG.34: *Spin rate during the beginning of the descent (RASU median) assuming a spin reversal. The superimposed tendency lines will be used for a smooth spin characterization.*

7.2 Using the AGC signal

Looking for more evidence on the spin direction topic, let's turn to the AGC. In fact, we observed that the spin movement was clearly visible on the AGC signal and thought of usefully deducing a spin rate from the clearly dominant frequency by examining its Fourier transform. But by doing this, we actually strongly underevaluated the possibilities of a direct analysis of the AGC time signal. Let's explain this in more detail.

The gain of the probe's antenna (we consider channel B only, since channel A didn't work properly) depends on both PAA[20] and azimuth; the following *figure 35* represents this dependence as obtained from the flight module antenna characterization carried out by SAAB industries and presented in document [11].

[20]Remember that the Probe Aspect Angle is defined as the complement of the elevation of the telecommunication link direction, or equivalently as the angle between the probe-to-orbiter direction and the antenna vertical = probe X axis.

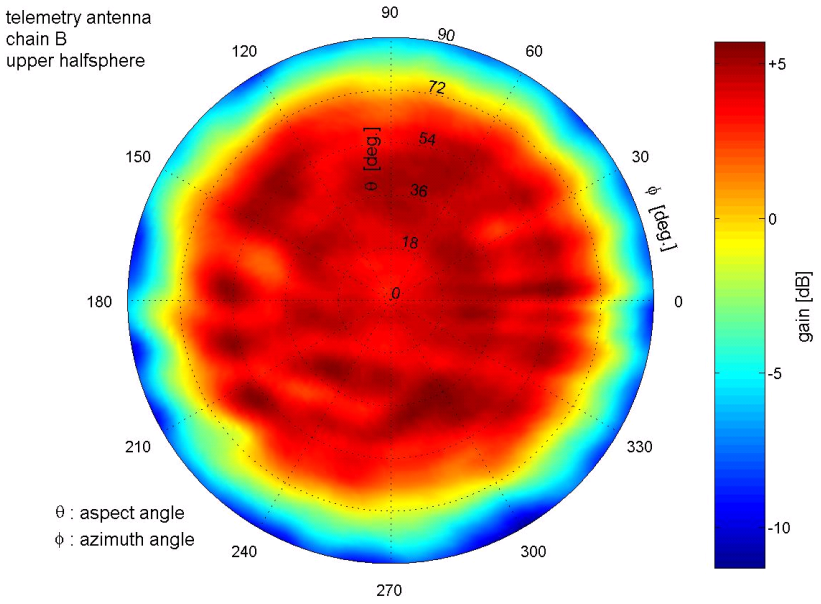

FIG.35: *The channel B antenna gain pattern (figure from DWE-team presentation at meeting HSWT# 29, Florence, February 28, 2005).*

When the probe moves in any way with respect to the orbiter, the link direction follows a continuous path in this half-sphere, encountering different gains which lead to adequate AGC adjustments. But there is an additional effect on the AGC signal, namely the varying distance between probe and orbiter: this induces a slow variation in power density received by the orbiter because the strength of the electromagnetic power at a distance R from the probe is proportional to $\frac{1}{R^2}$.

The resulting AGC signal was presented above. The green line indicates the original signal, the blue one is corrected for probe-orbiter distance variations; the actual probe-orbiter distance needed for this correction was easily computed from accurate probe and orbiter positions provided by the DTWG and the JPL respectively. The red line which is superimposed on some figures indicates a mean gain averaging the spin-induced variations.

When the probe had landed and thus did not move anymore, there only subsisted a very slow variation of PAA and orbiter azimuth which corresponds to the orbiter's movement across the horizon. But this does not explain the sharp gaps in the telecommunication link's gain; Ir. Miguel Pérez Ayúcar is currently evaluating the possible influence of a multi-path, coming from a reflection of the radio signal on Titan's ground, and good correspondence with the AGC signal's shape has been found[21].

Assuming that the probe remained roughly horizontal during the major part of its descent[22], the long timescale variation of PAA due to the orbiter's motion across the horizon during the duration of the mission can be easily deduced from geometrical transformations since we exactly know the probe and orbiter positions at every moment. This yields the following PAA variation during mission. It is very slow compared to the spin movement and

[21]See Lebreton J.-P. et al., Huygens descent and landing on Titan: Mission overview and science highlights, Nature, submitted may 2005.

[22]The angle of attack has been taken into account at the beginning of the descent; its rapid variation until the probe vertically hangs under the parachute causes the rapid variation of the PAA at the beginning, until 2.5 mn after T_0.

the resulting mean gain variation, represented by the red line on the AGC signal graph, corresponds to the variation of the antenna's gain with link direction elevation presented in the introduction.

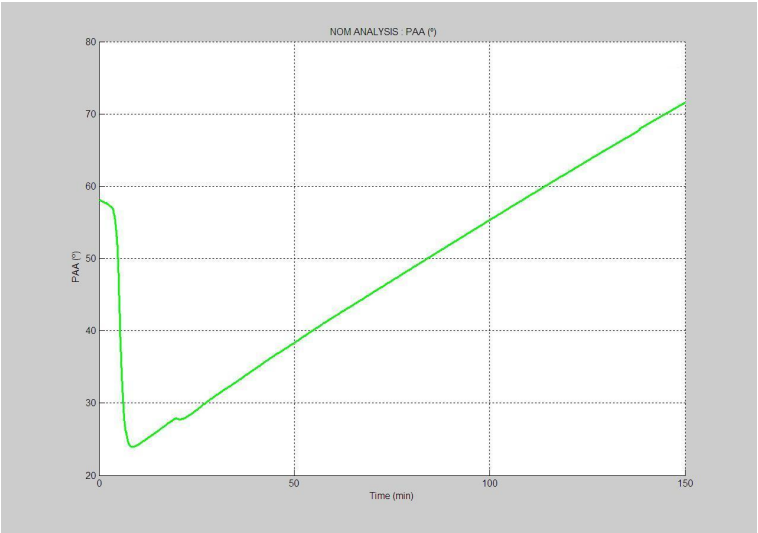

FIG.36: *Evolution of the Probe Aspect Angle during mission. Time is given in minutes after JPL-ESA interface time; this is roughly 4.5 minutes before* T_0.

Going on in that way, we plotted the azimuthal antenna gain variation for all different constant PAA values and found a very satisfactory match of the AGC signal observed at a certain moment with the azimuthal antenna gain pattern corresponding to the PAA of that moment. As an example, *figure 37* shows a zoom on the AGC signal observed about 5800 *s* after T_0, which corresponds to a PAA of about 56 *deg*, to be compared with the azimuthal antenna gain variation represented below for that PAA.

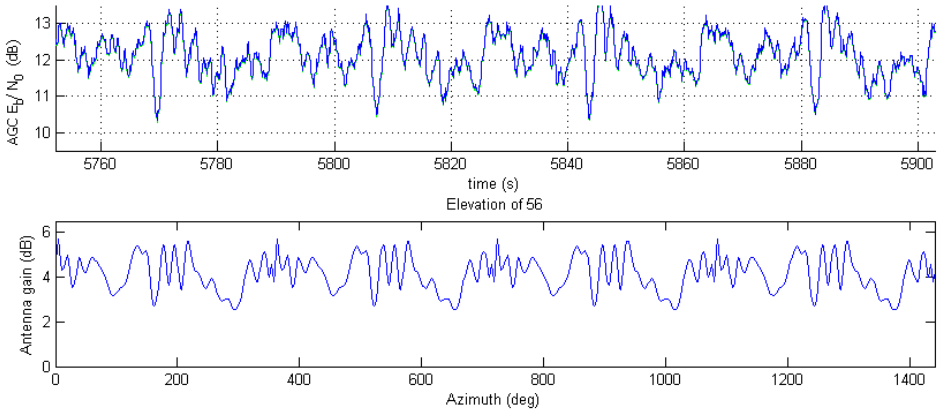

FIG.37: *Example of the good agreement between the observed AGC signal and the azimuthal antenna gain variation pattern for the corresponding PAA.*

We clearly see that there's a good agreement between the AGC signal observed and the use we want to make of it assuming a horizontal, spinning probe with only azimuthal antenna

gain variations. Differences between the observed curve and the theoretical curve for a strictly horizontal probe could be investigated for further information on Huygens' attitude (despite there's a significant noise and atmospheric effects are certainly interfering).

Now let's turn to the spin direction issue; indeed, it should be possible to infer the spin direction from the AGC signal shape. We cannot directly study what happens at the moment of the spin annihilation because at this time, the AGC signal varies so slowly that noise and attitude effects dominate its shape and make it incomparable to the ideal azimuthal AGP variation, but we have AGC time signals for the phases before (although just a few cycles were made during the short time between the start of the relay link to Cassini, 50 s after T_0, and the assumed spin reversal which would take place between 450 and 700 s after T_0) and after this assumed rotation direction inversion.

Examining a representative sequence from the AGC signal, we actually observe the apparent motion of Cassini in probe reference frame. If the AGC indicates a positive evolution direction, this means that Cassini's apparent movement with respect to the antenna (thus the probe) is counterclockwise as seen from above, meaning that Huygens was rotating clockwise as seen from above; the inverse observation leads to the opposite conclusion.

As the probe was ejected from Cassini (and supposed to spin during the entire descent) with a counterclockwise rotation as seen from above, Cassini's apparent movement for the probe's antenna should be clockwise. So let's try to fit the **inversed** AGC signal at the beginning of the link with the theoretical pattern for the corresponding PAA of 40 *deg*.

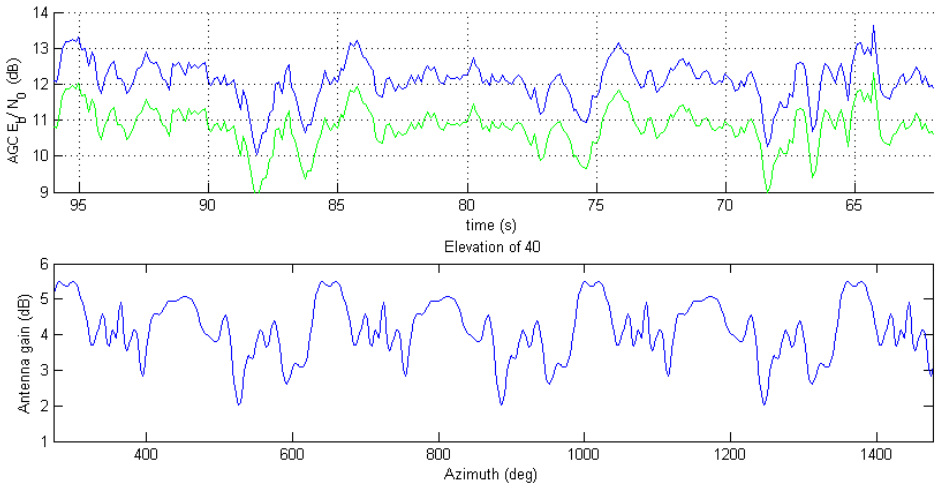

FIG.38: *Comparison between the* **inverted** *AGC signal at the beginning of the descent and the azimuthal antenna gain variation for a PAA of 40 deg.*

The good correspondence is obvious and allowed an easy superposition of initial point and period. This first result showing that the probe was rotating counterclockwise at the beginning is not surprising but totally independently confirms all our other information. To provide more redundancy on the comparison, we want to investigate the behaviour after spin annihilation for the same PAA[23]. So taking the antenna gain pattern for a PAA of 40 *deg* again, we directly see that the AGC signal at the corresponding time after spin annihilation, which

[23]By chance, this is possible for the particular configuration of the Huygens mission where the spin annihi-

is around 3000 s after T_0, does not have to be reversed to show an indisputable similarity. Thus, the probe was effectively spinning the other way, which means clockwise, after spin annihilation.

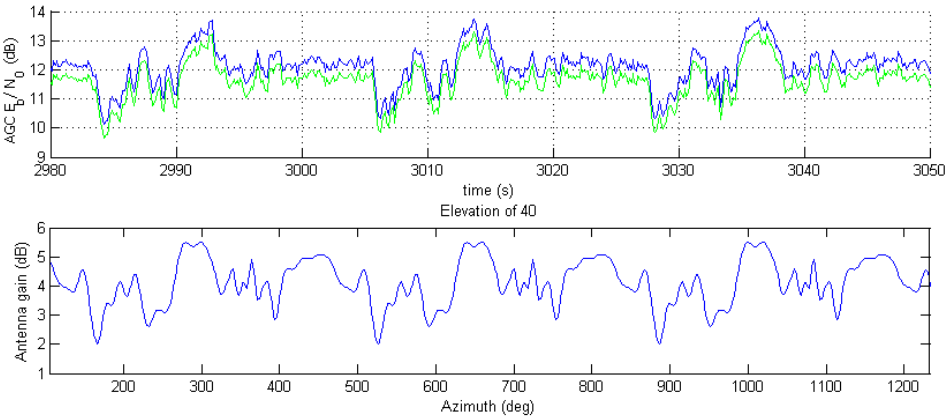

FIG.39: *Comparison between the* **non-inverted** *AGC signal at the end of the descent and the azimuthal antenna gain variation for a PAA of 40 deg.*

It is even seen more easily when directly comparing the two AGC samples, before and after spin annihilation, that they fit best when one is reversed with respect to the other.

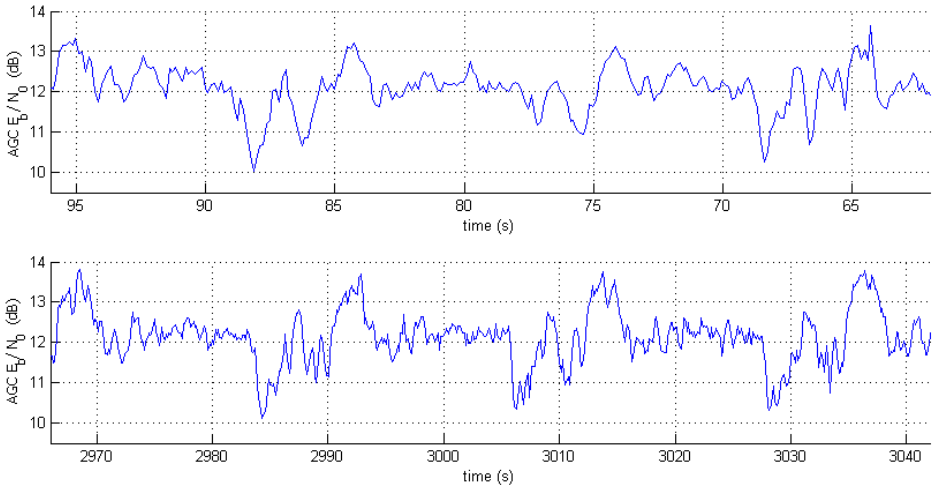

FIG.40: *Comparison between the* **inverted** *AGC signal at the beginning of the descent and the* **non-inverted** *AGC signal at the end of the descent for the same PAA.*

This provides the ultimate evidence: **the Huygens probe was spinning counter-clockwise (as seen from above) when ejected from Cassini, during coast and entry phases and at the beginning of the descent. A torque to be identified then slowed**

lation point lies before the PAA minimum when Cassini passed at its highest point above Huygens' horizon (see *figure 38*); as a result, the PAA was decreasing when it passed 40 *deg* at the beginning of the descent and through the spin annihilation phase, and passed 40 *deg* again while increasing after spin annihilation.

down the spin movement very rapidly until annihilation and reversal, triggering a spin motion in clockwise direction (as seen from above) for the rest of the descent phase under both parachutes.

7.3 Looking back to the SM2 test flight

Now that we were sure that the Huygens probe made a spin reversal to rotate in a clockwise direction during its descent, the major question to be answered was: why??

Checking the plans of the Huygens probe, the spin vanes were oriented in order to induce a counterclockwise spin motion, so parachute-induced anomalies, torques due to instruments' protuberances, an improper behaviour of the probe during its Titan mission,... were suggested to explain that anomaly.

A routine check was of course to try to know how the probe was spinning during the SM2 test flight; remembering the unexplained reduced efficiency of the spin vanes, we thought that the hypothetic unknown secondary torque which was responsible for this effect may have taken much more relative importance in the actual mission's flight conditions, surpassing the spin vanes' effect in order to induce spin reversal. Considering the instrument protuberances hypothesis, we noticed that SM2 had no HASI booms.

We already saw that no spin annihilation, and thus no reversal, occurred during the SM2 test flight; this seems quite natural since the probe was released without any initial spin, so that it would directly start spinning in the preferred direction, whatever it may be. According to axes definitions, the positive values measured by the gyroscope (see chapter 3, *figures 15 and 17*) would indicate clockwise rotation (thus spinning the wrong way!); however this conclusion is dangerous since a simple inversion anywhere on the way from the probe's dynamics to the dataset we finally got would lead to wrong results. A trial to use the $Y-$ and $Z-$ axes accelerometers in order to obtain radial and tangential accelerations to independently check this result had to be abandoned, no such clearly dominant accelerations being found when combining their measurements according to their location and orientations.

The only remaining sources of information to infer the probe's spin direction were the very short video sequences recorded during the test flight to verify proper separation processes. The reduced video sequences at our disposal last only a few seconds around the three events: back cover separation, front shield release and main chute jettison.

According to the flight sequence and the fact that the rotation movement was induced by spin vanes mounted on the fore-dome, no significant spin motion should have taken place before front shield release. This means that zero spin had to be observed in the first excerpt, a starting spin motion in the second and an ongoing spin motion in the third.

Looking at the sky for the first and third separation, it seems difficult to find adequate reference points to infer the probe's motion, especially since the beautiful spring morning in Sweden provided an entirely blue sky. A small white point was found to be related to a fixed reference frame, but the other probe motions made a reasonable spin deduction from this observation impossible. During front shield release, the Earth's surface could not easily be seen because of some fog and very intense solar irradiation on the camera; a relative rotation of the front shield with respect to the probe could not be made out during this too short video excerpt. Returning to the upward-looking camera, probe motion was tried to be inferred from the behaviour of the ejected parachutes, their wires and other ejected parts. However, aerodynamic flow effects were clearly dominant on these particles which followed

very different and clearly wind-induced paths.

Damning the sun for its blinding effect on the downlooking camera, the final solution came up: as suspected, a sun ray was visible on the uplooking camera as it is on most pictures taken on sunny days; our brain is simply so used to that vision that it automatically made abstraction of that feature. Now having another look at the last video sequence, we clearly identified that the sun ray was slowly but regularly moving clockwise on the screen. Knowing that in reality, the sun should be fixed and the probe moving during these few seconds rather than the opposite, after the following deduction sequence

$$SUN_{wrt}PROBE_{(uplooking)} = -SUN_{wrt}PROBE_{(downlooking)} = -\left(-PROBE_{wrt}SUN_{(downlooking)}\right) \ ,$$

we could conclude with absolute certainty that the SM2 model was also rotating **clockwise** as seen from above, the opposite of what was wanted and supposed to occur. So the cause of the spin direction anomaly observed during the Huygens mission was actually already present and showed its full effect during the SM2 test flight.

Surprisingly, absolutely no comment was made in the SM2 reports (see [15], [14], [17] and [5]) about the spin direction. We guess that the probe was simply assumed to rotate in the right direction; since a (nearly) acceptable rotation rate was observed, what indeed could have led to a wrong spin direction? The anomaly on the X-axis gyroscope, if detected, would obviously have been attributed to a sign reversal on the measuring instrument.

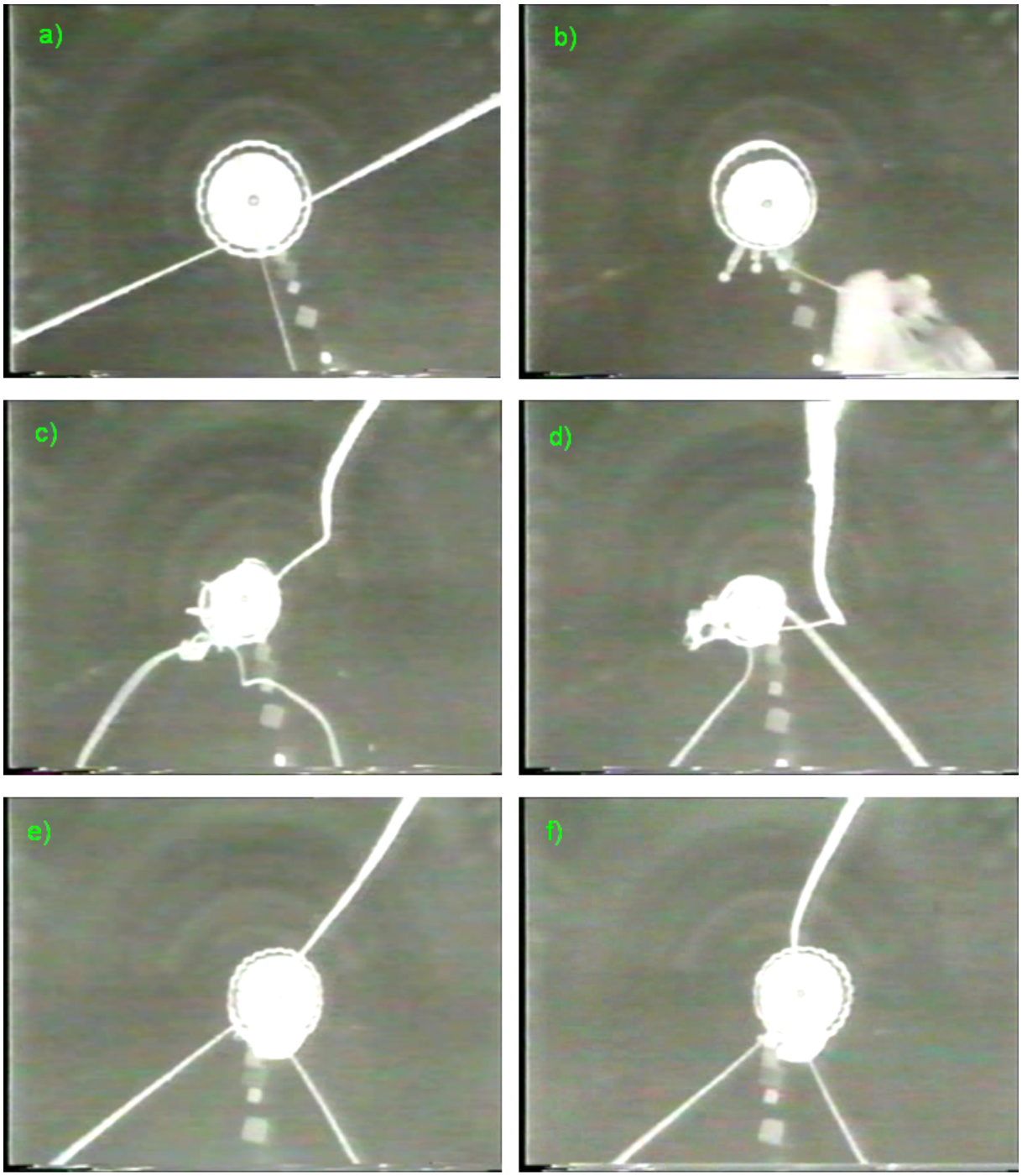

VID.1: *Extracts from the SM2 uplooking video camera recording during main chute release at successive times.*

7.4 Searching for the reason of the Huygens spin direction anomaly

As after reversal of the rotation direction, the spin rate profile follows the predicted curve quite well (however, remember the uncertainty on this curve since much reduced spin vane

efficiency compared with initial assumptions was observed during the SM2 test flight) and after the observations made on the SM2 data, the most straightforward answer to the question of what suddenly caused this spin reversal and previous sharp slowing down seems to be that the spin vanes were mounted in the wrong way. This sounds quite incredible! Even more when you know that the plans show a correct orientation with respect to the expected effect.

To verify the spin vane orientation, as all flights to Titan were overbooked, we turned to the SM2 model (which also rotated in the wrong direction) stored at an ESA facility a few kilometres from ESTEC. The following pictures were taken as a proof of our statement that the spin vanes were indeed **correctly** oriented[24].

[24]Some vanes had been damaged by the landing, but those could easily be identified and excluded from the measurements.

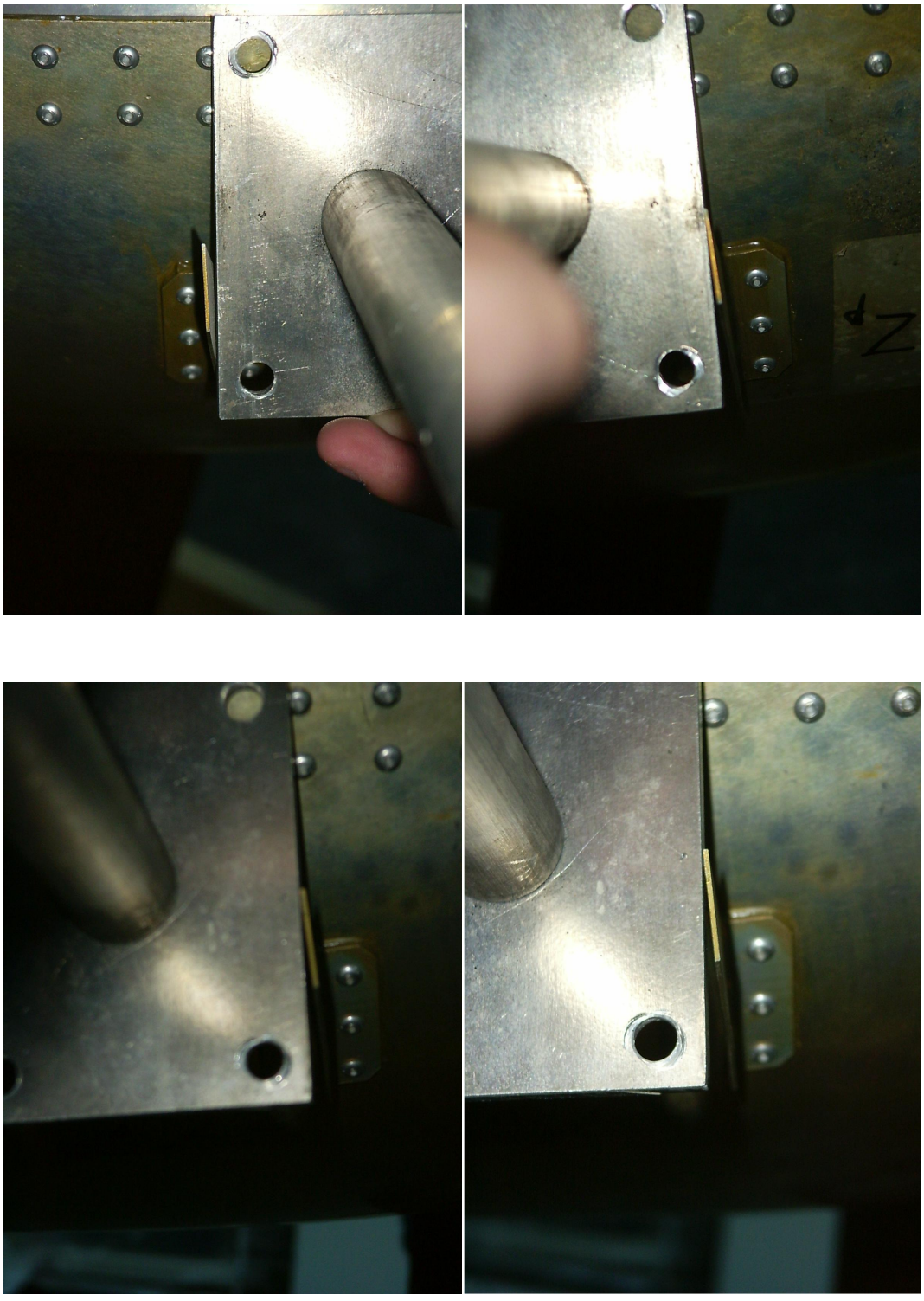

FIG.41: *Pictures taken during the spin vane measurements on SM2.*

This leads to a major problem in the comprehension of the phenomenon. At least, it shows that there had to be another motor torque than those considered for the preliminary

design; the "reduced efficiency" of the spin vanes observed during the SM2 test flight gets a totally different meaning as, if they were behaving as expected, they would have slowed down the spin motion. But what could be the reason of this Huygens spin anomaly?

Was there an additional motor torque due to slight irregularities, not identified so far? In that case, what could it be that had the same effect on SM2 and the newly built and differently instrumented Huygens probe? If the swivels unexpectedly blocked and the parachutes' motions caused this effect, what a chance would it be that not only the same torque direction was observed on both main chutes and both stabilizer chutes (the last ones additionally being of different design, single and double gap, on SM2 and Huygens) but also the same spin rate evolution as under the static spin vanes is observed, although the parachutes change during the descent; furthermore, under recovery chute where no swivel was incorporated, the SM2 probe was not steadily turning in the same direction but oscillated from one direction to the other, as would happen under torsion of the suspension cable; this seems to indicate that the parachute rather tends to damp spin motions than to act as a rotation motor.

Another possibility could be that the effect of the spin vanes was not understood in a proper way; this could be either directly their aerodynamic effect, or the air flow around them under full flight conditions, or even a perturbation induced by the spin vanes on the flow in order to generate other aerodynamic interactions on the probe leading to an inverse spin direction. This hypothesis which seems quite plausible but questions the whole pre-flight spin vanes analysis is further supported by the fact that increasing the spin vanes' incidence after the SM2 test flight effectively led to an increased spin torque efficiency, the spin rate during the mission being very close to the predicted curve under stabilizer (and not 2 times lower as for SM2). Thus, increasing the spin vanes' incidence angle seems to increase the efficiency of the dominant motor torque.

Or is this difference due to a reduced tilt with respect to the SM2 test flight? This might result (how and why should be investigated) in an enhanced motor torque, or simply reduce the spin vanes' efficiency and thus reduce the braking torque due to their predicted effect. This last hypothesis could be supported by the fact that for the SM2 flight, the spin rate was mainly slowed down under stabilizer chute, where the probe's stability was significantly reduced and the resulting tilt should have increased the spin vanes' efficiency. But the wrong spin direction can also imply that previous deductions about the spin vanes are wrong; for example, it might be that the efficiency of the spin vanes is actually reduced when the probe is tilted but that when performing the test on the entire probe[25], the reduction of their braking effect with respect to the unidentified dominant torque led to higher spin rates when the probe was tilted.

To properly rule out some possibilities and select investigation issues, we should know what aerodynamic simulations and wind tunnel tests were actually carried out by industry: were probe models used? If yes, how detailed? How was the flow defined? Did they maybe forget to check the direction of the induced torque? Could it be that the spin vanes intrinsically have another effect, or is the flow perturbed at their vicinity under flight conditions? However, it is most probable that the responsible industrial partner itself will carry out this analysis and communicate the obtained result. Anyway, the reasons for which the probe spun in the wrong direction were not included in the present study.

[25] We do not know if this was the case; further information from industry would be required to conclude.

8 The spin rate and azimuth (part 2)

After having addressed and solved the problem of the spin direction, we can eventually have an accurate idea of the azimuthal behaviour of the Huygens probe. To precisely determine the spin rate, we will make even further use of the AGC signal on which this movement was so clearly visible. In fact, we will rather provide the absolute azimuth of the probe at each time, which is much more useful, and hence be able to easily deduce the spin rate as an accessory information.

8.1 Determining the ground azimuth of the Huygens probe from the AGC signal

The rationale for deriving the probe's azimuth from the AGC is the following. If we have been able to match, at least at certain places, the observed AGC signal to the gain curve for the corresponding PAA, it should be possible, knowing the exact evolution of the PAA along the mission, to operate this fitting for all times with an evolving (according to PAA) gain pattern. Since each position on the gain curves corresponds to a particular antenna azimuth, this would actually relate time to the azimuth of the probe-to-orbiter link in antenna reference frame.

As the positions of probe and orbiter are known very accurately, the probe-to-orbiter direction can actually be considered as exactly defined for all times in an "absolute" reference frame (we will choose it with respect to Titan). Thus, the azimuth of this direction in antenna reference frame characterizes the orientation of the reference frame rather than the orientation of the link direction; in fact, we finally obtain the azimuthal orientation of the antenna - and hence of the Huygens probe - at each moment by a simple geometrical transformation.

8.1.1 Azimuth of the link direction

The first step of the method is to derive the azimuth of the probe-to-orbiter link direction as seen by the antenna; this means that we have to compare the AGC signal to the Antenna Gain Pattern.

A first problem encountered was that although the antenna gain pattern clearly repeats itself in the AGC signal, it can be quite different (and thus quite different from the ideal shape) from one cycle to the next one; the correspondence is far from always being as clear as in the chosen example. Some maximum or minimum peaks are missing, peaks are shifted or exchange relative importance, become wider or narrower,... under the effect of different perturbations (including maybe the effect of the sampling instants). An automatic analysis tool would have difficulties to accommodate with all these perturbations.

In addition, we have to take into account the varying (and *a priori* unknown) frequency at which the AGP pattern is "played" on the AGC and the variation of the actual azimuthal AGP variation pattern to be considered when the PAA changes. In practice, an automatic process could not be used to superimpose the rather idealized, "theoretical" antenna gain pattern on the perturbed, "experimental" AGC signal.

We consequently had to choose a manual treatment. It consisted in identifying one particular point (in fact the first deep minimum which can easily be seen on *figures 37 to 40* describing the spin direction) of the azimuthal Antenna Gain Pattern on each period of the

AGC signal and determining its position in time, even if this peak was deformed or missing, in which case an examination of the whole signal during the period usually allowed easy deduction of the missing peak's position. We will call this point the **peak** from now on, although it was not a clearly dominant extremum during the whole descent.

In fact, as the PAA changes between 24 *deg* and 72 *deg*, the shape of the peak which was initially identified also changes. This is illustrated on the following *figure 42* showing the "theoretical" antenna gain pattern for different PAAs; the step of 2 *deg* used in its variation corresponds to the step available from measurements; thus, we see all the discrete information at our disposal for the antenna gain pattern reconstruction.

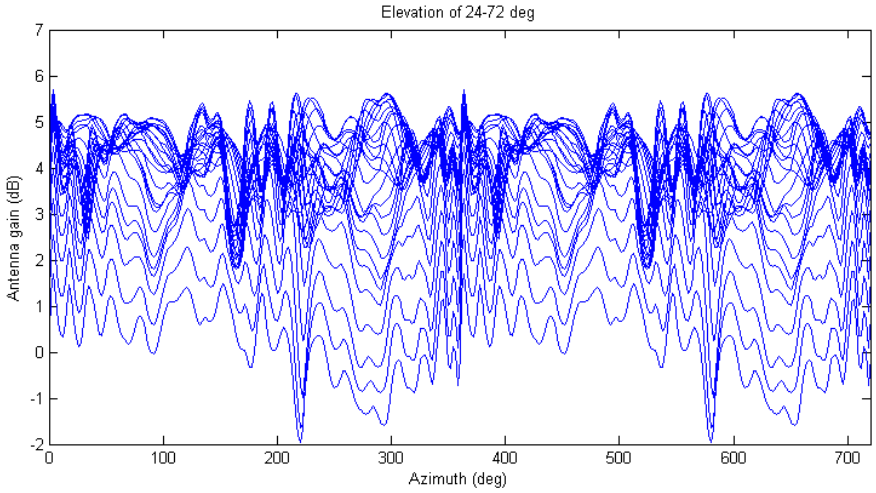

FIG.42: *Evolution of the azimuthal antenna gain pattern with Probe Aspect Angle (evolving from 24 deg at the top to 72 deg at the bottom of the diagram).*

The position of the extrema is progressively shifted, so that a `AZPEAKvPAA.TXT` look-up table had to be made with the azimuth corresponding to the used peak as a function of PAA; this had also to be constructed manually and represents the second and last manual intervention in the data processing.

The necessity of a manual treatment becomes more clear as the PAA increases and the peak initially used nearly disappears, becoming an average irregularity in the antenna gain's azimuthal evolution; it now requires much attention to recognize the peak on the AGC signal and the evolution of the antenna gain pattern with PAA had to be clearly visualized to see how the initial peak continuously evolves. Even considering the help of other peaks, for some values of the PAA, the pattern seems quite clear and a recognition routine could be easy to implement but for others this task turns out to be much more complex; for example, as the amplitude and position of the minima and maxima of the AGP pattern change, some clear peaks exchange their roles (a big one becoming small and vice versa) over a few revolutions.

During our manual analysis, to provide regularly spaced time-steps, it was avoided to jump to other, more easily detectable peaks for building the `PEAKTIME.TXT` table; however, we cannot deny that the latter were actually used to visualize the signal's evolution and help locate the weak, initially chosen peak. The number of turns between two consecutive peaks was also indicated in `PEAKTIME.TXT`, to represent the spin direction and to allow skipping one peak if its position was too unclear.

Using the known variation of PAA with mission time, we can combine the two tables `PEAKTIME.TXT` and `AZPEAKvPAA.TXT` and get $Ant2Orb_{az}$, the azimuth of the telecommunication link (=orbiter) with respect to the antenna reference, at given instants; according to document [11], the antenna reference coincides with the probe $Y-$ axis.

During two timeslots, the peak identification failed; those concern

- the zone of spin reversal: the signal slows down so much (*i.e.* the azimuthal antenna gain variation signal is so dilated, in fact infinitely at the spin annihilation point) that the actual "peaks" become slow variations of a highly perturbed average curve; furthermore, they become very seldom since the probe rotates very slowly. Extrapolation was very difficult at this place where the spin rate variation is also significant. However, though this gap in our data analysis lasts from 340 s to 940 s after T_0, only a few revolutions are concerned. A particular problem concerns the spin reversal. Indeed, there has to be a period during which no full rotation is made but the signal reverses at a certain time; this cannot be rendered using a simple interpolation between two peaks, but as anyway we do not have any reliable data the problem cannot be solved;

- the zone of maximal spin rate around 1300 s after T_0. As no particular PAA could explain those difficulties, it led us to suspect that a too low AGC sampling rate could be their cause and thus also play a significant role on the deformation of the signal, particularly the steep peaks, at other times. Another cause might be strong attitude perturbations since the probe was very unstable during this period.

For these periods, a "best-guess" peak position was derived, manually interpolating nearby spin rates, using the spin rate from FFT analysis,... . As those are actually not measurement data, they should be discarded: an error of ± 180 *deg* has been attributed to their value and the corresponding data has been marked in red, as inaccurate, in the Excel files.

8.1.2 Error evaluation on the link direction azimuth

The error on the regular data (*i.e.* where the peaks were clearly identified) comprises the following contributions.

- Uncertainty on the exact position of the peak on the antenna gain pattern for each PAA: the measurements of the AGP carried out by SAAB industries used a 2 *deg* step in azimuth direction, leading to an uncertainty on peak localization of ± 2 *deg*.

- Peak localization on the AGC signal on screen during the manual identification: this error could be reduced if needed. The choice of 5 periods on a 1000 pixels screen made by the operator implies about 200 pixels per rotation (let's say 180 to take into account the margins of the figure) so that we have 180 points for 360 *deg*, thus leading to a positioning error of maximally: ± 2 *deg*.

- PAA evaluation error: the same 2 *deg* step was used in elevation direction by SAAB industries, providing the azimuthal AGP for PAAs separated by 2 *deg*. As a maximal azimuthal shift of 2 *deg* (one point) on the peak's position can occur from one PAA to the next one, the error on azimuth due to a discrete PAA knowledge is ± 1 *deg*.

- Time resolution of the AGC signal: 8 Hz provide 8 samples per second, or $(8 \cdot Rot.Per.)$ samples per turn of 360 *deg*, leading to an error of $\pm \dfrac{180}{8 \cdot Rot.Per.}$ *deg*.

Remark: it is easily understood that, depending on the evolution of the signal, the exact position of an extremum could be anywhere between the three extremal points. Thus, the uncertainty on the position of a peak due to sampling should include a full sampling step of 2 *deg* in both directions; this has been done for the first two terms of the error. The other two uncertainties, concerning the resolution in *PAA* and in *time*, which evolve continuously, can just consider the classical half-step round-off error in both directions.

As all those contributions are independent, a root-of-squares estimator has been computed. As the numerical value of the last term depends on the actual spin rate, we cannot give any value for the error in this report. In the Excel file containing the peaks' times and azimuths, the error on their value is given in a separate column. It does never exceed ± 5 *deg*.

8.1.3 Ground azimuth of the probe

By "ground azimuth", we mean the azimuth of the Huygens probe with respect to Titan's ground, which is with respect to East in a reference frame located on Titan's surface, vertically under the probe.

Once we have determined the azimuth of the orbiter as seen by the antenna, deriving the absolute azimuthal orientation (or ground azimuth) of the antenna requires a simple geometrical transformation using the positions of the orbiter and the probe. Those, provided by the DTWG for Huygens and by JPL/nav for Cassini, are very accurately known.

Using MatLab, we expressed the probe-to-orbiter link direction in the reference frame corresponding to the surface of Titan under the probe's location; this reference frame is equivalent to Huygens' one if its X_P- axis was perfectly vertical. The method we use makes the assumption that the probe is horizontal at every moment.

Remark: in fact, we do not have accurate information (yet) on the instantaneous tilt of the probe, so that this is currently the only possible way to proceed. In reality however, the probe does not remain horizontal during the whole descent but oscillates according to both pendulum and coning motions; as it turns the antenna with respect to the orbiter and to Titan vertical, this has an impact on the azimuth deduction from the AGC which must be studied in section 8.1.4 dedicated to the error estimation.

From this, we readily obtain $Abs2Orb_{AZ}$, the azimuth of the orbiter with respect to Huygens in Titan ground coordinates; subtracting $Ant2Orb_{az}$, the relative position of the orbiter with respect to the antenna reference (which coincides with the Y_P- axis of the probe) that was presented in the previous section, we finally get the orientation of the Huygens probe with respect to Titan's ground coordinates by the simple formula

$$Abs2Ant_{AZ} = Abs2Orb_{AZ} - Ant2Orb_{az} \ .$$

Since all the data at our disposal is discrete - having the time and azimuth of one peak per rotation, the position of the probe and orbiter at different times and the antenna gain variation at different angles separated by 2 *deg* - interpolation had to be used to obtain intermediate values. In particular, the azimuth of the probe should be provided at every time instead of once per rotation when a peak is encountered.

As variations are not supposed to happen rapidly on those data, but irregularities may appear at longer timescales, we thought that it would not be a good idea to include many successive samples to construct a smooth interpolation curve. Since it additionally is simpler

and thus faster, linear interpolation has been used between 2 consecutive samples for all calculations; this requires that the provided data is

- sufficiently tightly sampled to avoid large interpolation errors and
- covers most of the used range (since linear extrapolation usually gives inaccurate results).

The resulting probe azimuthal orientation as a function of time, given with respect to local East, is computed assuming a linear variation of the azimuth between two successive peaks, thus at a constant average spin rate, so that strong spin changes during a single period could induce some errors (but still in a very acceptable range to characterize in which direction an experiment was looking). Such variations did not appear during the Huygens mission, except in the two zones where we anyway already had problems to usefully characterize the AGC signal; the way of enhancing this "sampling rate" for other missions where significant perturbations would lead to a poor accuracy using linear interpolation between consecutive peaks, would be to pick out two or more different peaks per cycle; this however would require much more work since every peak would have to be identified manually along both the AGC signal and the azimuthal antenna gain variation pattern.

Before going on, we want to emphasize the big advantage of the direct azimuth deduction using the AGC signal.

It is widely known that if we used spin rate integration to deduce the probe's azimuth, the accumulation of errors on prior times would lead to a significant uncertainty on the orientation of the probe at later times; in fact, after a certain time, this uncertainty could become larger than $\pm 180\ deg$ so that no information at all would be obtained. Imagine the impact of the huge uncertainty about the results during the two critical timeslots on such a method: how could we ever recover from the largely unknown orientation at spin reversal and the many rapid cycles?

The immense advantage of the "manual AGC method" is that, using no integration to compute the azimuth, it presents no bias of that kind: at each peak identification, the azimuth of the probe is known with the same good accuracy, the error being proportional to the quite small[26] peak location uncertainty. The azimuth of the probe being linearly interpolated between the consecutive peaks, no significantly higher error should be made since the probe's inertia and the absence of strongly varying torques prevents rapid spin rate oscillations which could lead to an irregular azimuth evolution.

A problem subsisted to characterize the orientation where peaks are difficult to locate, especially around the spin annihilation which occurs for an unknown azimuth, but as soon as we identified another clear peak, full accuracy was recovered for subsequent azimuth determinations.

8.1.4 Error evaluation on the ground azimuth

As the ground azimuth computation directly uses the peak data obtained in the previous section and the positions of Huygens and Cassini are known with a very good accuracy, the

[26] Without considering errors due to deviations from our assumptions, to be discussed later in the next section.

basic error on the ground azimuth of the peaks is the same as the error on the azimuth with respect to the orbiter.

But, as we made the - definitely wrong - assumption that Huygens remained horizontal during the whole descent, there is one important additional uncertainty which concerns the tilt of the probe. The effect of a non-zero tilt strongly depends on the tilt direction with respect to the telecommunication link.

The first problem of such a tilt is that it changes the Probe Aspect Angle with respect to its value when the probe is horizontal. Indeed, in this last case the PAA is simply the complement $\frac{\pi}{2} - El$ of the probe-orbiter direction's elevation above the local horizontal plane, easily computed from probe and orbiter coordinates. When an α *deg* tilt is considered, the actual PAA takes values between $\frac{\pi}{2} - El - \alpha$ and $\frac{\pi}{2} - El + \alpha$, depending on the tilt's direction with respect to the telecommunication link.

The quantitative impact of such a change in PAA mainly depends on the way in which the azimuthal antenna gain pattern changes as the PAA varies. The perturbations on signal shape are not so important, since it is up to the user to manually identify the peak using a sufficient resemblance between the observed signal pattern and a "theoretically idealized" antenna gain pattern; but if the same peak slightly (or more brutally) shifted position when changing the PAA, this position shift would have to be accounted for.

For the Huygens case, the extreme values for the azimuth of the peak we used are 164 *deg* to 178 *deg*, for PAAs of respectively 54 *deg* and 24 *deg*. However, tilts of more than 10 *deg* absolutely had to be avoided for mission functional needs as parachute behaviour, cover ejections and the actual feasibility of the telecommunication link with a sufficient safety margin. In addition, do not forget that to actually obtain the maximum bias, the extreme values, observed when the tilt axis is perpendicular to the orbiter direction, have to be reached precisely at the moment of a peak measurement. In the extreme case thus, when all bad conditions add, meaning a precise synchronization of the peak measurements with extreme tilt values and a perpendicular tilt direction, a 10 *deg* change in PAA could maximally induce a ± 4 *deg* shift on the azimuth of the proposed peak; this is truly acceptable since it is roughly equal, for very worst case, to the uncertainty on $Ant2Orb_{az}$.

The second problem is a purely geometrical one, related to the fact that what is called azimuth depends on which reference plane is considered. This means that the orbiter azimuth seen by the antenna, related to the probe reference plane, when tilted is different than what it would measure if the probe was horizontal. As a consequence, we may not simply subtract angles to deduce the probe's absolute azimuthal orientation since these angles are defined in different reference planes:

- Orbiter azimuth seen by the antenna $Ant2Orb_{az}$: probe reference frame, tilted;
- Probe-to-orbiter azimuth $Abs2Orb_{AZ}$: local Titan reference frame[27], not tilted;
- Antenna reference = Probe orientation azimuth $Abs2Ant_{AZ}$: local Titan reference frame, not tilted.

One might have wondered why we used uppercase and lowercase letters to write the azimuth indices; this was made just because of the present problem: the uppercase (in Titan ground

[27]Meaning that this reference frame's vertical is defined aligned with the local gravitational attraction direction.

coordinates) and lowercase (in probe coordinates) angles are actually measured in different planes.

In addition, the antenna reference direction is actually not horizontal and the azimuth given in local planet reference frame would thus characterize its projection, which would not evolve exactly continuously even if the probe was spinning at a constant rate around its tilted axis.

A calculation showing how to correctly relate the different angles in order to obtain the absolute azimuth of the Huygens probe, in local Titan reference frame, has been worked out and is reported in Appendix B. The rather complicated formulas obtained are not reproduced within this report. To simplify the analysis, the common reference direction has been taken as the intersection line of Titan- and Huygens-related horizontal frames; when expressing the azimuths with respect to a fixed reference, you simply have to subtract the angle between tilt axis and local East before applying the formulas and add it again at the end.

The influence of different tilts on the characterization of different azimuths turns out to strongly depend on tilt direction, as expected, and also on PAA. Numerical simulations have been carried out to investigate the qualitative and quantitative effects. The results are shown in the following figures.

The first figures show the (absolute value of the) difference between the real probe azimuth, as it should be given using the formulas developed in Appendix B, and the result obtained when making the wrong assumption that the probe is horizontal. It includes both geometrical contributions. The error increases when different tilt angles are considered from top left to bottom right. We can also observe a strong variation of the error along the horizontal axis, showing that it strongly depends on the relative orientation of the tilt axis with respect to the probe-to-orbiter direction (*i.e.* strongly varying during coning motions), while spin movements (along the vertical axis) have much less effect. Notice that the error is minimal, actually zero, when the tilt axis is perpendicular to the orbiter direction; this can in fact easily be visualized. Interestingly, it indicates that the tilt orientation leading to a maximal geometrical error corresponds to a minimal error on PAA and similarly, a maximum error on PAA implies a zero geometrical error. This seems logical since changing the elevation and changing the azimuth of a point when a constant tilt angle is allowed are two complementary effects.

Last but not least, we notice that the error increases with decreasing PAA (or increasing link direction elevation). This can also be intuitively understood by considering a point at an elevation close to 90 *deg* and a point close to the horizon: by slightly tilting the probe, the high point could be seen at very different azimuths while the azimuth of the low one barely changes.

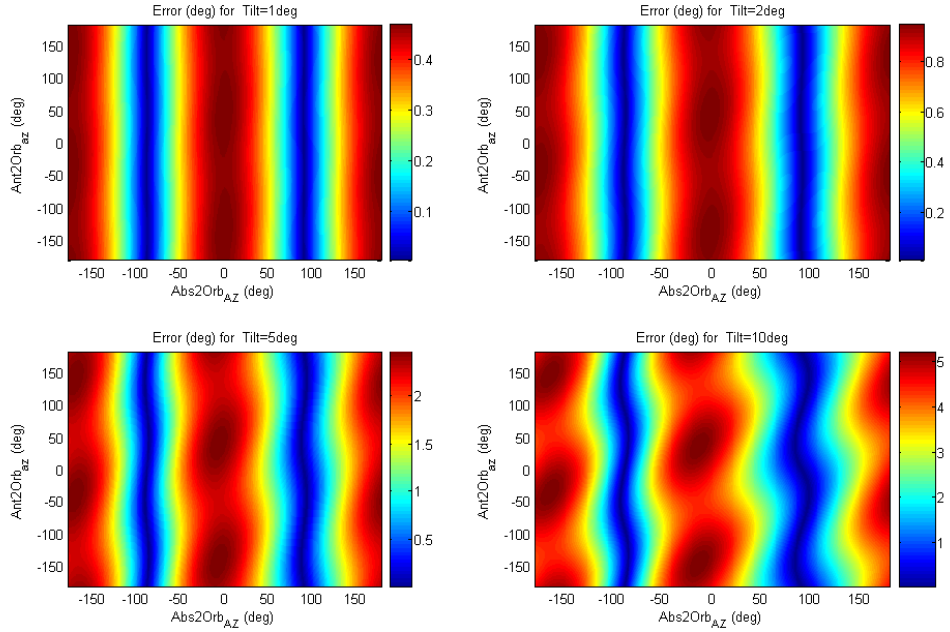

FIG.43a: *Error on the azimuth computation for different tilt angles, different orbiter azimuths measured by the probe's antenna $Ant2Orb_{az}$ and different link azimuths with respect to tilt axis $Abs2Orb_{AZ}$ for a link elevation of* **25** *deg.*

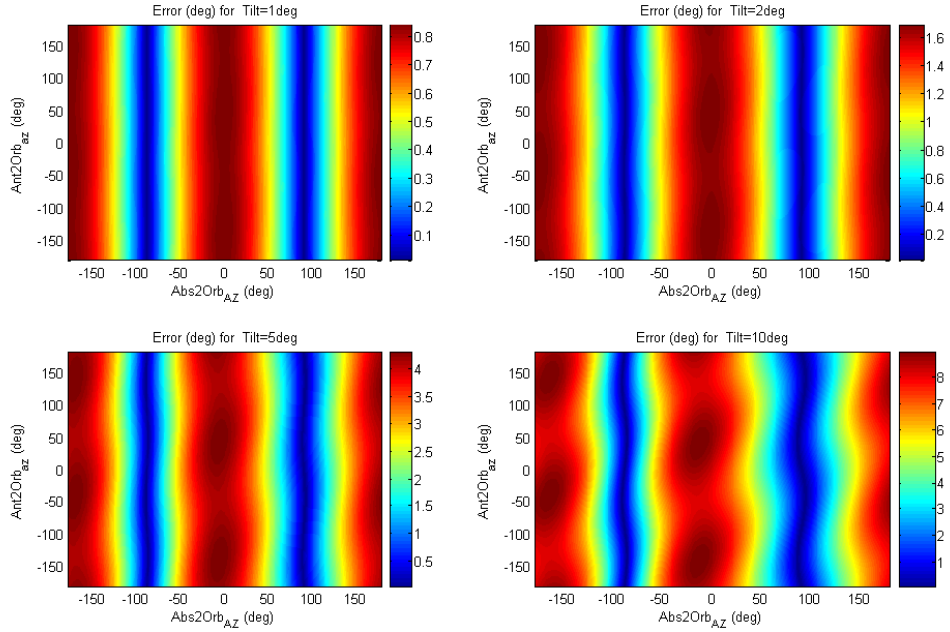

FIG.43b: *Error on the azimuth computation for different tilt angles, different orbiter azimuths measured by the probe's antenna $Ant2Orb_{az}$ and different link azimuths with respect to tilt axis $Abs2Orb_{AZ}$ for a link elevation of* **40** *deg.*

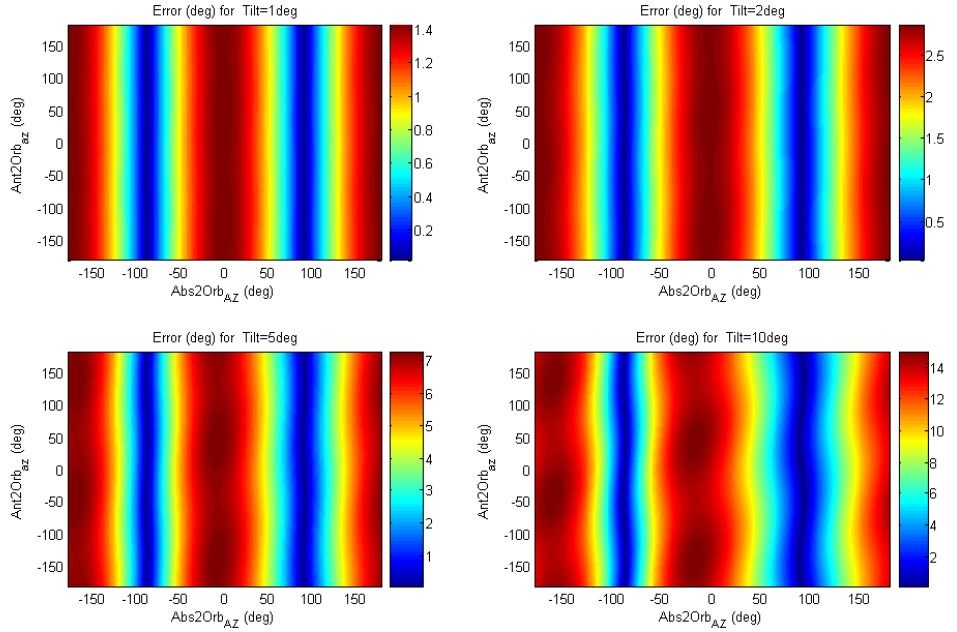

FIG.43c: *Error on the azimuth computation for different tilt angles, different orbiter azimuths measured by the probe's antenna $Ant2Orb_{az}$ and different link azimuths with respect to tilt axis $Abs2Orb_{AZ}$ for a link elevation of* **55** *deg.*

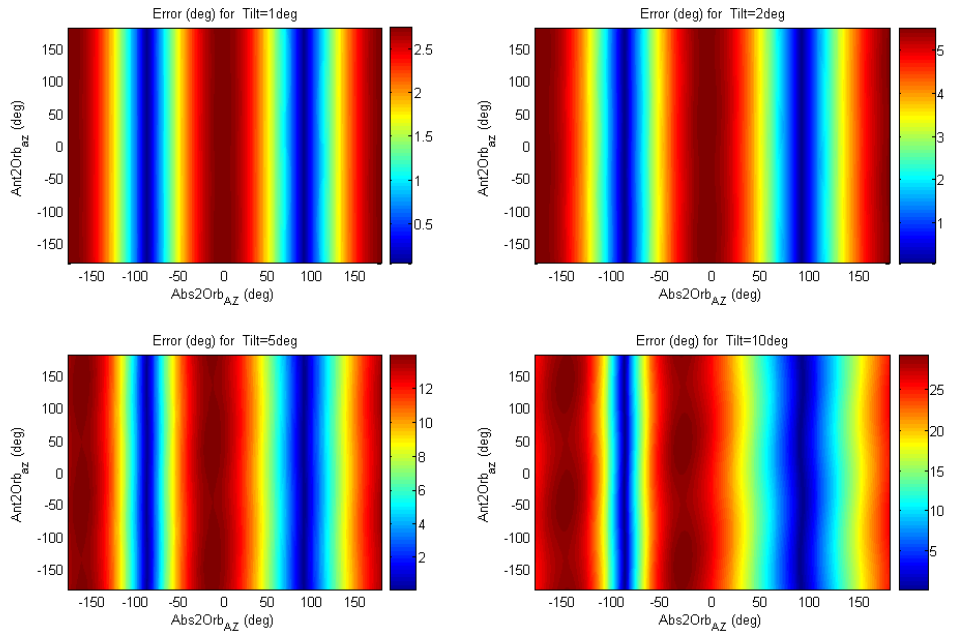

FIG.43d: *Error on the azimuth computation for different tilt angles, different orbiter azimuths measured by the probe's antenna $Ant2Orb_{az}$ and different link azimuths with respect to tilt axis $Abs2Orb_{AZ}$ for a link elevation of* **70** *deg.*

As a result of this investigation, *figure 44* shows the maximal error for different tilt angles as a function of the PAA; a random antenna orientation has been chosen as spin movements were seen to nearly not affect the error.

Very high error values are observed for a low PAA: at the maximal tilt of 10 *deg* certified for the Huygens mission, the error can reach up to ± 25 *deg* for the lowest PAA of 24 *deg*. Looking back to the evolution of PAA with mission time, we notice that the minimum PAA which would lead to this huge error is reached about 167 *s* after T_0; this is still under main chute, which is more stable than the stabilizer chute so that the extreme tilt values should not be reached; furthermore, the very low PAAs are only kept during a short period compared to the whole duration of the mission; the error indeed progressively decreases while the PAA increases towards the end of the mission, where it cannot be higher than 4 *deg*.

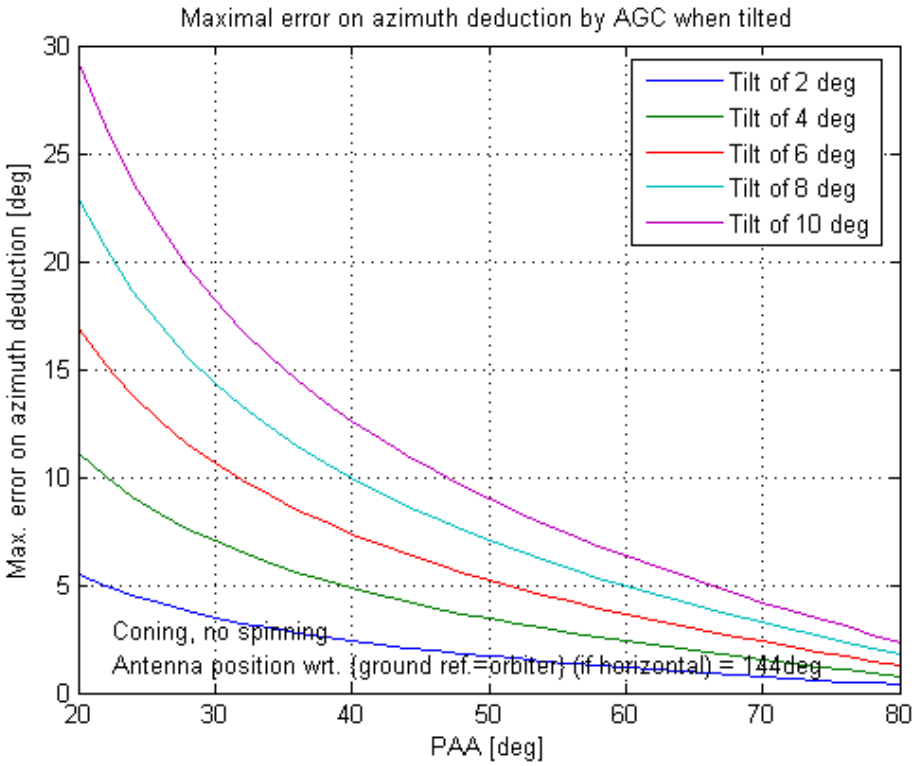

FIG.44: *Maximum error (for all possible tilt directions) on azimuth deduction that could be induced by a tilt of the probe as a function of PAA, for different tilt angles and a random antenna azimuth of 144 deg.*

We may thus be quite optimistic about a reduction of the geometrical error after having investigated the attitude issue, but at the present time we must still conclude that the contribution of the geometrical error is dominant, rather than negligible as we would like it, and that it can introduce a bias reaching from ± 25 *deg* about 170 *s* after T_0 to ± 4 *deg* at the end of the mission. However, it is most likely that the error will not be a constant offset but oscillates between the extreme values as the probe's attitude changes. For a pendulum motion with a constant favourable direction, it may even be very small.

If we knew the instantaneous probe attitude, we could correct the deduced probe azimuth from this bias to obtain more accuracy; however, as we will see, getting the same precise instantaneous information for the probe attitude as we did now for the azimuth is much less trivial, so that we do not have any reliable results whose incorporation could enhance the obtained azimuth precision. Furthermore, we can suspect that azimuth or spin information will be used (to remove their effect from the sensors' measurements) to determine the probe's attitude so that a parallel, iterative solving of both problems would be required if attitude aspects were included in the spin deduction. Whether such algorithm complications might be useful or not, strongly depends on what attitude information we will be able to deduce.

After having classified the attitude issue, we might maybe come back to these corrections and try to see whether

a) strong perturbations could effectively occur and significantly perturb the azimuth deductions and

b) it is possible to improve the results by including attitude information.

Moreover, if the investigation of the attitude issue shows large oscillation amplitudes during the maximum-spin timeslot[28], where we could not clearly identify the AGC signal, simulations of the Antenna Gain Pattern variations using the reconstructed attitude - if available at some time in the future - would maybe allow to watch this segment of the signal from a better point of view.

8.2 Deducing the Huygens probe's spin rate from the AGC azimuth analysis

The spin is a by-product of the ground azimuth knowledge; in fact, we already used sort of a spin rate when interpolating between two consecutive peaks. There are two possible methods to compute the actual spin rate of the Huygens probe from the manual peak count, depending if we consider the ground azimuth or the azimuth of the orbiter seen by the antenna. The deduced spin rates, during the periods where the peaks were clearly identified, should be much more accurate than what we had so far and in addition, the rotation direction is directly included.

8.2.1 Spin rate computed by the two different methods

As the number of rotations - usually one - between two successive peaks is precisely known, even without any orbiter information the spin rate could be approximated as

$$Spin[rpm] = \frac{60[s/mn] \cdot TurnNumber_{T_1 \to T_2}}{T_2 - T_1} \ ,$$

assuming that the absolute azimuth of two successive peaks was nearly the same. This means that the orbiter may not move about several degrees through the sky while the probe makes one rotation, including that the absolute azimuth of the orbiter may not change significantly

[28] Since the probe then descends rapidly and could thus experience bigger external perturbations, it even seems quite realistic that this would be the case.

and that the elevation variations (similar to PAA variations) may not induce a significant change in the peak's position.

The advantage of this method is that it provides a spin profile directly after peak identification on the AGC signal, even before considering the particular position of the peak on the AGP: the only information that is needed is the time at which we cross the peaks (and possibly the number of turns between consecutive peaks if it is different from one).

We will see a bit further that the methodical error on the spin rate due to the approximation that all peaks have the same azimuth is actually truly negligible with respect to other, unavoidable contributions.

The second, academically correct method considers the actual azimuth of each peak to compute the spin by the same formula as above where $TurnNumber$ is no more an entire number but a fraction, very close to one, that takes into account the really traversed angle between two consecutive peaks. The actual formula is thus

$$Spin[rpm] = \frac{Az_2 - Az_1(\pm 360\,deg)}{T_2 - T_1}\,\frac{60[s/mn]}{360[deg/rot.]}$$

and can only be implemented after having identified the peak azimuths on the PAA as a function of time and applied the whole geometrical transformation to obtain the probe's ground azimuth.

The 360 *deg* in brackets have to be added when, due to the *modulo* 360 *deg* definition of angles, the two peaks used for spin rate computation have azimuths that differ by nearly 360 *deg*.

The spin rate computed by those two methods, thus actually being an average spin rate over one period, was attributed to the middle of the interval used to compute it, in agreement with linear approximations.

8.2.2 Uncertainty on the spin profile deduced by these methods

Both methods used to compute the spin rate comprise two common error terms: the first one related to the uncertainty on the position of the peaks, the second one related to the uncertainty on turn number. Using a Taylor expansion of the formulas here above and replacing the uncertainty on the peaks' localization in time by the uncertainty on $Ant2Orb_{az}$ - as both results characterize the same basic uncertainty on the accurate localization of the peaks - by the formula

$$\Delta T = -\frac{\Delta Ant2Orb_{az}}{Spin} = -\frac{\Delta Ant2Orb_{az} \cdot (T_2 - T_1)}{360\,deg}\,,$$

we get

$$Err_{Spin}[rpm] = \frac{60[s/mn]}{(T_2 - T_1) \cdot 360[deg/rot.]}(\Delta Ant2Orb_{az_2} - \Delta Ant2Orb_{az_1}) + \frac{60[s/mn]}{T_2 - T_1}\Delta TurnNumber\,.$$

In the first term, $\Delta Ant2Orb_{az}$ contains the basic uncertainty component of the error on the azimuth. In the second term, $\Delta TurnNumber$, we may not include this uncertainty again, as the effect of the uncertainty on the localization of the peaks has already been considered. It

should rather contain the uncertainty on the number of turns which have been made between two hypothetically perfectly identified peaks. This error comes from the consideration of tilt influence, which was not present on the first azimuth. Remembering the maximum possible shift of 25 deg on a peak's position, we could be considering a period of 310 deg or 410 deg in place of the assumed ~ 360 deg. This implies a value of $\frac{50\,deg}{360\,deg}$ for $\Delta TurnNumber$ which makes it the dominant contribution to the uncertainty. However, it is most probable that this error is strongly overestimated, since an exact match between spin and coning motions to provide exactly a variation from maximum shift to minimum shift between two consecutive peaks would be needed.

Actually, since a single peak is shifted in the same direction for the computation of the preceding spin rate and for the computation of the following spin rate, there cannot be a steady bias on the spin rate: we would rather observe oscillations as we pass from peaks which are brought closer by the shift to peaks which are drawn aside. In fact, at least during the phase where peak identification succeeded, **all errors present on the deduction of the probe's spin using the second method are oscillations, no bias at all can be added by any inaccuracy or attitude influence in this method.**

This statement is not perfectly true for the first spin deduction method. Indeed, the shift induced by the motion of the orbiter goes in the same direction during the whole descent; in fact, we are constantly underestimating the number of degrees between two consecutive peaks while the probe is turning clockwise at the end of the descent and overestimating the number of degrees between two successive peaks at the beginning of the descent when the probe turns counterclockwise. The corresponding PAA variation does not imply a monotonous increase of the azimuth, but as the oscillation takes place over a very long time period (you could say the whole duration of the mission for one "period") it is also unfair to call it an oscillating effect. Both effects are superimposed in a slow variation of the peak's ground azimuth.

The impact of the orbiter motion on the spin deductions is expected to be very small, as Cassini is obviously moving very slowly compared to the spin period. The ground azimuth is varying from a minimum of -17.5 deg at $T_0 + 254$ s to a maximum of 10 deg at $T_0 + 6912$ s. This implies a difference of 27 deg over 6650 s and, assuming a typical spin rate of 2 rpm, an average error of $\frac{27\,[deg]}{6912\,[s]}/12\,[deg/s] = 0.03\%$ on the spin rate. I think that this is truly negligible.

Considering the influence of the PAA variation, we noticed that the PAA changes slowly with respect to the probe's rotation period (*i.e.* the probe makes several revolutions, or at least one revolution at the beginning, before the PAA has changed by one 2 deg step) and that the peak position variation when going from one PAA to the next one is always less than 2 deg, so that here also, no substantial change of the peak's azimuth can occur over a single period. The maximum error occurs while the probe's velocity vector is approaching vertical at the beginning of the mission; the quickest PAA variation can then shift the azimuth of a peak by about 2 deg during one single period so that the error due to this effect reaches the still very low maximum value of $2\,[deg]/360\,[deg] = 0.56\%$.

Thanks to this very little difference between the two methods, we can actually not make out the difference on the spin profiles computed by them. As the first one is much simpler, it is the one we recommend and use in the following spin rate discussion (although, as we just said, it makes no difference when talking about the results).

It is important though to be aware that, even if this spin rate is computed directly from

the $Ant2Orb_{az}$ data, its error includes all (oscillating) uncertainties about the real, ground azimuth of the probe since it is that one that should ideally be considered to derive an accurate spin rate by using the exact (non entire) turn number associated to the time interval between two consecutive peaks.

One important exception to this procedure would be if we got accurate instantaneous attitude data that show large perturbations on our azimuth deductions (see section 8.1.4). Indeed, this would allow to make the big contribution of maximally 25 *deg* to the error on the spin rate not uncertain anymore, but a determined difference between peak position and actual azimuth. The azimuth difference between two consecutive peaks would then become much larger than 2 *deg*, since the identified attitude variations would imply shifted azimuth positions in place of centred ones with high associated errors. In this case, the second method should be used to deduce an accurate spin rate. However, as we already said, the error on the spin rate induced by wrong azimuth positioning can only be alternating, so that using the second method would just remove the artificial oscillations on the spin rate computed with the first one[29], the average, smoothed spin profile always being the same (to the accuracy of the very little error associated to orbiter motion and PAA peak shift).

8.2.3 Comparison of the AGC-azimuth spin profile to the previous results

As what concerns the absolute azimuth of the probe, no other information is available to verify the results provided by the AGC peak method; but that is what makes this method so interesting: **it is the only engineering method capable of providing the absolute orientation of the Huygens probe at any moment (well, except during the two small timeslots where the method failed) during the descent, limiting the error by periodical recalibration at each identified peak.**

But the spin profile(s) that we have just been discussing can, and should, be analyzed in comparison with the previously provided ones.

To do this, we first have to show the spin profile resulting from the AGC peak count method; since the associated error could be evaluated, minimum and maximum values are also plotted. The narrower uncertainty interval only considers the basic error, while the larger one includes the effect of a possible tilt, which has to be considered unknown until useable attitude data are available (remember that they are very worst case errors, assuming the highest possible tilt in the worst direction and a perfect antiphase synchronization between two consecutive peaks). An "infinite" error is attributed to the phases where the peak identification failed.

[29] Or maybe even add some new ones.

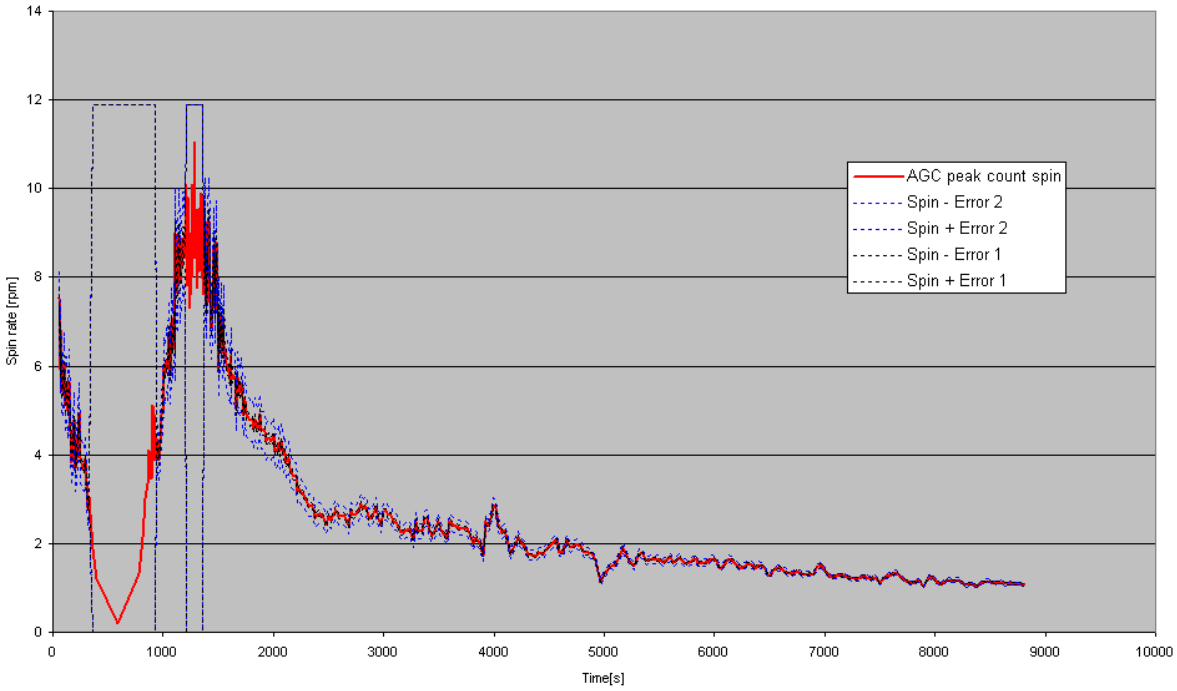

FIG.45: *The spin profile deduced by the AGC peak count method and the associated errors: without considering tilt motions* `(Err 1)` *and considering them* `(Err 2)`.

As the errors can only be oscillating and not biasing, the fact that the intervals are large at some places does not necessarily imply a bad accuracy; they were rather plotted to see whether the observed oscillations are likely to be due to biasing attitude motions or if they must be real (in case they were bigger than what the very maximal error interval tolerates). We see from *figure 45* that apparently, the maximal error is indeed smaller than what oscillations show; as the spin rate should nevertheless be quite regular, this rather creates a problem, questioning the reliability of our error analysis.

Trying to further investigate the probability that the observed oscillations may be real, we may turn to the other spin profiles. *Figure 46* superimposes the three spin profiles we have obtained during our investigations.

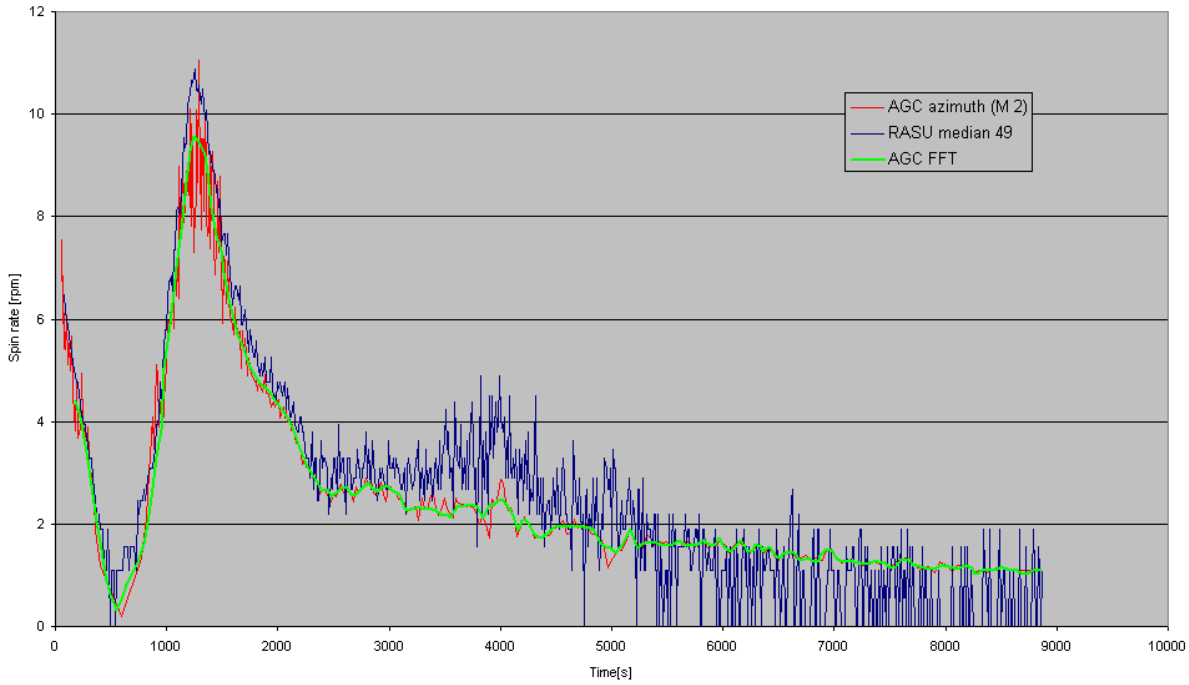

FIG.46: *The spin profiles deduced by the AGC peak count method, the AGC spectrum method and the RASU median method.*

It is not surprising to observe that the AGC Fourier transform spin profile nearly perfectly matches the AGC peak count curve; in fact, at most places it just seems to be a smoothed, averaged version of the AGC peak count profile. We can see that the anomaly around 5000 s on the AGC Fourier transform was envisaged in the right way, as the tendency is the same on the AGC peak count spin profile; however, the amplitude of this variation was underevaluated, as some other peaks were too; it is most probable that it was actually the strength of the spin variation around 5000 s that caused problems on the Fourier transform, specially since perturbing lines can also be observed on the AGC spectrum around other peaks in the spin curve (as shortly before 4000 s for example).

RASU is mostly higher than the AGC spin rate, and as no bias can exist on the AGC spin profile, we have to conclude that the bias on RASU tends to increase the average radial acceleration, leading to a slightly overevalueted spin rate even without considering the averaging problem due to the absence of negative values. At the end of the descent, RASU seems to be lower but again, the very low resolution does not allow us to make proper conclusions.

The fact that RASU's spin profile is higher before *and* after spin inversion is interesting in relation with the influence of coning motions on RASU. Indeed, as already said, the bias induced by a coning movement on RASU's spin rate estimation depends on the relative spin and coning directions. So, if different offsets were observed before and after spin inversion, we would be able to identify coning motions as their origin and determine the coning direction (as the spin direction is known); the fact that this is not the case only leads to the conclusion that pendulum motions dominate the error.

Considering the oscillations, some have to be real as they are present on both the AGC peak count and the independent RASU median spin profiles. Others are only present on the

AGC, or even show different directions on both spin profiles; while the absence of a peak on RASU could still be explained by the smoothing effect of the median in the RASU method, the opposite peaks obviously don't make any sense as a spin feature.

However, don't forget that the spin deduction from the RASU median is also subject to errors, including not only a varying but also a biasing contribution, which are influenced by attitude motions as the AGC spin profile is. The opposite peaks on the RASU and AGC spin profiles could thus be due to tilt motions which have opposite effects on RASU and on the AGC signals.

During the phases where problems were encountered for peak identification, very large and rapid excursions are visible on the AGC peak count spin profile. These are very probably not real, a comparison with the DISR sun sensor or images, depending on what is available for the concerned timeslots, should help to clarify the situation.

8.3 Presentation of the `ProbeAzimuth` MatLab routine

When the AGC signal analysis turned out to be so useful for azimuth characterization, we decided to write a MATLAB ® function which is able to perform the automatic part of the process to derive the ground azimuth and the spin of a probe by making use of the AGC signal of a probe-to-orbiter telecommunication link for a very general mission. This routine, called `ProbeAzimuth`, was then used with the data of the Huygens mission to provide the spin and ground azimuth of the probe at any time, but it is intended to be useable with any future mission if the same data as for this Huygens mission analysis are provided. The "only" manual steps to be carried out are the peak identification on the "experimental" AGC signal and on the "theoretical" azimuthal gain variation patterns for encountered PAA's. Using those two files as well as other data which should be directly accessible in the normal mission case (see list below), the rest is done automatically to provide spin rate and absolute azimuth with respect to planetary East using the assumptions previously discussed.

The use of linear interpolation is justified if a minimal care is given to sufficient resolution with respect to the mission specific variations on PAA, peak azimuths,... (see discussion above). To try to improve accuracy, it was extended to the peak azimuth variations as a function of PAA. If end points are missing, linear extrapolation produces much less accurate results, to be regarded with mistrust.

To simplify, and thus accelerate the table searches and calculations[30], and as the methodical error associated to these approximations is well below the unavoidable error contributions[31] , we used the first method for spin computation and also to interpolate the azimuth between two consecutive peaks: the linear interpolation just considers a 360 *deg* period with the same peak azimuth for neighbouring peaks. This can lead to very small (2 *deg* maximum for the Huygens mission), non physical jumps on the azimuth value when passing from one period to the next one.

In agreement with our linear approximations, the average spin rate value obtained between two successive peaks at T_1 and T_2 is attributed to the middle of the interval $T_1 \rightarrow T_2$ and linear interpolation is made between two successive interval centres to get a continuous spin

[30] By avoiding to compute the absolute azimuth for two points before getting a spin rate result.

[31] Remember that for the extreme case at the beginning of the Huygens mission, where the PAA changes by 2 *deg* over one single period, this can imply an error on azimuth of about ± 1 *deg*, and an error on spin rate of $\frac{2}{360} = 0.56\%$.

curve. However, the assumed linear evolution of the azimuth is equal to stating a constant, average spin rate during the whole interval; this is very normal for a linear interpolation, but it means that the spin obtained by deriving the azimuth is **not** equal to the smooth, interpolated one provided as the output.

Some effort has been made to get a more consistent output keeping the continuity of the 2 curves, spin and azimuth, but as we know the azimuth at the interval boarders (exactly) and the spin at their centre (as a first order approximation), it has turned out to be impossible to find a common higher-order interpolation meeting this criterion.

As an input, the function accepts time as a single scalar or as a row vector, not necessarily ordered in increasing order; it also detects if $t > t_{touchdown}$ and provides after-landing orientation information in the form of $MinAzimuth + i \cdot Uncertainty$ for those cases, using the method described in the next part of this work. It even allows different initial time definitions for the different datasets, in order to facilitate the use of simply copy-pasted raw data. All variables are in MKS units, except the angles that are given in *deg* and the spin rate output which is in *rpm*.

The following files have to be provided to the `ProbeAzimuth` function; the ones corresponding to the Huygens mission have been included in a .zip-file on the attached CD-Rom.

Data used by the function `ProbeAzimuth`.

- `'PROBEDATA.TXT'` : probe data to be provided as column (only first element used for the present task)

```
+Azimuth angle of "0 azimuth in antenna reference frame" on the probe
```

- `'PEAKTIME.TXT'` : time of successive AGC peaks, with number of turns made between the peak and the previous one (positive if counterclockwise as seen from above), to be provided manually as 2 columns

```
+PeakTime1   ArbtitraryValue
+PeakTime2   TurnNumber1->2
+PeakTime3   TurnNumber2->3
+...
```

- `'AZPEAKvPAA.TXT'` : azimuth of AGC peak used for each PAA considered, to be provided manually as 2 columns:

```
+PAA1   PeakAzimuth1
+PAA2   PeakAzimuth2
+...
```

- `'PAAvTIME.TXT'` : Probe Aspect Angle as a function of time, to be provided as 2 columns:

```
+Time1   PAA1
+Time2   PAA2
+...
```

- 'XYZORBvTIME.TXT' : orbiter position in planet reference frame, to be provided as 4 columns

```
+Time1  X1  Y1  Z1
+Time2  X2  Y2  Z2
+...

 NB: X, Y and Z directions are defined to form a direct orthogonal
 axis system, Z being the North, X pointing eastwards orthogonal to the
 longitude reference plane and Y in the longitudinal reference plane.
```

- 'XYZPROBEvTIME.TXT' : probe position in planet reference frame, to be provided as 4 columns

```
+Time1  X1  Y1  Z1
+Time2  X2  Y2  Z2
+...
```

- 'VRTTLANDED.TXT' : after-landing data, used to compute final orientation, to be provided as column

```
+Time of first touchdown
+Time of AGC signal stabilization
```

- 'TO4ALL.TXT' : initial times used for the above files, to allow correction if different reference times are used; t0 is defined as the value of 't' (function variable) for which the corresponding clock/file indicates 0 as time value. To be provided as column

```
+t0 for PeakTime
+t0 for Orbiter position
+t0 for Probe position
+t0 for touchdown definition
+t0 for AGC stabilization definition
+t0 for PAA evolution
```

As previously discussed, the absolute azimuthal orientation of the antenna is deduced from the orbiter azimuth seen by the antenna and the absolute orbiter azimuth in local horizontal reference frame assuming a horizontal probe. This second angle, $Abs2Orb_{AZ}$, is computed from the instantaneous (interpolated) probe and orbiter locations in planet reference frame: after having computed the probe-to-orbiter direction vector by simple subtraction of Cartesian coordinates, a coordinate change consisting in several rotations is operated to express it in

local horizontal reference frame (this means, relating directions to the horizontal plane and East direction defined by the probe's location). Then passing to spherical coordinates, we directly get the orbiter's azimuth and elevation as seen by the probe; if the probe is horizontal, the elevation might provide direct knowledge of the PAA, defined as the angle from the probe-to-orbiter direction to the probe's zenith, but as the probe usually has a defined angle of attack resulting from the entry phase and can thus be purposely far from horizontal at the beginning of the descent, it was decided that a file containing the evolution of the PAA with mission time should be provided. This type of data is usually available from telecommunication link analyses; if not, a first approximation giving excellent results at least for the end of the descent phase would be to consider the complement angle of the elevation, in place of an external input, as the Probe Aspect Angle.

> During the Huygens mission, the Cassini orbiter passed roughly above Titan's equator while the probe was descending to a landing site approximately 10-15 deg below the equator; thus, Huygens saw Cassini in the North. At the very beginning of the radio link, the obiter was nearly at its maximum height above horizon, which it passed from right to left as seen by the probe, subsequently descending through Titan's heaven with an azimuth increasing from 90 deg to a bit less than 180 deg while the elevation decreased from 66 deg ($PAA = 24$ deg) to 18 deg ($PAA = 72$ deg) at probe touchdown and finally 0 deg when Cassini disappeared behind the horizon.

A small lack of flexibility of the programme is that you may skip peaks by specifying it in the `TurnNumber` value of the `PEAKTIME.TXT` file, but the possibility to use several peaks per period for slower movements is not included: **for a given PAA**, consecutive peaks should all have the same azimuth[32]. In the opposite case, the programme would have to be adapted.

8.4 Combining all available sensors to provide a final spin profile

To close the spin and azimuth issue, we want to present the spin profile which, according to us, seems to be the best one we can obtain from our engineering data, that are RASU and the AGC signal (as CASU was not used).

The spin profile provided by the AGC peak count is probably the best one we can obtain and, furthermore, the only one where we can exactly estimate the error. In fact, the uncertainty is such that it can only induce artificial oscillations on the spin profile, no bias at all can be introduced.

But this ideal method cannot be used during two timeslots, one around spin annihilation and another around maximum spin. We chose to replace the whole segment between 333 s and 1485 s after T_0 by data provided by other methods. As the AGC Fourier transform spin rate matches very well the average of the AGC peak count spin profile during the phases of the descent where both methods are reliable, it was preferred, when available, to the RASU spin, which could not only strongly oscillate but also be biased according to our previous analysis.

[32] This means that if it turns out to really be impossible to use the same peak through the whole mission, you could change peak after a certain PAA and simply enter the new `PeakAzimuth` value in the `AZPEAKvsPAA` file; there would just be an error on the time interval during which the transit takes place; take care that this interval, during which the `PeakAzimuth` value is computed by interpolating between the two actually discontinuous peak positions, might be long if the PAA changes slowly.

We consequently used the AGC Fourier transform spin profile around the maximum spin rate, between 1015 s and 1485 s after T_0.

Around spin inversion, we have to use the RASU median as it is the most valid (if not only, since the identification of spectral lines on the AGC spectrum was also questionable around this point) data at our disposal. This is very annoying since the low spin region is also the worst case for RASU (though luckily, we are still under main chute at spin inversion so that the oscillations are not too large): lots of missing negative values make a proper processing difficult, the median being the best estimator we can use, and the resolution is very bad due to the square root on the quantification steps.

To smooth out these instrumental variations, the raw RASU median spin estimation was replaced by two second-order tendency curves, one during the main chute phase and one under stabilizer to allow a discontinuity in the slope of the spin profile when the descent velocity suddenly increases after main chute release.

The resulting spin profile has been transmitted to all Huygens working groups. *Figure 47* shows its evolution in time; positive values correspond to a clockwise rotation as seen from above.

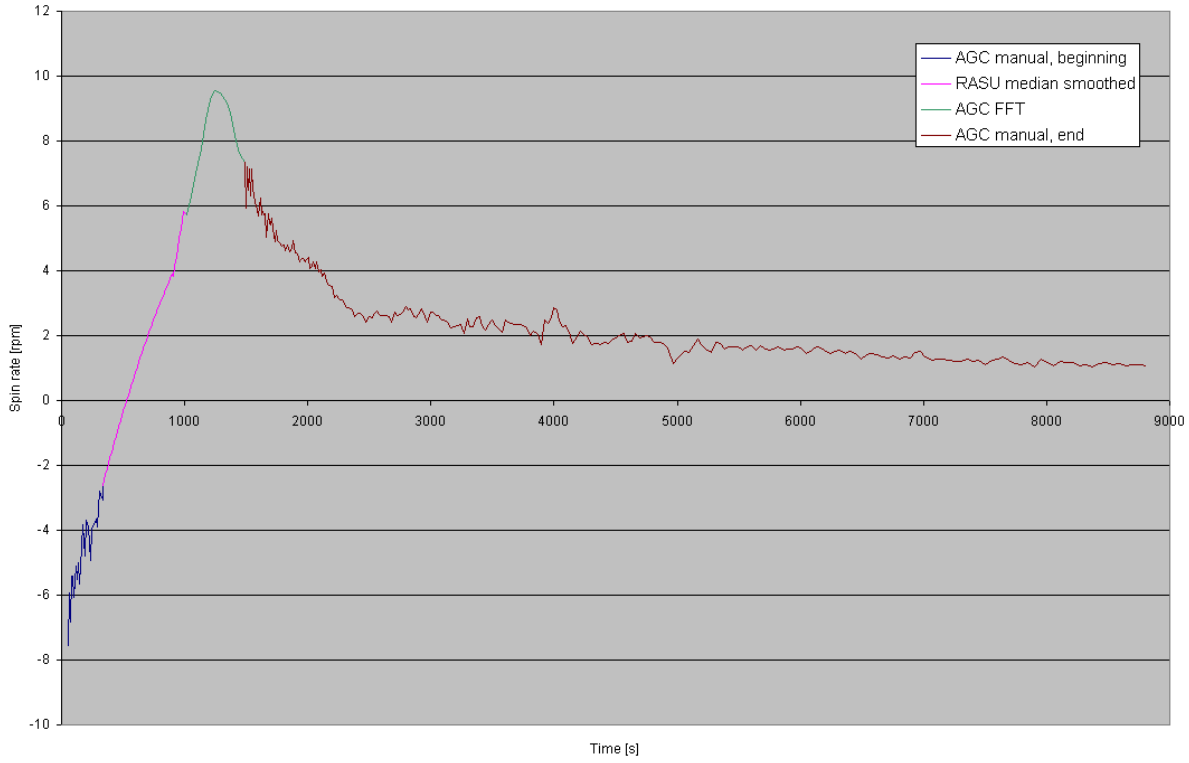

FIG.47: *Spin profile resulting from the best possible combination of engineering data.*

Part IV
Determining the probe's orientation after landing

In the previous part, we focused on the spin and azimuth characterization during the descent phase. However, the knowledge of the probe's orientation after landing is equally important as during the descent; in particular, it would be interesting to know in which direction the pictures were taken. The few information at our disposal is of course the same as before.

We will thus again use the AGC method, with a somewhat reduced accuracy, for direct azimuth characterization.

9 Deducing the ground azimuth from the AGC signal

Using our peak count strategy, we were able to derive the azimuth and spin of the probe while it was turning, until shortly before touchdown; we should thus be able, using short extrapolation or trying to fit the azimuthal variation of the AGP to the AGC signal, to determine the azimuth at landing time, 8870 s after T_0.

But looking at the AGC signal around touchdown, we can clearly make out that its stabilization is not at 8870 s but a bit later (3.5 s exactly); this is not surprising since the shock of the landing has certainly perturbed the probe, inducing much larger attitude oscillations than during the descent. Those attitude perturbations, damped within a few seconds, would explain the observed large amplitude variations. However, we cannot extract any spin information from the AGC during this short period and as RASU's spin resolution is bad for low spin rates, there is actually no way for us to accurately determine how the spin of the probe decreased to zero during this period.

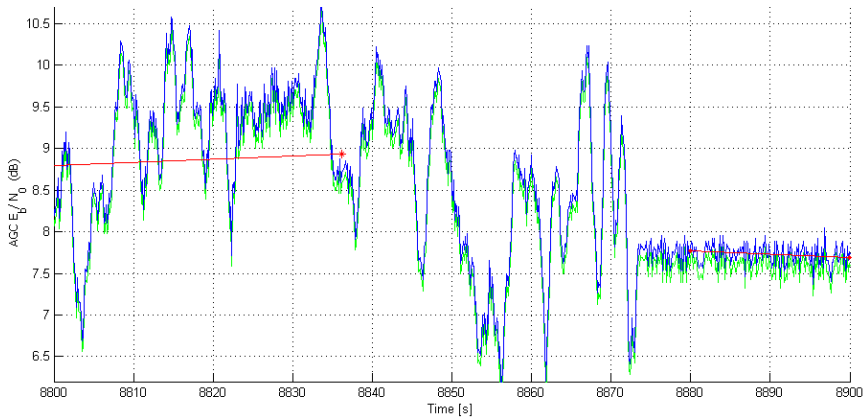

FIG.48: *The AGC signal around landing time; the red curve representing the mean gain is broken, since the probe stops spinning and the power level consequently sets down to a value corresponding to one particular azimuth after landing.*

To place ourselves at the safe side, we considered the two extreme cases where either the probe instantaneously stopped spinning when touching the ground or it kept spinning at maximum speed until the AGC signal fully stabilizes. It is obvious that none of those two cases is very realistic, especially the second one. Using the spin rate of 1.06 rpm computed from the AGC signal at the end of the descent, we see that the difference on probe azimuth between them lies around

$$3.5\,[s] \cdot 1.06\,[rpm] \cdot \frac{360\,[deg]}{60\,[s/mn]} = 22.26\,deg\ .$$

Fortunately, the high PAA value of 72 deg at the end of the mission implies a low value for the azimuth error induced by a tilt of the probe, which could maximally reach ± 4 deg for a tilt of 10 deg in the worst direction. Adding[33] the basic uncertainty associated to our measurement method, which sums about ± 3 deg for the typical end-of-descent spin rate, we obtain the basic uncertainty on the azimuth of the probe after landing as being

$$\pm 5\,deg - 22.26\,deg\ .$$

Writing a minus sign on the last term means that we will consider as the primary azimuth evaluation, the result obtained when assuming that the probe stopped spinning as soon as it touched the ground (remember that the probe was spinning clockwise).

9.1 First method: using the developed automatic tool

As has already been said, a calculation to determine the after-landing orientation was included in the automatic tool developed to compute a probe's azimuth from its AGC signal; this result is inserted, associated to a zero spin, whenever the azimuth is asked for a time superior to landing time.

To estimate the uncertainty on the provided azimuth, the program not only considers the two different ending times for the spin movement presented above, but also assumes different evolutions of the spin rate when extrapolating from the last peak to touchdown time: it is assumed either to linearly decrease at the same rate as between the last two peaks (which should be exaggerated since the spin profile has its concavity upwards for the end of the descent) or to stay constant at the average spin rate computed for the last full revolution.

The two extreme cases are obtained by considering the earliest stop time with the lowest spin rate and the longest spin duration with the highest velocity. These results are displayed in the format

$$Azimuth_{Min.Speed/Min.Time} + i \cdot \Delta Azimuth_{Max.Speed/Max.Time}\ .$$

As the probe was spinning clockwise as seen from above, $\Delta Azimuth$ should be negative. Indeed, the result provided by the programme is an azimuth of the probe's $Y-$axis of

$$162 - i \cdot 27.5\,deg$$

with respect to East; the uncertainty is higher than the basic 22.5 deg one calculated in the introduction, since it includes in addition an estimation of the extrapolation error[34]. The

[33] In a root-of-squares estimator as before: $\sqrt{4^2 + 3^2} = 5$.

[34] Considering extreme cases, we do not have a root-of-squares estimator but a worst case margin. This has been done because the stabilization time and the spin rate may not be seen as totally independent factors: the faster the probe was spinning, the longer time it may have taken to slow this movement down.

other components of the error ($\pm 5\ deg$) remain unchanged; they are small compared to the one resulting from our uncertainty about the probe's behaviour at touchdown, but we should keep them in mind since at one hand, extreme cases might have to be considered to see if results from different working teams might agree and at the other hand, it is probable that accurate information about the probe's behaviour at touchdown will be available in some future when data from HASI and SSP have been interpreted.

9.2 Second method: linear extrapolation using the four last rotations

(This part wasn't done by myself, but by my supervisor Ir. Miguel Pérez Ayúcar.) Taking the time and azimuth - actually always the same, given the very slow peak azimuth variation associated to PAA changes - of the four last peaks, a linear fit on this longer timescale was used to extrapolate the value of the azimuth; this is equivalent to taking as a constant spin rate the average spin rate over the last three periods.

It is difficult to know if this method actually improves our azimuth estimation in comparison with the previous one, since considering a longer period might imply a gain in accuracy by better rejecting alternating perturbations if the spin rate was really constant, but a lack in accuracy if the spin rate was really varying as well. However, given the very tiny variations of the average spin rate at the end of the descent (the actual existence of the oscillations still having to be assessed), it seems more probable indeed that the error considered by the previous method using quite different spin rate evolutions is overestimated and just considering an average over the last periods is the most realistic way to carry out our extrapolation.

The error thus includes, in addition to the two basic terms $-22.5 \pm 5\ deg$, an extrapolation error which is difficult to estimate but might remain small enough, if the spin was really smooth and the oscillations are really perturbations - to be discarded - on the AGC deduction method.

The azimuth given by this method considering a spin stop at touchdown time, 8869.77 s after T_0, is

$$151.8\, deg$$

which is somewhat lower than the deductions of the automatic tool. In fact, the actual correction to be made to this result should be the same for the error terms

- spin stop time
- error induced by a tilt angle

so that the difference should be explained by the remaining terms, which include a very small error from manual peak localizations (more peaks being used for the second method, this one should be more accurate) and the uncertainty on the spin rate's evolution. As a consequence, a difference of up to 10.5 deg has to be taken into account when considering different extrapolation methods for the spin rate. The fact that the second method provides a smaller azimuth means that it considers a higher spin rate; using the high spin rate for our first method as well, the difference between extreme cases should be reduced to 22.5 deg so that a $27.5 - 22.5 = 5\ deg$ uncertainty can be attributed to the extrapolation itself. But this still leaves a 5.5 deg error coming from the different views about the evolution of the actual spin rate during the mission - regular with perturbed measurements or perturbed itself; which view is the best one should be decided together with others teams and maybe industrial partners who have studied the behaviour of the probe and could tell us how smooth its spin profile should be.

9.3 Third method: manual superposition of the AGP curve on the AGC signal

To try to reduce some of the problems related to the definition of the end-of-mission spin rate and the extrapolation method, another straightforward way to deduce the azimuth from the AGC signal is to directly inspect the time signal at the end of the descent rather than just using peak values from the previous analysis. To do this, a few periods of the azimuthal evolution of the Antenna Gain Pattern for a PAA of 72 *deg*, corresponding to the end of the descent, have been drawn; the signal was then handled with a transparent background, allowing zooming and displacement, to try to fit it on the end of the AGC signal; after correct superposition, the azimuth indicated on the AGP at 8869,77 *s* gives the azimuth of the orbiter as seen by the antenna[35] and as we know that the orbiter was seen by the probe at an azimuth of exactly 175 *deg* with respect to East at the end of descent, a simple subtraction provides the probe's azimuth.

In practice, it turned out to be somewhat difficult to perfectly superimpose the patterns. The visual inspection of the varying correspondence of the two curves was a good way to gain insight into the perturbations associated to the AGC signal; in particular, the oscillations of the correspondence with time confirms a small variation of the speed at which the AGP signal is played on the AGC with a period of about 110 *s*, which was already seen on the spin profile deduced from the peak counts; whether this is a real spin variation or an artefact due to perturbing effects - probably those of tilt motions on the orbiter azimuth seen by the antenna - is still not clear.

As a consequence, different guesses were made for the best superposition, leading to somewhat different azimuth deductions. The following figures illustrate the two extreme cases, leading to a difference of 10 *deg* on the orbiter's azimuth seen by the antenna at touchdown.

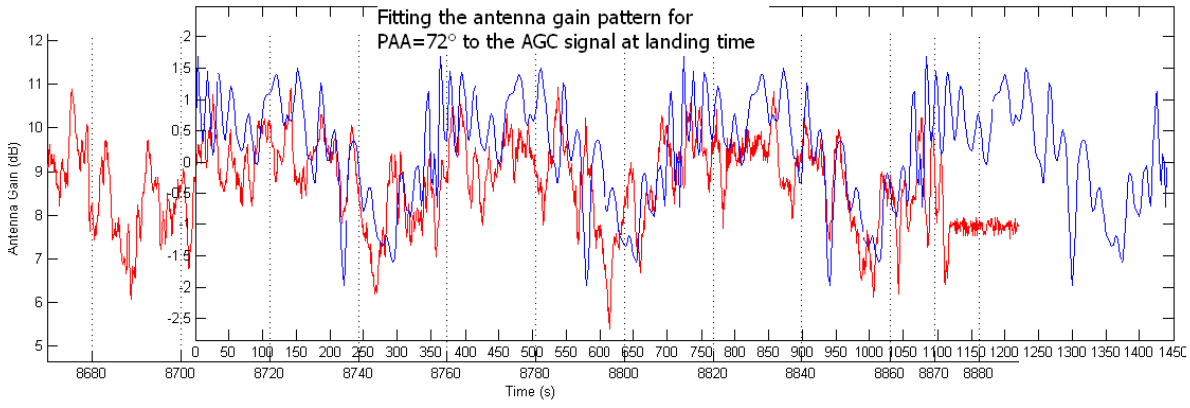

[35] Actually, the azimuth at 8870 *s* was taken and a difference of 1.4 *deg* was added, according to the end-of-mission spin rate.

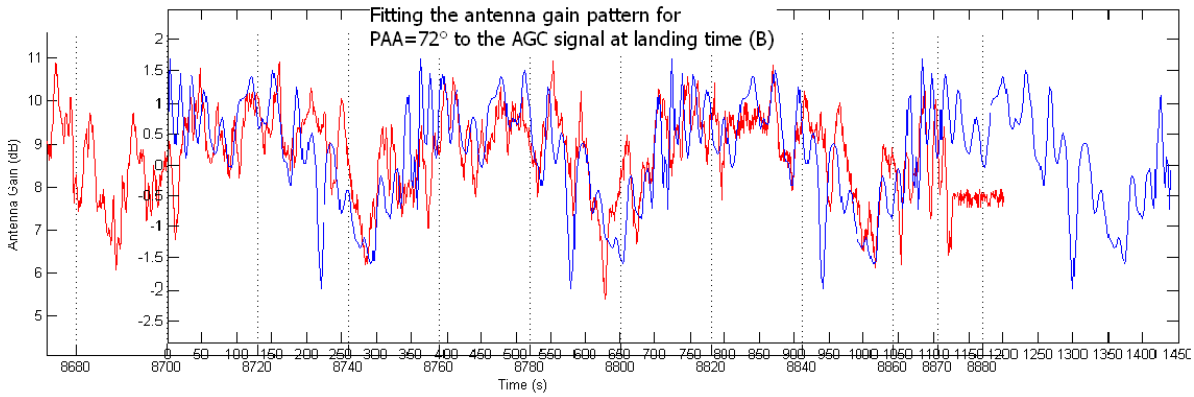

FIG.49: *Superposition of the AGP on the AGC signal at the end of the descent to deduce the after-landing azimuth.*

The result of this analysis is an orbiter azimuth with respect to antenna of 20 *deg* (+22.5 *deg* for the spin-ending uncertainty) which implies a probe azimuth with respect to ground of $175 - 20 = 155$ *deg* (-22.5 *deg* for the spin-ending uncertainty).

In addition to the uncertainty on the time at which the spin movement stopped, the error includes a ± 5 *deg* uncertainty on the fitting (equivalent to the previous extrapolation error); the other error terms (due to measurement and screen resolutions and the bias introduced by a possible tilt of the probe) associated to the AGC method sum up to ± 5 *deg* as well. The final result for the probe's azimuth after landing is thus, considering as basic case the early immediate spin stop[36],

$$155\,deg\ [-28\,deg,\ +7\,deg]\ .$$

The following figure shows the corresponding orientation of the probe.

[36] And again considering the worst case (simple addition) combination of extrapolation and spin-ending time errors.

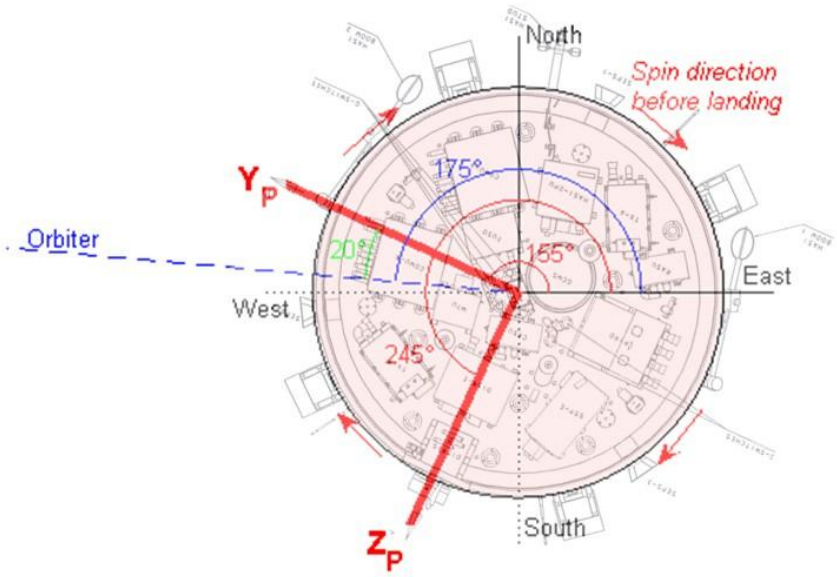

FIG.50: *The azimuthal orientation of the Huygens probe after its landing on Titan according to our deductions from the AGC signal.*

9.4 Comparison of our results with those from the DISR team

Determining the direction in which the pictures were taken on the surface was a principal goal of this section. The DISR team is also working on Huygens' trajectory and orientation reconstruction, using the images and other DISR sensors to deduce mainly the spin and azimuth information by direct inspection and extrapolation. As the agreement with our results is still being discussed, we cannot present any conclusions but we will now briefly discuss what has been done on this topic.

As can be seen from the previous figures, our results imply that the camera, directed along the probe's $Z-$ axis, was looking between South-South-West and South-West after landing - depending on if the probe stopped spinning directly when touching the ground or at AGC signal stabilization respectively.

The DISR team thought that it was looking more eastwards, around South-South-East. This difference, of 30 *deg* at least (*i.e.* considering the different possibilities for the end of the spin movement), is not compatible with our uncertainties. The different possibilities to be investigated in this direction include

- a conceptual or reliability problem on our method or the one from DISR;

- an error in the uncertainty attributed to our method or to the one from DISR, including maybe a very strong permanent tilt of the probe biasing the AGC deductions; however, at this low PAA, the required tilt would be over 40 *deg*, far above the realistically possible values and the less than 18 *deg* necessary to ensure the possibility of telecommunication, so this feature alone cannot explain the observed difference;

- a systematic error somewhere when defining the azimuth reference; for our method, this concerns the antenna reference where a definition error could maybe have occurred during AGP measurements or post-measurement operations have maybe changed the antenna's orientation; this last possibility probably requires that the whole top platform has been turned with respect to the probe since the variations of the AGP were mainly conditioned by other elements on the probe, so that it has to be excluded.

The stabilizer parachute should lie on Titan's ground "in front of" the probe, *i.e.* in the direction of its horizontal movement before landing, since the wind which was moving the probe-parachute system should still have blown into the parachute once the probe had landed. As the probe was moving from East to West at the end of the descent, the parachute should lie to the West. Assuming this position for the parachute, both azimuth values (from DISR and from ourselves) could agree with the fact that it is not seen on the DISR picture.

10 Characterizing the attitude using the accelerometer measurements

When the probe has landed, the measurements made by the accelerometers are purely static; by deleting all derivatives in the expressions of $\mathbf{Acc} \cdot \mathbf{e}_x$ (CASU) and $\mathbf{Acc} \cdot \mathbf{e}_y$ (RASU), they are found to be (see FIG.12 for the definition of the angles)

$$CASU_{meas.} = \cos(\theta)\mathbf{g}_{Titan} \ , \ RASU_{meas.} = -\sin(\theta)\cos(\psi - \phi)\mathbf{g}_{Titan} \ .$$

As we know g_{Titan} and the azimuth ψ of the probe, it seems easy to deduce θ and ϕ - or at least some possibilities for these angles since the inversion of a sine or cosine allows two angular values - from the two accelerometer measurements in order to obtain the complete probe orientation.

10.1 The tilt angle

As it is the only variable present in CASU's measurement, the tilt angle θ should be straightforwardly deduced by inverting the expression of $CASU_{meas.}$. Unfortunately, CASU's resolution of about $0.04\mathbf{g} \approx 0.4\ m/s^2$ is quite low so that we do not have any accurate value for $\cos(\theta)$.

Knowing that Titan's gravity is $1.354\ m/s^2$, the value of $CASU_{meas.}$ should lie slightly under $0.138\mathbf{g}$; it is obviously impossible to reach an acceptable relative error at these values with quantification steps of $0.04\mathbf{g}$.

In practice, the signal is not constant but oscillates between the values just below and just above Titan's gravity, that is 0.1184 $\mathbf{g}$ and 0.1577 $\mathbf{g}$, before stabilizing to the lower value. These oscillations should be very small in reality, so the fact that the limit between the two quantification values is repeatedly crossed indicates that the average value lies very close to this limit; how close can unfortunately not be accurately known. The value of the quantification limit is probably

$$\frac{0.1184\mathbf{g} + 0.1577\mathbf{g}}{2} = 0.1381\mathbf{g}$$

which is seen to correspond very closely to the value of Titan's gravity; the tilt should thus be "quite small". The fact that the stabilization is slightly below this value unhappily gives no additional, quantitative information: as $\cos(\theta)\mathbf{g}_{Titan} < 0.1381$ for all values of θ, it just indicates that CASU's measurement is consistent.

However, RASU's measurements might help us to put some limit value on the tilt angle of the probe. Here we have a much better resolution, the quantification steps being of approximately 0.0005 $\mathbf{g}$.

Despite this fact, the RASU signal does not oscillate as CASU's one does. This implies that the probe was actually very stable after touchdown (which, of course, is not surprising) and that the oscillations on CASU, if induced by real tiny probe orientation perturbations and not by any local artefact as a vibration mode or the operation of nearby instruments, can only be justified if the average was very close to the quantification limit. But we still get no quantitative result since the type and direction of the oscillations strongly influence the possibility to detect movements with CASU which are not seen on RASU; just imagine a pendulum motion (the most probable case) where RASU is aligned with the tilt axis.

We actually can derive one quantitative limit - the minimal tilt angle, as expected since we just tried to determine the maximal one and we failed - from RASU's measurement. The value indicated by RASU after touchdown is 0.00189 ± 0.00025 **g**. A positive value indicates that the gravitational acceleration measured by RASU after touchdown was in the same direction as the centrifugal acceleration during the descent, thus radially towards the edge of the probe, meaning that RASU was on the lowered half of the probe.

Since $\mid \cos(\psi - \phi) \mid < 1$, there is a minimum tilt angle under which RASU's measurements would be inconsistent. We are thus able to deduce the minimum tilt angle of the Huygens probe after touchdown, which corresponds to

$$\theta_{min} = \mathsf{asin}\left(\frac{\mathsf{min}(RASU_{meas.})}{\mathbf{g}_{Titan}}\right) = 0.68\, deg\ .$$

As a conclusion, our attempt to retrieve the probe's attitude after touchdown, from accelerometer measurements only, turns out to run to a dead end at the first step, due to the low resolution of CASU.

We anyway wanted to use RASU's accurate data to deduce the tilt direction, ϕ or $\psi - \phi$, but the results could reach from 0 to nearly 90 *deg* for different tilt angles so the characterization of the latter was a crucial step.

We thus turned to information from other working groups; in particular, the HASI servo-accelerometer as well as an information from the SSP tilt sensors seemed to indicate that the probe was tilted about 10 *deg* after landing. However, the tilt sensor indicated a permanent tilt of 10 *deg* during the descent as well, about which we were quite sceptical since it would imply a whole mission scenario at the very limit of the requirements and expectations. We should thus be very careful about this tilt value on the surface of Titan since a bias is probable on the measurements of the tilt sensor. That's among others why we desperately tried to put limits on the possible tilt angles in order to see if the tilt values provided by SSP and HASI could be validated.

Just to notice in case you were wondering, this tilt does not imply any correction to be applied to our azimuth results since they were deduced from prior to touchdown data.

10.2 The tilt direction

Whatever the real tilt may be, we will thus use the one provided by the SSP and HASI sensors. The HASI accelerometer provides the same information as CASU, though with a much higher accuracy, allowing to deduce only the tilt angle but not its direction. The SSP tilt sensor, sensing along two perpendicular axes, indicates a tilt direction very close to the probe axis Y_P, with the DISR camera looking upwards. Let's see what we can deduce from RASU.

Considering tilt values of 9, 10 or 11 *deg*, we immediately get corresponding values for $\mid \cos(\psi - \phi) \mid$ which lead to two different possibilities for the angle itself[37].

[37]The absolute value leads to angles between $-\pi/2$ and $\pi/2$; the actual position with respect to the tilt direction is derived knowing that RASU is on the lower half-plane.

Tilt angle	$(\psi - \phi)^*$
9 *deg*	± 85 *deg*
10 *deg*	± 85.5 *deg*
11 *deg*	± 86 *deg*

This value of $(\psi - \phi)^*$ is the difference between RASU's azimuth and the highest-to-lowest-point direction[38]. The result is thus that RASU should be very close to the tilt axis; as we know RASU's azimuth (120 *deg* more than the azimuth of DISR = the Z_P axis), we should actually say that the result is that the tilt axis is very close to RASU's radial position. *Figure 51* shows the situation.

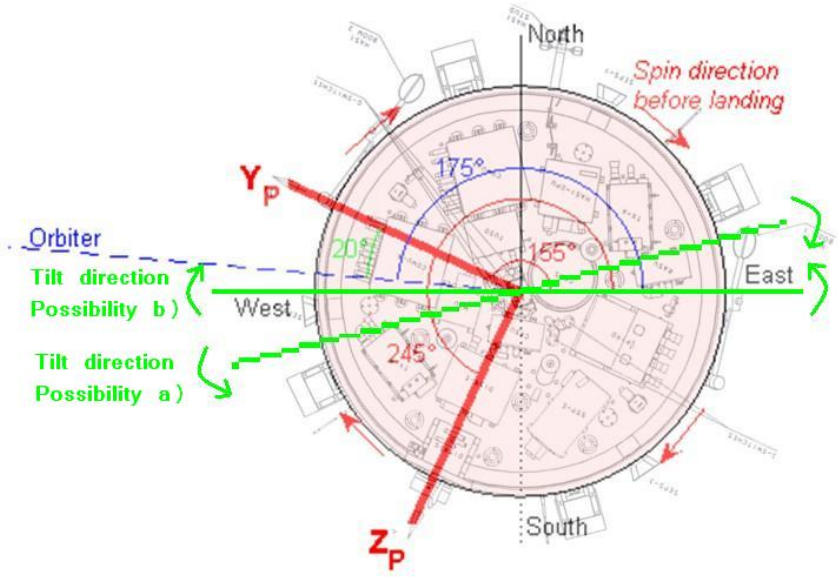

FIG.51: *The two different possibilities for the tilt direction assuming a tilt of 10 deg.*

We see that a 1 *deg* difference on the tilt angle implies a 0.5 *deg* difference on the tilt direction, but this is only valid around the relatively high tilt value. Indeed, computing the Taylor series of the formula

$$\psi - \phi = \mathsf{acos}\left(\frac{RASU_{meas.}}{\sin(\theta)\mathbf{g}_{Titan}}\right) ,$$

the impact on the $(\psi - \phi)$ result of differences on $RASU_{meas.}$ and θ can be expressed as

$$\mid \Delta(\psi - \phi) \mid \leq \frac{1}{\mid \sin(\psi - \phi) \mid \sin(\theta)\mathbf{g}_{Titan}} \cdot \mid \Delta RASU_{meas.} \mid + \frac{RASU_{meas.} \cos(\theta)}{\mid \sin(\psi - \phi) \mid \sin^2(\theta)\mathbf{g}_{Titan}} \cdot \mid \Delta\theta \mid \ .$$

Examining this expression, we see that

[38] And not the lowest-to-highest-point direction as would be the case for $(\psi - \phi)$.

- for given values of $RASU_{meas.}$ and $\sin(\psi - \phi)$, both terms of the error increase towards infinity when the tilt angle tends to zero. Infinity will of course never be reached since realistic values for $RASU_{meas.}$ and $\Delta RASU_{meas.}$ should compensate this evolution. However, it means that for the value which we observe, the accuracy of our deductions strongly increases with the tilt angle.

- for given values of $RASU_{meas.}$ and $\sin(\theta)$, both terms of the error strongly increase when $\psi - \phi$ tends to zero (meaning that RASU tends to be aligned with the highest-to-lowest-point direction).

Thus, the fact that θ is quite large and that our consequent results tend to show that RASU is close to the tilt axis ($\psi - \phi$ close to 90 deg) indicates that we are in optimal conditions for a good accuracy.

Replacing the variables in the formula by the values that we have observed and considering

- the quantification uncertainty for $\Delta RASU_{meas.}$ and

- an uncertainty of 1 deg for $\Delta\theta$ (totally arbitrary since we are not confident at all in the tilt angle provided by the SSP tilt sensor),

we get a maximal error of

$$41.86 \cdot \mid \Delta RASU_{meas.}[\mathbf{g}] \mid + 0.45 \cdot \mid \Delta\theta[deg] \mid = 0.46\, deg$$

on the tilt direction, which is, as expected, very small; the uncertainty on RASU's exact value turns out to have a particularly small influence.

As a consequence, our results seem to be incompatible with the information provided by the SSP tilt sensor about the tilt direction. An additional error could be present on the value of $\mathbf{g}_{Titan}$ if we landed at a significantly different altitude than the assumed nominal radius, but the DTWG told us that the uncertainty on altitude was much smaller than the kilometer required to have a significant influence. In any case, the error due to gravitational anomalies should be lower than the terms which were already considered before, so that the incompatibility of our results remains.

10.3 Investigating the compatibility of our deductions with the surface images from the DISR camera

In order to verify which results seem to be more plausible, we had a look at the famous images taken by the camera when the probe had landed. In fact, we wanted to see how the horizon was tilted on the images and check if, assuming that it was horizontal in reality, this agrees with the tilt angle and direction which we have just presented.

To simulate what would have to be seen by the camera if our results (and the horizontal horizon assumption) were right, we took two horizontal vectors close to the direction of the camera and applied a coordinate change in order to express their direction as seen in a reference frame attached to the camera. The following views of the horizon were obtained for possibilities *a*) (left) and *b*) (right) of FIG.51.

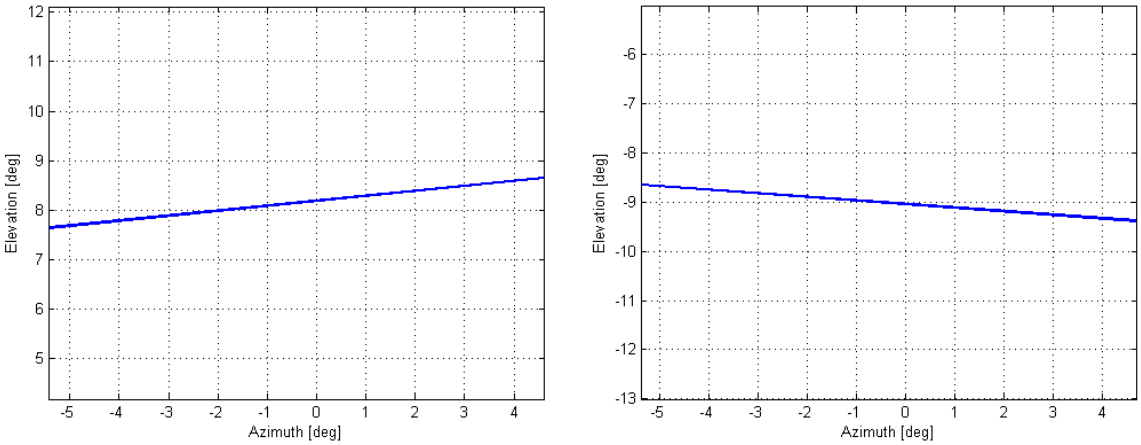

FIG.52: *The view which DISR would have of a horizontal horizon assuming a 10 deg tilt angle and the two tilt directions shown on FIG.51 (possibility A on the left, possibility B on the right).*

The tilt direction of the horizon depends as expected on the tilt direction of the probe and the horizon is seen more tilted for the a) case where the tilt axis is farther away from the perpendicular to the camera direction. The numerical values for the tilt of the horizon are 5.7 *deg* and 4.2 *deg* for the a) and b) possibilities respectively. These values can also be directly obtained by the following reasoning.

As on *figure 53*, let $Tilt$ be the maximum tilt angle and θ the direction of the camera (in red) with respect to the tilt axis. The tangent to the probe experiment platform at camera position is parallel to the diameter which is perpendicular to the antenna direction. As a result, θ also represents the angle between the lowest-to-highest point direction and this diameter. The horizon tilt which we want to compute would then correspond to the angle α characterizing the inclination of this special diameter.

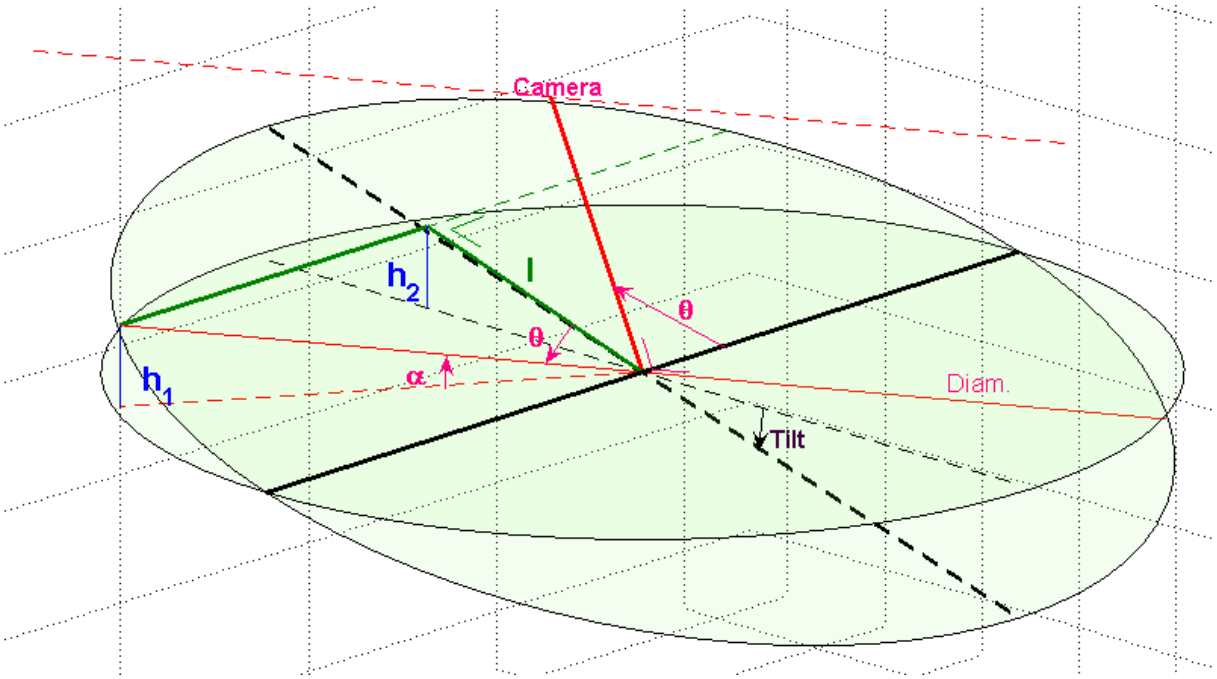

FIG.53: *Figure used to derive the tilt angle of the horizon that would be seen by DISR for a given tilt angle and tilt direction.*

Taking a unit length for the circle's radius, we have, considering the vertical triangles

$$\sin(\alpha) = h_1 = h_2 = \sin(Tilt) \cdot l$$

and considering the green rectangular triangle in the probe's horizontal plane, $l = \cos(\theta) \cdot 1$ which finally leads to

$$\alpha = \mathsf{asin}(\sin(Tilt)\cos(\theta))$$

providing the same two values as before for the tilt of the horizon.

The following figure shows a superposition of these horizon tilts on the surface picture taken by the DISR camera.

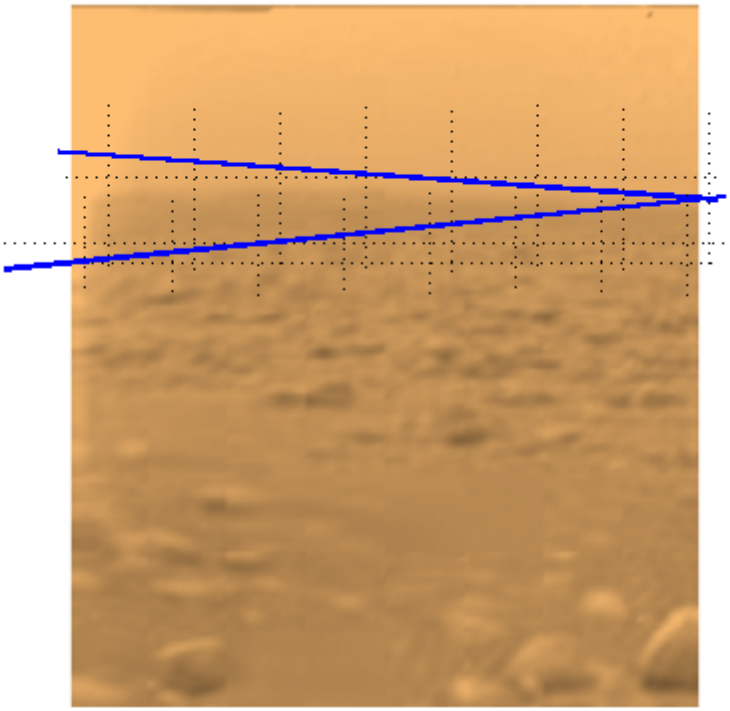

FIG.54: *Superposition of the tilted horizons on the surface picture taken by DISR.*

Possibility *a*) clearly has to be rejected when looking at the picture, it implies a (too) wrong tilt direction of the horizon with respect to what DISR sees. The second one agrees somewhat better, but both solutions need a higher tilt angle of the horizon; in fact, the official value for the tilt of the horizon seen on this picture has been published as being 0.5 *deg* clockwise. This can indicate either that the geomorphology of the landing site's surrounding implied a tilted horizon, or that our deductions about the probe's tilt are wrong.

So what about the SSP deductions? They would imply a very low tilt of the horizon, as on the picture. But considering the height of the horizon on the picture, the DISR team got a camera up-looking elevation of roughly 2 *deg*, while it should be very close to 10 *deg* according to SSP. Considering that some features might be attributed to hills in the neighbourhood of the landing site, another 2 *deg* could be added to the measurements of the camera team but not more.

Furthermore, taking a 1.7 *deg* tilt angle of the Huygens probe and repeating our calculations using RASU would place the camera at the top of the probe as well, thus agreeing in tilt angle and direction with the DISR pictures and in tilt direction with SSP; the tilt angle however would not agree with the SSP and HASI deductions.

We finally have to conclude that further analysis of the reliability of the different sensors is necessary before closing this issue with agreeing results.

•

Part V
Investigating the pendulum/coning motions to provide complete probe orientation during the descent

11 Preliminary considerations

While the spin motion was controlled by spin vanes and RASU was used to monitor its actual evolution, no active element and no specific engineering sensor were dedicated to the attitude of the probe. In fact, the primary goal was just to reach a sufficient stability to allow a proper operation of the probe; this was achieved in a purely passive way by ensuring acceptable limits of the probe-parachute system's proper behaviour, and it obviously succeeded (though maybe not as well as was expected for the nominal case).

Once this is ensured, the second objective, to characterize the attitude and attitude motions of the probe during the descent for a perfect reconstruction of the scientific measurement conditions, takes much less importance since no huge movements can occur; it is more a matter of intrinsic curiosity to know how the probe behaved. In this sense, it is not surprising that no specific engineering sensor for attitude reconstruction was incorporated; anyway, even in case of an improper behaviour of the probe, there would have been no alternative to the operating mode, consisting for example in a different front shield ejection in order to deal with large pendulum oscillations: the best possible method assuming worst case conditions was already implemented.

As a consequence, a large part of the attitude investigations will normally be carried out by the industries who designed the probe and DCSS; they are probably also most interested in the attitude issue as properties turning out to be important for future mission designs might be discovered. However, we will try to contribute a bit to this study using our basic knowledge.

11.1 Pre-mission analysis

The stability of the probe attitude was controlled through the parachute system. As already mentioned, the probe was suspended by 3 bridles, connecting to a single rope with incorporated swivel about 3.9 m above the experiment platform; the top of the parachutes were 27 m and 12.03 m above the probe respectively for main and stabilizer parachutes.

Given the much bigger diameters and drag coefficients of the parachutes compared to the probe, associated to their very low mass (about 1 kg), the basic dynamic model considers the probe simply pulled down by Titan's gravity, suspended under the parachute which mainly experiences the aerodynamic deceleration force that slows the whole system down. The static, equilibrium position of the probe would thus be located vertically under the parachute[39]; the

[39] At least at the end of the descent, where the initial horizontal velocity component from the entry phase has been completely rejected.

fact that the drag force is higher than the gravity force implies that the system is decelerated and tends towards a limit speed.

The task of the pre-mission analysis was to examine what is the stability of this equilibrium when subjected to perturbations; in particular, the dominant modes had to be identified and their rapid damping towards acceptable limits ensured.

The bridles being made of very stiff Kevlar, we can be absolutely certain that the probe-parachute system could not make any spring-like motion; in fact, all possible motions should be envisaged by assuming rigid suspension cables. What may have happened, but is very unlikely and should anyway have been rapidly damped according to studies and experience with parachutes on Earth, is that the shape of the canopy itself, made of fabric, oscillated periodically, leading to a very small spring-like sensation for the probe. According to the parachute specialists, this issue can be excluded from a first analysis of the probe's motions.

As a result, all oscillatory movements of the probe concern attitude variations (assuming a rather constant deceleration). The mission requirements stated that these were acceptable if

- the tilt of the probe did not exceed 10 deg and

- the angular velocity of the attitude motions did not exceed 6 deg/s.

This was necessary as well for operational needs (proper shield and cover ejections) as for instrumental needs (sufficient stability to take pictures for example). The 10 deg tilt limit was also imposed because of the parachute system itself. Indeed, for pendulum motions inducing angles above 10 deg between the probe's $X-$ axis and the vertical direction, it may happen that all three suspension bridles would have to be misaligned on the same side of the vertical rope. As this would not respect the force balance principle, it leads to what is known as bridle collapse: as represented on *figure 55*, in place of pursuing its normal pendulum movement, the probe stops, one of the three bridles loosens and the probe rotates in a way to place the two remaining bridles so that an additional tilt does not violate the force balance principle. Such behaviour has to be avoided. We may actually say that it did not happen during the Huygens mission: according to parachute specialist J. Underwood who studied this phenomenon, a bridle collapse would imply huge perturbations on the probe's attitude, which would definitely have been readily noticed.

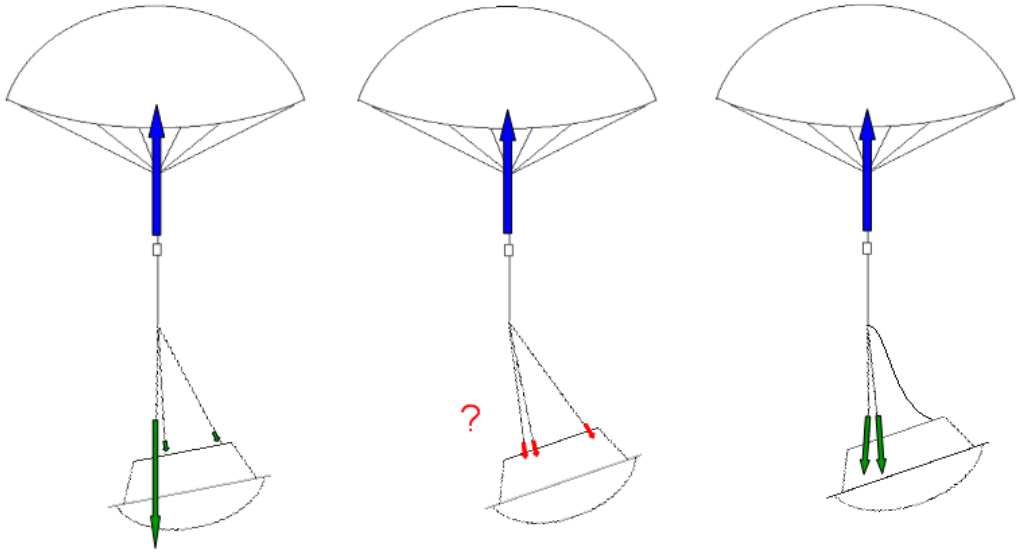

FIG.55: *Illustration of the phenomenon leading to bridle collapse; from left to right: the limit case, the impossible future behaviour keeping all bridles tight and the actual behaviour leading to bridle collapse.*

One more thing related to the pre-mission stability study, which has to be pointed out because it has to be taken into account for our analysis, is that the inertia of the parachute, associated to its aerodynamic behaviour, is sufficiently large to consider it as a fixed point, *i.e.* it may not constantly move from one side to the other. Its "moment of inertia" (in fact, its resistance to attitude variations under steady vertical flow conditions) however is not so big, so that it may rotate a bit in several directions to allow position and attitude variations for the probe.

One example of such a movement, where the attitude of the probe may vary quite a lot and rapidly without the probe having to move too much through the sky, would be a synchronized double pendulum oscillation with fixed probe and parachute positions and the swivel as a central turning point.

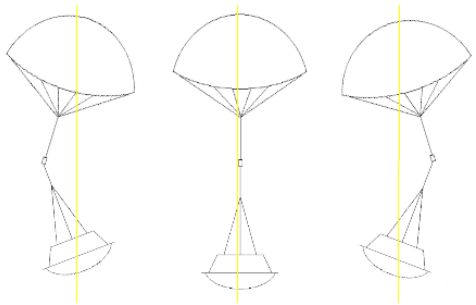

FIG.56: *Illustration of the synchronized double pendulum oscillation.*

This kind of motion is a mode which may appear; its frequency depends on various factors as the gravity experienced by the probe (basically $\mathbf{g}_{Titan} + Deceleration$), the distance from

probe to swivel and the moment of inertia of the probe. To efficiently damp such kinds of motions, it was necessary to enforce the stability of a parachute orientation perfectly aligned with the flow direction. This stabilizing effect was obtained by locally increasing the porosity of the parachute by introducing single (stabilizer chute) and double (main chute) gaps in the parachutes; they were of "disc gap band" type. Simulations show that movements as the one described above are then fully damped within less than one minute.

Checking the behaviour of the probe during the SM2 test flight however, undamped probe motions were present during the whole descent under stabilizer parachute. Examining the gyroscope data, it turned out to be precisely the double pendulum motion which we just described. Although the amplitude of the oscillations remained well within limits - the main amplitude is 2 deg with peaks up to 4 deg - the rapidity of the oscillations at a frequency of 2.6 Hz led to high angular velocities of up to 60 deg/s which are not acceptable. To solve this problem, as this type of motion should be rapidly damped according to DCSS analyses, the major question which had to be addressed was to find what was counteracting the damping effect by triggering this mode. Exactly knowing the passive system, different investigations were carried out to try to identify which aerodynamic effect could be the cause of these oscillations.

One possibility which was mentioned is vortex shedding: the probe passing at various places in front of the parachute would disturb the flow in such a way that this particular synchronized double pendulum movement is not damped. Tests were carried out on scale models in wind tunnels and during additional helicopter drops to try to put this particular movement to the fore and study it. However, the movement observed on SM2 did not appear.

Trying to characterize what could have been different during the SM2 flight and during these other tests, it was noticed that the SM2 test was carried out on a windy day. Particularly high wind shears were present at altitudes where the probe descended under stabilizer chute. Moreover, the power spectrum of the induced wind gusts on the probe showed a predominance of energy around 2.5 - 3 Hz. This corresponds to the frequency of the observed movement, at 2.6 Hz[40]. As a consequence, it seemed most probable that the strong attitude oscillations observed under stabilizer chute during the SM2 test flight were excited by wind gusts; this would explain why were not observed during the other tests made in calmer conditions. Everybody eventually got confident enough in this explanation to consider the stability problem solved.

Indeed, as such wind gusts (*i.e.* of significant amplitude and with similar dominant frequencies) were very unlikely to occur on Titan according to the current models of its atmosphere, there would be no trigger for the synchronized double pendulum oscillations, so they would simply be damped; as a consequence, no changes had to be made to the probe - parachute system to avoid large oscillations. To be somewhat safer though, the stabilizer parachute was upgraded to double gap for the Huygens mission to enhance its stability.

[40]We will see towards the end of this report that this also corresponds to the proper frequency of the synchronized double pendulum motion.

11.2 Information from the spin analysis

11.2.1 Qualitative information obtained from RASU anomalies

The comparison between the RASU median and the (normally much more accurate, at least on average) AGC spin profiles did not allow us to make spectacular conclusions about the attitude. Indeed, at the end of the descent the too low resolution of RASU limits its own possibilities and around spin inversion, there is no other reliable data to compare with.

Let's briefly summarize what we could nevertheless deduce from this comparison.

The attitude motions induce an offset on RASU which consists of

- a positive term dominated by the pendulum velocity and
- a term related to coning motions whose sign depends on the relative coning and spin directions.

Since the observed offset is positive before and after spin inversion, we think that we may conclude that the pendulum motions dominate with respect to the coning motions.

Under main chute, the RASU and AGC spin curves are very close. This implies a reduced influence of the pendulum velocity under main chute, since a significant positive offset should be observed if its addition had a significant effect. Since coning motions should have even less effect, we may conclude that the descent under main chute was very stable. This agrees with the observations that we have already made in the introduction when looking at the accelerometer signals.

A high RASU offset is observed between 3000 and 5000 s after T_0. This might be due to large oscillation amplitudes[41] or to a synchronization between the spin movement and other motions.

Finally, the inversed peaks observed on RASU and the AGC spin profiles and the peaks which are present on only one of those curves should certainly be explained by attitude motions.

11.2.2 Effect of the attitude on the AGC signal

We have already talked about the error induced by attitude motions on the AGC azimuth deduction. In the present section, we want to have a different look at these effects, trying to actually characterize the attitude motions from irregularities in the way the azimuthal antenna gain pattern is played on the AGC signal.

At first sight, there appear to be two methods which could prove interesting to investigate the probe's attitude during descent using the AGC signal.

The first one would be to examine the amplitude modulation of the AGC signal due to tilt effects. This method provides tilt information in the form of real PAA value: since the antenna gain decreases with increasing PAA, power drops could be attributed to a worse alignment between antenna vertical and orbiter direction and power peaks to better alignments; in

[41] However, don't forget that the offset represented on the spin profile is not on acceleration but on its square root, so that acceleration deviations appear bigger for low spin values. The hypothetical large oscillations may thus actually be present from the beginning of the descent under stabilizer chute - where the spin rate is much higher - which would be more consistent with what we observed on the CASU signal.

particular, "missing" extrema in the azimuthal AGP might be attributed to tilt-induced power drops or peaks.

After a few efforts, we concluded that we could not make any profitable use of this amplitude modulation. Searching the whole AGC signal for amplitude variations seemed to be worthless since much noise induced by other - for example atmospheric - effects was superimposed on the local variations and no long timescale variations could be made out. While the big extrema were indeed weaker at some places, here also no periodic pattern could be made out. In fact, it is most probable that the random modulation of the peaks' amplitude is due to sampling effects. Indeed, we may not forget that the AGC signal was sampled at a finite frequency of 8 Hz, which is quite high but could still make us skip the top of a steep peak.

The second method is directly related to our previous error calculations; indeed, as we noticed there, attitude motions induce phase modulations of the AGC signal. Having a closer look at these influences could help to deduce attitude properties. Therefore, let's more clearly represent the influence of different motions on the AGC azimuth deduction.

First of all, we examined the exact influence of a spin movement on the deviations of the AGC from a constant AGP play rate. Indeed, the error on the probe's azimuth turned out to vary very slightly with the antenna's azimuthal orientation and we wanted to rule out the possibility that this influence becomes dominant. To do this, we had to separate the two components of the previous geometrical error. Indeed, while the second component of the geometrical error is effectively due to the fact that the antenna sees the orbiter at a wrong place and is thus reflected on the AGC, the first component is only due to the projection of the antenna direction on a horizontal frame: it has no influence on the AGC signal but represents the variation of the actual azimuth of a tilted axis with respect to its azimuth if its reference plane was not tilted. As a consequence, we may expect to trace back the attitude motions of the probe by examining a varying influence of the second deviation term on the AGC signal, but the first term must not be considered.

The following figure shows the evolution of these two error terms when the probe has a constant tilt (angle and direction) and is just spinning.

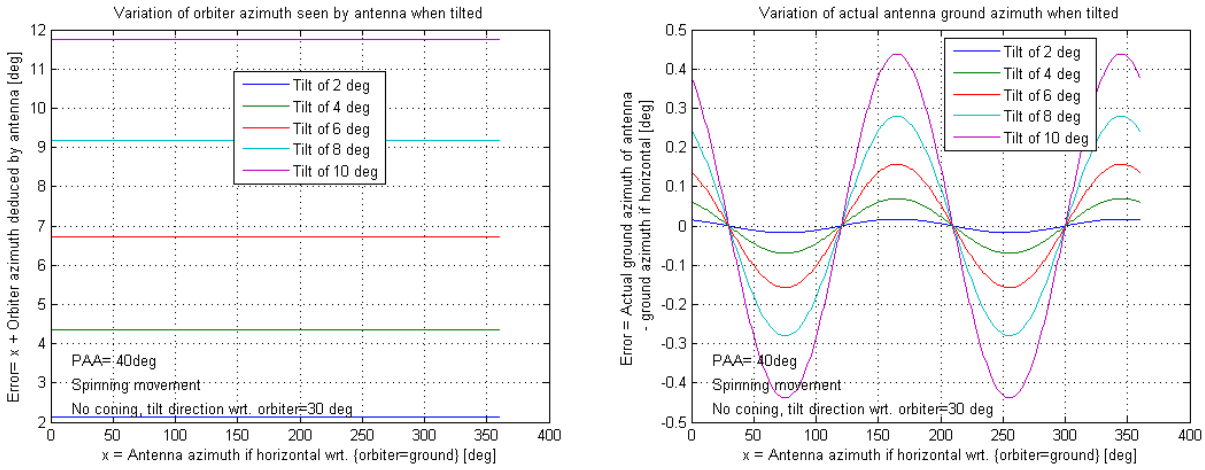

FIG.57: *Azimuth deviations while the probe is spinning with a constant tilt angle and tilt direction: the second (left) and first (right) components of the geometrical deviation presented in Appendix B.*

We observe that the second component, representing the deviation of the AGC signal, does not vary at all. We can thus conclude that **the dependence of the previously computed azimuth error on spin motions is only dictated through the first component of the geometrical error, which has no influence on the AGC signal; as a consequence, for a constant spin rate, deviations from a constant AGC play rate are only dictated by the attitude of the probe,** *i.e.* **the tilt angle and tilt direction.**

As the tilt direction turned out to have a very strong influence on the AGC azimuth deduction error, let's clearly visualize both components of the geometrical azimuth deviation for a coning movement.

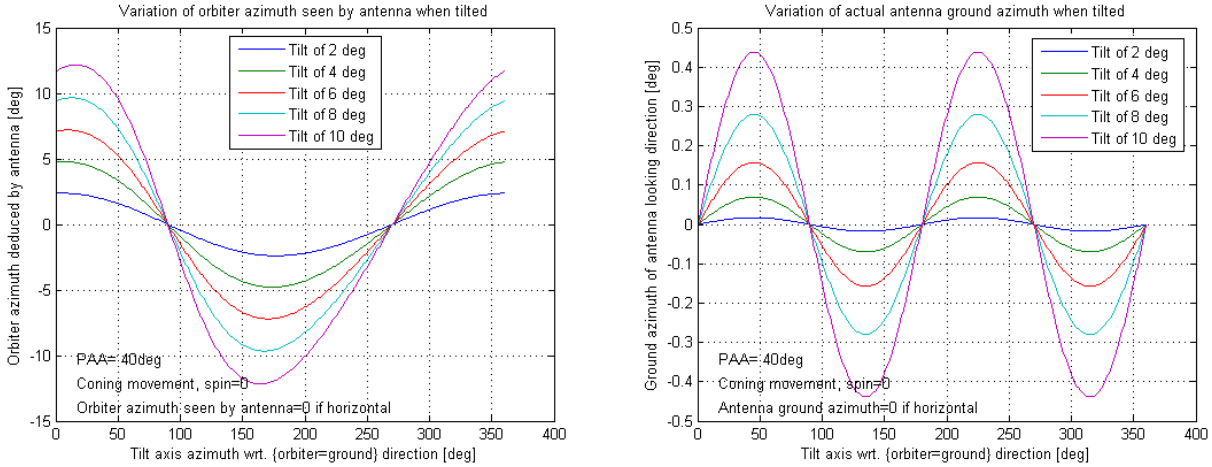

FIG.58: *Azimuth deviations while the probe is coning with a constant tilt angle: the second (left) and first (right) components of the geometrical deviation presented in Appendix B.*

The first component of the deviation behaves exactly as during spin motions (the antenna reference being similarly tilted in all possible directions during a coning period), but the second component is now dominant; it is thus actually very similar to what would be observed when travelling along a horizontal line on the 2-dimensional error plots shown in the section about the estimation of the uncertainty on the probe's azimuth deduction from the AGC signal.

Finally, the effect of a pendulum motion is very simple to imagine: just take a constant tilt direction, *i.e.* choosing a point on the horizontal axis of *figure 58*, and vary the tilt angle, *i.e.* going from one curve to the next one and jumping 180 *deg* further on the horizontal axis when you reach a zero tilt.

To illustrate what these influences would exactly imply on the AGC signal, we made a simulation, using the Huygens probe's B channel AGP, and superimposed the signal as it would be played for a constant spin rate and a horizontal probe (in green) or a tilted probe making a coning movement (in blue).

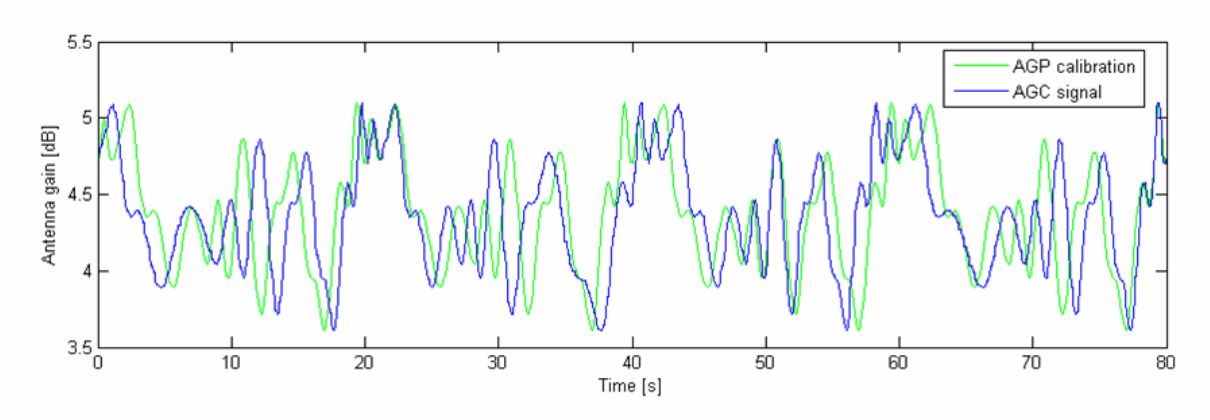

FIG.59: *Possible (simulated) AGC signals for the Huygens mission at* $PAA = 25$ *deg. In green: horizontal probe with a spin period of* 20 *s. In blue: tilted probe with a spin period of* 20 *s and a coning period of* 28.8 *s; the aperture angle is* 10 *deg.*

The periodic correspondence of the two patterns after one coning period is clearly visible. However, this is because we consider two idealized signals and the extreme cases for tilt angle and PAA. It is not so simple to make the same thing by comparing the real AGC signal, with all the superimposed noise and the varying spin rate, to the idealized AGP. A major problem is that we have no idea of the possible frequency of the perturbation which we should look for.

A first trial to get this worthy information may be made by observing the AGC deduced spin profile. Indeed, since it is most probable that the probe attitude angles oscillated with time during pendulum and coning motions, perturbations should be observed on the AGC azimuth and spin deductions following this periodic pattern[42].

Such secondary period oscillations seem to be visible at the end of the AGC spin profile. Their period is about 110 s, which is very long so that it is difficult, specially given the small number of consecutive oscillations, to rule out the possibility that they might be actual spin variations. Anyway, since our spin profile was constructed by using one peak per rotation period, its analysis will never give any hints about AGC perturbations with a shorter period than the spin period.

Another, more useful way to search for attitude induced secondary frequencies on the AGC signal is, of course, to consider its spectrum. No very low frequency can be made out, but looking at higher frequencies than before, a line appears at the end of the descent, starting at a frequency of 0.6 Hz around 6000 s and ending at the end of the descent with a frequency of 0.47 Hz; a harmonic of this signal is also visible.

[42]This conclusion may be wrong if the spin and the other motions have the same frequency; but this should obviously not remain the case by chance during a whole descent, under different parachutes.

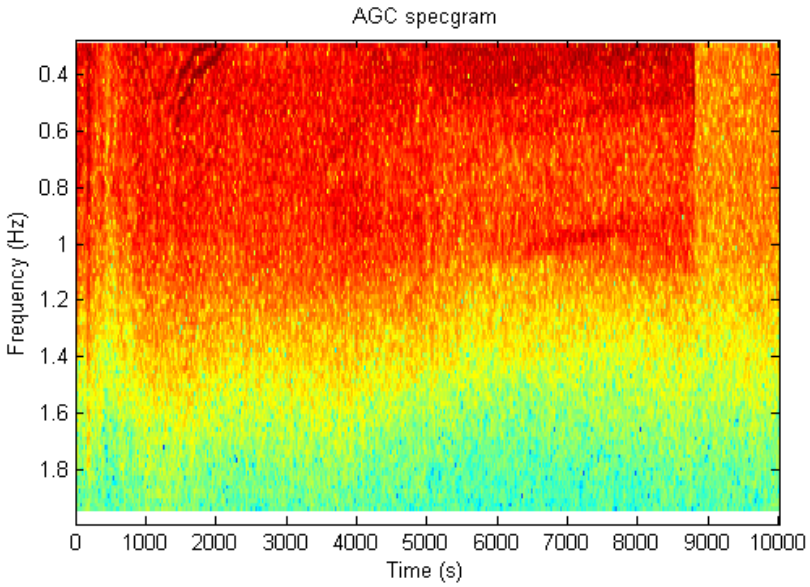

FIG.60: *Spectrum of the AGC signal up to frequencies of 2 Hz. The very low frequencies have been skipped because their strong dominance would completely flatten the rest of the signal.*

A first thing which has to be done is to rule out the possibility that it is simply a strong high-order harmonic of the spin movement. Checking the azimuthal AGP for the PAAs of the end of the descent, no strong harmonic was standing out above the tenth one, while the observed frequency would have to be at least the 18th one since

$$\frac{0.47\,Hz}{1.5\,rpm/60} = 18.8\ .$$

In fact, looking back to the RASU spectrum presented in the first section, this line seems to agree quite well with the decreasing frequency line starting around 3500 s. The following figure superimposing copies of the two frequency lines is meant to support the fact that they are caused by the same phenomenon.

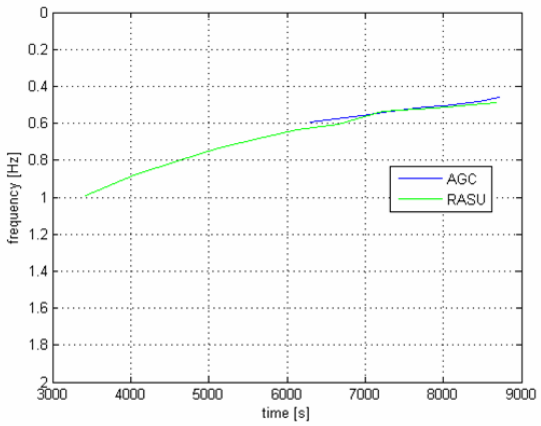

FIG.61: *Comparison of the decreasing frequency lines on the spectra of RASU (in green) and of the AGC (in blue).*

Trying to identify what phenomenon is reflected by this line, a first question which might be asked is: why does it only appear at the end of the descent? A possibility could be that the corresponding movement itself only appears at the end of the descent, but this is obviously wrong since RASU detects it much earlier. Another possibility might be that the conditions to detect it on the AGC signal improved towards the end of the descent.

Considering the respective effects of different attitude motions on the AGC signal, at least one plausible theory may be worked out. Imagine a pendulum motion in a fixed vertical plane; its effect on the AGC strongly depends on the orientation of this plane. Indeed, the perturbation would be small if the tilt axis was perpendicular to the orbiter direction[43], while it would be large if the pendulum motion was perpendicular to the orbiter direction. Now, there is no reason to suspect that the pendulum direction should absolutely remain constant during the whole descent; allowing a slow rotation of the pendulum plane from parallel to the orbiter direction, at the beginning of the descent, to perpendicular to the orbiter direction, at the end of the descent, would justify why the effect of the pendulum is only seen on the AGC at the end of the descent.

This theory however gives no explanation for the other frequency lines which are present on RASU; what could they be indeed once spin, pendulum and coning motions are attributed? In addition, it implies a strongly decreasing pendulum frequency for which there is no plausible theoretical explanation, while precisely the rather constant frequencies are not considered.

These constant frequency lines in turn are not observed at all on the AGC spectrum. Under main chute, one may argue that the probe was so stable and the attitude motions so small that effects cannot be extracted out of the noisy background on the AGC spectrum. Under stabilizer, the higher PAA values lead to a much reduced and steadily decreasing effect of attitude motions on the AGC signal. This additional remark makes our previous explanation for the frequency line reaching from 0.6 Hz to 0.47 Hz even more curious.

In fact, if the attitude variations indeed take place at the high frequencies of about 1 Hz observed on RASU, their influence on the AGC signal may be difficult to identify.

One problem might be that we are approaching the resolution limit of the AGC signal (8 Hz) and of the AGP (180 points per period, implying minimum 3 Hz for a spin period of 1 rpm); for manual identification, a 1 Hz attitude motion superimposed on the average 2 rpm spin would imply to identify 30 attitude-induced oscillations during one spin period. In addition these frequencies become quite close to the rapid noisy oscillations observed on the AGC signal[44]. At these frequencies, it is actually not easy to decide on the time signal whether observed oscillations are due to probe movements or to noise. As already said, the RASU frequencies have not been identified through the whole descent on the AGC spectrum, indicating that periodic movements are probably not visible in the oscillations.

This is consistent with the facts that amplitude modulations are difficult to make out on a perturbed signal and phase modulations need a high sampling rate to be made out.

[43]Notice that, as we are not considering only one peak on the AGP but the whole signal, we do not have to worry about the effects of the PAA on peak positions; indeed, the shape of the signal will slightly change for different PAAs, but this should obviously not be visible as a secondary frequency since the variation is not uniform for all azimuths. We may thus indeed consider the geometrical effect as the predominant one.

[44]To prove that these are indeed not induced by rapid attitude motions, one can have a look at the end of the AGC signal, after landing, where they are still present despite the fact that the probe is at rest.

We think that further characterization of the attitude motions is needed, especially concerning the reality of high frequency and low frequency attitude and low frequency spin movements, before a more detailed analysis of the AGC variations may refine our knowledge of these attitude motions.

12 Trying to identify the probe's attitude motions using the CASU and RASU accelerometers

In this section, we present a more detailed, quantitative analysis of the accelerometer outputs, the goal being to infer attitude motions.

According to the formulas in the introductory part, the measurements made by CASU (similar to $\mathbf{Acc} \cdot \mathbf{e_x}$) and RASU (similar to $-\mathbf{Acc} \cdot \mathbf{e_y}$) are the following.

$$\begin{aligned} CASU_{meas.} &= \{\cos(\theta)(Decel + \mathbf{g}_{Titan}) - \sin(\theta)\cos(\phi)\ddot{y} - \sin(\theta)\sin(\phi)\ddot{z} \\ &+ l[\dot{\theta}^2 + \sin^2(\theta)\dot{\phi}^2] \\ &+ r[\cos(\psi-\phi)\ddot{\theta} + \cos(\psi-\phi)\sin(\theta)\cos(\theta)\dot{\phi}^2 + \sin(\psi-\phi)\sin(\theta)\ddot{\phi} \\ &\quad -2\sin(\psi-\phi)\dot{\theta}(\dot{\psi}-\dot{\phi}) + 2\cos(\psi-\phi)\sin(\theta)\dot{\phi}(\dot{\psi}-\dot{\phi})]\} \end{aligned}$$

$$\begin{aligned} RASU_{meas.} &= -\{\sin(\theta)\cos(\psi-\phi)(Decel + \mathbf{g}_{Titan}) + (\cos(\theta)\cos(\phi)\cos(\psi-\phi) - \sin(\phi)\sin(\psi-\phi))\,\ddot{y} \\ &+ (\cos(\theta)\sin(\phi)\cos(\psi-\phi) + \cos(\phi)\sin(\psi-\phi))\,\ddot{z} \\ &+ l[\cos(\psi-\phi)\ddot{\theta} - \cos(\psi-\phi)\sin(\theta)\cos(\theta)\dot{\phi}^2 + \sin(\psi-\phi)\sin(\theta)\ddot{\phi} \\ &\quad +2\sin(\psi-\phi)\cos(\theta)\dot{\phi}\dot{\theta}] \\ &- r[\Big(\cos(\psi-\phi)\dot{\theta} + \sin(\psi-\phi)\sin(\theta)\dot{\phi}\Big)^2 + \Big((\dot{\psi}-\dot{\phi}) + \cos(\theta)\dot{\phi}\Big)^2]\} \end{aligned}$$

The positions of the accelerometers were not provided as accurate numbers yet. Luckily, RASU's radial position was included in the POSW's algorithm for the determination of the DDB spin rate, where we read that $r = 0.353\ m$; from rough, manual measurements on scaled plans, we derived the value of $r = 0.113\ m$ for CASU. The value of l, the vertical position of the suspension point (or, more mathematically, the fix point of the movement or centre of rotation) with respect to the accelerometers, depends on what is considered as the suspension point and will thus be discussed. The movement of this suspension point is represented by $Decel$, $\ddot{y}$ and $\ddot{z}$. We will usually neglect the horizontal accelerations, thus deleting the terms in $\ddot{y}$ and $\ddot{z}$.

The two following methods were successively considered to try, using these formulas, to make sense of the CASU and RASU measurements during the Huygens mission and relate them to actual movements of the probe.

The first, more theoretical method did not lead us to positive results and as a consequence their description has been kept short. The second method was more experimental and, though it did not lead to a full characterization of the Huygens probe's attitude motions (which is not surprising given the reduced information at our disposal), it allowed us to put a bounding box on the probe-parachute system's possible behaviours.

12.1 First trial: rigid system motions assuming the canopy top as fixed point

The present first method is a trial to find a very simple movement of the probe-parachute system which may be consistent with the accelerometer measurements. The structure of this

system being very simple indeed, it is not expected to move in exotic ways including many different movements of subsystems separated by many articulation points.

In fact, the rigid body movements which we study here consider no articulation point at all. As the parachute has a very dominant inertia under flight conditions, due to the stabilization of its position by the air flow, we should use the top of its canopy as the fixed "suspension point" for an oscillatory movement. The probe will thus be supposed to passively hang under the parachute, as a mass at the end of a rope attached to a fixed point. The fact that the parachute is actually not fixed but descends through Titan's atmosphere does not cause any major problem: according to Galileo-Newton and Einstein, we just have to consider the combined influences of the acceleration constant associated to the gravitational force and of the actual acceleration (which can actually not be differentiated according to Einstein) in place of the only gravitational acceleration for a "really fixed" suspension point or the only "real" deceleration in the "absence of any gravitational field", leading to replace $\ddot{x}$ by $(Decel + \mathbf{g}_{Titan})$ as has already been done in the above equations.

As a consequence of our assumptions, the distance l from the accelerometer platform to the fix point is simply equal to the distance from the same platform to the parachute's top; the values are thus 27 m and 12.03 m under main chute and stabilizer chute respectively.

12.1.1 Presentation of the theoretical models used

To allow an easy theoretical study, rather strong model simplifications were made.

A first simplification is that the spin of the probe is not taken into account. Knowing the spin profile, we might indeed include the gyroscopic effect associated to this movement in the study of the probe's attitude motions, especially since this gyroscopic effect was used to stabilize the probe during the entry phase. However, I think that the spin rate is too slow during most of the descent to induce a significant gyroscopic effect. In addition, we may not say that there are no torques acting on the probe during the descent, which is an important hypothesis to apply the theory of gyroscopic effects; in fact, the spin vanes were even designed to induce torques along the spin axis, so that the rotation rate along the probe's $X-$ axis is constantly adapted to external influences: I think that we may thus actually not speak about a real gyroscopic effect.

Going even further, we considered the probe as a point mass, totally discarding its moment of inertia. This is justified by the fact that, for the rigid system motions with the canopy top as fix point which we consider for the present study, an attitude variation of x *deg* for the probe requires a displacement of $l \cdot x$ *deg*. Under these conditions and given the dimensions of the probe, it seems acceptable to state that the translational effects largely dominate the rotational effects from a dynamic point of view.

A third simplification is that we will consider no damping effects; this is done because the actual movement of the probe actually seems not to have been (significantly) damped during the Huygens mission according to the accelerometer observations.

As a result, the movement of the probe is described as the behaviour of a point mass suspended under a rigid, massless cable[45] which is attached at a fixed point in a gravity field of $(\mathbf{g}_{Titan} + Decel)$ acceleration constant. The value of $Decel$ has been taken from DTWG trajectory reconstructions; it turned out to be negligible with respect to $\mathbf{g}_{Titan}$ once we leave

[45]The additional assumption that the cable has a very low mass should not surprise anybody.

the transition regions close to parachute deployments.

The simplest movement which may describe the motion of such a system is the simple, two-dimensional pendulum. The results of the theoretical study of this system are well known: the sinusoidal behaviour of the mass' position is entirely characterized by the freely chosen amplitude of the oscillations and the frequency, which cannot be varied but is fixed by external conditions; for small oscillations[46], it is given by the well-known formula

$$f = \frac{1}{2\pi}\sqrt{\frac{\mathbf{g}}{l}}$$

which, replacing $\mathbf{g} = \mathbf{g}_{Titan} + Decel$ and l by their values for the present model of the Huygens mission, yields pendulum frequencies of 0.0357 Hz and 0.0535 Hz under main and stabilizer chutes respectively. It is maybe better to consider the periods, which would be 28 s and 18.69 s respectively.

Another very simple movement, considering the possibility of 3-dimensional motions, would be a circular coning movement; in this case, the aperture angle would be a chosen constant and again, the frequency (we should better speak about a rotation velocity) of the movement is imposed by external conditions (and by the aperture angle, with a very weak influence for small apertures). By equating the vertical force components, since the probe remains at the same height during the whole movement, we first obtain the value of the tension T in the suspension rope

$$T = \frac{m\mathbf{g}}{\cos(\theta)} \ .$$

Then equating the horizontal component to the centrifugal force C, we get

$$C = T\sin(\theta) = m\mathbf{g}\tan(\theta)$$

and since the centrifugal force is expressed by the following equation (where r is the radius of the circle which is drawn by the probe's successive positions)

$$C = mr\dot{\phi}^2 = ml\sin(\theta)\dot{\phi}^2 \ ,$$

we get the rotation rate of the coning movement

$$\dot{\phi} = \sqrt{\frac{\mathbf{g}}{l\cos(\theta)}}\,[rad/s] = \frac{1}{2\pi}\sqrt{\frac{\mathbf{g}}{l\cos(\theta)}}\,[rot./s] \ .$$

As $\cos(\theta)$ is very close to 1 for low aperture angles θ, this rotation rate will only slightly vary with aperture angle and remains very close to the pendulum frequency computed above. As a consequence, it seems impossible to differentiate these two motions, pendulum and coning, on the basis of frequencies.

A third motion which was investigated is the complete, 3-dimensional free pendulum with pendulum and coning components. Its dynamic analysis has been reported to Appendix C. As this movement is more complex, three different methods were used for its investigation. The first one considers the evolution of the variables in time using the approximated formula

[46]The acceptable amplitude range, where $\theta \approx \sin(\theta)$, reaches up to 30 *deg* which is much more than the maximum amplitude of 10 *deg* allowed for the Huygens mission.

obtained in Appendix C and the second one considers the exact theoretical results for extreme values of the variables; as the coning period could not be derived by the exact method, numerical simulations starting with the basic, exact differential equations have been made to provide a third set of values for cross-checks. Some results obtained by these three different methods are reported in the `3DConingPendulum.xls` Excel file. The agreement of the results may vary, being worst for the approximated method when the amplitude of the pendulum motion approaches the value of the offset angle[47], but it stays acceptable for most cases. The behaviour of the energy for the approximated and simulated methods is a good indicator of their level of accuracy, since the energy should be conserved in the real case; the size of the energy variations over a few periods has been included as a last parameter in the Excel sheets, and the observed values show a good agreement particularly for the numerical simulations.

The coning and pendulum frequencies of the combined movement are again very close[48] for low pendulum amplitudes (simulations with higher amplitudes than those expected for the Huygens mission and presented in the Excel file have been carried out to see that the difference indeed increases for high pendulum amplitudes), which is not surprising as the pure coning and pendulum movements had a very similar frequency. This is not a particularity of the Huygens mission but a very physical behaviour since the similarity is contained in the formulas. It reflects the fact that the transition between a coning-pendulum motion, as shown on *figure 62*, and a 2-dimensional pendulum should be continuous, the actual movement being very similar though its description using θ and ϕ angles is very different.

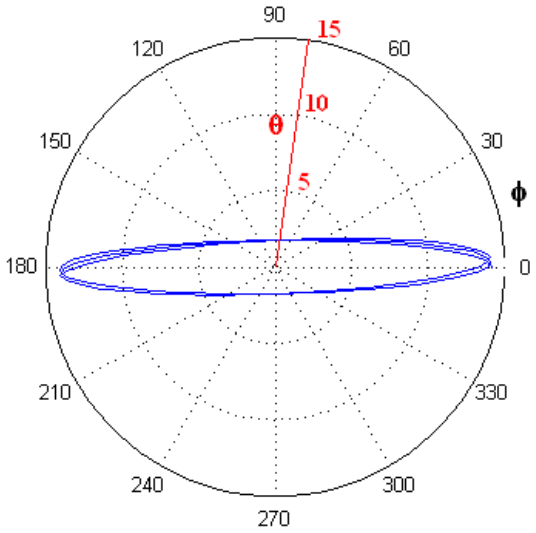

FIG.62: *The trajectory of a point mass executing a few periods of a free coning-pendulum motion in polar coordinates, (radial = θ, angular = ϕ, thus very similar to what would be seen when watching it from above). The direction of the "pendulum movement" (the major axis of the quasi-ellipsis, which is actually described as a combination of coning and pendulum components) slowly rotates according to the difference between coning and pendulum frequencies.*

[47] See Appendix C to understand the meaning of these terms.

[48] In fact, there is a factor of 2 because the pendulum motion is considered in a different way: a new period is started every time the pendulum reaches its maximum amplitude in the present case, while for the 2-dimensional pendulum, a whole period includes two maximum amplitude points.

12.1.2 Comparison with the measurements of the Huygens mission

Using the mathematical descriptions of the three types of movements presented above and the known spin profile, we now wanted to investigate how they might agree with the accelerometer measurements of the Huygens mission.

We therefore considered each term of the expressions of $CASU_{meas}$ and $RASU_{meas}$ presented in the introduction to this section, one by one, examining their maximum and minimum values and the point of the movement where they were reached; simulation results had sometimes to be used for the third type of movement since the absence of exact solution for the evolution in time of the variables caused some problems for the analysis of terms combining θ and ϕ effects.

I do not want to present this analysis in detail; let's just say that usually, a few dominant terms could be made out to infer the behaviour of the total $CASU_{meas}$ and $RASU_{meas}$ signals. The amplitudes considered for the 3-dimensional pendulum are presented in the Excel file `3DConingPendulum.xls`; for the simple pendulum and coning motions, we went up to θ values of 10 deg, the maximum expected for the Huygens mission. The results of these investigations are the following.

- On CASU under main chute, the constant offset and the minimal oscillations are compatible with whatever movement and θ value.
- On CASU under stabilizer chute, except in the transition region after parachute deployment, the offset (local average) variations remain under the resolution-imposed accuracy limit (*cfr.* Appendix A). No general trend is observed, the offset must thus be considered as constant and very close to Titan's gravity. This is also consistent with our theoretical analyses, where the offset variations on CASU should be small as well. But the much larger oscillation amplitudes cannot be explained by the theoretical rigid system movements considered for our theoretical study; indeed, the induced amplitudes on CASU would be so small that they would remain within the resolution limit, leading to similar observations as during the main chute phase. This is thus a first indication that we may not be studying the right movement patterns.
- The offset of RASU with respect to the spin profile was already investigated, for both flight phases, in previous sections. We should just add that the region of maximal offset which we previously identified also corresponds to the region of maximal activity (amplitude); it may thus be argued if it is a real offset induced by larger attitude oscillations or if these large amplitudes just led to problems for estimating the right average value without having any negative acceleration values.
- The oscillation amplitudes on RASU of
  - 0.01 to 0.03 m/s^2 under main chute
  - 0.15 to 0.35 m/s^2 under stabilizer chute at the beginning
  - 0.07 to 0.12 m/s^2 under stabilizer chute at the end

  could all be explained by assuming that the probe-parachute system experienced one of the three simple theoretical motions considered.

However, there are not only amplitudes but also frequencies to be compared. Looking at the oscillations of the RASU signal, we see that they actually occur at frequencies of about 1 Hz which are very close to the ones identified on its spectrum; the latter are thus really reflecting the main behaviour of the accelerometer signals. But this is totally different from what was deduced by our theoretical study and thus causes another, major problem for the consideration of rigid body motions under a fix canopy top as the likely Huygens probe behaviour.

A higher frequency would also explain the higher oscillation amplitudes observed on CASU under stabilizer chute: higher frequencies imply higher angular velocities for a same amplitude, and thus higher centrifugal accelerations which would be visible on the accelerometers.

If the attitude motions really take place at those high frequencies, we also have to consider the averaging made on RASU to deduce the spin rate in another way: in fact, we are rather averaging the attitude motions themselves, more than their spin-induced variations on the RASU accelerometer. That's why our much shorter averaging period than what would have been necessary to delete spin-induced variations and was used for the DDB spin computation, still provided acceptable results; spin-induced variations were not filtered out, but the dominant attitude variations well.

It is important to notice that no longer timescale variations, which could be related to the frequencies of the present simple pendulum and coning motions, were observed on the CASU and RASU signals. The 20 - 30 s periods provided by the theoretical study also do not agree with the oscillations observed on the spin profile, which were of about 110 s.

It is also impossible to justify the appearance of much higher frequencies by considering all effects which were discarded by our simplified study. Indeed, the probe's non-zero moment of inertia for example certainly has some effect, but I think that, since it adds inertia to the system, it should rather decrease than increase the frequency. Anyway, it seems impossible that this secondary effect might change the order of magnitude of the frequency. Damping should not significantly increase the probe's oscillation frequency and as the observed oscillations lasted during the totality of the 2 hours long descent, it may anyway not be dominant... unless another, excitatory phenomenon counteracts the damping effect. This is most probably the case and in fact questions the utility of the present study of an unexcited system. Moreover, as this trigger cannot be acting similarly on the whole parachute-rope-probe system but should rather be local, rigid body oscillations are not likely to be the dominant behaviour of the system.

We must thus conclude that the simple motions which were theoretically studied in this section are very unlikely to characterize the behaviour of the Huygens probe during its descent onto Titan. That's why we made a second study where more behaviours could be considered.

12.2 Second trial: considering a lower fix point height

The previous study seems to show that it is impossible to explain the accelerometer measurements by considering the canopy top as the fix point of a rigid body motion; in fact, just the high frequency of the oscillations already makes a motion implying large translations of the massive probe very improbable. We must thus find another way to relate the measurements of CASU and RASU to attitude variations of the probe.

12.2.1 Description of the method used

Rather than trying to theoretically modelize several other possible, more complex but still very simplified motions for the probe-parachute system in the hope of an agreement between one of them and the observations of CASU and RASU, we now want to start from the measurements themselves.

However, directly inferring the motion from accelerometer measurements is impossible; just look at the long expressions of $CASU_{meas}$ and $RASU_{meas}$ for the general case to see that, even when considering $\ddot{y} = \ddot{z} = 0$ and a perfectly known spin and deceleration, too many parameters interact (not only $\theta(t)$ and $\phi(t)$ are unknown, l is also undefined) in a too complex way to allow a useful analysis of these relations. We must thus make some assumptions to study the movements of the probe; the goal is to make them weaker than for the previous analysis, replacing the theoretical considerations about dynamically possible motions by observations made on the accelerometer signals.

As we found no other way to explain the high frequencies of the oscillations observed on the accelerometer signals, we had to use them as the basic frequencies of the movements which we will analyze. This goes in the right direction of using the accelerometer measurements as a starting point, while our previous theoretical analyses could not justify the appearance of such a rapid movement.

We further have to somewhat reduce the possibilities to be considered for the type of movement. The simplest way to carry out our analysis without having to care about in-phase and off-phase variations according to unavoidable dynamic rules as the angular momentum conservation, is to separate coning and pendulum motions. We will thus consider at one hand a pure pendulum movement and at the other hand a pure coning movement; anyway, our previous analysis showed that they produce similar results, as a combined pendulum and coning motion does. We may thus consider only the extreme cases without being too far from reality.

The big difference with the previous analysis is that we will not consider the canopy top as the rotation centre anymore, but allow it to be located anywhere on the symmetry axis at a distance l from the probe. We are actually just worrying about the behaviour of the probe, so to be rigorous we should define the fix point as the rotation centre for the movement of the probe: what happens to the rope and parachute above this point is totally discarded since it has no influence on the accelerometer measurements once a fixed rotation centre has been defined for the coning or pendulum movement of the probe; our description is thus now of purely kinematic nature. However, the big inertia of the parachute under flight conditions makes a swinging movement of the whole system around the fix point very unlikely; it is much more probable that the parachute stays at rest, and thus constitutes a second centre of rotation, governing the motions of the upper part of the system, as would be the case for a synchronized double pendulum motion for example.

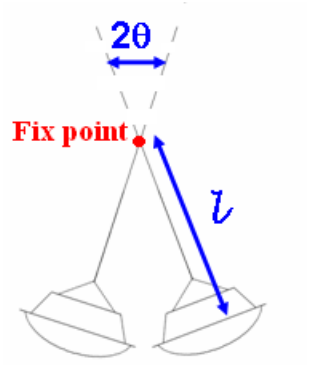

FIG.63: *Schematic illustration of our kinematical description of the probe's motion for the present analysis: the movement takes place around a fixed rotation centre at height l from the accelerometers, to which the probe is connected with a rigid rope; the aperture angle / pendulum amplitude is θ. The movement of the rest of the system, having no effect on the accelerometers, is discarded.*

Having defined the type and frequency of the movement, the method which we use consists in varying the amplitude or aperture angle for the pendulum and coning motions respectively, and the height of the fix point. We then simulate the effect which such probe oscillations would have on CASU and RASU and compare them with the actual accelerometer measurements in order to verify if a particular amplitude and fix point height could be consistent with the observations of the Huygens mission.

More precisely, we compared the minimum and maximum values reached by the simulated CASU and RASU signals to the observed minimum and maximum values on the actual signals; this implies 4 values to be compared. As RASU and CASU have a limited resolution, we do not have to look for equalities which would anyway never have been observed; instead, a value will be considered as matching when the (high resolution) simulated signal lies between $Min.$ and $Max.$, the possible acceleration values according to the RASU or CASU output assuming respectively the minimal or the maximal possible activity (*i.e.*, the minimal and maximal acceleration oscillation amplitudes compatible with the quantified output values of the accelerometer).

The known spin and deceleration profiles allow us to replace $\dot{\psi}$ and $\ddot{x} = \mathbf{g}_{Titan} + Decel$ by known values.

As the behaviour of the probe was not steady during the whole descent, we considered three different times at which a match was tried to be made.

The first one is under main chute, the two others are at the beginning and at the end of the stabilizer chute phase; indeed, the amplitude of the CASU oscillations changed and we wanted to examine what this implies for the probe motions. The considered spin and deceleration values for these three periods are 2 rpm and 0.02 m/s^2, 3 rpm and 0.02 m/s^2 and 1.5 rpm and 0.002 m/s^2 respectively. The observed extreme values on the accelerometer oscillations for these periods are listed in the tables below. Notice that we had to use the offset and amplitude (observed only in positive direction) of the RASU signal to reconstruct the negative values which should correspond to the minimum accelerations experienced by the RASU accelerometer but erased by quantification. Another problem was encountered to identify the minimal needed amplitude of the CASU oscillations under main chute; indeed, it

may not be zero but it might be very small indeed. Our choice is quite arbitrary, but we will notice when turning to the results that it still allows the lowest amplitude (1 *deg*) motions, so that its potential overevaluation has no effects on our conclusions.

	RASU minimum	RASU maximum	CASU minimum	CASU maximum
$Min.$	- 0.00123 **g**	0.00513 **g**	0.135 **g**	0.140 **g**
$Max.$	- 0.00149 **g**	0.00538 **g**	0.099 **g**	0.177 **g**

RASU and CASU extreme outputs for the Huygens mission under main chute.

	RASU minimum	RASU maximum	CASU minimum	CASU maximum
$Min.$	-0.0220 **g**	0.0295 **g**	0.099 **g**	0.216 **g**
$Max.$	-0.0224 **g**	0.0300 **g**	0.059 **g**	0.256 **g**

RASU and CASU extreme outputs for the Huygens mission during the first half of the stabilizer chute phase.

	RASU minimum	RASU maximum	CASU minimum	CASU maximum
$Min.$	-0.00851 **g**	0.0104 **g**	0.135 **g**	0.177 **g**
$Max.$	-0.00921 **g**	0.0111 **g**	0.099 **g**	0.216 **g**

RASU and CASU extreme outputs for the Huygens mission during the second half of the stabilizer chute phase.

Simulations were carried out for θ values reaching from 1 to 10 *deg* in steps of 1 *deg* and for four different fix point heights.

The largest height considers the length of the whole system, 27 m or 12.03 m under main and stabilizer chutes respectively; we already studied this case in our previous investigations to notice that it turns out to be impossible, but by taking this value, we could be sure to have considered the upper boundary for the position of the fix point; accessorily, we wanted to have an idea of the difference which this movement would imply on the accelerometers with respect to what had actually been observed.

The next fix point height which was considered is the point at which the three suspension bridles of the probe connect to the single rope. Indeed, as long as all three bridles were tensed, these bridles and the probe had to be considered as a rigid system so that the connecting point seemed to be the lowest possible material point around which oscillations could take place; this point is located 3.9 m above the probe's experiment platform where the accelerometers were fixed on. Going further down, the fix point becomes a fictive point, corresponding to no materially fixed element, but maybe to a physical point as the centre of mass, or to nothing particular, just happening to be the rotation centre of the probe's oscillations.

As a minimal height, we arbitrarily chose the length which would correspond to a 1 Hz oscillation frequency for a point mass pendulum. As it turns out to be a bit more than 3 cm, this has absolutely no meaning for the present case since the probe may definitely not be regarded as a point mass at this scale. However, it provides a useful minimal height different from zero; in addition, the computation of this value clearly shows that pendulum motions

in the sense of a mass suspended under an oscillating cable would definitely have no sense at 1 Hz frequencies for the Huygens mission.

The last value corresponds to nothing and was just chosen to have an intermediate point, at 0.3 m, for more accurate interpolation of the behaviour of the accelerometer signals as a function of the fix point height.

The simulations were simply made by considering the evolution in time of the different orientation angles for the considered movements. The formulas which were then used to represent the evolution in time of the accelerometer signals are presented in Appendix D. Finally, we just had to identify the maximal and minimal values reached by these signals during their evolution; this was much easier than trying to manually analyze at which moment the different signals reached their extreme values, especially since their qualitative behaviour might also change with amplitude and fix point height.

The results of our investigations are presented in the Excel file `AttitudeMovements.xls`. For each of the three phases and each type of motion (pendulum or coning), the resulting maximal and minimal RASU and CASU accelerations obtained by simulation of a movement at each considered amplitude and for each of the four fix point heights have been reported in a table. These values were then used to draw (by simple linear interpolation) curves representing the variation of the measured accelerations with fix point height, for each amplitude and each variable (CASU min & max, RASU min & max). The intersections between these curves and the horizontal lines corresponding to the values observed on the Huygens signals were then used to define the possible motions.

Considering the uncertainties about our measurements (the main uncertainty comes from the fact that the frequency lines on RASU's spectrum are rather broad) and since the assumptions of

- pure and perfectly regular pendulum and coning motions
- a perfect confidence in our spin profile
- a perfectly smooth behaviour of the fix point, *i.e.* no lateral acceleration of the probe-parachute system at all and no oscillations in its vertical behaviour (which could actually be induced by atmospheric effects as varying densities or vertical wind components)
- an absolute exclusion of spring-like motions

are definitely not realistic, the following deductions should not be regarded as the perfect truth, but as orders of magnitudes which might help to characterize the movement of the probe. For example, if the possible fix point heights according to RASU and CASU do not agree but are very close for a particular movement, it could be that, including all secondary effects, they perfectly match in reality and the corresponding movement should thus not be rejected but considered as a possible behaviour of the probe. In contrast, a movement which turns out to be impossible according to several observations may be excluded, since a hypothetical secondary effect would then be needed to explain several features of the accelerometer measurements, which makes it not secondary anymore.

In fact, as the positions of the accelerometers (their exact radial position as well as their height above the experiment platform) were not exactly communicated yet, there could be rather large uncertainties on our results; it might be that the accelerometers are not located

at exactly the same height for example; this could explain small differences on the location of the fix point deduced by CASU and RASU: the fix point height is defined with respect to the position of the accelerometers, which has thus to be known to actually locate the fix point.

It may even be that the height of the rotation centre changes during the oscillations, in which case there would not be any real fix point; if the motions of the rotation centre remain small however, our trials to define its height might provide acceptable results which could be regarded, as all our conclusions, as helpful orders of magnitudes.

12.2.2 Conclusions about likely attitude motions for the Huygens mission

Let's now present the results of these investigations.

First of all, we examined the shape of the different acceleration *versus* fix point height (or "length") curves obtained by simulation; they are very similar for all three phases of course.

For a pendulum motion, the minimum acceleration experienced by RASU regularly decreases as the fix point height increases; the maximal acceleration increases in the same regular way. This reflects the fact that the maximum and minimum values experienced by RASU are modulated with the azimuthal orientation of the probe with respect to the tilt direction, leading to symmetrical results for a pendulum motion; there is just an additional offset, mainly due to the spin, which leads to higher absolute values for the positive measurements than for the minimal ones; this justifies our operation using the offset and positive amplitude of the RASU signal to deduce the missing negative values. As expected, a higher oscillation amplitude leads to lower minimal and higher maximal accelerations.

The minimal value measured by CASU turns out to be independent of the height of the fix point. This is consistent with the fact that the term relative to l (see Appendix D) is squared; it will thus constitute a positive offset, which can at very best reach zero for the minimal value of $CASU_{meas}$. It is interesting to notice that here also, the higher amplitudes lead to lower values; this is consistent with the Huygens signal, where indeed higher oscillation amplitudes lead to lower acceleration values and are not (totally) countered by a positive offset. The behaviour of the maximal CASU acceleration is somewhat trickier. Indeed, the curves are not linear anymore; while an acceptable regularity is still present for low amplitudes, the higher accelerations for big amplitudes create a real break in the curves, where the beginning (between 0.034 and 0.3 m) is horizontal while the remaining part is very steep. This indicates that there could be a change in the qualitative behaviour of the probe somewhere between 0.3 and 3.9 m.

Our limited resolution in fix point height does not allow us to precisely locate the place of this change. As a consequence, the interpolation lines may be wrong and thus the consequent intersection points between them and the actual measurement values too. However, we see that those values are in fact not used to conclude about the likely probe motions, so that it is not necessary to refine our analysis. Interpolation errors are certainly present on other values as well but their effect concerning a bias of the deductions should not be stronger than the ones discussed at the end of the previous section: it is sufficient to derive orders of magnitudes.

For the coning motions, the evolution of the first two curves, concerning RASU's measurements, is very similar to what was observed for pendulum motions: the amplitude of the experienced acceleration steadily increases with increasing fix point height and higher oscil-

lation amplitudes; the offset, mainly due to the commonly imposed spin, is the same. As a conclusion, it might be very difficult to differentiate coning and pendulum motions based on RASU measurements.

Looking at CASU however, the behaviour is very different. The curves of the minimum acceleration *versus* fix point height are not horizontal anymore but rather steep (though linear) and cross each other: for a low fix point (below about 50 cm), larger oscillations lead to a lower minimal acceleration, but for a high fix point, it seems that the offset induced by larger oscillations dominates the increase in amplitude of the accelerometer variations so that larger oscillation amplitudes lead to higher values for the minimum acceleration on CASU. As a consequence, if the fix point turned out to be high, we could exclude coning motions and favour pendulum motions since we actually observed lower minimum acceleration values for larger oscillation amplitudes during the Huygens mission; however, if the fix point turns out to be low, there would be no difference on the behaviour of CASU's minimum for coning and pendulum motions.

The curve of the maximum acceleration on CASU as a function of fix point height is again much more similar to what was observed for pendulum motions, except that there is no break in the curve and no associated horizontal part at the beginning; as we anyway do not have the acceleration as a function of fix point height, but for one defined position of the fix point for the Huygens mission, this will never be noticed and is thus of no use for trying to differentiate pendulum and coning motions.

The next step to understand the behaviour of CASU and RASU measurements implied by these movements, which becomes necessary since qualitative changes seemed to occur on the acceleration *versus* fix point height curves, is to have a look at the actual time signals. A couple of time signals for each type of movement, covering the different flight phases, amplitudes and fix point heights, have been saved to a specific directory `simCASURASU`; a `readme.txt` file explains how the content of an image is related to its name. I do not want to discuss them all in detail, nor to fill this report with all these figures; when referring to these images, you should just know that for each flight phase, fix point height and type of motion, images have been saved for different amplitudes if a qualitative change was observed between 1 deg and 10 deg; in contrast, if only one image is available, there was no qualitative change when considering different amplitudes. Again, the results are similar when considering the different flight phases.

First considering the pendulum motions, we encounter a problem regarding the definition of the frequency of the oscillations. Indeed, a 1 Hz pendulum motion can actually induce 1 Hz or 2 Hz oscillations on the accelerometer signals, depending on the height of the fix point; we will call them main and double frequency oscillations.

Starting with the highest value, the RASU signal shows main frequency oscillations, but CASU shows mainly double frequency oscillations, slightly modulated by a main frequency signal; this modulation is better seen for low oscillation amplitudes. The spin period can be clearly made out on the RASU signal.

For the 3.9 m fix point height, the main frequency modulation of CASU is seen on the high amplitude oscillation signal as well, and it even tends to erase the double frequency movement for low amplitudes; the spin period now also appears, mainly modulating the minimum peaks for high amplitudes and clearly modulating the whole low amplitude, nearly main frequency signal. The qualitative behaviour of the RASU signal remains unchanged.

For the third fix point height, main frequency oscillations modulated by the spin frequency dominate both signals for all considered amplitudes.

Finally, when turning to the last, minimal fix point height, CASU's behaviour does not change but now the peaks of the RASU signal begin to separate in to subpeaks for intermediate amplitudes, until a significant double frequency component is superimposed on the RASU signal when the oscillation amplitudes become large. Under stabilizer, the RASU oscillations are even totally dominated by the double frequency for the extreme case of large oscillations with a low fix point.

These changes in the qualitative behaviour of the accelerometer signals do luckily not imply any problems about our deduction of the oscillation frequency:

- as the frequency line was observed on RASU, the qualitative changes of CASU do not have to be considered; as anyway, the fix point will more probably be quite low, the double frequency oscillations on CASU might actually not have appeared during the Huygens mission (this would be consistent with the fact that a frequency line corresponding to the frequencies observed on RASU has been identified on the CASU spectrum under main chute);

- on RASU, the main frequency is always dominating, though an important double frequency component is added for large oscillation amplitudes and a low fix point; however, we actually observed both frequencies, the main frequency and the first harmonic, on RASU's spectrum, at least under main chute where the double frequency was not cut out by the 2 Hz filter.

About the change in the qualitative behaviour of CASU's maximum value accelerations observed on the acceleration *versus* fix point height curves, we may suspect, given that the evolution was more regular for low amplitudes and that the break for high amplitudes occurred between the two intermediate fix point heights, similarly to the change in dominant frequency, that these two phenomena are directly related.

The coning motions cause much less trouble on the accelerometers: CASU shows a very regular main frequency oscillation for all amplitudes and fix point heights, while RASU's behaviour is similar to the case of pendulum motions; for a high fix point, the oscillations take place at main frequency, a strong double frequency component appearing for the lowest fix point value and even becoming totally dominant under stabilizer. As had already been expected from the acceleration *versus* fix point height curves, the influence of coning motions barely differs from pendulum motions on the RASU accelerometer but a clear difference is observed on CASU.

Let's now turn to the comparison of the simulated curves with the actual CASU and RASU measurements during the Huygens mission. When an acceleration *versus* fix point height curve crosses the interval of possible values for the Huygens mission, the intersection points define an interval of fix point heights which could possibly reflect a Huygens mission case, associated to the respective amplitude corresponding to the particular curve. When one curve, corresponding to a particular amplitude, did not cross the interval of the Huygens mission values, this amplitude was stated as impossible for the corresponding movement and flight phase.

This leads to a first reduction of possible amplitudes, namely those whose curves (at least one: RASU minimum, RASU maximum, CASU minimum or CASU maximum) do not cross

the interval of Huygens mission values; the cases corresponding to these amplitudes have been coloured in yellow in the `AttitudeMovements.xls` file. The remaining possible amplitudes, still on white background, are between (extreme values excluded)

- **0 and 4** *deg* under main chute;
- **4 and 8** *deg* (pendulum motion) and **5 and 9** *deg* (coning motion) for the first half of the descent under stabilizer chute;
- **1 and 5** *deg* for the second half of the descent under stabilizer chute.

As you can see, here also the conclusions are very similar for coning and pendulum motions.

A last step is to investigate the corresponding fix point heights. As a matter of fact, it was impossible to find an agreement between all values on this topic: no amplitude could be found where the intervals corresponding to Huygens mission intersections for all 4 variables overlapped. As a consequence, we can not further reduce the sets of possible amplitudes. We were very close to a positive conclusion under main chute though, where the only problem is that the RASU maximum tends to imply a higher fix point than the RASU minimum. Remember however how many assumptions and simplifications we made for this analysis, so that a slight disagreement should not be regarded as significant for our conclusions. The likely zone for the height of the fix point under main chute would lie between 4 and 12 *cm* above the accelerometers, similarly for coning and pendulum motions.

It is much more difficult to conclude for the first half of the stabilizer chute phase, where maximally two of the 4 examined parameters can agree on a same fix point height and amplitude. But here also, the possible values for the fix point height are very low, around 8 *cm*. During the second half of the stabilizer chute descent, the fix point height intervals lie somewhat closer, but here also no more than two values can agree at a time. Again, the most probable fix point heights lie between 4 and 11 *cm* for pendulum as well as for coning motions; the value of the CASU maximum tends to imply a much too high fix point height, but the problem becomes smaller as the largest possible amplitude of 5 *deg* is approached; this seems to be a very plausible amplitude seems it is close to the values of the first phase, out of which the lower second phase amplitudes should be reached continuously.

As a general conclusion, we may say that

- the amplitudes mentioned above are the most probable ones for the attitude motions of the Huygens probe. The very low amplitude under main chute and the higher, but decreasing amplitude under stabilizer chute deduced by our simulations agree with all other observations;
- the 4 considered variables tend to agree on a fix point around 8 *cm* above the probe's accelerometers. This point is very low, it obviously lies within the probe; thus, it would be more correct to speak about different wobbling motions of the probe than about coning and pendulum movements. Precise accelerometer positions should be known to exactly decide to which point this corresponds. If the accelerometers are located higher than the probe's centre of mass, it may even be that the fix point for the probe's wobbling movements is actually located under the accelerometers, which we did not consider in the present study.

We should quickly work out how these motions agree with the mission requirements. The found amplitudes are lower than 10 deg and would thus meet specifications. However, on SM2, we also had an acceptable oscillation amplitude under stabilizer parachute of 2 to 4 deg, but associated to the frequency of about 2.6 Hz, it led to unacceptable angular velocities of 30 to 60 deg/s. According to the present study of the Huygens mission, we have a maximal amplitude of 4 deg at least and a frequency of about 1 Hz, which logically lead to angular velocities which are 2.6 times lower than for the SM2 worst case; this corresponds to 23 deg/s, which is still above the safest mission requirements of 6 deg/s. Luckily, it seems that this did not create any problem for DCSS operations.

The fact that our conclusions about amplitude and fix point height are similar for pendulum and coning motions for all three cases considered by the present analysis, despite the fact that the acceleration *versus* fix point height curves were different for both cases so that the conclusions would totally disagree at other places than the ones imposed by the measurements made during the Huygens mission, seems to support the fact that our deductions should be right. Indeed, the similarity between coning and pendulum motions (and a combination of both) had already been observed during our previous, theoretical analysis; as a consequence, the fact that here also, the results seem to agree on a common amplitude and fix point height for both types of movements, justifying the accelerometer measurements in the same way, provides a very consistent picture of the attitude motion analyses.

Now that we were able to characterize probable amplitudes and fix point heights for the probe's attitude motions, the fact that these agree so well for all types of movements leads us to a last question which has to be solved using a new approach: we still have to identify the type of movement.

13 Comparison of the probe attitude during the Huygens mission and during the SM2 test flight

There is no doubt about the fact that the attitude of the Huygens flight module was much more perturbed during its descent than expected.

This had also been the case for the SM2 flight. In fact, it seems that the order of magnitude of the perturbations followed a same pattern for the two flights (although the amplitude of the small oscillations under main chute during the Huygens mission can not be deduced from engineering sensors): a very calm descent under main parachute followed by a rough descent under stabilizer, where the perturbations were not efficiently damped. The slow damping observed during the Huygens mission does not show its effect at the beginning of the descent under stabilizer, so that it would not have been detected during the SM2 test flight even if present; we should also remember that the Huygens stabilizer chute had a double gap which was expected to enhance the stability of the parachute - and hence better damp oscillations of the probe - with respect to the SM2 test flight.

The oscillations appearing during the SM2 test flight were thought to be induced by wind gusts. However, for the Huygens mission, such wind gusts were not present to counteract the stabilizing effect of the parachutes. At least, no information about unexpectedly strong wind shears has been reported until now and even if there were some, what a chance would it be if they had again the right frequency to excite an oscillation mode of the probe-parachute system.

I think that we may, or even should, assume that the Huygens probe's attitude motions were not induced by wind gusts. This can lead to two different conclusions. Either the oscillations observed during the SM2 test flight and during the Huygens mission correspond to different motions and an explanation has to be found for the attitude variations during the Huygens mission, or SM2 and Huygens presented the same (dominant component of the) movement pattern, which should thus be intrinsic to the behaviour of the probe-parachute system under the dynamic conditions of a descent through a planetary atmosphere.

Trying to make a decision between these to hypotheses, we had a more detailed look at the characteristic steady frequencies of the oscillatory attitude motions. Let's first summarize them again:

- SM2 test flight, main parachute: 2.1 Hz ;
- SM2 test flight, stabilizer parachute: 2.6 Hz ;
- Huygens mission, main parachute: 0.775 Hz ;
- Huygens mission, stabilizer parachute: 1 Hz .

The present study does not consider the second RASU frequency line, decreasing towards the end of the mission, which was also identified on the AGC spectrum.

A first very interesting observation is that the ratios of the SM2 frequencies divided by the Huygens frequencies are similar for both flight phases:

$$\frac{2.1\,Hz}{0.775\,Hz} = 2.71 \;\approx\; \frac{2.6\,Hz}{1\,Hz} = 2.6\;.$$

Moreover, these ratios are very similar to the square root of the gravitational accelerations ratio:

$$\sqrt{\frac{\mathbf{g}_{Earth}}{\mathbf{g}_{Titan}}} = \sqrt{\frac{9.81}{1.354}} = 2.7 \ .$$

This is important since the square root of $\mathbf{g}$ intervenes on the frequency of all oscillatory movements governed by gravity. Remember that $f = \frac{1}{2\pi}\sqrt{\frac{\mathbf{g}}{l}}$ for a pendulum motion, $f = \frac{1}{2\pi}\sqrt{\frac{\mathbf{g}}{l\cos(\theta)}}$ for a coning motion,...

For the particular synchronized double pendulum movement identified on SM2, an approximated formula for the frequency is

$$f = \frac{1}{2\pi}\sqrt{\frac{m\mathbf{g}l}{I}}$$

where m is the mass of the probe, I its moment of inertia and l is the height of the flexion point (actually, the point at which the parachute pulls on the lower part of the double pendulum) above the fix point, which should coincide more or less with the probe's centre of gravity; the value of this last length was 3.9 m for both parachutes during the SM2 and Huygens flights. To validate our comparison, we should be certain that m and I were also the same for the SM2 and Huygens probes, so that $\mathbf{g}$ is the only varying parameter. We have already said that matching the Huygens mass was a primary requirement for the SM2 test flight; no clear information is available about the moment of inertia. But since the mass and structure of both probes were the same and the additional mass on Special Model 2 was placed in a way to "ensure that the centre of gravity of the probe is very close to the symmetry axis and that the probe is well balanced", which seem to be reasonable objectives for the Huygens probe as well, there should be no major difference.

But the above formula does not show any difference between the main chute and stabilizer chute phases, while frequency differences are clearly observed on the spectra. By reorganizing the previous equation, it is not surprising to obtain a good agreement on the ratios between stabilizer chute phase and main chute phase frequencies for both missions:

$$\frac{1\,Hz}{0.775\,Hz} = 1.29 \ \approx \ \frac{2.6\,Hz}{2.1\,Hz} = 1.24 \ .$$

Considering the expressions of the frequency for a simple pendulum and a simple coning motion, a trial may be made to match this ratio to the square root of the suspension lengths ratio. Taking the 27 m suspension length of the main chute and the 12.03 m suspension length of the stabilizer for both flights, the matching ratio should be

$$\sqrt{\frac{L_{Main}}{L_{Stabilizer}}} = 1.498$$

which, as you see, is too far from the above values. This is consistent with the fact that rigid body motions involving the whole probe-parachute system at the observed high frequencies are impossible.

However, we still have to identify what could explain the frequency difference between main chute and stabilizer chute phases. Further considering the synchronized double pendulum motion, specialist J. Underwood from Vorticity reminded us that the above frequency formula

is approximated; it is valid for small amplitudes, but actually when the amplitude increases, the frequency of the movement does as well. Thus, a higher frequency under stabilizer chute would be consistent with the larger oscillation amplitude. But while the amplitude of the oscillations decreases with time, on the spectrum there is a constant frequency line around 1 Hz which does not similarly decrease; thus this explanation must also be rejected.

Investigating all possible differences between both parachute phases, but with a constant effect through the whole phase, another possibility would be the different drag coefficient and thus the different flow experienced by the probe, which might be important since the trigger of the attitude oscillations should be of aerodynamic nature.

The conclusion of this analysis is that it seems very probable that the attitude motions of the probe were the same under both parachutes and for both the SM2 test flight and the Huygens mission. This would be a synchronized double pendulum movement, the probe and parachute being tilted but remaining roughly at the same position, the fix point for the probe's attitude oscillations being very close to its centre of gravity; this agrees quite well with the deductions made during the previous accelerometer analysis, showing a very low fix point for the probe's motions. However, some unsolved problems remain.

The first one concerns the identification of the trigger which excited this oscillation mode and counteracted its damping. As, though the trigger should not be wind gusts as suspected for the SM2 test flight, the examination of scale models did not show similar motions, further analysis, probably of theoretical nature, is required; the hypothesis of vortex shedding will maybe turn out to be right at last. This analysis will be done by industrial partners.

But there are still major problems about our characterization of the attitude movement too. These concern among others the fact that

- no satisfactory explanation has been found for the clear frequency differences between main chute and stabilizer chute phases;
- a second frequency line appearing very clearly on the spectra of RASU and the AGC has not been considered.

In every case, we think that we may state that the actual attitude motions take place at the high frequencies observed on RASU and not at the low frequencies observed on slow AGC oscillations; the latter may be due to secondary attitude motions involving maybe the whole probe-parachute set as a rigid system, actual spin rate variations or aliasing when considering only one peak per rotation period on the AGC signal.

•

Part VI
Conclusions

As a conclusion of our investigations, we may say that the spin and azimuth of the Huygens probe during the whole descent as well as its azimuth after landing have been successfully characterized.

The analysis of the AGC signal variations, due to the antenna gain's inhomogeneity, turned out to be particularly useful in this issue and could seriously be considered as a means of getting orientation information for future missions; the uncertainty on azimuth, going from maximally 27 *deg* for low PAA to 6 *deg* for high PAA, could be reduced if accurate attitude information turned out to be available in the future.

Precisely, regarding the attitude issue, it was much more difficult to extract useful information from the engineering dataset. Some restrictions could be made about the probe's possible motions but no actual result was obtained, though the oscillation frequencies tend to show that a major component could be the same movement as during the SM2 test flight; as a next step, the corresponding frequencies should be used to have an additional look at the AGC signal.

Luckily, the stability of the probe seems to have been sufficient to allow, as a first approximation, to consider it horizontal.

About the orientation of the probe on the surface, questionable results were obtained by making use of an external tilt angle value, which cannot be brought into agreement with other observations.

One of the engineering data, namely the radar signal, was not used for the present analysis. Future investigations might show that it also provides very useful information about the probe's attitude.

Finally, the Huygens spin direction anomaly which was discovered/confirmed is still under investigation.

•

References

[1] Technical Report HUY.ASP.HIT.RE.0005, 2004.

[2] Martin Baker Aerospace. Huygens SM2 test descent control sub-system requirements. Technical report, Huygens Briefing Munchen, March 21, 1995.

[3] Aerospatiale. Huygens SM2 flight video. Technical report, 1995.

[4] Aerospatiale. Huygens SM2 presentation. Technical report, Huygens Briefing Munchen, March 21, 1995.

[5] Aerospatiale. Huygens SM2 test evaluation report. Technical Report HUY.AS/C.530.TR.0425, 1995.

[6] Aerospatiale. Huygens flight acceptance review / system design report. Technical Report HUY.AS/C.100.RE.0505, 1997.

[7] M. Pérez Ayúcar. Use of PDRS TLM parameters for attitude reconstruction (issue 2). Technical report, ESA/ESTEC Noordwijk, 2003.

[8] K.C. Clausen, H. Hassan, M. Verdant, P. Couzin, G. Huttin, M. Brisson, C. Sollazzo, and J.-P. Lebreton. The Huygens probe system design. *Space Science Reviews*, 104:155–189, 2002.

[9] Fulchignoni et al. The characterization of Titan's atmospheric physical properties by the Huygens atmospheric structure instrument (HASI). *Space Science Reviews*, 104, 2002.

[10] E. Jaekel, P. Rideau, P.R. Nugteren, and J. Underwood. Drop testing the Huygens probe. *ESA bulletin*, 85, 1996.

[11] F. S. Johansson. Step by step test procedure for the Huygens antenna radiation pattern test. Technical Report HUY.PRC.0542.SE, Saab Ericsson Space, 1994.

[12] J.-P. Lebreton and D.L. Matson. The Huygens mission to Titan: overview and status. *Space Science Reviews*, 104, 2002.

[13] Deimos Space. Huygens descent trajectory analysis tool implementation details. Technical Report HUY.ESOC.ASW.TN.1002.TOS.OFH, 2004.

[14] Fokker Space. Huygens SM2 balloon air drop test report. Technical Report HUY.FOKK.532.RE.0030, 1995.

[15] Fokker Space. Huygens SM2 flight data report. Technical Report HUY.FOKK.532.RE.0029, 1995.

[16] Fokker Space. Huygens SM2 gondola & specimen system description. Technical report, Huygens Briefing Munchen, March 21, 1995.

[17] Fokker Space. Huygens SM2 inspection report of recovered items. Technical Report HUY.FOKK.532.RE.0031, 1995.

Datasets used

- SM2 test flight data: Time reference frame, Accelerometer and Gyroscope measurements carried out during the SM2 test flight in Kiruna, Sweden, on May 14, 1995.
- Huygens mission engineering data: CASU and RASU measurements, AGC signal directly from probe measurements during the descent on January 14, 2005; PAA and orbiter position from mission preparatory activities; probe position and descent velocity from DTWG releases.
- Data from scientific instruments: qualitative attitude-related information coming from other working groups, mainly from DISR, and presented throughout the report.
- Data provided by SAAB-aerospace: characterization of Huygens' B-channel Antenna Gain Pattern for all elevations and azimuths at 2 *deg* steps.
- SM2 probe: measurements carried out by ourselves on the SM2 probe model to verify the spin vanes' orientation, made in Katwijk on March 10, 2005.

Appendixes

Appendix A: Resolution enhancement on the average value measured by a quantifying instrument resulting from the addition of a varying signal

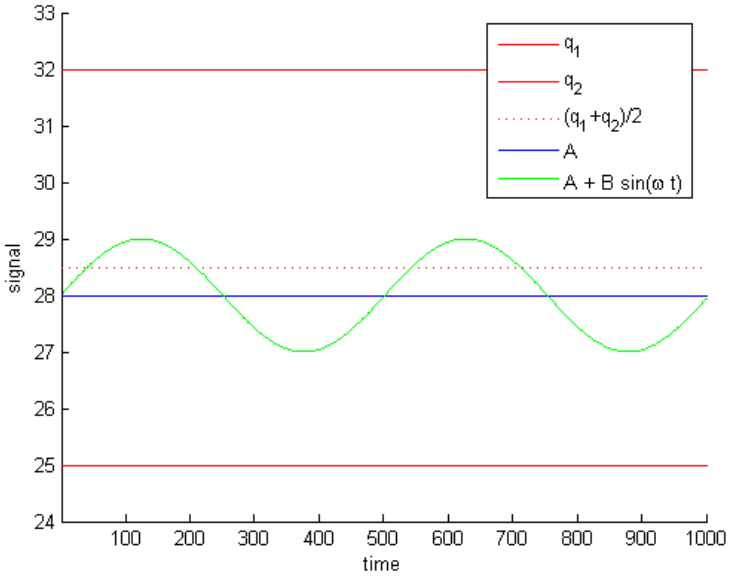

To illustrate the benefit of a varying signal superimposed on a constant value to precisely deduce the average when the measurement's quantification is raw, let's consider the case represented on the figure above. The constant average value lies between quantification steps $q_1 < q_2$, at a level A. If absolutely no noise was present, the output of our instrument would indicate either constantly q_1 or constantly q_2, depending on the position of A with respect to $\frac{q_1+q_2}{2}$ (in the case represented on the figure, the output would be $q_1 = 25$). The resulting error on our measurement would be $\pm\frac{q_2-q_1}{2}$.

Let's now imagine the presence of a sinusoidal perturbation of amplitude B, very small but sufficiently large to cross the frontier $\frac{q_1+q_2}{2}$ leading to different outputs. To simplify our analysis, the amplitude will be chosen so that no other values than q_1 and q_2 are obtained as output and frequency sampling will be neglected by assuming a sufficiently long averaging time and a sampling frequency that is incommensurable with the signal's one.

The instrument's output is now varying, indicating q_2 while the signal is above $\frac{q_1+q_2}{2}$ and indicating q_1 when it is below this limit; as a consequence, the respective times during which q_1 and q_2 are indicated can give us a hint about the location of the constant average with respect to $\frac{q_1+q_2}{2}$. If we simply compute the average of the output, we will obtain

$$\begin{aligned}\bar{\mathsf{Output}} &= q_1 \cdot \mathsf{prob}\left[A + B\sin(\omega t) < \frac{q_1+q_2}{2}\right] + q_2 \cdot \mathsf{prob}\left[A + B\sin(\omega t) > \frac{q_1+q_2}{2}\right] \\ &= q_1 \cdot \mathsf{prob}\left[\sin(\omega t) < \left(\frac{q_1+q_2}{2} - A\right)/B\right] + q_2 \cdot \left(1 - \mathsf{prob}\left[\sin(\omega t) < \left(\frac{q_1+q_2}{2} - A\right)/B\right]\right) .\end{aligned}$$

The fraction of time during which $\sin(\omega t) < \left(\frac{q_1+q_2}{2} - A\right)/B$ corresponds to

$$\frac{2 * (\arcsin\left(\left(\frac{q_1+q_2}{2} - A\right)/B\right) + \pi/2)}{2\pi}$$

so that the final result obtained after averaging of the instruments' output would be

$$\frac{q_1+q_2}{2} + \frac{q_1-q_2}{\pi} \cdot F$$

where F replaces

$$\arcsin\left(\left(\frac{q_1+q_2}{2} - A\right)/B\right) .$$

The following graph represents the error $\bar{\mathsf{Output}} - A$ for the different values of A and B compatible with our assumptions (zero values being given to the error in parts of the graph where the assumptions are not verified); the values used for q_1 and q_2 are the same as on the first graph.

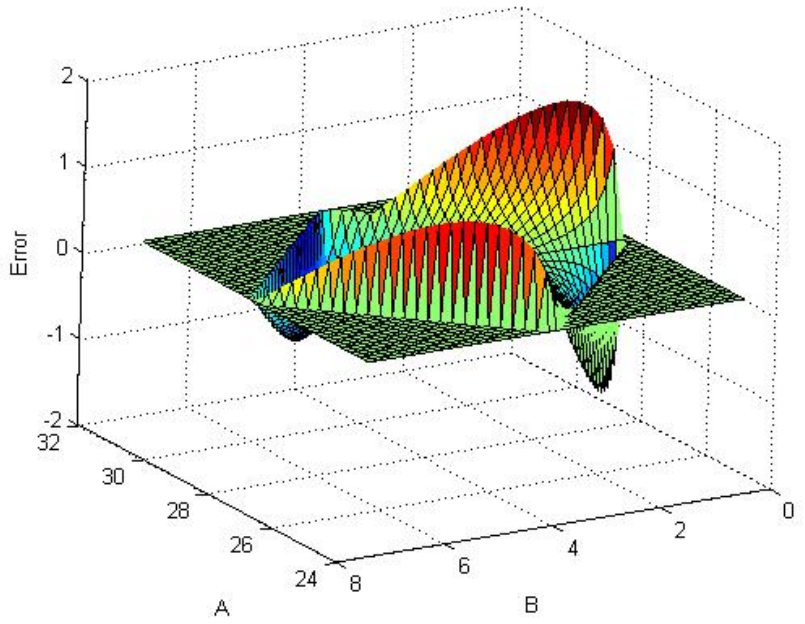

The maximum error encountered is ± 1.55, much less than the ± 3.5 in the static case; notice as well that this is due to a strong increase at the edge of the explored region, which

should just be used exceptionally. We can thus conclude that the error on the average of our measurements made during dynamic phases should be lower than the quantification error by a factor of 2 at very least.

•

Appendix B: How to correctly compute the probe's ground azimuth using AGC azimuth characterization when the probe tilt is known

The problem to be solved is, knowing

- probe and orbiter positions
- probe tilt and tilt direction
- the azimuth of the probe-orbiter direction as seen by the antenna in probe reference frame (this is the part directly obtained from the AGC signal),

to compute the ground ("absolute") azimuth of the antenna reference (thus projected in horizontal plane) in order to provide probe orientation.

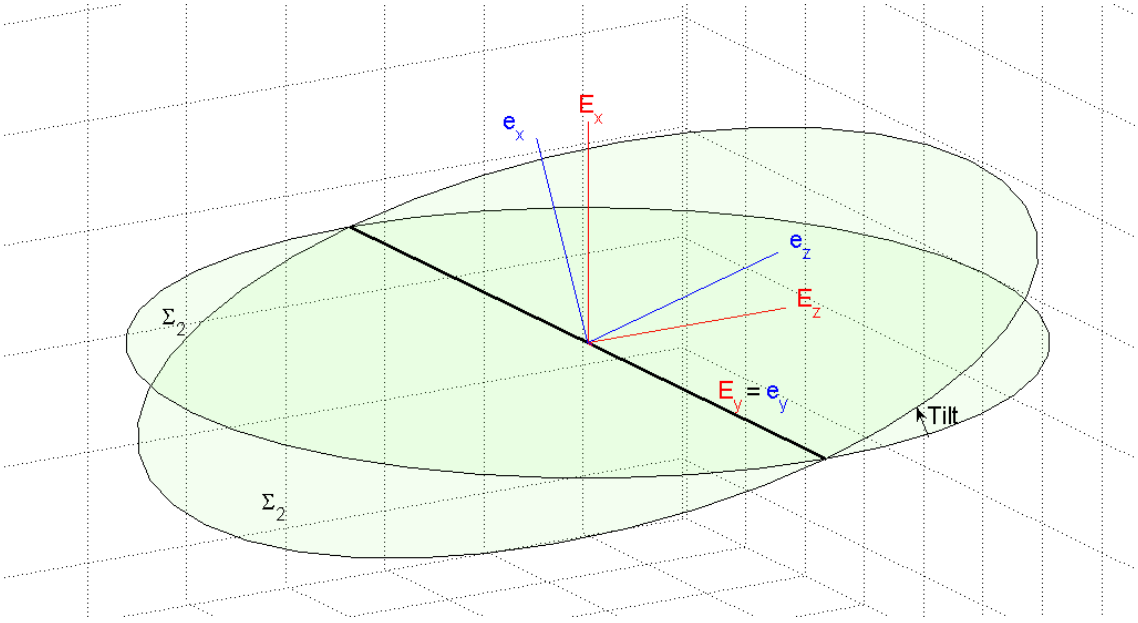

The azimuth of a point is defined by the angle which the orthogonal projection of its position vector onto a reference plane makes with a reference direction in that plane; to be rigorous, let's specify that all positions are given with the probe as the reference centre, although it should seem obvious.

To facilitate the analysis, we'll choose, as indicated on the figure above, a common reference direction $\mathbf{E}_y = \mathbf{e}_y$ with respect to which azimuth is given in both the horizontal reference frame related to Titan ground Σ_1 and the tilted reference frame related to probe Σ_2. We then have no other choice than taking as reference direction the intersection of Σ_1 and Σ_2, which can also be regarded as the axis around which the probe is tilted; its direction is chosen to always provide a positive tilt angle.

In doing this, we are fixing the tilt direction in the reference frame considered as "absolute"; that's why, to simulate the variation of this tilt direction, we will allow the orbiter azimuth to change from 0 to 360 *deg* while it is actually fixed at each moment.

The angles to be related are represented in the figure below; uppercase letters are used to indicate angles in ground reference frame, lowercase letters to indicate angles in probe-related (tilted) reference frame. We distinguish

- the ground azimuth of the orbiter, $Abs2Orb_{AZ}$ (known);
- the ground elevation of the orbiter, $Abs2Orb_{EL}$ (known);
- the tilt of the probe, $Tilt$ (known);
- the orbiter azimuth as seen from the antenna, $Ant2Orb_{az}$ (known);
- the ground azimuth of the antenna, $Abs2Ant_{AZ}$ (to be computed).

Intermediary angles to be used are

- the antenna azimuth in tilted reference frame, $Abs2Ant_{az}$;
- the orbiter azimuth in tilted reference frame, $Abs2Orb_{az}$.

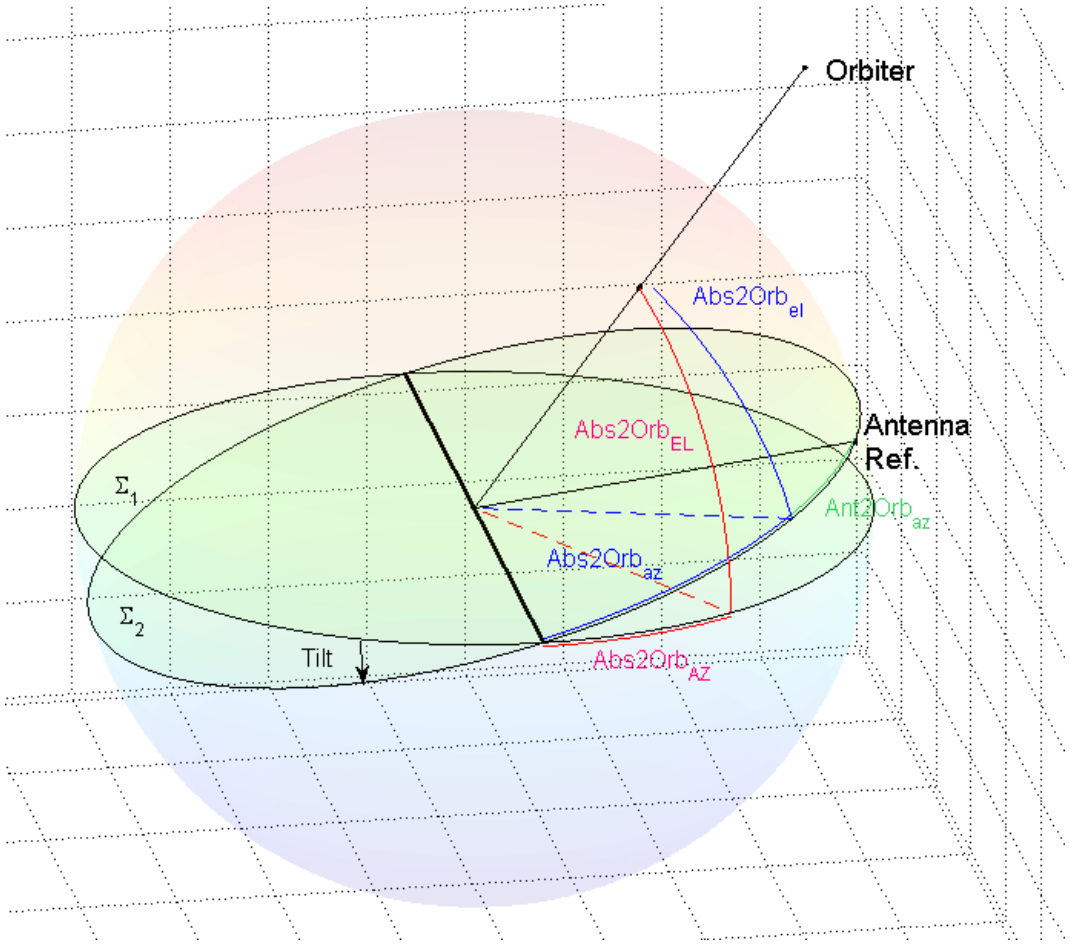

As we can see, we'll have to carry out some spherical trigonometry to obtain the wanted relation. Let's quickly recall its basic formulas:

$$\frac{\sin(\beta)}{\sin(B)} = \frac{\sin(\alpha)}{\sin(A)} = \frac{\sin(\gamma)}{\sin(C)}$$

and

$$\cos(\alpha) = \sin(\beta)\sin(\gamma)\cos(A) - \cos(\beta)\cos(\gamma)$$

where A, B and C are the "lengths" (measured as central angles) of the edges of the spherical triangle in face of the angles α, β and γ respectively.

If we knew $Abs2Orb_{az}$, it would be easy to infer $Abs2Ant_{az} = Abs2Orb_{az} - Ant2Orb_{az}$ since they're all defined in the same reference frame. Then having $Abs2Ant_{az}$ and looking at the following figure

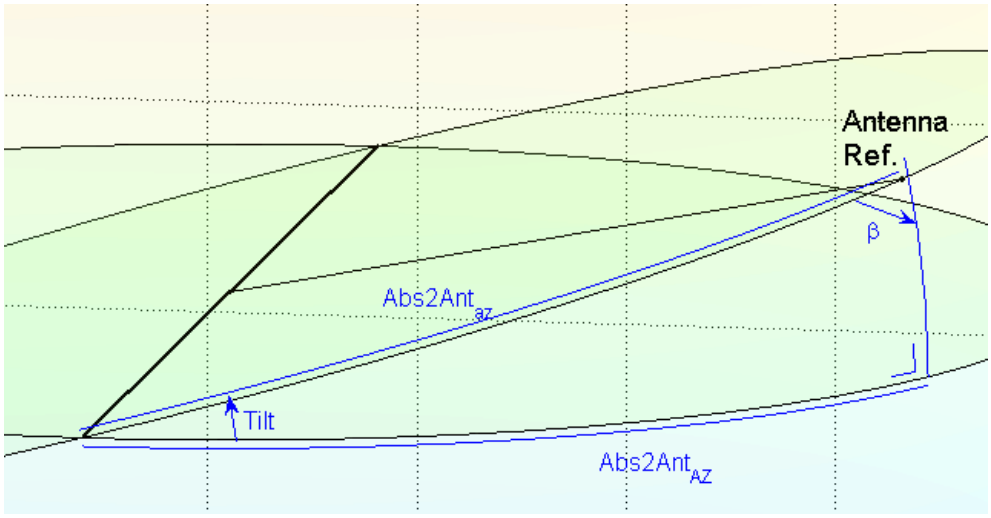

we see that

$$\frac{\sin(Abs2Ant_{AZ})}{\sin(\beta)} = \frac{\sin(Abs2Ant_{az})}{\sin(\pi/2)} \Leftrightarrow \sin(Abs2Ant_{AZ}) = \sin(Abs2Antaz)\cdot\sin(\beta)$$

where β has to be computed from

$$\cos(\pi/2) = \sin(Tilt)\sin(\beta)\cos(Abs2Ant_{az}) - \cos(Tilt)\cos(\beta) = 0$$

$$\Leftrightarrow \tan(\beta) = \frac{1}{\tan(Tilt)\cos(Abs2Ant_{az})}\,.$$

This yields

$$|\sin(\beta)| = \sqrt{\frac{1}{1+\frac{1}{\tan^2(\beta)}}} = \sqrt{\frac{1}{1+\tan^2(Tilt)\cos^2(Abs2Ant_{az})}}$$

and after replacement in the preceding equation,

$$| \sin(Abs2Ant_{AZ}) | = | \sin(Abs2Ant_{az}) | \cdot \sqrt{\frac{1}{1 + \tan^2(Tilt)\cos^2(Abs2Ant_{az})}} \ .$$

To deduce angles from the $|\sin|$ values, observe that

$$\begin{aligned} -\pi \leq Abs2Ant_{az} \leq -\pi/2 &\Leftrightarrow -\pi \leq Abs2Ant_{AZ} \leq -\pi/2 \\ -\pi/2 \leq Abs2Ant_{az} \leq 0 &\Leftrightarrow -\pi/2 \leq Abs2Ant_{AZ} \leq 0 \\ 0 \leq Abs2Ant_{az} \leq \pi/2 &\Leftrightarrow 0 \leq Abs2Ant_{AZ} \leq \pi/2 \\ \pi/2 \leq Abs2Ant_{az} \leq \pi &\Leftrightarrow \pi/2 \leq Abs2Ant_{AZ} \leq \pi \end{aligned}$$

with corresponding equalities.

This formula represents the correction to be made to the absolute azimuth at which you are looking when you're staying on a plane which can be tilted: if you stay at the same azimuth on the plane, your actual ground azimuth resulting from the horizontal projection of your position vector changes; it could be argued that taking this bias into account or not is a question of convention about how you should define your azimuth.

But a first correction, which absolutely has to be considered, intervenes on the calculation of $Abs2Orb_{az}$. It is of the same kind as the previously discussed one, except that the fact that the orbiter isn't located in any of the two reference planes induces more complications. The following figure shows the problem to be solved.

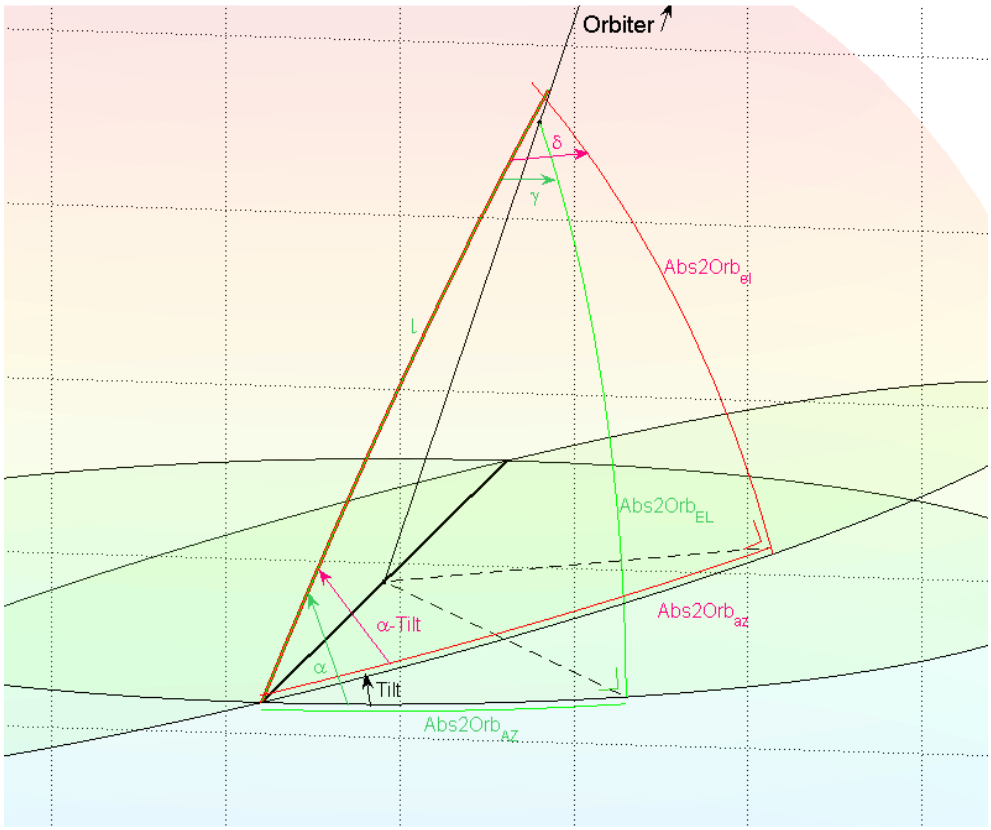

In a first (green) rectangular spherical triangle, $Abs2Orb_{AZ}$ and $Abs2Orb_{EL}$ are known and should thus allow deduction of all remaining quantities. After this, considering the other (red) rectangular spherical triangle, the knowledge of $(\alpha - Tilt)$ and l should allow to compute $Abs2Orb_{az}$. We can again derive the angle from the absolute value of its sine or cosine by adapting the equalities and inequalities used in the previous case for $Abs2Orb_{AZ}$ and $Abs2Orb_{az}$; complications arise from the fact that the orbiter has a non-zero elevation in both reference frames, so that we'll have to establish the trigonometric relations before getting the rule. We should also notice that neither α nor $(\alpha - Tilt)$ may be negative since in those cases, the telecommunication link would be lost either for a nominal (horizontal) probe or for the actual tilted case respectively.

We then have in the red spherical triangle

$$\frac{\sin(Abs2Orb_{az})}{\sin(\delta)} = \frac{\sin(l)}{\sin(\pi/2)} \Leftrightarrow \mid \sin(Abs2Orb_{az}) \mid = \mid \sin(l) \mid \cdot \mid \sin(\delta) \mid$$

where $\mid \sin(\delta) \mid$ has to be computed from

$$\cos(\pi/2) = \sin(\delta)\sin(\alpha - Tilt)\cos(l) - \cos(\delta)\cos(\alpha - Tilt) = 0$$

$$\Leftrightarrow \tan(\delta) = \frac{1}{\tan(\alpha - Tilt)\cos(l)}$$

as being

$$\mid \sin(\delta) \mid = \sqrt{\frac{1}{1 + \frac{1}{\tan^2(\delta)}}} = \sqrt{\frac{1}{1 + \tan^2(\alpha - Tilt)\cos^2(l)}} \ .$$

We still have to compute $\mid \sin(l) \mid$ or $\mid \cos(l) \mid$ and α (here the angular value is needed, or at least the equivalent information to permit to deduce it, since we have to subtract angles) from the green spherical triangle. Let's use for example

$$\begin{aligned}
\frac{\sin(l)}{\sin(\pi/2)} &= \frac{\sin(Abs2Orb_{AZ})}{\sin(\gamma)} \Leftrightarrow \sin(\gamma) = \frac{\sin(Abs2Orb_{AZ})}{\sin(l)} \\
\frac{\sin(l)}{\sin(\pi/2)} &= \frac{\sin(Abs2Orb_{EL})}{\sin(\alpha)} \Leftrightarrow \sin(l) = \frac{\sin(Abs2Orb_{EL})}{\sin(\alpha)} \\
\cos(\alpha) &= \sin(\gamma)\sin(\pi/2)\cos(Abs2Orb_{EL}) - \cos(\pi/2)\cos(\gamma) = \sin(\gamma)\cos(Abs2Orb_{EL}) \ .
\end{aligned}$$

Successively injecting the first and the second equation in the third one yields

$$\cos(\alpha) = \frac{\sin(Abs2Orb_{AZ})\cos(Abs2Orb_{EL})}{\sin(l)} = \frac{\sin(\alpha)\sin(Abs2Orb_{AZ})}{\tan(Abs2Orb_{EL})}$$

$$\Leftrightarrow \tan(\alpha) = \frac{\tan(Abs2Orb_{EL})}{\sin(Abs2Orb_{AZ})}$$

which leads to

$$\alpha = \mathsf{atan}\left(\frac{\tan(Abs2Orb_{EL})}{\sin(Abs2Orb_{AZ})}\right)$$

with the **unusual** convention $0 \leq \alpha \leq \pi$.

Finally, we can compute $\mid \sin(l) \mid$ as being

$$\begin{aligned} \mid \sin(l) \mid &= \frac{\mid \sin(Abs2Orb_{EL}) \mid}{\mid \sin(\alpha) \mid} = \mid \sin(Abs2Orb_{EL}) \mid \cdot \sqrt{1 + \frac{1}{\tan^2(\alpha)}} \\ &= \mid \sin(Abs2Orb_{EL}) \mid \cdot \sqrt{1 + \left(\frac{\sin(Abs2Orb_{AZ})}{\tan(Abs2Orb_{EL})} \right)^2} \end{aligned}$$

to possess all necessary elements for a full computation.

Searching for a rule to deduce an angle from the $\mid \sin(Abs2Orb_{az}) \mid$ value obtained, we first observe that $Abs2Orb_{AZ}$ and $Abs2Orb_{az}$ are equal for $\pm\pi/2$.

When $Abs2Orb_{az} = 0$, considering the red triangle, we have

$$\alpha - Tilt = \pi/2 \;\Leftrightarrow\; \tan(\alpha) = \frac{\tan(Abs2Orb_{EL})}{\sin(Abs2Orb_{AZ})} = \frac{-1}{\tan(Tilt)}$$

so that

$$Abs2Orb_{AZ} = -\mathsf{asin}\left(\tan(Abs2Orb_{EL})\tan(Tilt)\right) \ ,$$

the negative value close to zero being obvious from the figures.

In a similar fashion, we get for $Abs2Orb_{az} = \pi$ the value of

$$Abs2Orb_{AZ} = \pi + \mathsf{asin}\left(\tan(Abs2Orb_{EL})\tan(Tilt)\right)$$

whose sign can again be checked on the figures.

We can thus conclude with the final rule

$$\begin{aligned} -\pi + \mathsf{asin}\left(\tan(Abs2Orb_{EL})\tan(Tilt)\right) \le Abs2Orb_{AZ} \le -\pi/2 &\;\Leftrightarrow\; -\pi \le Abs2Orb_{az} \le -\pi/2 \\ -\pi/2 \le Abs2Orb_{AZ} \le -\mathsf{asin}\left(\tan(Abs2Orb_{EL})\tan(Tilt)\right) &\;\Leftrightarrow\; -\pi/2 \le Abs2Orb_{az} \le 0 \\ -\mathsf{asin}\left(\tan(Abs2Orb_{EL})\tan(Tilt)\right) \le Abs2Orb_{AZ} \le \pi/2 &\;\Leftrightarrow\; 0 \le Abs2Orb_{az} \le \pi/2 \\ \pi/2 \le Abs2Orb_{AZ} \le \pi + \mathsf{asin}\left(\tan(Abs2Orb_{EL})\tan(Tilt)\right) &\;\Leftrightarrow\; \pi/2 \le Abs2Orb_{az} \le \pi \ . \end{aligned}$$

Let's now summarize all the stuff worked out, in the order in which it would be used to compute the exact probe azimuthal orientation $Abs2Ant_{AZ}$ from the AGC-provided $Ant2Orb_{az}$ angle and the known tilt. I won't combine them all in a single, huge and unreadable equation.

$$\alpha^* = \mathsf{atan}\left(\frac{\tan(Abs2Orb_{EL})}{\sin(Abs2Orb_{AZ})}\right)$$

If $-\pi/2 \le \alpha^* \le 0$ then $\alpha = \pi + \alpha^*$

If $0 \le \alpha^* \le \pi/2$ then $\alpha = \alpha^*$

$$| \sin(\delta) | = \frac{1}{\sqrt{1 + \tan^2(\alpha - Tilt)\left(1 - \sin^2(Abs2Orb_{EL}) \cdot \left(1 + \left(\frac{\sin(Abs2Orb_{AZ})}{\tan(Abs2Orb_{EL})}\right)^2\right)\right)}}$$

$$| \sin(Abs2Orb_{az}) | = | \sin(Abs2Orb_{EL}) | \cdot \sqrt{1 + \left(\frac{\sin(Abs2Orb_{AZ})}{\tan(Abs2Orb_{EL})}\right)^2} \cdot | \sin(\delta) |$$

If $-\pi + \mathsf{asin}\left(\tan(Abs2Orb_{EL})\tan(Tilt)\right) \leq Abs2Orb_{AZ} \leq -\pi/2$
then $-\pi \leq Abs2Orb_{az} \leq -\pi/2$

If $-\pi/2 \leq Abs2Orb_{AZ} \leq -\mathsf{asin}\left(\tan(Abs2Orb_{EL})\tan(Tilt)\right)$
then $-\pi/2 \leq Abs2Orb_{az} \leq 0$

If $-\mathsf{asin}\left(\tan(Abs2Orb_{EL})\tan(Tilt)\right) \leq Abs2Orb_{AZ} \leq \pi/2$
then $0 \leq Abs2Orb_{az} \leq \pi/2$

If $\pi/2 \leq Abs2Orb_{AZ} \leq \pi + \mathsf{asin}\left(\tan(Abs2Orb_{EL})\tan(Tilt)\right)$
then $\pi/2 \leq Abs2Orb_{az} \leq \pi$

$$Abs2Ant_{az} = Abs2Orb_{az} - Ant2Orb_{az}$$

$$| \sin(Abs2Ant_{AZ}) | = | \sin(Abs2Ant_{az}) | \cdot \sqrt{\frac{1}{1 + \tan^2(Tilt)\cos^2(Abs2Ant_{az})}}$$

If $-\pi \leq Abs2Ant_{az} \leq -\pi/2$
then $-\pi \leq Abs2Ant_{AZ} \leq -\pi/2$

If $-\pi/2 \leq Abs2Ant_{az} \leq 0$
then $-\pi/2 \leq Abs2Ant_{AZ} \leq 0$

If $0 \leq Abs2Ant_{az} \leq \pi/2$
then $0 \leq Abs2Ant_{AZ} \leq \pi/2$

If $\pi/2 \leq Abs2Ant_{az} \leq \pi$
then $\pi/2 \leq Abs2Ant_{AZ} \leq \pi$

-

Appendix C: A brief mathematical analysis of the three-dimensional free pendulum

This appendix presents some results that we derived about the three-dimensional free pendulum; much better and at least more complete analyses of this system are certainly available in specialized literature but as we did it ourselves we are not able to provide any reference, so we present our own deductions.

The model of the three-dimensional free pendulum is basically the same as the classical pendulum, except that a three-dimensional space is considered. The point mass, attached at the end of a rigid and massless rope, then moves on a spherical surface under influence of its inertia, the planet's gravity and the tension of the rope which is attached at a "fix" point[49].

The ideal case which we will study here as a basis to the understanding of this motion considers no other forces, nor torques. In particular, there is no influence of a spin movement since we consider a punctual mass and no damping is included.

As a consequence, a first conserved quantity is the total energy of the system. It comprises the kinetic and potential energies of the point mass (the rope being unable to store any energy since it is massless and rigid) and, defining the angles as in the rest of this report, can be expressed as

$$\frac{2E}{ml^2} = A_2 = \sin^2(\theta)\dot{\phi}^2 + \dot{\theta}^2 - 2\frac{g}{l}\cos(\theta) \ .$$

Notice that E, and thus A_2, will usually be negative.

The fact that all forces (gravitation and tension in the rope) act in the vertical plane containing the rope and the point mass implies that their torque is zero with respect to the vertical axis containing all those planes, which is the vertical axis passing through the fix point. This means that the angular momentum around this axis will also be a conserved quantity:

$$\frac{L_x}{ml^2} = A_1 = \sin^2(\theta)\dot{\phi} \ .$$

Expressing the equilibrium of the forces and accelerations along a meridian line (to avoid having to consider the tension in the rope), we get as a third equation

$$\sin(\theta)\cos(\theta)\dot{\phi}^2 - \ddot{\theta} = \frac{g}{l}\sin(\theta)$$

[49]For the case of the Huygens probe, there is no actual fix point, since the whole system is descending through Titan's atmosphere. However, as according to Galileo-Newton and Einstein,

- the Newtonian laws of physics are equally valid in two referential frames which move at constant speeds relative to each other and
- the inertial corrections to be made when considering an accelerated reference frame in order to recover the Newtonian laws of mechanics may be expressed as a gravitational force,

we can easily derive that a pendulum motion in a horizontally inertial, but vertically decelerated reference frame can be simply described as a pendulum motion in an inertial reference frame, but with an experienced gravitational acceleration of $g = \mathbf{g}_{Titan} + Deceleration$; for this to be valid, the decelerating force must of course be applied to the fix point (parachute) and not to the mass.

which we can multiply by $\sin(\theta)$ to get

$$\cos(\theta)\sin^2(\theta)\dot{\phi}^2 - \sin(\theta)\ddot{\theta} = \frac{g}{l}\sin^2(\theta)$$

where the first term can be simplified by introducing the energy conservation equation to get

$$\cos(\theta)\left(A_2 - \dot{\theta}^2 + \frac{2g}{l}\cos(\theta)\right) - \sin(\theta)\ddot{\theta} = \frac{g}{l}\sin^2(\theta)$$

$$\Leftrightarrow \frac{g}{l}(1 - 3\cos^2(\theta)) = A_2\cos(\theta) - \dot{\theta}^2\cos(\theta) - \ddot{\theta}\sin(\theta) = A_2\cos(\theta) + \frac{d^2}{dt^2}[\cos(\theta)] \ .$$

This is an ordinary differential equation in $x = \cos(\theta)$, where the only non-linear term, in x^2, is in the first member.

A first way to solve this equation is to linearize it for small tilt angles, which means using $x = 1 - \delta$ with δ positive and small. This yields a very classical linear differential equation with constant coefficients

$$\ddot{\delta} + \left(A_2 + \frac{6g}{l}\right)\delta = \left(A_2 + \frac{2g}{l}\right)$$

whose solution is

$$\delta(t) = \frac{A_2 + \frac{2g}{l}}{A_2 + \frac{6g}{l}} - C_1\sin(\sqrt{A_2 + \frac{6g}{l}}t)$$

or

$$\cos(\theta(t)) = 1 - \frac{A_2 + \frac{2g}{l}}{A_2 + \frac{6g}{l}} + C_1\sin(\sqrt{A_2 + \frac{6g}{l}}t)$$

where the pendulum oscillation amplitude C_1 has to be smaller than $\dfrac{A_2 + 2g/l}{A_2 + 6g/l}$ for $\cos(\theta)$ to remain smaller than one (notice from the expression of A_2 that $A_2 + 2\frac{g}{l}$ is always positive).

All other quantities may then be expressed as a function of time and of the initial conditions using this approximated time evolution for $\cos(\theta)$, in order to derive the CASU and RASU measurements implied by this behaviour. We get among others

$$\dot{\phi} = \frac{A_1\left(A_2 + \frac{6g}{l}\right)^2}{1 - (C_1)^2\left(A_2 + \frac{6g}{l}\right)^2\sin^2\left(\sqrt{A_2 + \frac{6g}{l}}t\right) - \left(\frac{4g}{l}\right)^2 - 8C_1\frac{g}{l}\left(A_2 + \frac{6g}{l}\right)\sin\left(\sqrt{A_2 + \frac{6g}{l}}t\right)}$$

$$|\ \dot{\theta}\ | = \frac{C_1\sqrt{A_2 + \frac{6g}{l}}\cos\left(\sqrt{A_2 + \frac{6g}{l}}t\right)}{\sqrt{1 - \left(\frac{4g/l}{A_2 + 6g/l} + C_1\sin\left(\sqrt{A_2 + \frac{6g}{l}}t\right)\right)^2}} \ .$$

The coning period is obtained by integrating the coning speed until reaching $\Delta\phi = 2\pi$. The resulting equation can be easily solved and is

$$2\pi = \frac{A_1}{b\alpha\sqrt{1 - \left(\frac{C_1}{b}\right)^2}}\left[\mathsf{atan}\left(\frac{\tan\left(\frac{\alpha}{2}t\right) - \frac{C_1}{b}}{\sqrt{1 - \left(\frac{C_1}{b}\right)^2}}\right) - \mathsf{atan}\left(\frac{-\frac{C_1}{b}}{\sqrt{1 - \left(\frac{C_1}{b}\right)^2}}\right) + k\pi\right]$$

where

$$k = \mathsf{floor}\left[\frac{2b\alpha\sqrt{1-\left(\frac{C_1}{b}\right)^2}}{A_1} - \frac{1}{2}\right]$$

and the constants $b = 1 - \frac{4g/l}{A_2+6g/l}$ and $\alpha = \sqrt{A_2 + \frac{6g}{l}}$.

But these are only approximations. Maximal and minimal angles, angular velocities and accelerations should be accurately known to clearly decide about CASU and RASU. Some exact analytic expressions can also be obtained to investigate the accuracy of the approximated results.

For example, the (exact) time evolution for a pure coning motion can be retrieved by assuming $\dot{\theta} = \ddot{\theta} = 0$ in the non linear differential equation. Let's remind the value of $\dot{\phi}$ as a function of the aperture angle, which defines the whole movement: $\dot{\phi} = \frac{1}{2\pi}\sqrt{\frac{g}{l\cos(\theta^*)}}$.

Using the approximate formula with $C_1 = 0$ associated to the exact expression of $\dot{\phi}$ for a coning movement to compute the value of A_2, we get the relation

$$\frac{6g}{l} = \frac{6g}{l}\left(\cos(\theta) + \frac{\sin^2(\theta)}{2}\right)$$

which proves that the approximation is very acceptable for coning motions with small aperture angles.

Notice that for a combined pendulum and coning motion, as the angular momentum has to be conserved, θ can never reach zero. In fact, the mass may pass very close to vertical but never exactly vertically, so that the movement is seen as a very rapid coning motion through nearly 180 *deg* with a varying but always positive aperture angle in place of a pure pendulum movement where the sign of θ would change; nevertheless, the two actual movements are very similar and tend to each other as the minimal value for θ tends to zero.

Let's consider the exact equations of the three-dimensional pendulum and define initial conditions by

- the initial value of θ, defined as θ^*
- the value of A_1
- an initial zero value of $\dot{\theta}$, the initial value of A_1 being chosen so that the initial θ value is the maximal aperture angle.

A first quantity can be easily derived; indeed, by replacing $\dot{\phi}$ in the energy conservation equation using the angular momentum conservation, we first express A_2 as a function of the initial conditions

$$A_2 = \frac{A_1^2}{\sin^2(\theta^*)} - \frac{2g}{l}\cos(\theta^*)$$

and can then express $\mid \dot{\theta} \mid$ as a function of θ and initial conditions:

$$\mid \dot{\theta} \mid = \sqrt{A_2 + \frac{2g}{l}\cos(\theta) - \frac{A_1^2}{1-\cos^2(\theta)}}\ .$$

Deriving this expression with respect to $x = \cos(\theta)$ and equating it to zero, we can guess the possible extremal values for $\mid \dot{\theta} \mid$. It is clear that $\dot{\theta} = 0$ for θ_{max} (defined as initial value θ^*) and θ_{min} (to be computed), so there should be just one extremal value between them. In fact, the equation giving the location of the maximum pendulum rate is the fourth order polynomial equation (stating $y = 1 - \cos^2(\theta)$)

$$\left(\frac{g}{l}\right)^2 y^4 + A_1^4 y - A_1^4 = 0$$

which yields two complex and one negative values, the only positive value, which turns out to always remain smaller than 1, thus being the solution. This value then has to be injected in the equation of $\mid \dot{\theta} \mid$ to provide its extremal value.

The minimal and maximal values for $\dot{\phi}$ are readily obtained from the angular momentum conservation equation

$$\dot{\phi} = \frac{A_1}{\sin^2(\theta)}$$

once the maximal and minimal values for θ are known; the first one being given as an initial value, we have to compute the second one.

For both extremal values of the aperture angle, $\dot{\theta} = 0$; using the energy conservation equation and replacing $\dot{\phi}$ using the angular momentum conservation equation as before,

$$A_2 = \frac{A_1^2}{\sin^2(\theta_{extr})} - \frac{2g}{l}\cos(\theta_{extr}) \ ,$$

we obtain a third order equation in $\cos(\theta)$,

$$\frac{2g}{l}\cos^3(\theta_{extr}) + A_2\cos^2(\theta_{extr}) - \frac{2g}{l}\cos(\theta) + (A_1^2 - A_2) \ .$$

Knowing one solution, namely θ_{max} which is given as the initial condition θ^*, we can divide the third order equation using the Horner technique to obtain a simple second order equation. The determiner of this equation

$$\rho = \left(A_2^2 + \left(\frac{2g\cos(\theta^*)}{l}\right)^2 - 4A_2\frac{g}{l}\cos(\theta^*)\right) + 16\left(\frac{g}{l}\right)^2(1 - \cos^2(\theta^*))$$

is always positive, which proves that there are two more real solutions. These can be expressed as

$$\cos(\theta_{extr}) = \frac{-A_2 - \frac{2g}{l}\cos(\theta^*) \pm \sqrt{\rho}}{\frac{4g}{l}}$$

which shows that there is at least one negative solution since $A_2 + \frac{2g}{l}\cos(\theta^*) = \frac{A_1^2}{\sin^2(\theta^*)}$ is positive. Our solution for $\cos(\theta_{min})$ however should be positive, since it should be bigger than $\cos(\theta_{max})$, for which no negative values will be allowed (taking aperture angles smaller than 90 *deg*). The second solution, taking the + sign, should thus directly provide θ_{min}. It

can be verified that this positive solution indeed exists by writing the classical expression for the product of the solutions of a second order equation

$$\frac{\left(\frac{2g}{l}\cos(\theta^*) + A_2\right)\cos(\theta^*) - \frac{2g}{l}}{\frac{2g}{l}}$$

and noticing that it is always negative since the first term of the numerator is positive (because equal to $\frac{A_1^2}{\sin^2(\theta^*)}$) but smaller than the absolute value of the second one (because A_2 is negative and $\cos(\theta^*)$ smaller than one).

The period of the pendulum movement can be computed by

$$T = 2\int_{Min}^{Max} \frac{d\theta}{\dot{\theta}} = 2\int_{Min}^{Max} \frac{\sin(\theta)}{\sqrt{\sin^2(\theta)A_2 + \frac{2g}{l}\sin^2(\theta)\cos(\theta) - A_1^2}} d\theta$$

or, defining $X = -\cos(\theta)$,

$$T = 2\int_{-\cos(Min)}^{-\cos(Max)} \frac{dX}{\sqrt{\frac{2g}{l}X^3 - A_2X^2 - \frac{2g}{l}X + A_2 - A_1^2}}$$

which we integrated numerically.

A last parameter which would be very interesting to know is the coning period. Unhappily, we were unable to work out a method to deduce a value for this parameter without having to integrate an explicit expression of the movement as a function of time. As pure pendulum and pure coning periods are very similar for small aperture angles, it can be expected that, at least for a small pendulum amplitude as well, the results given by the approximated study - which shows a very similar period for coning and pendulum motions[50] - should be acceptable.

•

---

[50] Actually, the "pendulum frequency" computed here is close to the double of the coning frequency, which comes from the fact that a whole pendulum movement corresponds to 2 oscillations from maximum to minimum and back.

Appendix D: Measurements made by CASU and RASU assuming pure coning or pendulum motions

The relations expressing the measurements made by CASU and RASU simplify to the following when considering pure coning or pendulum motions.

Notice that, while r is fixed by the radial position of the accelerometers ($r = 0.353\ m$ for RASU and $r \approx 0.113\ m$ for CASU), the fix point height l, denoting the distance from the probe horizontal plane at height of the accelerometer sets to the rotation centre, is not defined. We assume that this "fix point" experiences no lateral acceleration at all (*i.e.* $\ddot{y}$ and $\ddot{z}$ terms have been discarded) but allow a vertical acceleration (or rather deceleration for the case of the Huygens probe).

A star exponent has been attributed to constant orientation angles. Just to remember the meaning of these angles:

- θ represents the pendulum amplitude or the (half-)aperture angle of the cone;
- ϕ defines the orientation of the pendulum's vertical plane or the azimuthal position of the probe on the cone;
- ψ characterizes the azimuthal orientation of the probe (directions of the probe axes).

CASU and RASU measurements for a pure pendulum motion

$CASU_{meas} =$

$$\cos(\theta)(\ddot{x} + \mathbf{g}_{Titan}) + l\dot{\theta}^2 + r\cos(\psi - \phi^*)\ddot{\theta} - 2r\sin(\psi - \phi^*)\dot{\theta}\dot{\psi}$$

$RASU_{meas} =$

$$-\sin(\theta)\cos(\psi - \phi^*)(\ddot{x} + \mathbf{g}_{Titan}) - l\cos(\psi - \phi^*)\ddot{\theta} + r\left(\cos(\psi - \phi^*)\dot{\theta}\right)^2 + r\dot{\psi}^2$$

CASU and RASU measurements for a pure coning motion

$CASU_{meas} =$

$$\cos(\theta^*)(\ddot{x}+\mathbf{g}_{Titan})+l\left(\sin(\theta^*)\dot{\phi}\right)^2+r\cos(\psi-\phi)\sin(\theta^*)\cos(\theta^*)\dot{\phi}^2+2r\cos(\psi-\phi)\sin(\theta^*)\dot{\phi}(\dot{\psi}-\dot{\phi})$$

$RASU_{meas} =$

$$-\sin(\theta^*)\cos(\psi-\phi)(\ddot{x}+\mathbf{g}_{Titan})+l\cos(\psi-\phi)\sin(\theta^*)\cos(\theta^*)\dot{\phi}^2+r\left(\sin(\psi-\phi)\sin(\theta^*)\dot{\phi}\right)^2+r\left(\dot{\psi}+\dot{\phi}(\cos(\theta^*)-1)\right)^2$$

•